Characterisation of the effects of cosolutes on the stability of H-bonds in proteins by NMR spectroscopy

Anwar Mohammad

University College London

A thesis submitted for the degree of Doctor of Philosophy

January 2010

Thesis abstract

The strength of the hydrogen bond (H-bond) in biomacromolecules is significantly weaker compared to covalent bonds. Consequently, H-bonds readily form and break under physiological conditions. This property explains the key role H-bonds play in the stabilisation of biological macromolecules and as participants in many enzymatic reactions. Ubiquitin is often used in NMR experiments as a model protein due to its high solubility and stability. In addition, the folding of ubiquitin has been shown to follow a simple two-state process. As such, ubiquitin is an ideal protein to examine the subtle effects of different solvent conditions on secondary structure. In this research project a variety of NMR parameters are used to characterise the changes in the character (i.e. geometry/strength) of the H-bonds in ubiquitin under different physico-chemical conditions. In particular, the research project focuses on measuring H-bond scalar couplings (HBCs), and correlating the HBCs to other NMR parameters such as the amide 1H isotropic chemical shift and 15N relaxation data. The NMR data is complimented by circular dichroic data that provides a "global" picture of the protein structural state under the various co-solute conditions examined.

The H-bonds properties of ubiquitin where observed over a range of four temperatures 15 to 60 ºC in the presence and absence of 1.5 M trimethylamine-N-oxide (TMAO). TMAO is an organic osmolyte produced by certain species of fish to counteract high concentrations of urea found in their cells. In the absence of TMAO a global decrease in $^{h3}J_{NC'}$ couplings were observed with increasing temperatures. This observation indicates a thermal expansion of the protein as the temperature increased. The weakening of the HBCs correlated with an upfield shift of the amide $^{1}H_{N}$ chemical shift and a downfield shift of the donor ^{15}N chemical shift. The NMR results were supported by CD data in which a global decrease in ellipticity values was observed as the temperature was increased. In the presence of 1.5 M TMAO the average decrease in $^{h3}J_{NC'}$ couplings between 15 and 60 ºC were smaller (0.075 ± 0.001 Hz) compared to value 0.1 ± 0.001 Hz recorded in the absence of TMAO. Using these HBC values, the thermal expansion coefficient in the absence of TMAO was 3.3 (±0.2) 10^{-4} K^{-1}, whereas in the presence of TMAO a value of 2.2 (±0.2) 10^{-4} $K^{-1}$was calculated. The slower rate of thermal expansion of H-bonds in ubiquitin in the presence of TMAO

indicates that this co-solute slows the thermal denaturation of ubiquitin and shifts the melting point of ubiquitin to a higher value. In the presence of TMAO, the correlation between the HBCs and the ^{1}H and ^{15}N chemical shifts is significantly weaker compared to data recorded in the absence of TMAO. Presumably, the presence of TMAO not only indirectly influences the H-bond character, but also the chemical environment of the donor amide group. This is not unexpected since the HBCs are solely influenced by the H-bond geometry, whereas the chemical environment surrounding the donor group nuclei influences the ^{1}H and ^{15}N chemical shifts.

Urea and Guanidinium chloride (Gdn.HCl) are denaturants that have been used extensively in protein folding and stability studies. The H-bonds in ubiquitin where observed over different Gdn.HCl concentrations from 0 to 3.0 M. An increase in some of the $^{h3}J_{NC'}$ couplings were observed at Gdn.HCl concentrations below 1.5 M. This observation follows previous research that has shown that the salt stabilising characteristics of Gdn.HCl prevail at low concentrations. At 3 M Gdn.HCl a global decrease in HBCs was observed. Due to the two-state folding process of ubiquitin, the acquisition of NMR data beyond a Gdn.HCl concentration of < 3.0 M gave rise to second sets of peaks: one set of peaks represented the native state of ubiquitin, while the second set of peaks represents ubiquitin in the unfolded state. As such, the recording of data beyond this concentration would not provide any further insight into the denaturation of ubiquitin. At the concentrations examined (i.e. < 3.0 M), this study provided insights into the influence of Gdn.HCl on the stability and character of H-bonds in ubiquitin. In a similar series of NMR experiments, the effect of urea on the structure of ubiquitin was examined at concentrations ranging between 0 and 3 M.

"The knowledge of anything, since all things have causes, is not acquired or complete unless it is known by its causes"

Abu Ali Sina (Avicenna)

Acknowledgements

During my time at UCL I have been immensely privileged to have met and worked with some wonderful individuals who helped in along the way in accomplish my PhD. Without them, I could not have completed this project. Now I have the opportunity to spread my gratitude.

First and foremost I want to thank my supervisor Dr Andrew Dingley for his enormous help and support during my PhD project. I am very grateful for the time and effort he invested in helping me to understand NMR and structural biology. Without his support, patience, suggestions and guidance I would have never managed to complete my project.

I would like to express my deepest gratitude to Dr Michael Schmitz at the University of Auckland for all the help with the relaxation experiments, ModelFree analysis, and for all his analysis and input on the project.

My sincere thanks goes to my group members, Evanglous Diolets, Yen-Ching Yang and Hong-Gang Zoe for all their help in the lab and with experiments and for making the lab a joyful place to work in.

I would like to express my gratitude to all the experts who patiently taught me their skills. I would like to thank; Acely Garza, Andrew Sankar, Brian Ferguson, Diego Esposito and Mark Jeeves, for all the help they gave me especially during my first year. I would like to also express my gratitude to the NMR manager at UCL Dr Richard Harris for all his help with setting up NMR experiments, and Dr Tom Frenkiel the NMR manager at NIMR for his assistance with setting the experiments and pulse sequences.

There are a few people I want to thank for making the day-to day life at UCL a pleasant and enjoyable. I think of Beatriz, Sanjay and Igor for the good constant humour and discussions. As my close friend, colleague and my flat-mate I can not forget to thank Radwan. I miss the daily stimulating discussions ranging from politics to science.

And lastly, I would like to thank my parents for all the help and support they have given me during my education. I am very grateful for the unlimited belief in me and their constant encouragement.

Table of Contents

List of Figures

List of Tables

Abbreviations

ABBREVIATION	DEFINITION
1D	One-Dimensional
2D	Two-Dimensional
3D	Three-Dimensional
ASA	Accessible surface area
$^{1}J_{NH}$	One bond ^{1}H nuclei to ^{15}N coupling
$^{1}J_{CN}$	One bond ^{13}C nuclei to ^{15}N coupling
Å	Ångström
APS	Ammonium persulfate
ATP	Adenosine triphosphate
ATPase	Adenosine triphosphatase
A.U.	Absorbance Units
B_0	net magnetization vector
BPTI	Basic pancreatic trypsin inhibitor
CD	Circular dichroism spectroscopy
cDNA	Complementary deoxyribonucleic acid
GPC	glycerol phosphorylcholine
CPD	Composite-pulse decoupling
DIPSI	Decoupling In the Presence of Scalar Interactions
CPMG	Carr-Purcell-Meiboom-Gill
CSA	Chemical Shift Anisotropy
DFT	Density function theorem
E.coli	Escherichia coli
EDTA	ethylenediaminetetraacetic acid
FC	Fermi Contact
FID	Free Induction Decay
FRET	Fluorescence resonance energy transfer
FPLC	Fast protein liquid chromatography
GARP	Globally Optimized Alternating Phase Rectangular Pulse
Gdm^{+}	Guanidine ion
Gdn.HCl	Guanidinium Hydrochloride

ABBREVIATION	DEFINITION
ΔG	Gibbs free energy
HBC	Hydrogen bond scalar coupling
Hz	Hertz
H-bond	Hydrogen bond
HPLC	High performance liquid chromatography
HSQC	Heteronuclear Single Quantum Coherence
INEPT	Insensitive Nucleus Enhanced by Polarisation Transfer
IPTG	isopropyl-beta-D-thiogalactopyranoside
IR	Infrared spectroscopy
ITC	Isothermal titration calorimetry
$^{h3}J_{NC}$	trans hydrogen bond scalar couplings
kD	kilo Daltons
kHz	kio Hertz
kJ	kilo Jules
LB	Luria Bertani
MD	Molecular dynamic simulations
MG	Mannosylglycerate
MRE	Mean Residue ellipticity
ME	Molar ellipticity
mRNA	Messenger ribonucleic acid
$^{n}J_{ij}$	n-bond scalar coupling between nuclei i and j
NMR	Nuclear magnetic resonance
NOE	Nuclear Overhauser Effect
PDB	Protein Data Bank
ppm	Parts per million
QCC	Quadrupolar coupling constant
R_1	Longitudinal relaxation rate
R_2	Transverse relaxation rate
RF	Radio-Frequency
RNA	Ribonucleic acid
RMSD	Root mean square deviation
ROE	Rotating-frame Overhauser Enhancement
rpm	Rounds per minute
SCN^-	Thiocyanate

ABBREVIATION	DEFINITION
S/N	Signal-to-noise
SNase	nuclease A form Staphylococcus aureus
SD	Standard deviation
SDMA	Symmetric-L-N^{η}, $N^{\eta'}$-dimethylarginine
SDS-PAGE	SDS-polyacrylamide gel electrophoresis
SDS	Sodium dodecyl sulfate
SEC	Size exclusion chromatography
SW	Spectral Width
TEMED	N,N,N',N'-tetramethyl-ethylenediamine
TFA	Trifluoroacetic acid
TFE	Trifluoroethanol
TMAO	Trimethylamine-N-oxide
TROSY	Transverse Relaxation-Optimised Spectroscopy
τ_c	Rotational correlation time
WURST	Wideband, Uniform Rate, and Smooth Truncation
UPS	ubiquitin–proteasome system
UV	Ultra violet light

Chapter 1
Introduction

1.1 Hydrogen bonds

1.1.1 Definition

A simple definition of the hydrogen bond (H-bond) is the weak attractive interaction between a partial electropositive hydrogen atom attached to an electronegative donor atom D (D─H) and an electronegative acceptor atom A (Pimentel and McClellan, 1960). This interaction is largely attributed to the electrostatic attraction between a partial positive charge located at the position of the hydrogen atom in the D–H group and a partial negative charge on the acceptor atom A. Moore and Winmill (1912) were the first to suggest the presence of H-bonding when they solved the structure of trimethylammonium hydroxide. In 1920, Latimer and Rodebush suggested that a free pair of electrons on the water molecule might be able to exert sufficient force on a hydrogen atom held by a pair of electrons on another water molecule to bind the two molecules together. Furthermore, this study suggested that the hydrogen nucleus held between the two octets constitutes a weak bond. Approximately 20 years later in 1939 the chapter on hydrogen bonding in the book titled "*The nature of the chemical bond"*(Pauling, 1940) placed H-bonding into perspective. Pauling was one of the first scientists to use the term H-bond. Pauling suggested that a hydrogen atom can be attracted by the force of two atoms, instead of one, and thus this atom can act as a bridge between the two electronegative atoms (Pauling, 1960). In biomacromolecules the major kind of H-bonds are O–H•••O, O–H•••N, N–H•••O, and N–H•••N, while weaker H-bonds have been characterised which comprise of C–H groups as donors (Derewenda et al., 1994, Derewenda et al., 1995, Fabiola et al., 1997, Grzesiek et al.,

2001). The usual site of where the H-bonds attract is indentified as an electronic lone pair on either an oxygen or nitrogen acceptor atom. However, other acceptors have been recognised such as the π electrons of aromatic systems and sulfur groups or metallic cofactors (Table 1.1).

H-bonds play an important role in biology and chemistry due to the moderate energies required for their formation and breaking. Consequently, this feature enables H-bonds to play pivotal roles in many common enzymatic and chemical reactions in many common solvents such as water. Possibly the most important example of such a reaction is the formation of H-bonds in protein secondary structures and nucleic acids (Pauling, 1960). In biomacromolecules, H-bond energies are approximately an order of magnitude weaker (i.e. ≤ 30 kJ mol^{-1}) than covalent bonds. Strong H-bonds have bond energies similar to the magnitude of a covalent bond. One such strong H-bond is the bifluoride ion (HF_2^-) with energy of 163 ± 4 kJ mol^{-1} (Table 1.1) (Larson and McMahon, 1982).

In the geometric characterization of an H-bond, the H•••A and D•••A are the main parameters distances, as well as several bond and torsion angles such as the hydrogen bond angle D–H•••A. The H-bond is thought to be present when the distance $R_{D•••A}$ is equal to or smaller than the sum of the van der Waals radii of the two electronegative atoms. Studies have shown that the $R_{O•••O}$ distance of 2.75 Å in ice, which is much smaller than the sum of the van der Waals radii of 3.04 Å of the two oxygen atoms (Bondi 1964). In biomacromolecules the presence of backbone N–H•••O=C H-bond for a solved structure by X-ray crystallography or NMR spectroscopy is indicated by the spatial arrangement of the donor and acceptor atoms. For a structure solved by X-ray crystallography at medium resolution a large number of H-bonds are observed, e.g. for a 3.0 Å resolution structure, 85% of C=O and 75% of N–H donors are seen to form at least one H-bond according to standard geometric criteria. Whereas, at a higher resolution (i.e. < 1.5 Å resolution) more the 95% of C=O and 90% of the N–H are satisfied according to the geometric criteria (McDonald and Thornton, 1994). As a result of the weak hydrogen atom density, it is very hard to collect exact information `from X-ray diffraction data. However, with high structure resolutions of < ~1 Å resolution it is possible to obtain individual spatial positions for the hydrogen atoms which are independent of the use of standard covalent geometries (Dingley et al., 2001).

Table 1.1 Potential H-bond donor and acceptor groups classified according to the strength of the interaction.

	Donor	**Acceptor**
Very strong	$N^{+}H_3$, X+-H, F-H	COO-, O-, N-, F-
Strong	O-H, N-H, Hal-H	O=C, O-H, N, S=C, Hal-
Weak	C-H, S-H, P-H, M-H	C=C, Hal-C, π, S-H, M, Hal-M, Hal-H, Se

1.1.2 Role in protein structure

In 1936 Mirsky and Pauling were the first to suggest that H-bonding plays an important role in protein folding and stability and that H-bonds occur between the carbonyl carbon and the amide groups of the peptide backbone. Pauling and Corey (Pauling and Corey, 1951, Pauling et al., 1951) were the first to predict the two most common secondary structures found in globular proteins; the α-helix and β-sheet conformations. Both of these secondary structures were proposed to be held together by H-bonds.

The α-helix is observed when a polypeptide chain of consecutive residues all have ϕ and ψ torsion angle pairs with approximately –60º and –50º values, respectively (Branden and Tooze, 1999). The polypeptide chain is coiled into a helix with 3.6 residues per turn with a distance of 1.5 Å per residue. This leads to a rise in the helix of 5.4 Å per turn. The H-bonds occur between C=O group (acceptor) of residue *n* and the NH group (donor) of residue *n* + 4. A statistical analysis of a number of crystallographic structures (Baker and Hubbard, 1984) showed that the average values for N•••O and H•••O distances and for N–H•••O and H•••O=C angles are 2.99 ± 0.14 Å, 2.06 ± 0.16 Å, 157 ± 11˚, 147 ± 9˚ for the α-helix. In theory the α-helix turn can be right-handed or left-handed, depending on the direction of the chain. However with L-amino acids a left handed turn is not allowed due to the close approach between the C═O group and the side chains. Other types of helix are possible, notably the 3_{10}-helix, with three residues per turn, and the π-helix with 4.4 residues per turn (Branden and Tooze, 1999). The 3_{10}-helix is rarely observed in protein structures, probably because the C=O groups are spread out more from the helix axis and the H-bonding is less

favourable (and therefore the overall structure is less stable) than in the α-helix (Lehninger et al., 2005, Pauling et al., 1951, Whitford, 2005).

Helices are amphipilic and are more likely to be found on the exterior surface of a protein molecule; with one side of the helix carrying mostly polar side-chains and this surface is exposed to the external solution. The other side of the helix, consisting of primarily non-polar side-chains, faces into the molecular interior (Schiffer and Edmundson, 1967). These helices are often referred as being amphipathic. Helices may be bent or curved, and may mould around the non-polar "core" of a protein. There may even be breaks in the H-bonding associated with helix curvature (Blundell et al., 1983).

The second major secondary structural element found in globular proteins is the β-sheet. Unlike the α-helix which is built from one chain of consecutive amino acids, the β-sheet involves a combination of several regions of the polypeptide chain. The β-sheet consists of β-strands that are usually 5 to 10 residues in length and are in an almost fully extended conformation with a broader φ and ψ torsion angular space allowance. An extended single β-strand conformation is not stable because there are no interactions among atoms that are close in the peptide bond. The β-strand conformation is only stable when incorporated into a β-sheet. This is observed when β-strands are aligned adjacent to one another such that H-bonds can form between the backbone C=O of one strand and the backbone NH of the adjacent strand. Adjacent stands can form a parallel or anti parallel arrangement. A statistical analysis of a number of crystallographic structures (Baker and Hubbard, 1984) has shown that the average values for N•••O and H•••O distances and for N–H•••O and H•••O=C angles are 2.91 ± 0.14 Å, 1.96 ± 0.16 Å, 160 ± 10° and151 ± 12°. Consequently, the measured average H-bond N•••O and H•••O distances are about 0.1 Å shorter in β-sheets as compared to H-bonds present in α-helices. Parallel sheets are thought to be weaker than anti-parallel sheets, as a result of weaker, although this may be dependent on the amino acids present (Richardson, 1977). The strands of β-sheets are seldom long (maximum about 15 residues), and the H-bonding can be interrupted by β-bulges or by irregularities near the ends of the strands (Lehninger et al., 2005, Pauling and Corey, 1951, Whitford, 2005, Baker and Hubbard, 1984).

Some β-sheets are formed from a long polypeptide chain, which has a bend after a number of amino acids known as the β-turn, or β-bend, which consists of a sequence of four residues, frequently linked by a 1-4 (3_{10}-type) H-bond between the C=O of residue one and the NH of residue four. β-turns allow the complete reversal of the polypeptide chain direction and for that reason are frequently found between two secondary structure elements (two antiparallel β-strands)**.** They are also generally positioned externally to interact with solvent molecules or are positioned near polar side-chains leading to H-bonding between these side-chains and the NH and C=O groups of residues 2 and 3. Some turns have been identified to be associated with internal water molecules (Kuntz, 1972).

In addition to the secondary structures described above, which involve H-bonds between the atoms of the polypeptide backbone (main chain-main chain N–H●●●O H-bonds), many H-bond interactions are provided by amino acid side-chains. Polar side-chains including –OH (Ser, Thr, Tyr), carboxylic (Asp,Glu), carboxyamide (Asn, Gln), amino (Lys), guanidinum (Arg), and imidazole (His) groups are known to form H-bonds. H-bonds involving amino acid side chains play an integral role by stabilising interactions on the protein surface and sometimes in the molecular interior. These H-bond types include side chain-side chain and side chain-main chain forms, or, for surface groups, through the interaction with external solvents such as H_2O (Perutz and Raidt, 1975, Baker and Hubbard, 1984) (Figure 1.1).

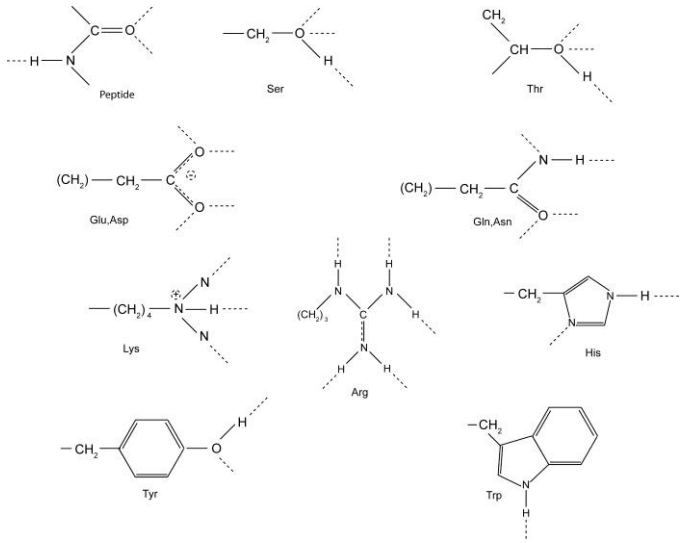

Figure 1.1: H-bonding groups in proteins, comprising the main chain peptide group and all the principal H-bonding side chains. In each case the maximum number of H-bonds expected is presented. (Adapted from (Baker and Hubbard, 1984))

1.1.3 Other non-covalent forces in proteins

Besides H-bonds, there are other crucial non-covalent interactions which are important in the stability (and fold) of proteins. This section briefly describes the general features of other non-covalent forces. Non-covalent interactions can be specific or non-specific. Non-specific interactions include van der Waals interactions. In contrast, specific interactions involve, for example, salt bridges which form between two opposing charged side-chains (e.g. Glu-Lys). Hydrophobic forces are often considered the driving force in protein folding processes, while electrostatic interactions are important in protein folding, stability, flexibility and function.

1.1.3.1 Hydrophobic interactions

Hydrophobic interactions are the influences that cause non-polar substances to minimise their contact with water. The magnitude of the hydrophobic interaction is usually measured by the transfer of free energy ΔG of a non polar molecule in a gas, liquid or solid state to water. Gibbs free energy (ΔG) is made of an enthalpy ΔH term and entropy $-T\Delta S$ term, where:

$$\Delta G = \Delta H - T\Delta S \qquad \text{Equation [1.1]}$$

Experiments indicate that the transfer of hydrocarbon molecule from nonpolar solvent to water is often exothermic ($\Delta H < 0$). Therefore, the fact that dissolving is not spontaneous must mean that entropy change is negative ($\Delta S < 0$). For example, the process of CH4 (in CCl4) CH4 (aq) have a $\Delta G = +12 kJ\ mol^{-1}$ at 25 °C. Substances characterised by a positive Gibbs free energy of transfer from a nonpolar to a polar solvent are classified has hydrophobic. The free energy of transfer is positive which indicates the non-polar molecule prefers a non aqueous environment (Lins and Brasseur, 1995).

Measuring the enthalpy of transfer from an organic solution to an aqueous solution at room temperature is insignificant, due to the interaction enthalpies being the same in both cases; however, the entropy is negative. The reduction in entropy is a result of the water molecules forming ordered cages around the non-polar molecule. However, the ordered cages become weaker than bulk water at high temperature (~ 110 °C), and the entropy contribution approaches to zero. Consequently, this results in positive enthalpy (unfavourable). This indicates that the temperature dependencies of entropy and

enthalpy are not equal; therefore there is a distinct temperature at which the hydrophobic effect is strongest. Subsequently, if the temperature increases or decreases beyond the set temperature the hydrophobic effect decreases. Techniques such as site directed mutagenesis or transferring model compounds from organic solvent to water (e.g. blocked amino acids, cyclic peptides and urea) on protein, are used to empirically estimate the role of the hydrophobic effect on protein stability. The transfer of free energy ΔG calculated is usually given as a function of the change in the solvent accessible non-polar surface area upon going from the unfolded to the folded state (Creighton, 1992).

1.1.3.2 Electrostatic forces

Salt-bridges or ion pairs found in proteins are found between hydrophilic side-chains that possess positive or negative charges. The charged side-chains are positioned in such a manner that opposing charges are attracted to each other at neutral pH. Such interactions are found to be vital for protein stability. Electrostatic interactions are dependent on the distance of the charged particles from each other. There are three main types of electrostatic forces; charge-charge interactions which are between oppositely charged side chains, charge-dipole interactions are between the charged side-chains and dipole of water molecules and dipole-dipole interactions is when some side-chains possess weak dipoles that can interact with the weak dipole force, for example, a water molecule (Lins and Brasseur, 1995). The electrostatic interaction energy between two atoms bearing single opposite charges separated by 3 Å in water has a value of ~6 kJ mol^{-1} (Stryer, 1995).

1.1.3.3 van der Waal forces

van der Waal forces are both attractive and repulsive and involve interactions between permanent and/or induced dipole interactions. The energies associated with van der Waals interactions are very small. Typical van der Waals interactions contribute between 2 to 4 $kJ \cdot mol^{-1}$ per atom pair. Although individual van der Waals forces are extremely weak relative to other forces governing protein stability and fold, it is the very large number of these interactions which gives rise to the three-dimensional structure of proteins and therefore collectively these forces provide significant protein stability (Lins and Brasseur, 1995).

1.2 NMR spectroscopy

1.2.1 Basic NMR theory

Nuclear magnetic resonance NMR is based on the fact that nuclei of atoms have magnetic properties. These properties can be utilised to extract chemical information about molecules. In quantum mechanics terms, subatomic particles (protons, neutrons and electrons) have spin. If the number of neutrons and the number of protons are both even, the nucleus has no spin. If the number of neutrons plus the number of protons is odd, then the nucleus has a half-integer spin (i.e. 1/2, 3/2, 5/2). If the number of neutrons and the number of protons are both odd, then the nucleus has an integer spin (i.e. 1, 2, 3)(Levitt, 2001).

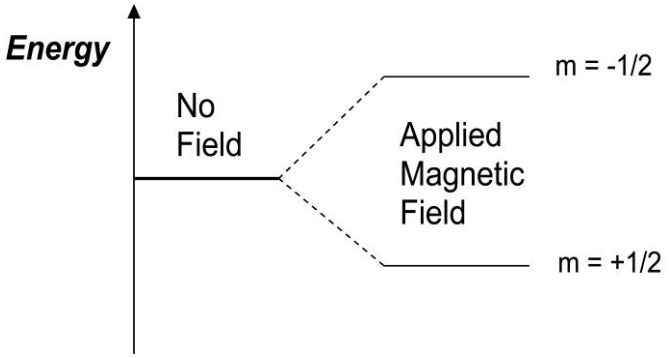

Figure1.2: Energy levels for spin quantum m = ±½.

The magnetic moment of a nucleus will align with an externally applied magnetic field of strength Bo**.** The nucleus will align in only two ways, either with or against the applied field Bo. The magnetic moment aligned parallel with Bo has a spin m=+1/2 and is often given the notation α, whereas the anti-parallel orientation (spin m=-1/2) is referred to as β (Figure 1.2). The rotational axis of the spinning nucleus cannot be orientated exactly parallel or anti-parallel to Bo which in a co-ordinate system is the *z* axis (Figure). The nucleus must precess like a motion similar of a gyroscope about this field at an angle. The angular velocity is given by the expression(Levitt, 2001, Keeler, 2005):

$$\omega o = \gamma Bo \qquad \text{Equation [1.2]}$$

Where ωo is the precession rate which is also called the Larmor frequency (Figure 1.3). The γ magnetogyric ratio (γ) relates the magnetic moment μ and the spin number I for a specific nucleus. Each nucleus has a distinct γ value, for a proton γ = 2.674x104 gauss-1 sec-1. This precession process generates an electric field with frequency ωo. If

a sample were to be irradiated with radio waves in mega Hertz (MHz) the proton will absorb the energy and be promoted to the less favourable higher energy state. This energy absorption is called resonance because the frequency of the applied radiation and the precession resonate (Keeler, 2005).

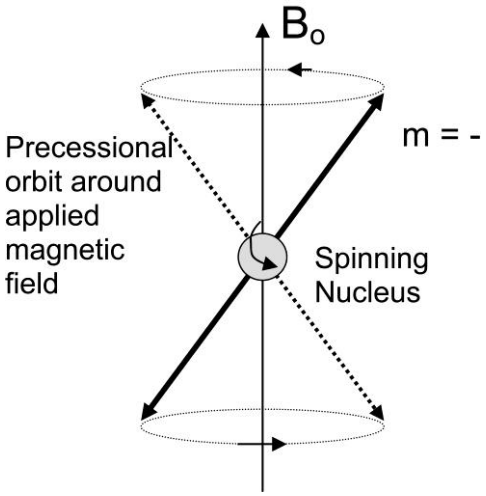

Figure 1.3: Spinning nucleus with charge precessing in a magnetic field Bo.

Spin states which are oriented parallel to the external field are lower in energy than in the absence of an external field. However, a spin state that has an opposite orientation to the external magnetic field possesses higher energy than in the absence of an external field. When a nucleus is irradiated with electromagnetic radiation of the correct energy which is determined by its frequency, the nucleus in a low energy state will change its orientation to a higher energy state. The absorption of energy during this transition forms the basis of the NMR (Keeler, 2005, Levitt, 2001).

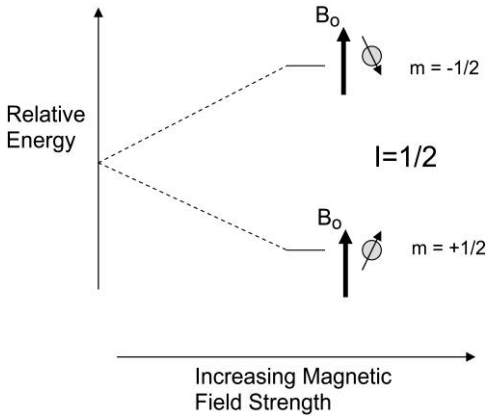

Figure 1.4: Magnetic Field strength on NMR energies.

1.2.2 NMR observations of the hydrogen bond

The understanding of H-bonds in macromolecules has been significantly enhanced by the role high resolution NMR. The various NMR observables such as, chemical shift,

reduced hydrogen exchange rates, covalent scalar coupling ($^1J_{NH}$) and many others have provided indirect evidence of H-bonds. However, presence of scalar couplings between magnetically active nuclei on both sides of the hydrogen bridge made it possible to directly observe such couplings in biomacromolecules and smaller chemical compounds.

1.2.2.1 Indirect NMR observations of the hydrogen bond

1.2.2.1.1 Chemical Shift

Chemical shift is the oldest and most fundamental parameter in NMR (Dyson and Wright, 2004). This NMR parameter is exquisitely sensitive to steric and electronic effects. Chemical shifts are particularly sensitive to changes in the secondary or tertiary structures of the protein. Various changes in chemical shift can provide important insights into a conformational change in protein structure. For example, the protein may undergo a conformational change when placed in a denaturing environment. Secondary structure chemical shifts can also depict if the residue is part of a α-helix or β-sheet. The amide proton (NH) chemical shifts of amide protons in β-sheets generally show an upfield chemical shift in comparison with the downfield chemical shift observed for amide protons located in α-helix secondary structure elements. One of the reasons why this difference in chemical shift exists for the two secondary structures can be attributed to the involvement of the NH groups in H-bonds (Oldfield, 2002, Pardi et al., 1983).

While chemical shifts of nuclei are directly related to the surrounding environment, nuclei involved in H-bond (Wagner et al., 1983) formation show chemical shift perturbations indicating the redistribution of the electron density upon the creation of an H-bond (Grant and Harris, 1996). The proton H-bonded between the electronegative acceptor and donor nuclei such as oxygen or nitrogen, always gives rise to an isotropic chemical shift to a higher frequency or downfield shift (Pardi et al., 1983). This downfield shift can be explained by a decrease in the electron density surrounding the hydrogen nucleus and deshielding effects from the electronic currents of the acceptor atom. A number of cases can be given for such proton downfield shifts on H-bond formation with oxygen or nitrogen acceptors e.g. in proteins the downfield chemical shifts have been acknowledged to be correlated to shorter H-bond lengths (Pardi et al., 1983, Oldfield, 2002, Wishart et al., 1991, Wang et al., 2007). Similar downfield shifts have been detected in nucleic base pairs with imino and amino protons. In some cases

the H-bonds hydrogen nucleus chemical shift may be as large as 15 to 20 ppm (Shoup et al., 1966, Fiala et al., 2004). The extreme downfield proton shift (i.e. > 15 ppm) has been used to measure the presence of "low barrier H-bonds, which are short H-bonds important in enzyme catalysis (Frey et al., 1994, Sharif et al., 2007). In contrast, H-bonding to aromatic ring electrons usually results in a change in the ^{1}H chemical shift to upfield shifts. This is the result of aromatic ring current shielding effects outweighing the electronic deshielding from the formation of the H-bond (Grant and Harris, 1996).

1.2.2.1.2 Reduced hydrogen exchange rates

One of the earliest methods used to study unfolded protein states is proton hydrogen exchange rates (Dyson and Wright, 2004). This technique observes the rate of exchange between the amide protons (NH) in the folded state and under different denaturing conditions (cosolutes, pH, and temperature) (Krishna et al., 2004, Dyson and Wright, 2004). The hydrogen exchange rates decrease considerably when the hydrogen atom is involved in an H-bond, even if the H-bond is located on the surface of the protein (Krishna et al., 2004). Magnetisation transfer techniques have been successfully applied to study exchange processes of protons between solvent water and exchangeable sites in proteins (Bai et al., 1993). The standard approach to detect such exchanges is to selectively excite water and observe magnetization transfer to other sites. However, this method is rather crude and is often complicated by artifacts due to other active magnetisation transfer pathways such as NOEs (nuclear overhauser effect) from CαHs or exchange-relayed NOEs from rapidly exchanging protons. Perhaps the most common method used to study slow-exchange processes (i.e. rates << 1 s^{-1}) are the hydrogen-deuterium exchange experiments. Faster exchange processes (i.e. > 2 s^{-1}) are measured using experiments such as water-NOE/ROE, water-exchange filter and CLEANEX (Hwang et al., 1998, Hwang and Shaka, 1998) experiments. All these methods have been developed to quantitatively measure exchanges rates over a large range and can be used to monitor H-bonding in backbone amide groups.

Hydrogen bond exchange rates are based on a two-step mechanism which involves the opening (step1) and closing (step2) of the H-bond. Step one is regarded as the equilibrium reaction between the closed and the open H-bond, whereas step two is the exchange between the open state and the solvent (Krishna et al., 2004, Hernandez and LeMaster, 2009).

$$\mathrm{NH(closed)} \underset{K_{cl}}{\overset{K_{op}}{\rightleftharpoons}} \mathrm{NH(open)} \xrightarrow{K_{cl}} \mathrm{NH(open)}$$

Equation [1.3]

From Equation 1.1, the K_{op} are the opening (unfolding) and K_{cl} is the closing (folding) rates of the protecting structure. Therefore, the hydrogen exchange rates K_{op} and K_{cl} represent the opening (unfolding) and closing (folding) of the H-bond respectively. However, the rate of hydrogen exchange depends on a number of factors such as pH, the pK of the donor group and of the base or acid, temperature, solvent accessibility, as well as the H-bond opening rate itself (Krishna et al., 2004). On the protein surface the exchange rates are in the millisecond to seconds time scale. H-bonded amide hydrogens located in secondary structure elements have been reported to have exchange times ranging between 10 to 10^6 min (Wagner and Wuthrich, 1982). Clearly, the very slow exchange rates of amide hydrogens observed in the interior of proteins may not only be due to H-bonding, but also may limited solvent accessibility (Wagner and Wuthrich, 1982, Daley et al., 2004). In contrast, nucleic acid hydrogens have a faster exchange rate, even if the molecule is structured, which reduces their benefit. However, hydrogens H-bonded in tRNA tertiary structure have a slower exchange rate (Nonin et al., 1997, Latham et al., 2009).

1.2.2.1.3 ^{2}H/^{1}H Isotope fractionation factor

In addition to the above methods to measure exchange rates, the ^{2}H/^{1}H fractionation factor Φ is a value which reflects the distribution of protons (H) versus deuterons (D) at exchangeable hydrogen positions of a solute, as compared with the corresponding relative concentration of labile hydrogens within a solvent of mixed proton and deuteron content, e.g., $^1H_2O/^2H_2O$

$$\Phi \equiv ([D - {}^2H]/ [D - {}^1H])_{solute} / ([{}^2H]/ [{}^1H])_{solvent}$$

Equation [1.4]

The equilibrium D/H isotope fractionation factor Φ, of a given NH in a protein corresponds to the population ratio of deuterated over protonated states, when equilibrated in a 50% D_2O / 50% H_2O solvent mixture which gives a value Φ = 1. The larger mass of *2*H results in a lower vibrational energy level than that of ^{1}H. Therefore during the exchange of the amide proton a value greater than one indicates a preference of D over H and a value less than one indicates a preference of H over D.

Studies have observed backbone NH Φ values in proteins ranging from 0.7 to 1.4. The Φ values recorded were based on the intensity measurements of ^{15}N-^{1}H correlations in

a range of H_2O/D_2O solvent mixtures. However complications arise when interpreting these results, due to the magnetization exchange between the solvent and the protein, which itself is also a function of the deuteration level. For example, solvent presaturation and/or the use of an interscan delays shorter than the (long) solvent T_1 attenuates resonances of protons in rapid exchange with solvent and, through the NOE, the intensities of other protons in their vicinity. The attenuation factor is roughly proportional to the H_2O/D_2O ratio and therefore decreases the apparent Φ value. The change in solvent viscosity is another factor that can affect the H_2O/D_2O ratio resulting in an increase in Φ value. Intramolecular dipole-dipole contributions between exchangeable protons result in a decrease in the measured Φ values.

Experimental results suggest a correlation between the fractionation factor Φ for H-bonded hydrogens and the strength of the H-bond, where a lower Φ value corresponds to a stronger H-bond. Although this is not an NMR parameter, NMR usually provides the most suitable method for its determination in small chemical molecules, and biomacromolecules. Bax and colleagues measured the NH fractionation factors in ubiquitin at 27 ºC. The values were observed to range between 1.01−1.21 (LiWang and Bax 1996). They found no clear correlation between H-bond length and fractionation; however, on average the α-helical residues (E24-E34) yielded slightly lower fractionation numbers (1.07 ± 0.03) than those involved in β-sheet H-bonds (1.14 ± 0.04). The data also do not support a statistically significant correlation between fractionation and the N─H●●●O angle, or a combination of this angle and hydrogen bond length. However, the data indicate a larger value when the N─H●●●O angle falls in the 180 ± 40° range. This finding coincides with a theoretical study which showed a sharp increase in the hydrogen bond potential energy surface for N─H●●●O angles outside this range (LiWang and Bax 1996).

The fractionation factors observed in staphylococcal nuclease showed a large range in Φ values, from as low as 0.3 to as high as 1.5 with an average value of 0.85 for ligated and un-ligated species. The fractionation values for amide groups located in the β-sheets w found to lie between two extremes, where the highest value was 1.42 and the lowest being 0.34. The three α-helices showed the lowest average fractionation factor of (0.79 ± 0.10) (Loh and Markley, 1994).

1.2.2.1.4 Primary and secondary isotope shifts from substitution of ^{1}H by ^{2}H and ^{3}H

The substitution of one isotope for another (e.g., ^{2}H for ^{1}H) is known to affect the isotropic chemical shift of the substituted nucleus (primary isotope shift) and of magnetic nuclei, such as ^{13}C and ^{15}N, one or more covalent bonds away from the substituted nucleus (secondary isotope shifts). The primary isotope effects are obtained by comparing the nuclear shielding of different isotopes. The secondary isotope effect occurs because of differences in the nuclear shielding of nuclei caused by two different isotopes. The changes in nuclear shielding may also occur if isotope substitution causes a change in chemical equilibrium (Chan et al., 1970, Schilf et al., 2004).

The primary isotope effect of the NMR chemical shifts of ^{1}H, ^{2}H, and ^{3}H nuclei is usually very small, in the case of ^{3}H usually < 0.03 ppm for tritium bound to sp^2 or sp^3 type carbons. The difference in chemical behaviour of the three isotopes of hydrogen is mainly caused by the difference in their masses, which in turn influences the vibrational motions and the zero-point vibrational energies. Thus, from a measurement of an isotope effect in some property one can make a deduction about the shape of potential energy surfaces. Studies have shown that valuable information about the H-bond is obtainable from the isotope effect (Cassidy et al., 2000, Schilf et al., 2004).

The variation of the ^{1}H chemical shift with nuclear distance in H-bonded systems is such that the proton is deshielded as the proton moves towards the midpoint between the heavy atoms (O, N, or C) of the H-bond. This can be used to correlate the chemical shift with the shape of the H-bond potential. In the case of strong and short H-bonds the chemical shift is at a higher ppm (parts per million) value . Weaker H-bonds have an upfield chemical shift with a lower $\Delta\delta$ (delta ppm) (Rozwadowski, 2007).

The primary isotope shift for the substitution of hydrogen by either deuterium or tritium is usually small in weak H-bonds, whereas significant effects are observed for strong H-bonds. Primary isotope shifts have been used to characterize a number of H-bond systems and provide information on the shape and symmetry of potential energy wells for the H-bonded hydrogen nucleus. Secondary isotope effects have also been used to characterize the presence and properties of the weak H-bonds in biomacromolecules.

1.2.2.1.5 Covalent scalar couplings ($^1J_{NH}$)

Scalar couplings arise from interactions between nuclei through their bonding electrons rather than through space. Scalar couplings are a short-range interaction that usually occurs for nuclei separated by one to three chemical bonds. The redistribution of electron densities upon H-bond formation also gives rise to observable changes in scalar couplings between nuclei associated with the H-bond. In turn the chemical bonds involved in H-bonding present a distinct chemical shift, which can be measured using specific NMR experiments to observe these changes. Changes of one-bond couplings between hydrogen bonded proton and donor nuclei have been observed in a number of small chemical compounds in various organic solvents, where changes in $^1J_{NH}$ and $^1J_{CH}$ couplings were measured upon H-bond formation (Cordier et al., 1999a, Tolman and Prestegard, 1996).

Studies have shown that an absolute increase in the $^1J_{NH}$ coupling was associated with a decrease in the donor-acceptor distance and thus with an increase in the ‘‘strength’’ of the H-bond (Manalo et al., 2005). In proteins, the $^1J_{CN}$ coupling is strengthened when the carbonyl oxygen atom (C═O) is H-bonded. On the other hand, when the amide NH is involved in an H-bond this leads to a weaker $^1J_{CN}$ coupling. This observation has been used to correlate the measured $^1J_{CN}$ coupling constants with the various types of secondary structure elements in a protein (Delaglio et al., 1991).

1.2.2.1.6 ^{2}H Quadrupolar coupling constant

Deuterium possesses an electric quadrupole moment and therefore is exquisitely sensitive to its local electronic environment. The H-bond is electrostatic in nature, an ideal probe of this interaction reports on its local electric environment. Therefore a short N–^{2}H●●●O═C hydrogen bond results in a more symmetrical electrical environment at the deuterium nucleus relative to a long H-bond. That is, shorter hydrogen bonds will result in weaker electric field gradients and, therefore, smaller ^{2}H quadrupolar coupling constant (QCC) values. NMR studies on small peptide analogues showed the tight correlation between QCC and hydrogen bond lengths determined from X-ray and neutron diffraction using amide deuteron (^{2}HN) QCC measurements made by single-crystal solid-state. These experiments have led groups to develop a method for measuring QCC values of the backbone amide deuterons (^{2}HN) of a protein in solution, thereby providing quantitative information on H-bonding. NMR studies of inorganic molecules and single (zwitterionic) amino acids deuterated at the amide site

have shown that the ^{2}H QCC follows a simple relationship of the form QCC + $A + B/r^3$ kHz, where r is the distance between the deuterium and the acceptor group (in Angstroms), and the coefficients A and B depend on the nature of the donor and acceptor (Liwang and Bax, 1997, Tafazzoli and Amini, 2008).

1.2.2.2 Direct NMR parameters for observing the presence of H-bonds

1.2.2.2.1 Hydrogen bond scalar couplings

The interaction between two nuclear spins involves a direct dipolar coupling and an indirect interaction by way of electrons (or scalar coupling). Dipolar couplings are an interaction transmitted between two magnetic nuclei through space (no chemical bond connecting the nuclei) and have a distance and angular (between B_0) dependency. Although dipolar couplings contain a great deal of structural information, and can be on the order of tens of kilohertz, the dipolar interaction averages to approximately zero in solutions and gases as a result of the isotropic reorientation of the molecules. Dipolar couplings are synonymous with the Nuclear Overhauser effect, or NOE. The NOE is the name given to the transfer of z magnetization from one spin to another spin by cross relaxation induced by the dipolar interaction of the two interacting spins. This interaction is a purely through-space event. On the other hand the scalar interaction or J-coupling, is transmitted through the electron cloud of the molecule, hence the interaction is between nuclei that have electrons between them, i.e. which are connected by a chemical bond. A measurable J-coupling can be detected up to a distance of three to four bonds. The strength of the scalar interaction is measured by the size of the resonance splitting in hertz (Hz). This splitting defines the scalar coupling constant, $^{n}J_{ij}$, in which, n designates the number of bonds separating the two nuclei i and j (Pervushin et al., 1998). The value of the J-coupling constant can be either positive or negative.

A way to visualise the transmission of nuclear polarisation through a chemical bond (or hydrogen bond) can be viewed as follows. Taking two coupled nuclei X and Y, suppose nucleus X has its spin orientation parallel to the applied magnetic field, B_0. The magnetic moment of nucleus X gives rise to a magnetic field which will orient a nearby electron. The polarisation of this electron is transmitted to a second nearby electron (bonding electron) via electron-electron interactions, i.e. Pauli Exclusion Principle and electric forces. Due to this interaction, the second electron will orient antiparallel to that of the first electron or parallel to nucleus X. If the second electron is

close to a second nucleus, then the magnetic field produced by this second electron polarises this magnetic nucleus. This second nucleus, Y, will tend to orient antiparallel to this electron (Figure 1.5). Consequently, information about spin orientation of spin X is transmitted to spin Y via the bonding electrons. The lowest energy state, and therefore most favourable, occurs when X and Y are antiparallel; however, this is not the only state to be observed. Since the magnetic interactions are very small, the state when both spins are parallel is also observed at a slightly higher energy and with almost equal probability. As such, when nucleus X undergoes resonance and flips its spin state with respect to B_0, the energy of its transition depends on the initial orientation of Y relative to X, and two signals are present in the spectrum. The difference in frequency between the two signals is proportional to the energy (given in Hz) of the scalar coupling interaction between X and Y (Dingley et al., 2001).

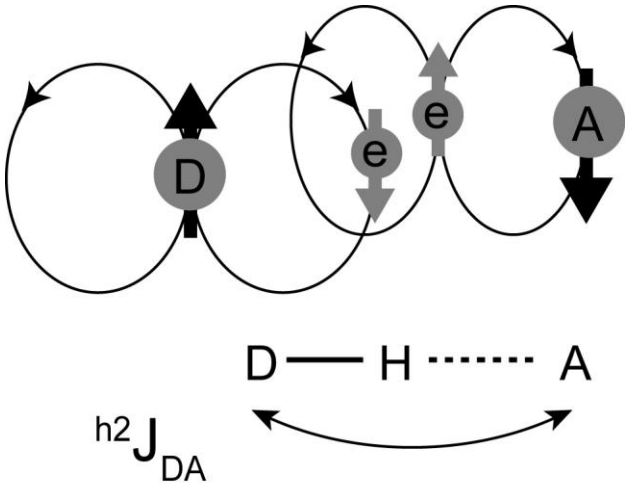

Figure 1.5: A representation of the scalar coupling mechanism across H-bonds. The two-bond coupling of type $^{h2}J_{DA}$ connects the nucleus to the donor atom D with the nucleus of the acceptor atom A. The electrons (e) transmit the magnetic polarization between the two nuclei. (Adapted from (Dingley et al., 2001)

H-bond scalar couplings (HBCs) can be used to identify donor and acceptor groups in individual H-bonds from COSY-type experiments (Dingley et al., 2000, Grzesiek et al., 2001). In favourable cases, complete H-bond networks in biomacromolecules can be established, thereby providing valuable data for structure determination. As the simplest explanation, HBCs are caused by the overlap of H-bond donor and acceptor electronic wave functions. Consequently, the magnitude of HBCs is proportional to the square of the electronic overlap integral (Grzesiek et al., 2004). Thus HBCs provide a

very sensitive measure of H-bond geometries, i.e. they depend exponentially on donor-acceptor distances) as (Cornilescu et al., 1999) well as on certain H-bond angles (Barfield, 2002).

Since the initial observation of HBCs for N–H···N H-bonds in Watson-Crick base pairs of nucleic acids (Dingley and Grzesiek 1998) and backbone N–H···O=C H-bonds in proteins (Cordier and Grzesiek 1998, Cornilescu et al., 1999), there have been numerous reports detailing the measurement of HBCs for other H-bond moieties in biomacromolecules (Wohnert et al., 1999, Dingley et al., 2000). Besides experimental observation of HBCs, there are a number of theoretical studies using quantum chemical calculations that have improved our understanding of the relationship between NMR H-bond parameters and geometric properties (Barfield et al., 2001) of biomacromolecular H-bonds (See section 2.5.1). Experimental and theoretical results have revealed that the same nucleus $\rightarrow$ electron $\rightarrow$ nucleus magnetization transfer mechanisms (see above) that underlie the detection of covalent bond scalar couplings also facilitate the observation of couplings via H-bonds. Consequently, the same experiments for the detection, quantification or magnetization transfer are applicable to H-bond scalar couplings. In the following sections, a detailed discussion is presented on studies examining HBCs in proteins. For completeness, a cursory presentation is given for HBCs observed in nucleic acids and theoretical studies examining HBC properties.

Table1.2: Observed trans-H-bond couplings in proteins.

Structure	Size (Hz)	Acceptor	Donor
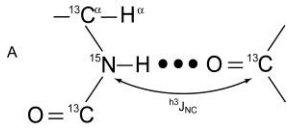	-0.2 to -0.9	Backbone amide	Backbone carbonyl or side-chain carboxylate
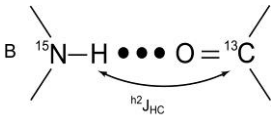	-0.6 to 1.3	Backbone amide	Backbone carbonyl
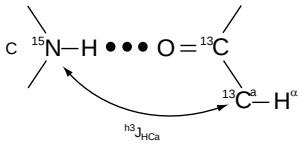	0 – 1.4	Backbone amide	Backbone carbonyl
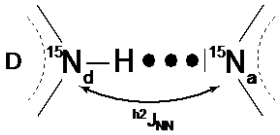	8 - 11	Histidine-Nε2	Histidine-Nε2
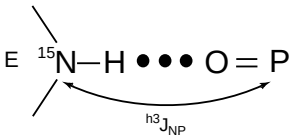	4.6[a]	Backbone amide	GDP-Phosphate
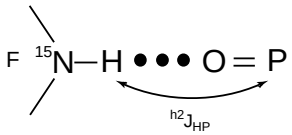	3.4[a]	Backbone amide	GDP-Phosphate
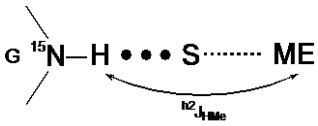	0.3 – 4[a]	Backbone amide	Cystine-S coordinating ^{113}Cd or ^{119}Hg

1.2.2.2.1.1 Proteins

The most common H-bond in proteins connects the backbone NH-group of one amino acid to a C═O group of another amino acid and is illustrated as N─H●●●O═C. Including this H-bond, the canonical patterns of H-bonds in proteins are H_i●●●O_k, O_i●●●H_k, H_{i-2}●●●O_{k+2}, O_{i-1}●●●H_{k+2} for anti-parallel β-sheets, H_i●●●O_k, O_i●●●H_{k+2}, H_{i+2}●●●O_{k+2}, O_{i-2}●●●H_{k+4} for parallel β-sheets, O_i●●●H_{i+4} for α-helices, and O_i●●●H_{i+3} for 3_{10}-helices, where the H_i and O_k stand for the backbone amide proton and oxygen atoms of the hydrogen bonded residues *i* and *k*, respectively (Grzesiek et al., 2001).

The carbonyl oxygen nucleus in proteins is not readily accessible for detection of scalar couplings across the H-bond. However, three-bond couplings across the H-bond can be detected between the ^{15}N donor nucleus and the acceptor ^{13}C nucleus of the C═O moiety. The detection of $^{h3}J_{NC}$ H-bond couplings is achieved by a modification of the conventional HNCO experiment used for protein structural studies. The conventional HNCO experiments follows an "out and "back" path according to $^{1}H^{Ni} \rightarrow {}^{15}N^{i} \rightarrow {}^{13}C^{'i-1} \rightarrow {}^{15}N^{i} \rightarrow {}^{1}H^{Ni}$ (see Section 2.5.2 for more detail on the HNCO experiment). However, in the long-range HNCO experiment used for detecting $^{h3}J_{NC}$ H-bond couplings the delays are modified such that the magnetisation transfers between the amide ^{15}N nucleus of residue *i* and the carbonyl ^{13}C nucleus of the hydrogen bonded residue *j* (Figure 1.3) (Cordier and Grzesiek 1999).

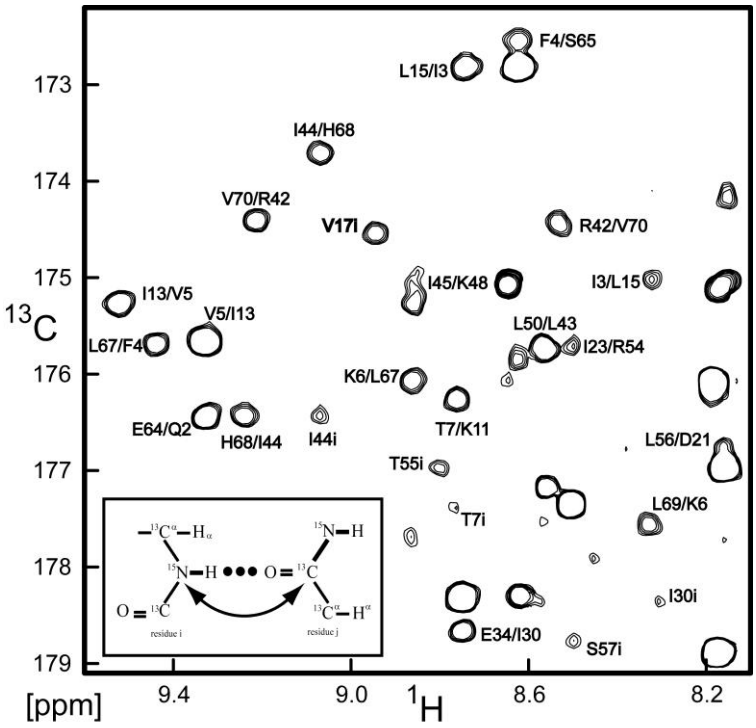

Figure 1.6: Selected region of the standard 2D long-range quantitative-$J_{NC'}$ H(N)CO spectrum recorded on a 2.5 mM sample of uniformly $^{13}C/^{15}N$-enriched ubiquitin. Resonances labelled as Res_i/Res_j are due to $^{h3}J_{NC'}$ scalar couplings between ^{15}N nucleus of residue *i* and $^{13}C'$ nucleus of residue *j*. Residues marked with an *i* denote not completely refocused one-bond correlations between the ^{15}N nucleus of residue *i* and $^{13}C'$ nucleus of residue *i*–1. Implemented from the original paper published on $^{h3}J_{NC'}$ scalar couplings of ubiquitin (Cordier and Grzesiek 1999).

The result of the modified 2D HNCO experiment is show in Figure 1.6, where the magnetisation is transferred by long-range J_{NC} scalar interactions between NH ^{15}N and C═O ^{13}C nuclei in ubiquitin. The spectrum shown in Figure 1.6 is a two-dimensional version of the HNCO and therefore only the ^{1}HN and the $^{13}C'$ chemical shifts are detected. The cross-peaks depict the H-bond $^{h3}J_{NC}$ correlations present in the secondary structure of ubiquitin (Cordier and Grzesiek 1999, Cornilescu et al., 1999). For example, two cross-peaks are visible between the backbone amide and carbonyl groups of residues leucine 67 and phenylalanine 4, respectively, which are part of an antiparallel β-sheet. A summary of these interactions is shown in Figure 1.7 by the dotted lines in the secondary structure schematic of ubiquitin.

Quantification of the $^{h3}J_{NC}$ coupling constants can be achieved by comparison of the cross-peak intensities from the long-range experiment, to the intensities of sequential $^{1}Hi - ^{15}Ni - ^{13}C'_{i-1}$ correlations measured in the reference experiment (see Section 2.4.2 for details on the method of quantifying the size of the couplings). Typical values

of $^{h3}J_{NC}$ coupling constants range from −0.1 to −0.9 Hz (Cordier and Grzesiek 1999, Cornilescu et al., 1999). Although the absolute size of these couplings is small, it is possible to trace out complete H-bond networks in smaller, non-deuterated proteins, i.e. 10 kDa in size, by using this long-range HNCO method (Cordier et al., 1999b).

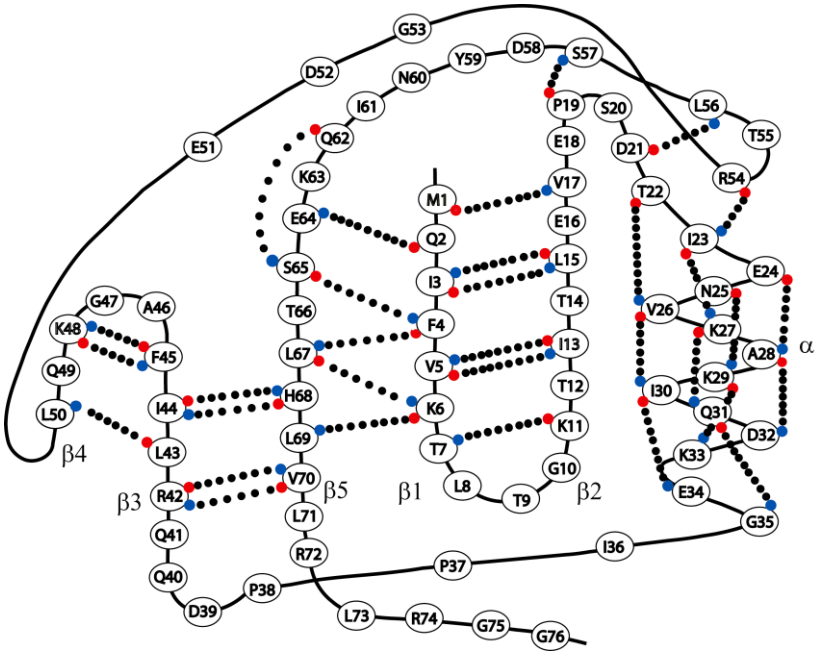

Figure 1.7: Secondary structure topology of ubiquitin, The Dotted lines mark the $^{h3}J_{NC}$ correlations which are observed in the long-range HN(C)O experiment.

The sensitivity of the long-range experiment is only sufficient to detect the small size $^{h3}J_{NC}$ couplings of backbone H-bonds in small and medium sized proteins. For larger proteins, the sensitivity of the long-range HNCO rapidly decreases due to ^{15}N transverse relaxation losses during the extended magnetization transfer periods (Section 2.4.1). Deuteration and TROSY-techniques (Pervushin et al., 1997) at higher fields are used to measure HBCs in larger proteins. Usually a 3D version of the pulse sequence is used, in which the third chemical shift axis (or z-axis) is the ^{15}N donor frequency. When such long-range 3D HNCO H-bond correlations are detectable, the assignment is usually unique due to the excellent dispersion of resonances that results from the strong variation of both $^{13}C'$ and ^{15}N chemical shifts as a function of H-bond geometry. Such a 3D HNCO-TROSY experiment was successful in observing $^{h3}J_{NC}$ couplings in the perdeuterated 30 kDa ribosome inactivating protein MAP30 (Wang et al., 1999).

Since the initial observations of HBCs in protein N─H●●●O═C H-bonds there have been a number of studies that have utilised this parameter to study H-bond character under various conditions and for structural analysis. The $^{h3}J_{NC}$ scalar couplings where used to determine the complete structure of the 64-residue α/β protein chymotrypsin inhibitor 2 (Bonvin et al., 2001) with the aid of secondary chemical shifts. The structures generated were close to 1 Å RMSD from the crystal structure. H-bond scalar couplings are dependent on H-bond geometries; therefore it is a sensitive parameter that can be used to characterise subtle changes occurring to the protein structure under various conditions (e.g. heat, temperature and pressure). A number of investigations have used the size of the $^{h3}J_{NC}$ couplings in proteins to monitor such changes in detail. Pressure variations up to 2000 bar were investigated by Gronenborn, Akasaka and coworkers for protein G (Li et al., 2000). As monitored by $^{h3}J_{NC}$ the H-bond strength was found to increase in peripheral regions and to decrease in the protein centre. Unfortunately sensitivity was severely limited in this investigation by the small (20 ml) volume of the pressure cell.

Markley and coworkers observed that mutants of the sweet protein brazzein (Assadi-Porter et al., 2003) exhibit distinct changes in $^{h3}J_{NC}$ detected H-bond patterns, which correlate with a variation in sweetness. All 'sweet' variants show the same $^{h3}J_{NC}$ correlations, whereas the 'non-sweet' variants lacked an H-bond in the centre of the α-helix and a second one in the centre of the β-sheet. The S-peptide of Ribonuclease A, was used to provide a model system for the study H-bond formation as the peptide formed a helix (Nelson and Kallenbach, 1989). Peptide-S is largely unfolded in aqueous solution, whereas the addition of trifluoroethanol (TFE) (Jaravine et al., 2001) induces a α-helical structure that is very similar to the structure of the equivalent N-terminal part of the full Ribonuclease A. In order to monitor the transition of the H-bonds from the unfolded to the folded state, $^{h3}J_{NC}$ correlations were followed in long-range HNCO experiments over a range of TFE concentrations from 0 to 90%. A quantitative analysis of the individual $^{h3}J_{NC'}$ coupling values yields a detailed picture of the folding transition.

Grzesiek and Cordier characterized the H-bond network of the A-state of ubiquitin (Cordier and Grzesiek, 2004) (ubiquitin in 60%/40% methanol/water) by $^{h3}J_{NC}$ couplings in an effort to understand the forces contributing to the stability of the protein. The measured couplings were quantitatively compared to the $^{h3}J_{NC}$ couplings

in the native state. The A-state of ubiquitin has been extensively characterised by a variety of biophysical methods NMR (Harding et al., 1991), CD, calirometry (Makhatadze et al., 1991) and MD. The structure of ubiquitin A-state does not have a hydrophobic core and is less globular than the native state. The N-terminal part of the A-state is similar to the native state with the first β-hairpin β1/β2 (residues M1 to V17) and the central α-helix α (residues I23 to G35). The C-terminal part beyond residue G35 undergoes a dramatic change from a β-structure in the native state to a helical structure for residues Q40 to R74 (helix α'). Furthermore Grzesiek et al. also characterised the changes in the $^{h3}J_{NC}$ couplings for the chicken c-Src Scr homology domain 3 (SH3) upon binding the class I proline-rich ligand RLP2 (RALPPLPRY). The small β-sandwich SH3 fold has been used extensively for studying protein stability and folding and for probing the structural response for a protein to ligand binding. The $^{h3}J_{NC}$ couplings measured showed reproducible changes of 0.3 Hz which can be translated into changes in H-bond length of up to 0.12 Å. This allowed the evaluation of the subtle changes in the protein structure upon the binding of the ligand to the SH3 domain (Cordier et al., 2000).

In a more recent study, the solvent effect on $^{h3}J_{NC}$ couplings in apoCaM (Juranic et al., 2007) (calcium free calmodulin) and haloCaM (calcium-loaded) were measured and compared to other NMR parameters and the X-ray crystal structure. The largest difference in the conformation of the apo and holoCaM is the backbone conformation of the linker connecting the two globular domains. The dynamic differences in crystal and NMR structures are seen in the backbone H-bonds in apoCaM, where a few are shown to be intramolecular in solution stucture and intermolecular in the crystal structure. Therefore it was hypothesised that in solution calmodulin H-bonds show a different dynamic behaviour influenced by the solvent which is not observed in the H-bonds measured in the crystal structure. This hypothesis was supported by only observing the $^{h3}J_{NC}$ couplings that had a threshold of > 0.2 Hz showing a correlation to H-bonds in the crystal protein and was supported by the protein dynamics in solution. In contrast, $^{h3}J_{NC}$ couplings with a threshold of < 0.2 Hz occupied the more flexible regions of the protein secondary structure and were not detected. The function of calmodulin requires large conformational changes which are occupied by the weaker H-bonds. This study illustrates how H-bond couplings are influenced by dynamic

processes and shows that the measured H-bond coupling is an ensemble average of all possible conformational states for a particular H-bond.

1.2.2.2.1.2 Theoretical studies

Computational studies using density functional theory (DFT) and *ab initio* molecular orbital methods have reproduced the trends, but not necessarily the magnitude, of the measured HBCs and donor and acceptor chemical shifts in nucleic acids (Barfield et al., 2001) and proteins (van Mourik and Dingley, 2005, Tuttle et al., 2004). Spin-spin couplings are recognized to be one of the most difficult molecular observables to calculate. Most studies have relied solely on calculating the dominant contribution of the Fermi Contact (FC) term to the overall coupling constant, and have neglected the diamagnetic spin-orbit, the paramagnetic spin-orbit, and the spin-dipole terms. Only a few recent studies, examining the H-bonds in the protein ubiquitin (Tuttle et al., 2004) and model peptides (Wieczorek and Dannenberg, 2003) have considered the influence of all four Ramsey (Ramsey 1953) terms to the size of the HBCs. Studies have shown a very good agreement between experimentally determined HBC constants and theoretical simulations were found for hydrogen bonds in nucleic acid base pairs and in the backbone of proteins. In these and other systems, such calculations have become a very powerful analytical tool that complements the experimental measurement of scalar couplings.

Studies using DFT and ab initio molecular orbital methods have shown correlations between $^{h3}J_{NC}$ scalar couplings and H-bond geometry by examining various H-bonds in biomolecular and chemical systems (e.g. N─H●●●O═C, N─H●●●N, N─H●●●C, and C─H●●●N) (Barfield, 2002, van Mourik and Dingley, 2005). In addition, H-bond cooperativity has been examined via theoretical calculations in which H-bond geometries are identical between the H-bonding moieties but there is a difference in the size of the HBC's throughout the H-bonding chain (Wieczorek and Dannenberg, 2005a, Wieczorek and Dannenberg, 2005b). Juranic´ and co-workers has shown that HBCs are sensitive to the extended environment of an H-bonded system and have provided correlations between intramolecular and intermolecular spin-spin couplings in a protein backbone context (Juranic et al., 2002).

1.3 Ubiquitin

1.3.1 NMR studies of ubiquitin

The model protein used in this research thesis is ubiquitin. Human ubiquitin is a small monomeric protein of ~8.6 kDa. Vijay-Kumar et al. solved the high resolution (1.8 Å) crystal structure in 1987(Vijay-Kumar et al., 1987) (Figure 1.8). Due to its high solubility and stability, extensive NMR studies have been carried out on ubiquitin. There are NMR resonance assignments in its native, (Di Stefano and Wand, 1987, Weber et al., 1987) denatured and A-state (Harding et al., 1991) (partially folded). Additionally, the two-step folding (unfolding) transition of ubiquitin has been well characterised (Wintrode et al., 1994). As a result, ubiquitin is an ideal protein to investigate the formation and subtle changes of individual H-bonds under different solvent conditions during the initial stages of denaturation using NMR spectroscopy.

Ubiquitin has been instrumental in developing many NMR experiments such as NH backbone dynamics, various two-, three- and four-dimensional experiments, backbone NH exchange experiments, residual dipolar couplings and H-bond scalar couplings in proteins (Denisov and Halle, 1995a, Denisov and Halle, 1995b, Bax and Tjandra, 1997, Grzesiek and Bax, 1997). The high stability of ubiquitin in conjunction with the high peak dispersion observed in the 2D ^{1}H-^{15}N HSQC (Figure 1.8) has led to ubiquitin acting as the model protein for the development of NMR experiments. The peak dispersion and high stability of ubiquitin makes this protein the ideal choice for studying small coupling $|< 1.0|$ Hz.

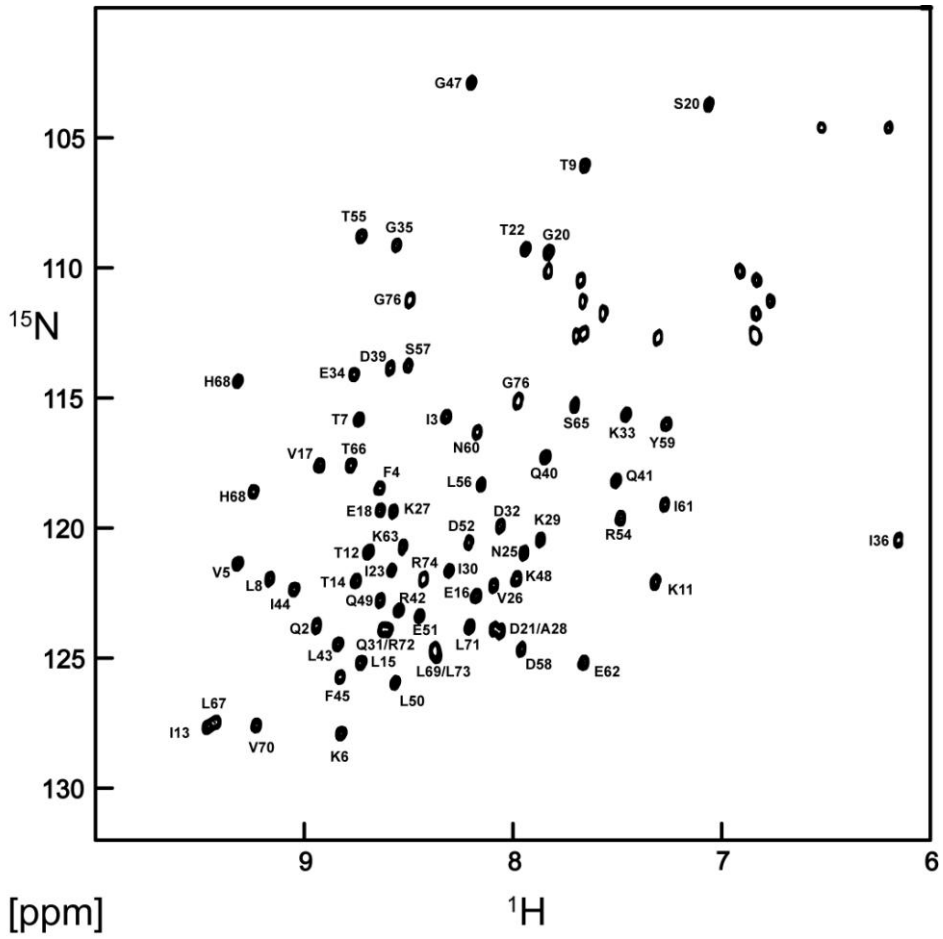

Figure 1.8: A 2D ^{1}H-^{15}N HSQC spectra of ubiquitin recorded at 25 ºC and pH 6.5. The ubiquitin HSQC spectra was recorded at UCL NMR facilities, and similar to spectra published in Protein NMR Spectroscopy: principles and practice (Cavanagh, 2007).

1.3.2 Function

Cell-cycle regulatory proteins are important for programmed degradation and cell-cycle progression. Ubiquitin-mediated degradation further controls cell growth and proliferation, by degrading tumour suppressors, protoncogens, and components of the signal transduction pathways. The ubiquitin system is involved in endocytosis and down-regulation of receptors and transporters, as well as in the degradation of resident or abnormal proteins in the endoplasmic reticulum. Dysfunction in several ubiquitin-mediated processes causes pathological conditions, including malignant transformation (Herrmann et al., 2007, Hershko and Ciechanover, 1992).

Ubiquitin targets proteins for degradation by covalently binding to proteins and this process forms the initial part of the ubiquitin-mediated protein degradation pathway. The ubiquitin degradation pathway requires three enzymes for ubiquitin to ligate with other proteins (Figure 1.9). ATP activates the C-terminal Gly residue of ubiquitin by a

specific activating enzyme, E1 (Step 1). In this step, ubiquitin binds to ATP forming an ubiquitin adenylate moiety with the release of PPi, followed by the formation of a thioester linkage between ubiquitin and the Cys residue of E1, with AMP being released. Activated ubiquitin is next transferred to an active site Cys residue of an ubiquitin-carrier protein, E2 (Step 2). In the third step, catalyzed by a ubiquitin protein ligase or E3 enzyme, ubiquitin is linked by its C-terminus in an amide isopeptide linkage to an amino group of the substrate protein's lysine residues (Figure 1*A*, Step 3) (Hershko and Ciechanover, 1998, Hershko and Ciechanover, 1992, Herrmann et al., 2007).

The proteasome 26 complex degrades the polyubiquitin chains and requires ATP hydrolysis. The 26S proteasome is formed by an ATP-dependent assembly of a 20S proteasome, a complex that contains the protease catalytic sites, with 19S "cap" or regulatory complexes. ATPase and other subunits found in the 19S complex are involved in the specific action of the 26S proteasome on ubiquitinylated proteins. The roles of ATP in the assembly of the 26S proteasome complex and in its proteolytic action are not fully understood. The actions of the 26S proteasome on ubiquitinylated proteins are presumed to generate certain products: free peptides, short peptides still linked to ubiquitin via their lysine residues, and polyubiquitin chains (Figure 1*A*, Step 4). The latter two products are converted to free and reusable ubiquitin by the action of ubiquitin-C-terminal hydrolases or isopeptidases (Steps 5 and 6). Some isopeptidases stop the proteolysis by the 26S proteosome by separating certain ubiquitin-protein conjugates (Step 7). Short peptides formed by the above processes are further degraded to free amino acids by peptidases present in the cytosol (Figure 1*A*, Step 8) (Herrmann et al., 2007, Hershko and Ciechanover, 1992, Hershko and Ciechanover, 1998).

There is one single E1 enzyme, whilst there are many species of E2 enzymes, and multiple families of E3 enzymes known as E3 multi-protein complexes. The selectivity of ubiquitin-protein ligation is due to E3 specificity resulting in protein degradation. The specific protein substrate contains a unique recognition signal which the E3 enzyme recognises, although in some cases E3 recognises the protein non-specifically through an adaptor protein. Different types of E3s may carry out the transfer of ubiquitin to the substrate protein by two different mechanisms (Hershko and Ciechanover, 1998).

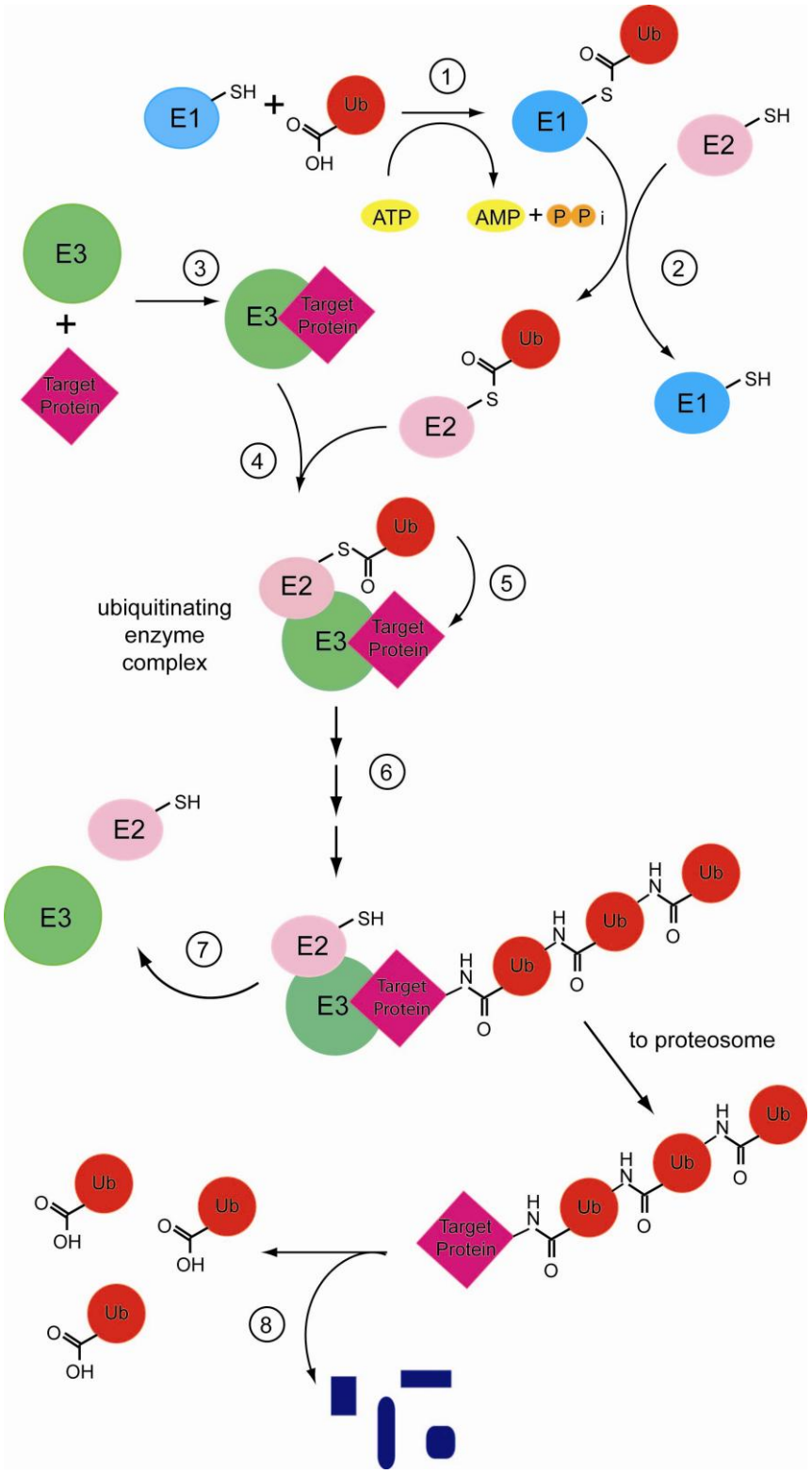

Figure 1.9: Enzymatic reactions of the ubiquitin system Ub:Ubiquitin. Adapted from (Hershko and Ciechanover, 1998)

1.3.3 Structure

Early NMR and chemical studies showed ubiquitin as a compact stable globular protein.(Weber et al., 1987, Briggs and Roder, 1992) The structure of ubiquitin

showed a pronounced hydrophobic core, with 16 of the 21 hydrophobic residues (valine, leucine, isoleucine, and methionine), buried within the interior of the molecule (Figure 1.11). The high thermal and chemical stability of ubiquitin may be attributed to this hydrophobic core. Prior to solving the structure of ubiquitin by X-ray crystallography, CD spectropolarimetry results predicted that the structure of ubiquitin consisted of 28% α-helix and 12% β-sheet., whereas a second research group predicted 6% α-helix and 10% β-sheet (Cary et al., 1980, Jenson et al., 1980). Definitive secondary structure composition came when the crystal structure was solved in 1987 (Vijay-Kumar et al., 1987). This structure showed a single α-helix which constituted 16% of the residues and 5 β-strands corresponding to 37% of the chain. In addition, there are seven reverse turns representing 37% of the chain. From the crystal structure it was also concluded that 90% of the polypeptide chain is involved in secondary structure H-bonding (Figure 1.13). The NMR structure solved by Bax and co-workers in crystalline medium (Figure 1.10) shows near identical structural similarity with the x-ray crystal structure with a calculated RMSD of 0.35 Å.

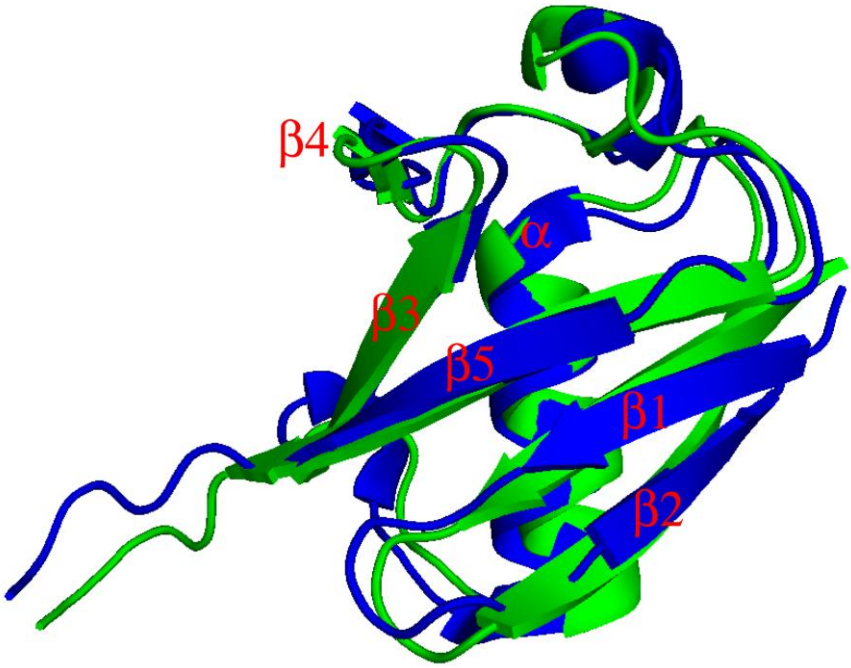

Figure 1.10: Overlay representation of human ubiquitin (76 residues) solved by X-ray crystallography 1UBQ (green) and NMR 1DZ3 (blue). Figure prepared using PyMOL (DeLano, 2002).

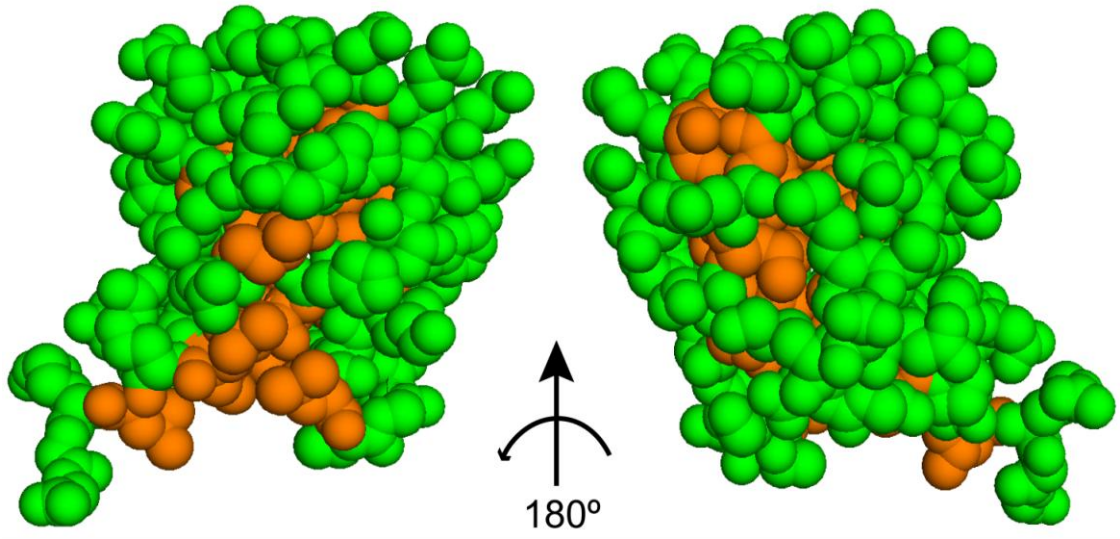

Figure 1.11: Sphere representations of human ubiquitin, the orange spheres depict the hydrophobic residues valine, leucine, isoleucine, and methionine.

NMR studies (Cary et al., 1980) were conducted on ubiquitin before the crystal structure was presented (Vijay-Kumar et al., 1985). NMR studies indicated that residues His68 and Tyr59 were located in hydrophobic environments. The study of the crystal structure of ubiquitin indicated otherwise and found these residues to be present on the surface of the protein. Tyr59 is involved in a reserve turn consisting of residues 57–60, and the tyrosine ring contributes to the stability of a loop involving residues 51–59 by forming an H-bond between the N of Glu51 and the OH of the Tyr59 side chain (Weber et al., 1987).

The α-helix of ubiquitin involves residues 23 to 35 (Figure 1.12) and there is a short 3_{10}-helix involving residues 56–59. Two of the β-strands, composed of residues 1 to 7 and 64 to 72, are parallel, whereas the other three strands, which are composed of residues 10 to 17, 40 to 45 and 48 to 50, run in an anti-parallel arrangement (Figure 1.11). The β-sheet has the characteristic left-handed twist, and the α-helix fits into the cavity formed by the sheet. NMR NOESY data showed that the overall solution structure is very similar to that of the crystal structure (Weber et al., 1987). Detailed secondary structure information was indentified through sequential and cross-strand NOEs (Wuthrich et al., 1984). Two small discrepancies in the interpretation of the crystal structure were found. The first is the short β-strand involving residues 48–50 forms part of a five-stranded β-sheet. The second is the turn region between residues 56–61, in the crystal structure this is described as a "reverse turn", but NMR data shows it is a short 3_{10}-helix (Figure1.12). Furthermore, the structure refinement study

of ubiquitin in crystalline medium by Bax and co-workers showed that ubiquitin has a high quality backbone geometry not observed in X-ray or liquid NMR structure (Bax and Tjandra, 1997).

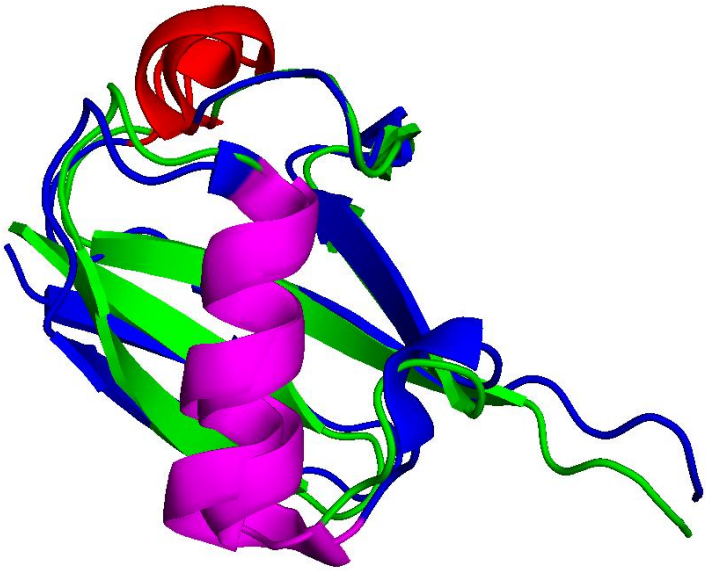

Figure 1.12: Overlay representation of human ubiquitin, X-ray crystallography 1UBQ (green) and NMR 1DZ3 (blue). The α-helix is depicted in magenta and residues 56-61 are shown in red.

Ubiquitin is an interesting protein not only because of its physiological role but due to its high stability. Although ubiquitin has seven lysine residues and four arginine residues ubiquitin is extremely resistant to tryptic digestion (Vijay-Kumar et al., 1985). Ubiquitin is very stable through a wide range of pH values and at very high temperatures with a Tm above 100 ºC (Herberhold and Winter, 2002). The structure of ubiquitin is very tightly packed and H-bonded (Figure 1.10), with the only portion of ubiquitin without intramolecular H-bonding located in the C-terminal region (residues 71–76). The stability of ubiquitin is also enhanced by the hydrophobic core formed by the residues present in the α-helix and β-sheet. The α-helix contributes three hydrophobic residues, and 11 of the 13 hydrophobic residues in the β-sheet participate in the formation of the hydrophobic core. Only Ile44 and Va170 are partially exposed to the surface. Other residues that contribute to this core include Ile36, Leu56 and Ile61.

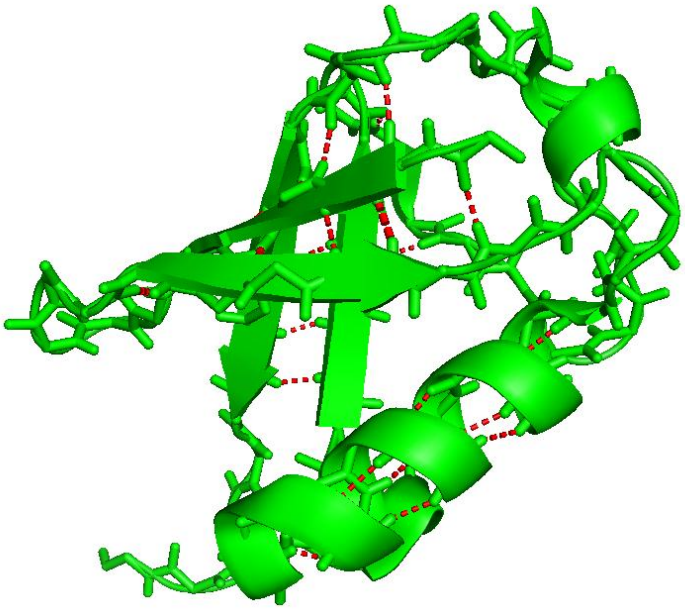

Figure 1.13: X-ray crystal structure of human ubiquitin (1UBQ), with the red dashes depicting the backbone H-bond of the secondary structure elements.

1.4 The influence of cosolutes on protein structure and stability

Cosolutes can be divided in two classes: 'kosmotrope' (order-favouring) and 'chaotrope' (disorder-favouring) (Moelbert et al., 2004). In general, kosmotropes are considered to stabilise proteins, whereas chaotropic solutes destabilise proteins. This terminology may not always hold, because such properties may vary and be dependent on the environment the kosmotrope/chaotrope is present in. For example a solute may not always act in the same way at different concentrations or in the presence of macromolecules or at different temperatures (Wiggins, 2001, Zhang and Cremer, 2006).

1.4.1 Denaturing cosolutes

The effect of cosolutes on protein stability has been used as a tool to understand protein folding and stability. Urea and guanidinum-HCl (Gdn.HCl) have been used widely to characterise the stability of proteins. This research has enabled scientists to extract different thermodynamic parameters (Gibbs energy, enthalpy, entropy, heat capacity and partial volume) and to derive the equilibrium of folded-unfolded protein states. The use of denaturants has also provided information on which parts of the protein are particularly influenced by solutes and this information aids our understanding of how proteins fold into their active states (Fersht, 1999). This research thesis examines the influence of the two denaturants guanidine chloride (Gdn.HCl) and urea on individual H-bonds in the protein ubiquitin. In particular, the research of the

thesis focuses on the initial stages of the destabilisation of the H-bond network in ubiquitin. The mechanisms of action of both Gdn.HCl and urea will be explained in detail in chapter 4.

1.4.2 Osmolytes

Numerous organisms have modified their cellular systems against environmental stress such as high temperature, salt and pressure. The organisms produce organic molecules called osmolytes, which are chemically diverse. Osmolytes can be divided into two classes, compatible osmolytes such as polyols and amino acids and counteracting osmolytes such as methylamines(Yancey et al., 1982, Baskakov and Bolen, 1998). Compatible osmolytes protect the protein against denaturation but do not affect the structure or function of the protein whilst counteracting osmolytes (trimethylamine-*N*-oxide (TMAO), betaine and glycerophosphocholine) protect the protein against the denaturant but also in addition influence the structure and function (Qu and Bolen, 2003, Yancey and Somero, 1979). This thesis focuses on the activity of the counteracting osmolyte trimethylamine N-oxide (TMAO) on the character of individual H-bonds in ubiquitin.

1.5 Project Aims

In this thesis, the $^{h3}J_{NC}$ couplings of ubiquitin have been measured during the early stages of chemical and thermal denaturation. Chapter 2 presents the methods used throughout the results sections presented in Chapters 3 and 4. In Chapter 3, HBCs have been observed over a temperature range in the absence and presence of TMAO. This study aims to characterise the influence of TMAO on countering the thermal expansion of individual H-bonds in the protein. The HBC data is correlated with other NMR parameters such as ^{1}H isotropic chemical shift, $^{1}J_{NH}$ and ^{15}N relaxation measurements. In Chapter 4 similar NMR parameters are used to observe and compare the effects of the chemical denaturants urea and Gdn.HCl on individual H-bond stability. Chapter 5 presents a summary and overview of the results and compares the influences of the compounds on ubiquitin stability.

Chapter 2

Materials and Methods

2.1 Materials

2.1.1 Preparation of media for protein over-expression

For the preparation of one liter of Luria-Bertani (LB) medium, 10 g of bacterial peptone (Sigma Aldrich, UK), 5 g yeast extract (Sigma Aldrich, UK) and 5 g NaCl (Sigma Aldrich, UK). To prepare LB agar plates, 15 g/l of agar is added to the prepared LB medium. After preparation, the LB media or LB agar is autoclaved, and upon cooling 100 μg/ml ampicillin is added as a selection marker.

For the preparation of one litre of ^{15}N- or $^{15}N/^{13}C$-labelled minimal growth medium the basic salts, 3 g of KH_2PO_4, 5 g of Na_2HPO_4, 0.5 g of NaCl and [^{15}N]-labelled $(NH_4)_2SO_4$ (Cambridge Isotope Lab. USA) were prepared and autoclaved. The trace elements MgCl (1 M), $CaCl_2$ (1 M) and $FeSO_4$ (0.01 M), as well as the vitamins (Pantothenic acid, Folic acid, Nicotinate, Pyridoxine HCl, Riboflavin, Thiamine and Myo-inositol) were filter sterilised. The uniformly ^{13}C-labelled D-glucose (Cambridge Isotope Lab. USA) was added to the trace elements and vitamins. The mixture was filter sterilised and added to the basic salt solution.

2.1.2 Preparation of SDS-polyacrylamide gel electrophoresis (PAGE) gels

SDS-PAGE of proteins was performed using the vertical gel apparatus from (Invitrogen XCell SureLock™ Mini-Cell, UK). Seventeen percent (w/v) Tris-glycine gels of 1.0 mm thickness were prepared according to the manufacturer's

instructions. Loading buffer containing contains 0.5M Tris-HCl (pH 6.8), 4.4% (w/v) SDS, 20% (v/v) glycerol, 2% (v/v) 2-mercaptoethanol, and bromophenol blue in distilled/deionized water (Invitrogen, UK) was added to samples. Samples were heated at 70 ºC for 10 min, quenched on ice, and loaded into the wells of the gel. Electrophoresis was at 200 mA for 35 min (until bromophenol blue dye reached the bottom of the gel). To visualise proteins, the gels were stained with Coomassie stain (Merril, 1990) for 45 min to 1 hr, and destained using a standard destaining solution (250 ml acetic acid, 400 ml methanol, 350 ml water). Standard molecular weight markers (Mark12 Unstained Standard, Invitrogen, UK) were used for the estimation of the molecular weight of protein bands appearing on the gel.

To prepare one SDS-PAGE gel, the stacking gel contained 0.375 M Tris-HCl, pH 6.8), 10 % SDS, H2O and 10% APS. The separating gel contained 1 M Tris-HCl, pH 8.8, 50 % sucrose, H_2O 10 % SDS 10 % APS and 40 % acrylamide

2.2. Protein expression of ubiquitin

2.2.1 Unlabelled protein expression

Transformation of competent cells proceeded as follows: two microliters of purified plasmid was added to 50 µl aliquots of thawed BL21(C+) (Invitrogen, UK) cells and left on ice for 30 minutes. The cells were heat shocked for 90 seconds at 42 °C. The cells were then chilled on ice for 2 minutes before the addition 250 µl of LB medium. The cells were allowed to grow for 30 minutes to one hour at 37 °C. 50 to 100 µl of cell mixture was plated onto an ampicillin selective 25 ml LB-agar plate and incubated overnight at 37 °C.

A single colony selected from a plate of freshly transformed BL21(C+) cells with the pET21b plasmid carrying the cDNA insert of human ubiquitin was used to inoculate 10 ml of LB medium containing 100 µg/mL ampicillin as the selection marker. The cells were incubated at 37 ºC and shaken at 250 rpm for six hours. The culture was subsequently used to inoculate a 200 ml LB culture and was incubated at 37 ºC and shaken at 180 rpm overnight. The cells from the 200 ml overnight culture were used to inoculate 500 ml of LB medium at a 1 % ratio (i.e. 5 ml of overnight culture was used to inoculate the 500 ml culture). The culture was incubated at 37 ºC and shaken at 220 rpm until the culture reached an optical density (OD_{600}) between 0.6–0.8. Absorbance measurements were obtained with a

Hitachi U-1800 single-wavelength UV/Visible spectrophotometer. At this point, protein over-expression was initiated by the addition of 0.1 mM of isopropyl-β-D-thiogalactopyranoside (IPTG; Melford Laboratories, UK). Culturing was continued for a further four hours. Cells were harvested (5000 rpm for 10 minutes), and resuspended in 40 ml of 50 mM Tris buffer, pH 8.0 (Trizma® base, Sigma Aldrich, UK) and frozen at –20 °C until further use.

2.2.2 Isotope enriched protein expression

A single colony selected from a plate of freshly transformed BL21(C+) cells with the pET21b plasmid carrying the cDNA insert of ubiquitin was used to inoculate 10 ml LB medium containing 100 μg/mL ampicillin as the selection marker. The cells were incubated at 37 ºC and shaken at 250 rpm for six hours. The small culture was subsequently used to inoculate 200 ml of modified minimal medium containing ampicillin (100 μg/ml) and incubated at 37 ºC and shaken at 180 rpm overnight. The cells from the 200 ml overnight culture were spun down at 3500 rpm for 15 minutes, and resuspended in 20 ml $^{15}N/^{13}C$-isotope-labelled minimal media. Five millilitres of this solution was used to inoculate 1 L of $^{13}C/^{15}N$ enriched modified minimal media. The culture was incubated at 37 ºC and shaken at 220 rpm until an OD_{600} = 0.6–0.8 was reached. Protein expression was induced by the addition of 0.1 mM IPTG and culturing continued for a further four hours at 37 ºC and 220 rpm. Cells were harvested (3000 *g* for 10 minutes), and resuspended in 40 ml of 50 mM Tris buffer, pH 8.0 and frozen at –20 °C until further use.

2.3 Protein Purification

2.3.1 Cell lysis

Purification of labelled and unlabelled material was performed using the same purification protocol. The cell pellets were passed three times over a French press (American Instrument Company, USA). The cell debris was pelleted by centrifugation (12,000 rpm for 60 minutes at 4 ºC) and supernatant decanted into sterile 50 ml screw-cap tubes. The pellet was discarded.

2.3.2 Anion-exchange chromatography

An anion-exchange column (Q-sepharose Amersham Biosciences UK, bed volume = 60 ml) was equilibrated with 50 mM Tris buffer pH 8.0. The column was connected to a semi-automated Pharmacia FPLC with a spectrophotometric

cell measuring the absorbance at 280 nm (Amersham Biosciences, UK). The supernatant was loaded on to the pre-equilibrated column at a flow rate of 2 ml/minute. Ubiquitin was collected in the initial flow-through as this protein does not interact with the column matrix. The remaining protein material was eluted using a NaCl gradient (0–1 M). The flow-through containing ubiquitin was collected and concentrated using 3 kDa centrifugal ultrafiltration vivaspin concentrators (Vivascience Limited, Gloucestershire, UK) to a final volume of ~20 ml.

2.3.3 Size exclusion chromatography

The size-exclusion column (SEC) (Superdex 75 Amersham Biosciences UK), bed volume = 120 ml was equilibrated with 20 mM potassium phosphate pH 7.0, 10 mM NaCl and 1 mM EDTA buffer. The column was loaded with 5 ml of the concentrated supernatant at a flow rate of 1 ml/min (Figure 2.1). SEC was attached to the same FPLC system used for the anion-exchange purification step. The purification of ubiquitin was monitored at three different wavelengths 215 (peptide bonds), 254 (phenylalanine) and 280 nm (tryptophan). Fractions containing ubiquitin were confirmed by SDS-PAGE (Figure 2.2). Protein concentration was determined by measuring the absorbance of collected fractions at 280 nm and a molar extinction coefficient of 1490 M^{-1} cm^{-1}. The SDS-PAGE result confirmed that protein impurities were minimal (i.e. purity ≥ 90%).

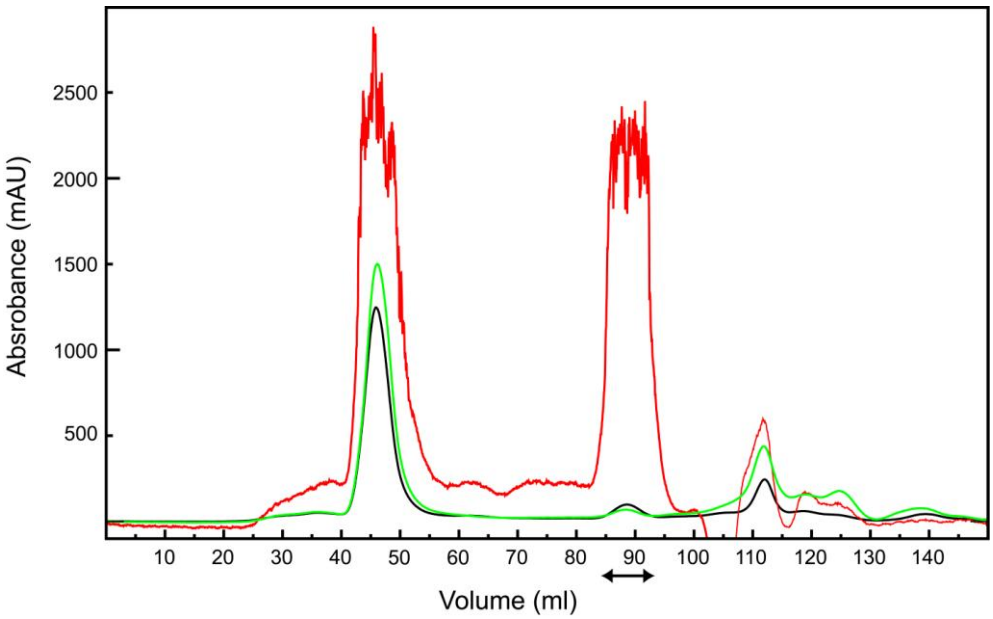

Figure 2.1: The size exclusion chromatogram of ubiquitin purification. The purification was monitored at three wavelengths 215 nm (red), 254 nm (green) and 280 nm (black). The peak with double headed arrow beneath it depicts where ubiquitin was eluted.

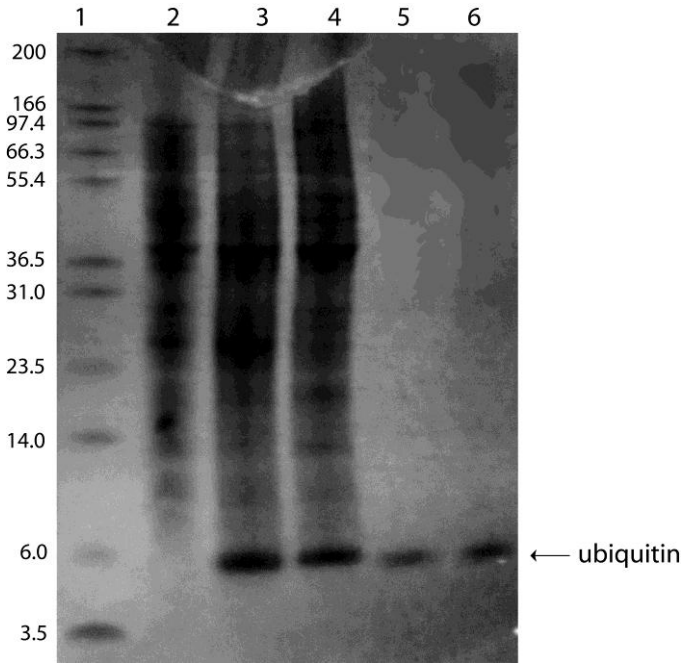

Figure 2.2: SDS PAGE gel of ubiquitin purification; lane 1 is mark12^{TM} standard, lane 2 is before IPTG induction, lane 3 is after IPTG induction, lane 4 is anion exchange purification, lane 5 size exclusion chromatography and lane 5 reverse phase chromatography. Ubiquitin appears at 6 kDa, this is due to ubiquitin running as a folded protein, therefore runs further on the gel.

2.3.4 Reverse phase chromatography

Ubiquitin was purified to homogeneity using C18 reverse-phase HPLC. A semi-preparative (Grace Vydac USA; 10 mm x 25 cm, 5 μm particle size) column was

used. The column was equilibrated with solvent A (0.1% v/v trifluoroacetic acid (TFA) in filtered degassed water). Five millilitre samples were loaded on to the column at a flow rate of 5 ml/min. Protein material was purified using a linear gradient of 100% solvent A to 75% solvent A: 25% solvent B (0.1% v/v TFA in acetonitrile) over 15 minutes, followed by a linear gradient of 75% solvent A:25% solvent B to 40% solvent A:60% solvent B over 30 minutes at a flow rate of 4 ml/min. The UV absorbance was monitored simultaneously at 215 nm (amide bond), 254 (phenylalanine) and 280 nm (tryptophan residues) using a fully-automated ÄKTA^{TM} HPLC system (Amersham Biosciences). The target protein eluted at approximately 63% Solvent A: 37% Solvent B. The purified material was lyophilised and stored at −20 °C (Figure 2.3).

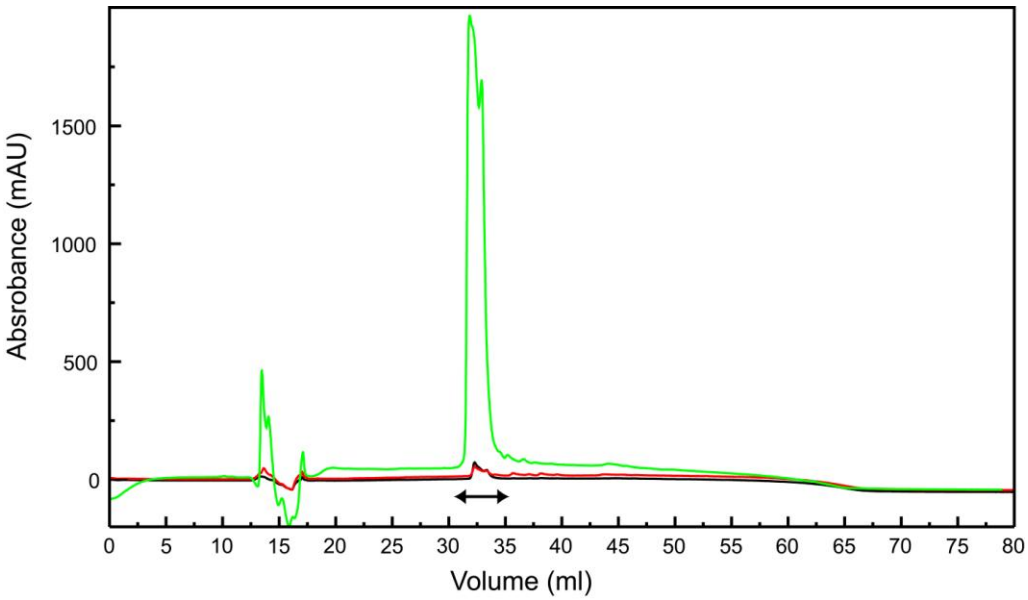

Figure 2.3: Reverse phase chromatogram of ubiquitin with only one main peak, of ultra pure ubiquitin. The collected peak was ran on a SDS PAGE gel Figure 2.2.

2.4 Nuclear magnetic resonance (NMR) experiments

2.4.1 Hardware

NMR experiments were predominantly recorded at the UCL NMR laboratory on Varian UnityPlus spectrometers operating at 500 and 600 MHz proton frequencies. Both spectrometers were equipped with a 5-mm z-gradient $^{1}H/^{15}N/^{13}C$ probes optimized for ^{1}H detection. Standard pulse sequences where established by Dr Richard Harris (NMR Facility Manager).

The long-range quantitative $^{h3}J_{NC'}$ H(N)CO experiments were also recorded at the MRC Biomedical NMR centre, Mill Hill (NIMR), London. The Bruker 600 MHz

spectrometer is equipped with a cryoprobe 5-mm z-gradient $^{1}H/^{15}N/^{13}C$ probe optimised for ^{1}H detection. The pulse programmes used at the NIMR were written by Dr Tom Frenkiel.

2.4.2 Sample preparation

2.4.2.1 No cosolute

Lyophilised ^{15}N- and $^{15}N/^{13}C$-enriched ubiquitin material was dissolved in water to a final concentration of 2.0 to 2.5 mM, pH 6.5. NMR experiments were run at four different temperatures: 15, 30, 45, and 60 ºC.

The temperature of the NMR probe was calibrated using the following equation:

$$y = -0.0032x^2 + 1.27x - 0.04911 \qquad \text{Equation [2.2]}$$

by using a methanol sample for low temperatures and ethylene glycol for high temperatures (Cavanagh, 1996).

2.4.2.2 TMAO

Lyophilised ^{15}N- and $^{15}N/^{13}C$-enriched ubiquitin material was dissolved in 1.5 M TMAO buffer at pH 6.5. NMR experiments were run at four different temperatures: 15, 30, 45, and 60 ºC.

The addition of 1.5 M TMAO to the protein sample visibly increased the viscosity of the solution. The viscosity of TMAO was measured using a ViscoSystem® AVS 350 viscosity measuring unit (Schott, Germany). A high viscosity viscometer (Schott, Germany) was connected to the ViscoSystem to measure the viscosities of 1.5 and 3.0 M TMAO solutions at 15, 30, 45 and 60 ºC. The temperature at each measurement was kept constant by a temperature controlled water-bath. 15 ml of TMAO was loaded into the viscometer and was left to equilibrate at the ambient temperature for 10 minutes. The measurements were recorded in seconds and repeated three times and the average value was multiplied by the viscometer constant K (0.004894) to calculate the kinematic viscosity [mm^2/s]. The viscosity was calculated by dividing the kinematic viscosity by the density of TMAO. This is illustrated in the following equations:

$$\text{Kinematic viscosity} = t \times K \qquad \text{Equation [2.3]}$$

$$\text{Viscosity} = \frac{K}{\rho} \text{ in centipoise [cp] } 1\text{Kg m}^{-1}\text{s}^{-1} \qquad \text{Equation [2.4]}$$

where *t* is time in seconds, *K* is the viscometer constant and ρ is the density [g/m^2] of the TMAO solution. The density of TMAO was calculated by careful weight analysis. Table 2.4 shows the TMAO viscosity values calculated from the measurements and using Equations [2.3] and [2.4]. Viscosity values for H_2O are taken from Atkins "*Physical Chemistry"*(Atkins, 1994). The viscosity values were used to estimate the rotational correlation time of ubiquitin in TMAO at various temperatures (Table 2.5) using the Stokes-Einstein- Deybe equation:

$$\tau_c = \frac{4\pi\eta_w r^3}{3K_B T} \qquad \text{Equation [2.5]}$$

were τ_c is the measurement of the time a molecule rotates through an angle of one radian and it is dependent on the size, shape and dynamics of the molecule, as well as the physical characteristics of the solvent, the viscosity is defined as η , *r* is the radius of the spherical particle, K_B is Boltzmans constant and T is absolute temperature. The τ_c of a protein is directly related to its volume and molecular weight (Cavanagh, 1996).

Table 2.4: The viscosity calculations in centipoise [cp] 1Kg m^{-1}s^{-1}

Temperature [ºC]	H_2O	1.5 M TMAO	3.0 M TMAO
15	1.139	1.665	–
25	0.890	1.21	1.69
30	0.798	1.128	–
45	0.596	0.807	–
60	0.467	0.625	–

Table 2.5: The correlation times τ_c (ns) for ubiquitin at different temperatures in the absence and presence of TMAO

Temperature [ºC]	H_2O	1.5 M TMAO	3.0 M TMAO
15	5.3	7.97	–
25	4.1	5.5	7.7
30	3.3	5.17	–
45	3.0	3.45	–
60	1.9	2.6	–

2.4.2.3 Guanidinium Hydrochloride (Gdn.HCl)

Lyophilised ^{15}N- and ^{15}N/^{13}C-enriched ubiquitin material was dissolved in 0 to 7.5 M Gdn.HCl at pH 4.7. All NMR experiments were run at 25 ºC.

2.4.2.4 Urea

Lyophilised ^{15}N- and ^{15}N/^{13}C-enriched ubiquitin material was dissolved in 0 to 8.5 M urea at pH 4.7. All NMR experiments were run at 25 ºC.

2.4.2 H-bond scalar coupling experiments

The detection of the $^{h3}J_{NC'}$ couplings in N–H•••O=C hydrogen bonds in proteins is achieved by a straightforward modification of the 3D HNCO experiment used for the sequential assignment of protein backbones. In the conventional 3D HNCO experiment magnetization follows an "out" and "back" path according to $^1H^{Ni} \rightarrow {}^{15}N^{i} \rightarrow {}^{13}C'^{i-1} \rightarrow {}^{15}N^{i} \rightarrow {}^{1}H^{Ni}$. In order to achieve the transfer between the amide ^{15}N nucleus of one amino acid and the carbonyl ^{13}C nucleus of the preceding amino acid, the delays for the magnetisation transfer between the $^{15}N^{i}$ and $^{13}C'^{i-1}$ step are usually set to values slightly shorter than $1/2(^1J_{NC'})$, where $^1J_{NC'}$ is the one-bond transfer from the amide ^{15}N nucleus of residue i to the carbonyl ^{13}C nucleus of residue i–1. With typical $^1J_{NC'}$ values in the range of 13 to 17 Hz, this corresponds to magnetisation transfer periods of approximately 30 ms (i.e. $1/2(^1J_{NC'}) \approx 1/30$ Hz ≈ 33 ms).

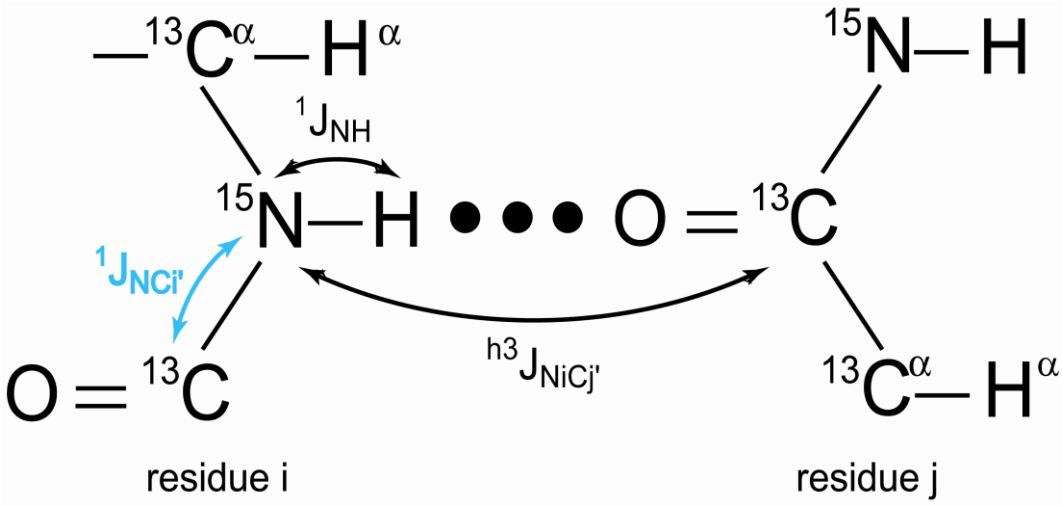

Figure 2.4: Schematic of a backbone N–H●●●O=C H-bond. The detection of the $^{h3}J_{NiCj'}$ correlations follow the "out-and-back" magnetisation transfer pathway shown by the black double-headed arrows. The blue double-headed arrow illustrates the magnetisation transfer pathway for the reference H(N)CO experiment. In both experiments, magnetisation is initially transferred from the amide proton to the amide nitrogen via the 90 Hz one-bond coupling between these two nuclei ($^{1}J_{NH}$).

In the long-range quantitative 2D H(N)CO experiment suitable for magnetization transfer via $^{h3}J_{NC'}$ couplings, the delays (2T in Figure 2.5) are set to 133 ms ≈ $2/^{1}J_{NC'}$ such that the $^{1}J_{NC'}$ transfer is essentially refocused (Figure 2.5A). In principle, such refocusing can be achieved by any choice of 2T ≈ $n/^{1}J_{NC'}$ with n being an integer. The maximum sensitivity for the detection of $^{h3}J_{NC'}$ correlations will be equal to $1/2(^{h3}J_{NC'})$ (e.g. one second for a 0.5 Hz coupling). However, such delay periods are not feasible due to relaxation mechanisms and the maximal sensitivity for the experiment is obtained when 2T is set to values close to the transverse relaxation time of the ^{15}N nuclei (Figure 2.5).

Although the delays are set to 133 ms, transfer by ^{15}N–$^{13}C'$ couplings with coupling constant values different from 15 Hz will still occur. As a consequence, the resulting 2D H(N)CO spectrum does not contain the normal $^{1}H^{i}$–$^{13}C'^{i-1}$ cross peaks, but cross peaks resulting from eventual long-range correlations, such as the $^{h3}J_{NiC'j}$ couplings between the amide ^{15}N nucleus of residue i and the carbonyl ^{13}C nucleus of the H-bonded residue j. Thus the magnetisation path for $^{h3}J_{NiC'j}$ correlations is $^{1}H_{N}$ (donor) → ^{15}Ni (donor) → $^{13}Cj'$ (acceptor) → ^{15}Ni (donor) → $^{1}H_{N}$ (donor).

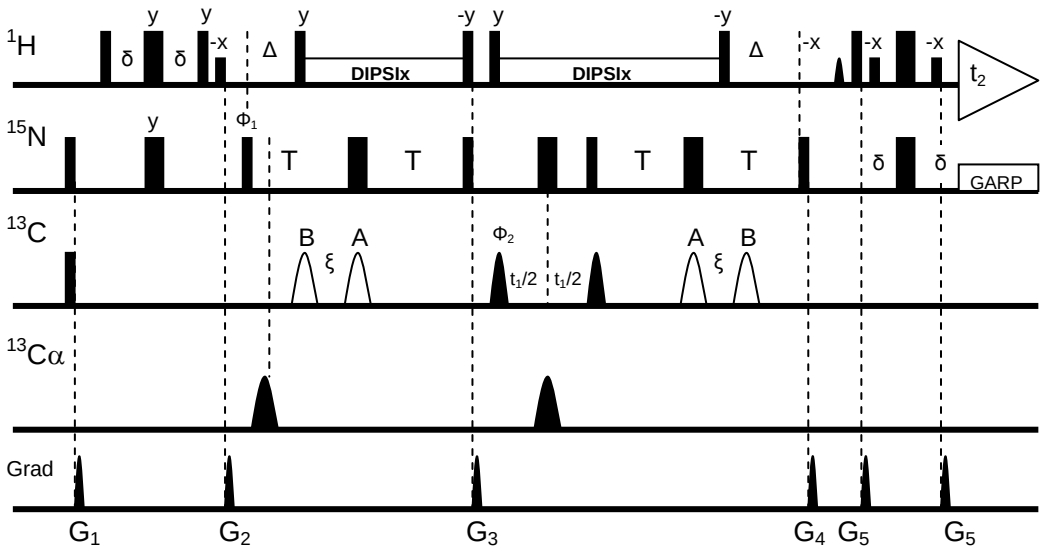

Figure 2.5: Pulse sequence of the long-range quantitative 2D H(N)CO experiment. Narrow and wide pulses denote the 90º and 180º flip angles, respectively, and unless indicated the phase is x. ^{1}H and ^{15}N carrier positions are on the $^{1}H_2O$ resonance and at 117.0 ppm. The ^{13}C carrier frequencies are set to 177 ppm and 56 ppm for $^{13}C'$ and $^{13}C^{\alpha}$, respectively. All regular ^{1}H pulses are applied at RF field strength of 29 kHz. DIPSIx (Shaka et al., 1988) refers to the ^{1}H decoupling, using the DIPSI-2 modulation scheme with the RF fields ($\gamma_H B_1$ = 14.5 kHz) applied along the x-axis and the carrier at the H_2O resonance. The ^{1}H decoupling is interrupted by the gradient pulse G_3. Rectangular low power ^{1}H pulses are applied using $\gamma_H B_1/2\pi$ = 200 Hz, whereas the shaped ^{1}H 90^{o}_{-x} pulse has a sine-bell amplitude profile and durations between 2.2 to 3.3 ms. All regular ^{15}N pulses are applied at an RF field strength of $\gamma_N B_2/2\pi$ = 6.1 kHz, whereas ^{15}N GARP (Shaka et al., 1985) decoupling is applied at an RF field strength $\gamma_N B_2/2\pi$ = 1.25 kHz during acquisition. The rectangular ^{13}C pulse at the start of the pulse scheme is applied at an RF field strength of $\gamma_C B_3/2\pi$ = 3.3 kHz. Both the initial ^{13}C and ^{15}N 90º pulses combined with the G_1 gradient remove unwanted ^{13}C and ^{15}N Boltzmann contributions which reduce the sensitivity of the experiment. All ^{13}C 180º pulses (e.g. at the midpoint the of 2T periods) have a Q3 amplitude profile, with durations of 256 ms, corresponding to an inversion bandwidth of 46 ppm. The ^{13}C 90º pulses bracketing the t_1 period have a Q5 amplitude profile and duration of 320 ms, corresponding to an excitation bandwidth of 2.3 kHz. The second shaped ^{13}C 90º pulse is applied as a time-reversal Q5 pulse. Delay durations: δ = 2.25 ms; Δ = 5.4 ms; T = 66.5 ms. Phase cycling Φ_1= 2(x), 2(-x); Φ_2 = x,-x; receiver = x, 2(-x), x. Quadrature detection in the t_1 dimension was achieved by incrementing Φ_2 in the States-TPPI (Marion et al., 1988) manner. Gradients are sine-bell shaped with an absolute amplitude of 25 G/cm at their center and durations of $G_{1,2,3,4,5}$ = 1, 1, 1.5, 1, and 0.4 ms. For the quantification of the $J_{NC'}$ couplings, two independent experiments are performed with the $^{13}C'$ 180º Q3 pulses (open) applied at either position A or B. Cross peaks observed for experiment A are primarily due to the small $^{h3}J_{NiCj'}$ couplings which evolve during the full period of 2T. Cross peaks observed in scheme B are a result of the sequential residue $^{1}J_{NC'}$ couplings which are active during the period 2(T–ξ), where ξ = 16.5 ms (Cordier and Grzesiek 1998, Cornilescu et al., 1999).

The size of the $^{h3}J_{NC'}$ couplings were quantitatively determined by a J correlation technique. Cross peaks that result from the transfer of magnetisation between $^{15}N_i$ and $^{13}C_j$' nuclei across the H-bond (Scheme A, Figure 2.4) are proportional to:

$$\sin^2\left(2\pi^{h3}J_{NiC'j}T\right)*\cos^2\left(2\pi^{1}J_{NiC'i-1}T\right) \qquad \text{Equation [2.6]}$$

In the 2D H(N)CO reference experiment, the effective time of magnetisation transfer from ^{15}N to ^{13}C' is equal to 2T, but the ^{13}C' 180º Q3 pulse in the centre of the 2T period is shifted by 16.5ms. This has the influence of reducing the effective time for the ^{15}N to ^{13}C' defocusing and refocusing time to a value equal to 2(T – 16.5 ms) while keeping the relaxation losses identical to the pulse sequence with scheme A. Therefore the cross peaks that result from the transfer of magnetisation between the $^{15}N_i$ and $^{13}C'_{i-1}$ nuclei in the reference experiment are proportional to:

$$\sin^2\left(2\pi^{1}J_{NiC'i-1}\left[T-16.5ms\right]\right)*\cos^2\left(2\pi^{h3}J_{NiC'j}\left[T-16.5ms\right]\right) \qquad \text{Equation [2.7]}$$

As described previously, to quantitatively determine the value of the $^{h3}J_{NC'}$ couplings, the ratio of the peak intensities recorded using schemes A and B is given by:

$$\frac{I_{lr}}{I_{ref}}=\frac{\sin^2\left(2\pi^{h3}J_{NiC'j}T\right)*\cos^2\left(2\pi^{1}J_{NiC'i-1}T\right)}{\sin^2\left(2\pi^{1}J_{NiC'i-1}\left[T-16.5ms\right]\right)\cos^2\left(2\pi^{h3}J_{NiC'J}\left[T-16.5ms\right]\right)} \qquad \text{Equation [2.8]}$$

By taking the square root on both sides gives:

$$\sqrt{\frac{I_{lr}}{I_{ref}}}=\frac{\sin\left(2\pi^{h3}J_{NiC'j}T\right)*\cos\left(2\pi^{1}J_{NiC'i-1}T\right)}{\sin\left(2\pi^{1}J_{NiC'i-1}\left[T-16.5ms\right]\right)*\cos\left(2\pi^{h3}J_{NiC'J}\left[T-16.5ms\right]\right)} \qquad \text{Equation [2.9]}$$

For small values of $^{h3}J_{NC'}$ such that $|2\pi^{h3}J_{NC'}T| << 1$ and values of $^{1}J_{NiC'i-1}$ close to 15 Hz the following relation is valid:

$$J_{NiC'j}\approx\frac{\sqrt{\frac{I_{lr}}{I_{ref}}}}{2\pi T} \qquad \text{Equation [2.10]}$$

To accommodate the different number of scans used in pulse schemes A and B, Equation [2.10] is modified to:

$$J_{NiC'j} \approx \frac{\sqrt{\left(\frac{I_{lr}}{NS_{ref}}\right)}}{\sqrt{\left(\frac{I_{ref}}{NS_{lr}}\right)}} \frac{}{2\pi T}$$ Equation [2.11]

In order to determine experimental reproducibility both long-range and the reference H(N)CO experiments were carried out at least twice, and the values of the $^{h3}J_{NiCj'}$ couplings and errors refer to the root mean square deviation (RMSD).

Figure 2.8B shows the result of a long-range 2D H(N)CO experiment recorded using the pulse sequence depicted in Figure 2.5 (scheme A) for a $^{13}C/^{15}N$-enriched ubiquitin sample. The resonances detected in the long-range 2D H(N)CO are between the amide $^{1}H^{N}$ and the carbonyl ^{13}C. The majority of the resonances depicted in Figure 2.8B correspond to HBC correlations. A total number of 17 $^{h3}J_{NC'}$ correlations were detected from an expected 33 H-bonds present in ubiquitin (based on examination of the 1.8 Å crystal structure of human ubiquitin) (Vijay-Kumar et al., 1987). For example, a cross peak is visible between the backbone amide and carbonyl groups of residues F4 as the donor nucleus and S65 as the acceptor nucleus. This H-bond forms between β-strands one and five. During the long-range and the reference H(N)CO experiments the intraresidue one-bond scalar coupling between the ^{15}N donor amide and the $^{13}C_{\alpha}$ nuclei is also active during the 2T periods, yet refocused using a Q3 180° selective pulse centred in t_1. The size of this $^{1}J_{NC\alpha}$ coupling is ~11 Hz (Figure 2.7). The $^{13}C_{\alpha}$ has a fast transverse relaxation rate due to the strong heteronuclear dipole-dipole interaction with the directly bonded $^{1}H_{\alpha}$ nucleus. Consequently, the scalar coupling (via the $^{1}J_{NC\alpha}$) mediated relaxation leads to a significantly weaker signal in the conventional long-range quantitative $J_{NC'}$ H(N)CO experiment due to the long $^{15}N_i$ $-^{13}C_j$' magnetisation transfer periods. The absence of the 16 $^{h3}J_{NiCj'}$ correlations in the pulse scheme depicted in Figure 2.5 presumably stem from this scalar coupling mediated relaxation process.

There are two solutions for overcoming the relaxation contribution to backbone ^{15}N from the J-coupling mediated $^{1}H_{\alpha}$-$^{13}C_{\alpha}$ dipole-dipole interaction. The first approach is to prepare a uniformly $^{2}H/^{13}C/^{15}N$ enriched ubiquitin sample. In this

sample the $^{1}H\alpha$ is replaced by $^{2}H\alpha$ and this change leads to a significant weakening (~6.5 due to γ_H/γ_D) of the heteronuclear dipole-dipole interaction. However, deuteration is a costly procedure and for this project is not economically tractable since we require multiple NMR samples of approximately 11 mg of protein per sample. As previously published, a simple alternative is to modify the pulse sequence presented in Figure 2.5 by the introduction of composite-pulse decoupling (CPD) or adiabatic decoupling. Figure 2.8 shows the long-range 2D-CPD-H(N)CO pulse sequence where WURST (Kupce and Freeman 1995) decoupling has been applied to the backbone $^{13}C\alpha$ during the entire 2T periods. This effectively quenches the scalar coupling mediated relaxation by preventing magnetisation transfer between the $^{15}N_i$ and $^{13}C_\alpha$ nucleus. 31 out of a possible 33 $^{h3}J_{NC'}$ correlations (Figure 2.8C) were observed when employing this pulse scheme.

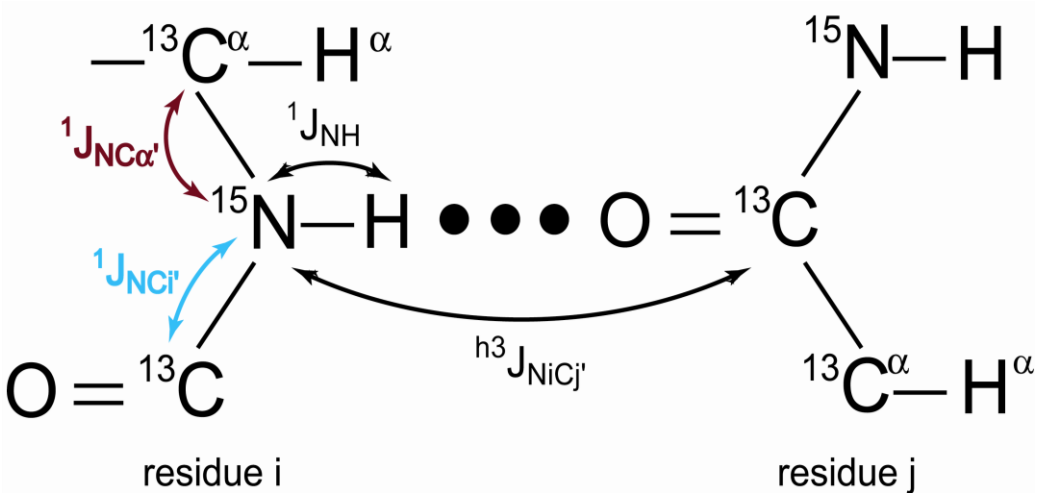

Figure 2.6: Schematic of a backbone N–H•••O=C H-bond. The detection of the $^{h3}J_{NC'}$ correlations follow the magnetisation transfer pathway shown by the black double-headed arrows, whereas the blue double-headed arrow illustrates the magnetisation transfer pathway for the reference 2D HNCO experiment. The red double-headed arrow represents the magnetisation transfer pathway between the amide ^{15}N and the $^{13}C\alpha$ nuclei via the 11 Hz one-bond coupling $^{1}J_{NC\alpha}$. In the 2D CPD-H(N)CO experiment, the $^{1}J_{NC\alpha}$ transfer is quenched.

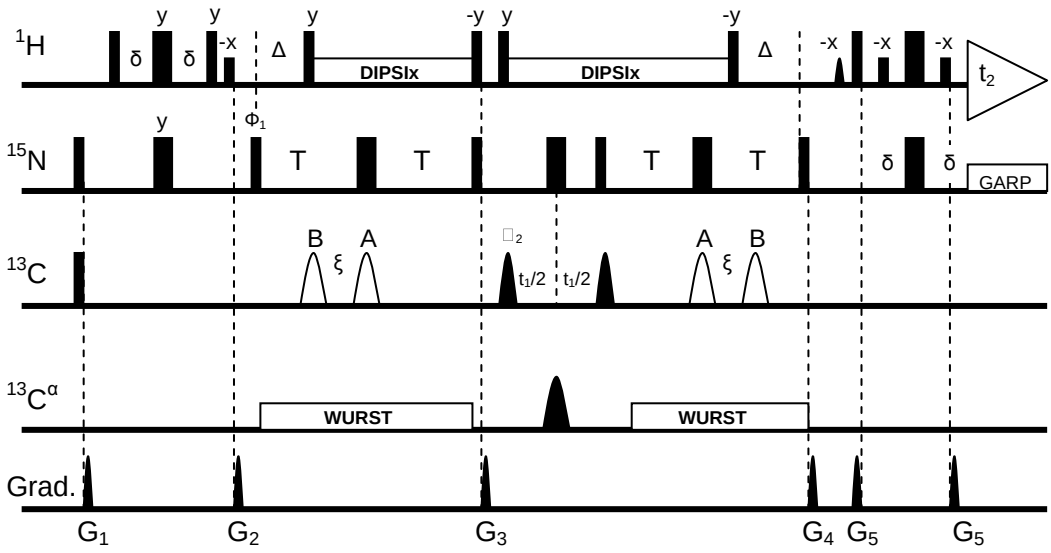

Figure 2.7: The pulse sequence of the long-range quantitative 2D CPD-H(N)CO experiment. The description to this pulse sequence is identical to Figure 2.4, except band-selective $^{13}C_{\alpha}$ decoupling during the N to C' INEPT transfer periods are used. WURST refers to the $^{13}C_{\alpha}$ decoupling, using a WALTZ-16 sequence with phase modulated pulses having the SEDUCE-1(Liu et al., 2000) profile with an RF field strength of 3.6 kHz.

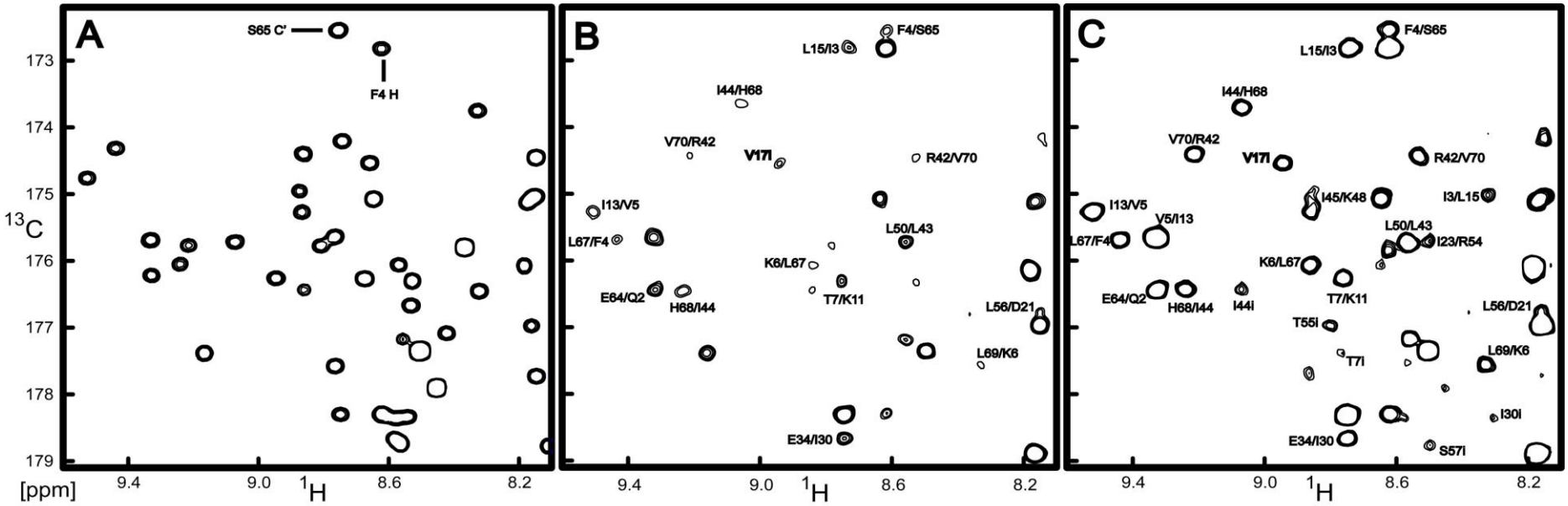

Figure 2.8: Selected region of the standard 2D long-range quantitative-$J_{NC'}$ H(N)CO spectrum recorded on a 2.5 mM sample of uniformly $^{13}C/^{15}N$-enriched ubiquitin. Resonances labelled as Res_i/Res_j are due to $^{h3}J_{NC'}$ scalar couplings between ^{15}N nucleus of residue *i* and $^{13}C'$ nucleus of residue *j*. Residues marked with an *i* denote not completely refocused one-bond correlations between the ^{15}N nucleus of residue *i* and $^{13}C'$ nucleus of residue *i*–1. Figure 2.8A shows the reference spectrum, Figure 2.8B shows the spectrum recorded with the pulse sequence, were the $^{13}C_\alpha$ is refocused by a selective 180º pulse and Figure 2.8C shows the similar spectrum recorded using the pulse sequence where WURST decoupling of the $^{13}C_\alpha$ nuclei has been employed throughout the 2T period.

$^{13}C/^{15}N$-enriched ubiquitin samples at ~2.5 mM concentrations were prepared (Section 2.5.2). The $^{h3}J_{NC'}$ and $^{1}J_{NC'}$ couplings of ubiquitin were determined at four different temperatures in the presence and absence of 1.5 M TMAO: 15, 30, 45, and 60 ºC using the 2D long-range CPD-H(N)CO experiment. The $^{h3}J_{NC'}$ and $^{1}J_{NC'}$ of ubiquitin in the presence of either Gdn.HCl or urea at various concentrations were determined at 25 ºC. The data matrix size was 65* (t_{CO}) x 1024* (t_{NH}) data points (where *n** refers to the number of complex points) and acquisition times of 39 (t_{CO}) and 110 ms (t_{NH}). Depending on the sample environment, the total measuring times for measuring $^{h3}J_{NC'}$ couplings ranged from 36 to 120 hours for a single spectrum recorded using a standard probe head. The acquisition times using the 600 MHz with cryoprobe ranged between 16 to 24 hours. Reference spectra for quantification of the $^{h3}J_{NC'}$ couplings were recorded with total measuring times of approximately two hours.

2.4.3 Two-dimensional (2D) $^{1}H–^{15}N$ heteronuclear single quantum coherence (HSQC) experiment

2D $^{1}H–^{15}N$ HSQC experiments were recorded using a pulse-field gradient sensitivity-enhanced pulse scheme with the incorporation of water flip-back pulses for optimal water suppression. The 2D $^{1}H–^{15}N$ HSQC experiment was recorded with the INEPT transfer delay set to 2.25 ms as a compromise between the fast relaxing amide protons and the optimal transfer time for the $^{1}J_{NH}$ couplings of ~90 Hz. The recycle delay was 1.2 s. The data matrix consisted of 128* × 384* data points (were n* refers to complex points) with acquisition times of 61 (t_N) and 96 ms (t_{HN}). A total of 32 scans per complex t_N increment was collected. The total measuring time was between 1 to 1.6 hours. The experiment was performed with the ^{1}H carrier positioned in the centre of the amide proton frequency (7.52 ppm) and the ^{15}N carrier at 118.4 ppm. ^{15}N decoupling was applied during data acquisition.

2.4.4 Measuring ^{15}N longitudinal R_1, transverse R_2 relaxation rates and [1H]-^{15}N nuclear Overhauser effects (NOE)

The ^{15}N R_1, R_2 and ^{1}H-^{15}N nuclear Overhauser effect (NOE) experiments were all recorded using experiments based on published pulse sequences (Kay et al., 1989). Experiments were recorded using 2.5 mM ubiquitin samples in the presence and absence of 1.5 M TMAO at 15 and 60 ºC. To obtain R_1 relaxation values, for no cosolute at 15 ºC 14 relaxation delays of 54, 154 (×2), 304, 454, 604 (×2), 754, 904,

1054, 1204 (×2), 1504 and 1804 ms were employed, whereas at 60 ºC 14 relaxation delays 54, 154 (×2), 304, 454, 604 (×2), 754, 904, 1054, 1204 (x2), 1404 and 1604 ms were used. In the presence of 1.5 M TMAO at 15 ºC 14 relaxation delays of 54, 154 (×2), 304, 454, 604 (×2), 754, 1004, 1104, 1404 (×2), 1704 and 2004 ms were employed, whereas at 60 ºC 14 relaxation delays of 54, 154 (×2), 304, 454, 604 (×2), 754, 904, 1054, 1204 (×2), 1404 and 1604 ms were employed.

For R_2 relation values, in the absence of TMAO at 15 ºC, 15 relaxation delays of 28.8, 43.2 (×2), 57.6, 72, 86.4, 115.2, 129.6, 144 (×2), 158.4, 172.4, 201.6 and 244.8 ms, whereas at 60 ºC relaxation delays of 28.8, 57.6 (×2), 86.4, 100.8, 115.2, 144 (×2), 172.8, 201.6, 216, 230.4, 259.2 and 302 ms, were used. In the presence of 1.5 M TMAO at 15 ºC relaxation delays of 28.8, 43.2 (×2), 57.6, 72, 86.4, 115.2, 129.6, 144 (×2), 158.4, 172.4, 201.6 and 244.8 ms were employed, whereas at 60 ºC relaxation delays of 28.8, 57.6 (×2), 86.4, 100.8, 115.2, 144 (×2), 172.8, 201.6, 216, 230.4 (×2), 259.2 and 302 ms, were employed.

The ^{1}H saturation period in the [1H]-^{15}N NOE experiment was 3.0 seconds with two experiments recorded in an interleaved manner. In the saturation experiment the offset was positioned on-resonance (i.e. amide protons), whereas in the reference experiment saturation was performed ~3 MHz off-resonance (i.e. no amide proton saturation). The data matrix consisted of 128* × 384* data points (were n* refers to complex points) with acquisition times of 61 (t_N) and 96 ms (t_{HN}). A total of 32 scans per complex t_N increment was collected. An additional recycling delay of 2 s was added to the saturation period during the [1H]-^{15}N NOE experiment.

2.4.5 Measuring $^{1}J_{NH}$ coupling experiment (IPAP)

The IPAP experiments were recorded using the published pulse sequence. The $^{1}J_{NH}$ couplings of ubiquitin were determined at four temperatures in the presence and absence of 1.5 M TMAO: 15, 30, 45, and 60 ºC. The $^{1}J_{NH}$ couplings of ubiquitin in the presence of Gdn.HCl or urea at various concentrations were determined at 25 ºC.

2.4.6 Chemical shift mapping

Chemical shift changes in ubiquitin were determined in Gdn.HCl (0 to 6.5 M) and urea (0 to 8.5 M) at 25 ºC using 2D ^{1}H–^{15}N HSQC experiments as mentioned in section 2.5.3. Proton chemical shifts were referenced to 3,3,3-trimethysilyl acid

(TSP), while ^{15}N and ^{13}C chemical shifts were indirectly referenced according to.(Markley et al., 1984)

2.5 NMR data analysis

2.5.1 Processing NMR data

All raw NMR data were processed using the nmrPipe program of Delaglio and co-workers. Standard manipulations of data sets included zero-filling, application of a shifted sine-bell function, base line corrections, and linear prediction of the indirect dimensions where possible and zero and first order phase corrections were applied using nmrPipe. Spectra were initially visualised in nmrDraw.

The processed spectra were exported into AZARA (http://www.bio.cam.ac.uk/azara/) format using the PIPE2AZARA software. Multiple spectra were visualised together and plotting of spectra was performed using Plot2 (http://www.bio.cam.ac.uk/azara/).

2.5.2 Peak Intensities

The peak picking program (Garrett et al., 1991) PIPP was used to determine peak intensities peak pick the long-range and reference HNCO experiments. As explained in Section 2.5.3 peak intensities were used to calculate the H-bond $^{h3}J_{NC'}$ couplings. The analysis software in the CCPN package (Vranken et al., 2005) was used to peak pick the resonances of the relaxation data.

2.5.3 Derivation of ^{15}N R_1, ^{15}N R_2, [1H] ^{15}N-heteronuclear-NOE values

^{15}N R_1 and R_2 experiments yielded a pseudo 3D-spectrum with the third dimension corresponding to the 2D NH correlation plane with incremented relaxation delays (See Section 2.5.4). For each set of relaxation data recorded, a reference 2D [^{1}H,^{15}N] spectrum was acquired. Only well resolved NH cross peaks in the reference spectrum were selected for further analysis. The signal intensity of each selected resonance from the 2D planes recorded was extracted using the analysis program which is part of the CCPN software package (Vranken et al., 2005). The intensity values of the resonances as a function of the relaxation delay were fit to:

$$I(t) = I_0 \exp\left[\frac{-t}{\mathrm{T}_i}\right] \qquad \text{Equation [2.12]}$$

using the fitting programme Curvefit which fits the data using a two parameter least square Levenberg-Marquardt method as described by Mandel and coworkers (Mandel

et al., 1995). The error on the fit was estimated using a Monte Carlo simulation based on the signal intensities of the resonances acquired for a pair of duplicated time points. The relaxation rates and standard deviations stated in the text correspond to the mean relaxation rate and standard deviation of the distribution of 500 such Monte Carlo iterations.

^{1}H–^{15}N heteronuclear NOE experiments were acquired as a pair of interleaved 2D NH correlation spectra in the presence of on- and off-resonance proton saturation. The signal intensity values of selected resonances were extracted as described for the R_1 and R_2 relaxation experiments. The steady-state NOE values were determined from the ratios of the intensities of the peaks with and without amide proton saturation. The experimental error σ_{NOE} was calculated based on the spectral noise value (σ_{Isat} and σ_{Iunsat}) in each 2D NH plane using the following relationship:

$$\sigma_{NOE} / NOE = ((\sigma_{I_{sat}} / I_{sat})^2 + (\sigma_{I_{unsat}} / I_{unsat})^2)^{1/2} \qquad \text{Equation [2.13]}$$

where I_{sat} and I_{unsat} are the measured intensities of a resonances in the presence and absence of proton saturation, respectively.

2.5.4 Modelfree dynamics analysis

The relaxation rates of proteins are affected primarily by the dipolar interactions and chemical shift anisotropy (CSA). The overall relaxation rates are the linear combination of all rates of the interactions. The relaxation rates can be expressed in terms of combination of spectral density functions, $J(\omega)$ where ω denotes the precession frequency. The function shows the amount of magnetic field fluctuations present in the sample as a function of ω. Since R_1, R_2 and [1H]-^{15}N NOE relaxation parameters are sensitive to these field fluctuations, they can be cast as functions of $J(\omega)$. These equations account for relaxation processes driven by the dipole-dipole interaction and the CSA of the ^{15}N nucleus.

$$R_1 = (d^2/4)\left[J(\omega_{\text{H}} - \omega_{\text{N}}) + 3J(\omega_{\text{N}}) + 6J(\omega_{\text{H}} + \omega_{\text{N}})\right] + c^2 J(\omega_{\text{N}}) \qquad \text{Equation [2.14]}$$

$$R_2 = (d^2/8)\left[4J(0) + J(\omega_{\text{H}} - \omega_{\text{N}}) + 3J(\omega_{\text{N}}) + 6J(\omega_{\text{H}}) + 6J(\omega_{\text{H}} + \omega_{\text{N}})\right] + (c^2/6)\left[3J(\omega_{\text{N}}) + 4J(0)\right] + R_{ex} \qquad \text{Equation [2.15]}$$

$$\mathrm{NOE} = 1 + (\gamma_{\mathrm{H}} + \gamma_{\mathrm{N}}) d^2 \left[6J(\omega_{\mathrm{H}} + \omega_{\mathrm{N}}) - J(\omega_{\mathrm{H}} - \omega_{\mathrm{N}}) \right] T_1 \qquad \text{Equation [2.16]}$$

where $T_1=1/R_1$.

where *d* and *c* are constants defined as:

$$d = (\mu_0 \gamma_{\mathrm{H}} \gamma_{\mathrm{N}} h / 8\pi^2) \left\langle r_{NH}^{-3} \right\rangle \qquad \text{Equation [2.17]}$$

$$c = \Delta\sigma \omega_{\mathrm{N}} / \sqrt{3} \qquad \text{Equation [2.18]}$$

where μ_0 is the permeability constant ($4\pi \times 10^{-7}$ H m^{-1}), *h* is the Planck's constant, γ_{H} and γ_{N} are the gyromagnetic ratios of the hydrogen and nitrogen atoms respectively, r_{NH} is the length of the N–H internuclear vector, Δσ is the CSA of the ^{15}N spin (–160 ppm), assumed to be axially symmetric, and ω_{H} and ω_{N} are the Larmor frequencies of the ^{1}H and ^{15}N nuclei, respectively.

The amplitudes and timescales of these protein motions are described by the Modelfree formalism of (Lipari and Szabo, 1982a,b), and the extended model by Clore and co-workers (Clore *et al.*, 1990) which models the spectral density function as

$$J(\omega) = \frac{2}{5} \left[\frac{S^2 \tau_m}{1 + (\omega \tau_m)^2} + \frac{(1 - S_f^2) \tau'_f}{1 + (\omega \tau'_f)^2} + \frac{(S_f^2 - S^2) \tau'_s}{1 + (\omega \tau'_s)^2} \right] \qquad \text{Equation [2.19]}$$

in which $\tau'_f = \tau_e \tau_m / (\tau_e + \tau_m)$, $\tau_s = \tau_s \tau_m / (\tau_{s+} \tau_m)$, τ_m is the isotropic rotational correlation time of the macromolecule, τ_e is the effective correlation time for fast (<200 psec) internal motions, and τ_s the correlation time for slow (~nsec) motions ($\tau_e < \tau_s < \tau_m$). Corrections for non-isotropic macromolecular tumbling are readily implemented (Woessner 1962, (Lee et al., 1997). $S^2 = S^2_f S^2_s$ is the square of the generalized order parameter that characterizes the amplitude of internal motions, and S^2_f and S^2_s are the order parameters for internal dynamics on the fast and slow time scales, respectively. The order parameter describes the amplitude of bond vector motions in the time range from picoseconds to nanoseconds and has values from 0 for unrestricted motions to 1 indicating a static bond vector in the molecular reference frame. Consequently, measurement of ^{15}N longitudinal and transverse relaxation rates in combination with the [1H]-^{15}N heteronuclear NOE allows sampling of the spectral

density function and thus amplitudes and time scales of protein motion can be determined.

The R_1, R_2 and NOE data were fitted to five spectral density models using equations 2.14 to 2.16 and the R_{ex} term added to equation 2.15. These models were used to describe the amide backbone dynamics (Clore et al. 1990). The five models each particular internal motional parameter (up to three), with an overall rotational correlation time. The models:

Table 2.6 The models fitted to five spectral density models with the internal motional parameters

Models	Parameters
1	S^2
2	S^2, τ_e
3	S^2, R_{ex}
4	S^2, τ_e , R_{ex}
5	S^2_f, S^2, τ_e

Model 1 is calculated by presuming the $S^2_s = 1$and $\tau_f \rightarrow 0$, this model ignores both fast and slow internal motions. Model 2 is obtained by assuming that $S^2_s = 1$ and is applicable if motions on the slow time scale are negligible; however, fast motions are includes, i.e. τ_e. Model 2 is the original formulation of Lipari & Szabo (1982*a*). Models 3 and 4 are similar to models 1 and 2; however, they include, a non-zero chemical exchange contribution, R_{ex}, in the relaxation model. Model 5 is obtained by assuming only that $\tau_f \rightarrow 0$. The form of the spectral density function for model 5 is isomorphous with an approximate spectral density function incorporating anisotropic rotational diffusion (Lipari & Szabo, 1982*a*; Stone et al., 1992).

Prior to determining which model to be used for individual residues, the global correlation time of the molecule τ_m was estimated from the R_2/R_1 ratio for the amide backbone resonances using the $R_2/R1$_diffusion programme released by Prof. Art Palmer. To determine $\tau_{m,}$ the numbers of nuclear spins with slow internal motions, or

short R_2 values due to chemical or conformational exchange were excluded. These nuclear spins skew the time estimate leading to incorrect estimates of the overall motion of the protein. The slow internal motion of a nuclear spin can be differentiated from the fast motion nuclear spin by the residue specific heteronuclear NOE values. If a residue exhibited an average NOE of smaller than 0.65 the residue was excluded from estimated τ_m. Moreover, the chemical exchange contribution can also lead to an over estimation of R_2/R_1, consequently leading to a longer correlation time. Consequently a standard deviation filter was applied to eliminate residues for which R_2/R_1 values were significantly different from the sample mean (Tjandra et al., 1995) *i.e*. when,

$$\left| \frac{(R_1) - R_{1i}}{(R_1)} - \frac{(R_2) - R_{2i}}{(R_2)} \right| > 1.5 \times SD \qquad \text{Equation [2.20]}$$

where R_1 and R_2 are the sample average longitudinal and transverse relaxation rates respectively, $R_{1,i}$ and $R_{2,i}$ are the individual residue N–H group relaxation rates and SD is the standard deviation over the complete data set of unfiltered ^{15}N R_2/R_1 values ((Tjandra et al., 1995).

The R_2/R_1 predicted values were optimized by estimating the orientation of the rotational diffusion tensor using the available atomic resolution structure. For a monomeric protein like ubiquitin there are six unknown parameters; D_{xx}, D_{yy}, and D_{zz}; the polar coordinates θ and Φ describing the orientation of D_{zz}; and the angle ψ to define the orientation of D_{xx}, where $D_{zz} \geq D_{xx} \geq D_{yy}$. In the case of ubiquitin, the protein is assumed to undergo axial symmetric rotational diffusion. Consequently, $D_{xx} = D_{yy} \neq D_{zz}$ and the only polar coordinates are θ and Φ describing the orientation of D_{zz} within the molecular frame. For the axial symmetric model, $D_{xx} = D_{yy}$ is defined as $D_\perp$ (perpendicular) and D_{zz} is given as $D_\parallel$ (parallel). The ratio of $D_\parallel/D_\perp$ provides a description of the asymmetry of the diffusion tensor. The isotropic rotational diffusion tensor value, D_{iso}, is determined by the following equation:

$$D_{iso} = (D_\parallel + 2D_\perp)/3 \qquad \text{Equation [2.21]}$$

D_{iso} can be used to determine the τ_m since:

$$1/6D_{iso} = \tau_m \qquad \text{Equation [2.22]}$$

Using the programme R_2/R_1_diffusion the four parameters (i.e. D_{iso}, $D_{\|}/D_{\perp}$, θ and Φ) were calculated (as initial estimates for Modelfree analysis) for the various conditions ubiquitin was studied under (see Chapter 3).

Using the calculated initial estimates of τ_m, $D_{\|}/D_{\perp}$, θ and Φ all model parameters for each of the models 1 to 5 were optimised by minimising the error function X^2.

$$X^2 = \frac{\sum_{i=1}^{N} \Gamma = \sum_{i=1}^{N} \sum_{j=1}^{M} \left(R_{ij} - \hat{R}_{ij}\right)^2}{\sigma_{ij}^2} \qquad \text{Equation [2.23]}$$

in which the total number of nuclear spins is N. For the ith spin, Γ_i is the sum squared error, M_i is the number of experimental relaxation parameter, R_{ij} is the jth experimental relaxation parameters, R_{ij} is the jth theoretical relaxation parameter, and σ_{ij} is the experimental uncertainty in the jth relaxation parameter. The statistical degrees of freedom for each model was calculated with a number M_i –p, were p is the number of free internal motional parameter of the statistical model. At one magnetic field strength, model 1 has two degrees of freedom (i.e. p = 1) whereas models 2 and 3 have one degree of freedom. Models 4 and 5 have zero degrees of freedom. By using Monte Carlo simulations using 500 randomly distributed synthetic data sets, the statistical properties of Modelfree parameters were acquired.

To select a model, the five theoretical models were fit to the experimental data, while the τ_m remained fixed. For each model, 500 randomly distributed synthetic data sets were generated as described previously (Palmer et al., 1991). In the first step the simulated data were compared with the experimental data. The results of the simulation were used to determine the cumulative X^2 probability distribution and α = 0.10 critical value (where α is the cut-off level, i.e. 10% of samples fall outside the expected range of values) of Γi (sum of squared errors) for each model. In the next step, the simulated errors generated using a particular model was compared to the simulated errors using a second model, which contains additional one or two parameters. F-test statistics was used to determine the cumulative probability distribution and α = 20 from the simulation results obtained from two models:

$$F_1 = \frac{p_2\left(\Gamma_{1i} - \Gamma_{2i}\right)}{\left(p_1 - p_2\right)\Gamma_{2i}} \qquad \text{Equation [2.24]}$$

in which Γ_{1i} and Γ_{2i} are the sum of squared errors for two models with p_1 and p_2 degrees of freedom ($p_1 > p_2$). To select model 1 the Γ_1 is less than the simulated critical value obtained at a α level equal to 0.1. Model 2 was selected if Γ_1 for model 1 was greater than the appropriate critical value, whereas Γ_2 for model 2 was smaller than the appropriate critical value and the F-statistic comparing models 1 and 2 was greater then the appropriate critical value. The same methodology was used for model 3. For models 4 and 5 the F statistical approach could not be used because these models contain three parameters and therefore have zero degrees of freedom. Instead, spins were fit with three parameter models if Γi was much greater than the critical values for one and two parameter models (generally Γi > 10-fold cut-off value) and Γi was zero for either model 4 or model 5. As additional constraints on model 5, τ_e was required to be less than τ_m and the relative uncertainty in τ_e was required to be less than 100%.

Using the selected models for each residue, Modelfree was subsequently used to optimise the overall (i.e. τ_m $D_{\|}/D_{\perp}$, θ and Φ) and internal motion parameters. The results from this Modelfree analysis are reported in Chapter 3.

Chapter 3

Measuring the stability of H-bonds in ubiquitin by NMR spectroscopy I: the effects of a counter-acting osmolyte

3.1 Introduction

In multicellular organisms some cells are bathed in a fluid which may be subjected to large changes in composition and physical properties, such as salinity, temperature and pH. Such conditions, in turn, lead to changes in the concentration of the intracellular solutes. Proteins are sensitive to changes in the cellular environment. As such, proteins that experience harsh cellular conditions are likely to undergo structural and functional changes that are ultimately fatal to the organism. Therefore organisms have adapted to the perturbations in the cellular environment to ensure that proteins remain stable and function under extreme conditions. Such a mechanism that has evolved in multicellular organisms to protect intracellular proteins involves the synthesis and accumulation of certain small organic solutes known as organic osmolytes (Yancey et al., 1982).

Osmolytes are typically accumulated in the intracellular environment at relatively high concentrations (400 mM) (Yancey and Somero, 1979). At these concentrations,

osmolytes increase thermodynamic stabilities of folded proteins without affecting the cellular processes or biomolecular interactions (Somero, 1986). Osmolytes are divided into two classes: compatible and counter-acting osmolytes. Compatible osmolytes provide protection against water and denaturation stresses without altering cellular process and present a strong selective advantage to the organism in adapting to harsh environments. Representatives of this class include certain amino acids (e.g. proline and glycine) and polyols (e.g. trehalose, sucrose and sorbitol) (Wang and Bolen, 1996, Qu and Bolen, 2003).

Counteracting osmolytes consist of mainly methylamines. Methylamines are generally found in organisms that accumulate high intracellular concentrations of urea (between 0.3 and 0.6 M) (Baskakov and Bolen, 1998b). The high concentrations of urea present in elasmobranches (sharks and rays) cells and mammalian organs such as the kidneys can alter the function of intracellular proteins. Therefore mammalian kidneys including rats, rabbits, possums and humans contain large amounts of methylamines such as glycine, betaine and glycerol phosphorylcholine (GPC), whilst in elasmobranches the predominant methylamine is trimethylamine N-oxide (TMAO) (Somero, 1986).

In contrast to compatible osmolytes which only stabilise proteins, counteracting osmolytes stabilise the protein against the denaturing effects and affect the function of proteins. An example of a biological system which has evolved to protect its intracellular proteins against any denaturant is the cells from the marine shark. Shark cells have high levels of urea (600 mM) that represent a potential denaturing effect on the cellular proteins. However, in these same cells TMAO is also present at a ratio of 3:2 or 2:1 (urea:TMAO) to counteract the denaturing effects of urea and permit normal cellular function by maintaining protein stability (Forster and Goldstein, 1976, Yancey and Somero, 1979). TMAO also plays a role in deep sea fish by counteracting the influence of high hydrostatic pressures on protein structure and function. TMAO may also contribute to the buoyancy of fish.

The ability of TMAO to affect the function of proteins has been shown in a study were the function of the enzyme lactate dehydrogenase (Baskakov and Bolen, 1998b) was measured in a 2:1 urea:TMAO mixture and urea and TMAO separately. The enzyme function decreased in the presence of urea. This was determined by

observing a decrease in k_{cat} (the maximum number of enzymatic reactions catalysed per second) and an increase in the K_m. As TMAO was added to the solution also containing urea, the k_{cat} and K_m values returned to the values observed in the absence of both cosolutes. The addition of TMAO alone to the enzyme solution showed an increase in k_{cat} and a decrease in K_m values which indicated that TMAO not only prevents the denaturation of the enzyme in the presence of urea but also influences the activity of the enzyme. Osmolytes have also been discovered in microorganisms such bacteria and archaea that withstand high temperatures up to 100 ºC (hyperthermophiles) (Martins et al., 1997, Lamosa et al., 2006). These organisms have evolved to accumulate solutes that preserve there cellular components at high temperatures such as mannosylglycerate (MG). A thermal denaturation study of the bacterial protein, nuclease A form Staphylococcus aureus (SNase) in the presence and absence of MG has been performed. The study showed an increase in the T_m by 7 ºC and a two-fold increase in the unfolding capacity where ΔCp increased from 1.7 (±0.5) in the absence of MG to 4 (±1) in the presence of MG. This further indicates that counteracting osmolytes prevent the loss of protein function (Faria et al., 2004).

Various mechanisms have been proposed on how osmolytes stabilise proteins against harsh environmental factors Bolen et al. (1997). have proposed that osmolyte-induced stability is related to backbone solvation. In this study, the protein backbone is considered osmophobic, and therefore the protein folds to bury the majority of the backbone atoms into the core of the protein. Such an effect provides significant stability in the presence of osmolytes (Bolen and Baskakov, 2001). The osmophobic nature of the protein backbone results from differences in the hydrated state of the protein backbone and the osmolyte molecules, which depend on the local water structure and interactions. TMAO thermodynamically stabilises proteins against denaturation due to the highly unfavourable interaction of TMAO with the peptide backbone of the denatured state. This mechanism is called the "osmophobic effect" (Bolen and Baskakov, 2001, Celinski and Scholtz, 2002, Takano et al., 2004).

Thermal unfolding of proteins is generally used to determine the thermodynamic stability of the protein, which is calculated as the Gibbs free energy between the folded and unfolded state ΔG = Gu (unfolded) − Gf (folded). In thermal unfolding

experiments the protein solution is heated at a constant rate and the changes in the protein conformation are monitored by different spectroscopic and calorimetric methods. The parameters recorded from the thermal unfolding experiments include the melting temperature (T_m), enthalpy ($\Delta H(T_m)$) and heat capacity (ΔCp) of unfolding, which are used to determine the protein stability ($\Delta G(T_m)$).

Proteins unfold by heat or denaturing cosolutes and this unfolding leads to an increase in entropy (or in broad terms an increase in disorder). Heating the protein sample shifts the equilibrium between the folded and unfolded states towards the unfolded state. This results in an increase in the transition temperature T1 resulting in an increase in enthalpy ΔH (T1). The other important parameter that increases as the protein is thermally denatured is the heat capacity (ΔCp). Increases in the ΔCp indicate increases in the volume of the protein which occurs as the protein unfolds.

Most natural osmolytes can increase protein thermal stability *in vitro*; however most of these osmolytes increase the thermal stability of proteins at concentrations higher than what is observed in nature. However studies in living organisms have shown that certain carbohydrates such as terhalose in yeast can protect enzymes against thermal denaturation,(Zancan and Sola-Penna, 2005, Faber-Barata and Sola-Penna, 2005) whereas in hyperthermophilic archaea from marine hydrothermal vents have been shown to accumulate β-mannosylglycerate, di-*myo*-inositol phosphate and K^+ as a way to protect the organism from high temperatures and salinities (Lamosa et al., 1998). Trehalose and anionic osmolytes such as these sugar phosphates (paired with K^+) can stabilize proteins at high temperatures, while other osmolytes are much less effective (Yancey, 2005). In general, osmolytes have no biological preference (Wang and Bolen, 1996) and counteract the effects of thermal denaturation of proteins in yeast, (Singer and Lindquist, 1998) mammals (Anjum et al., 2000) and bacteria (Venkatesu et al., 2009). In this chapter the counteracting effects of TMAO on thermal denaturation are examined at various temperatures. Human ubiquitin was chosen as the model protein for this study due to the abundance of NMR and other biophysical data describing the structure, folding and unfolding behaviour of this protein.

Previous studies using different biophysical techniques, such as CD, IR and ITC have illustrated the global effect of osmolytes on protein stability, including H-bond

stability. By directly observing H-bonds via $^{h3}J_{NC'}$ couplings combined with other NMR parameters (^{1}H chemical shifts, $^{1}J_{NH}$ couplings, standard ^{15}N laboratory-frame relaxation analysis) this chapter describes quantitatively the counteracting effect of TMAO against thermal denaturation on individual H-bonds during the initial stages of thermal expansion of ubiquitin.

3.2 The correlation between chemical shift and H-bonds

Many physicochemical factors influence the position of the $^{1}H_N$ chemical shift, including H-bonding. In general, when an amide donor proton forms an H-bond with a carbonyl acceptor group, a downfield shift of the $^{1}H_N$ chemical shift is observed (Wishart et al., 1991, Wishart and Case, 2001). This is due to a reduction in electronic shielding around the H_N nucleus as the acceptor group draws away electron density surrounding the hydrogen nucleus upon H-bond formation (Wishart et al., 1991). While other contributors to the $^{1}H_N$ chemical shift are known, such as ring current effects, H-bonding has been shown to be one of the dominant influences to the chemical shift of this nucleus. Here changes of ~2 ppm have been observed upon the formation of H-bonds (Wagner et al. 1983). Consequently, the $^{1}H_N$ chemical shift has been considered to be a reasonable parameter for measuring the presence of H-bonding in protein structures. Wagner et al. (1983) showed that the $^{1}H_N$ chemical shift is correlated to the H-bond donor-acceptor distance. In this paper, the atomic distances between the amide donor atom d_N and the H-bond acceptor oxygen atom d_O of the basic pancreatic trypsin inhibitor proteins (BPTI) were used to derive a relation between H-bond distance and $^{1}H_N$ chemical shift (Figure 3.2):

$$\Delta\delta H^N / ppm = 19.2 Å^3 d_{HO}^{-3} - 2.3 \qquad \text{Equation [3.1]}$$

Figures 3.2A and B show selected regions of 2D $^{1}H–^{15}N$ HSQC spectra of ubiquitin recorded at 15 (black), 30 (red), 45 (green) and 60 ºC (blue) in the absence and presence of 1.5 M TMAO. In both figures, the $^{1}H_N$ chemical shift values of the peaks shifted upfield as the temperature was increased which correlates with a general weakening of the N–H•••O=C H-bonds. In the presence of 1.5 M TMAO the average $^{1}H_N$ downfield shift observed at 15 ºC is similar to the average chemical observed in the absence of the cosolute (8.67 ppm). However the change in the $^{1}H_N$ chemical shifts ($\Delta\delta$) calculated between 15 and 60 ºC in the absence of cosolute showed an upfield shift of 0.12 ppm, whereas in the presence of 1.5 M TMAO this

shift was slightly less (0.1 ppm). This indicates that the H-bonds in the presence of 1.5 M TMAO are, on average, stabilised in the presence of this osmolyte. Although $^{1}H_{N}$ chemical shifts can be used as a tool to detect H-bonds and measure the changes in the H-bond character (e.g. length), there are other factors (e.g. ring-current effects) that influence the amide proton chemical shifts, resulting in a modest inaccurate analysis of the changes in the H-bond length. This is exemplified by the considerable scatter of the points in Figure 3.1.

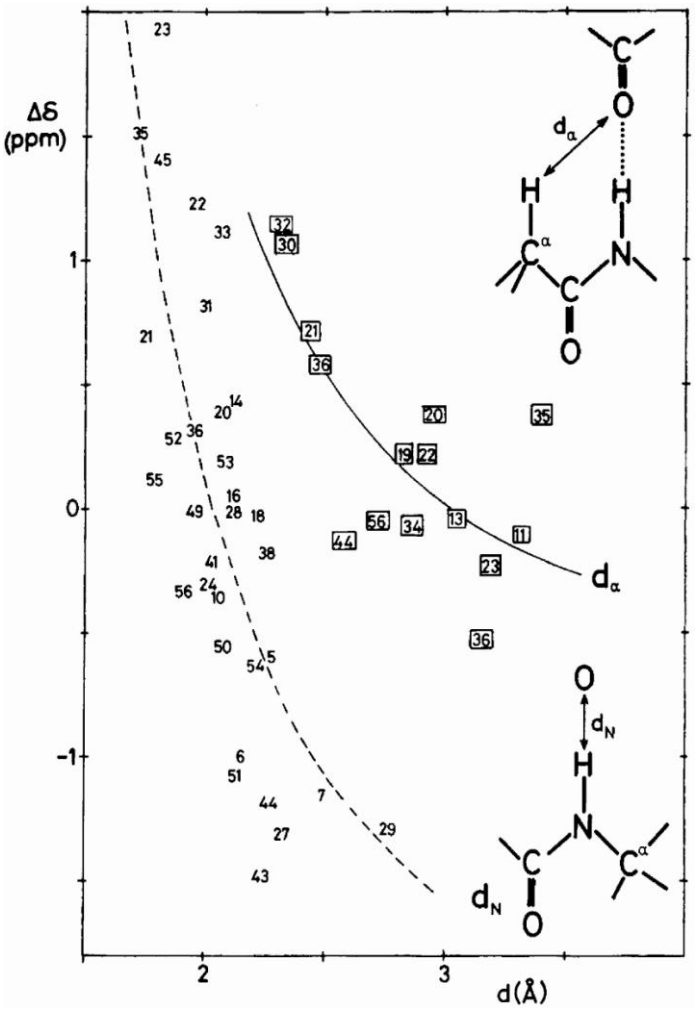

Figure 3.1: The relation between H-bond distance d_{NO} and the chemical shift of H-bonding amide protons in BPTI. The plot of the relation between the proton chemical shifts in the anti-parallel β-sheets versus their distance to the nearest oxygen atom (indicated in squares) is also shown. This figure is taken from (Wagner et al. 1983).

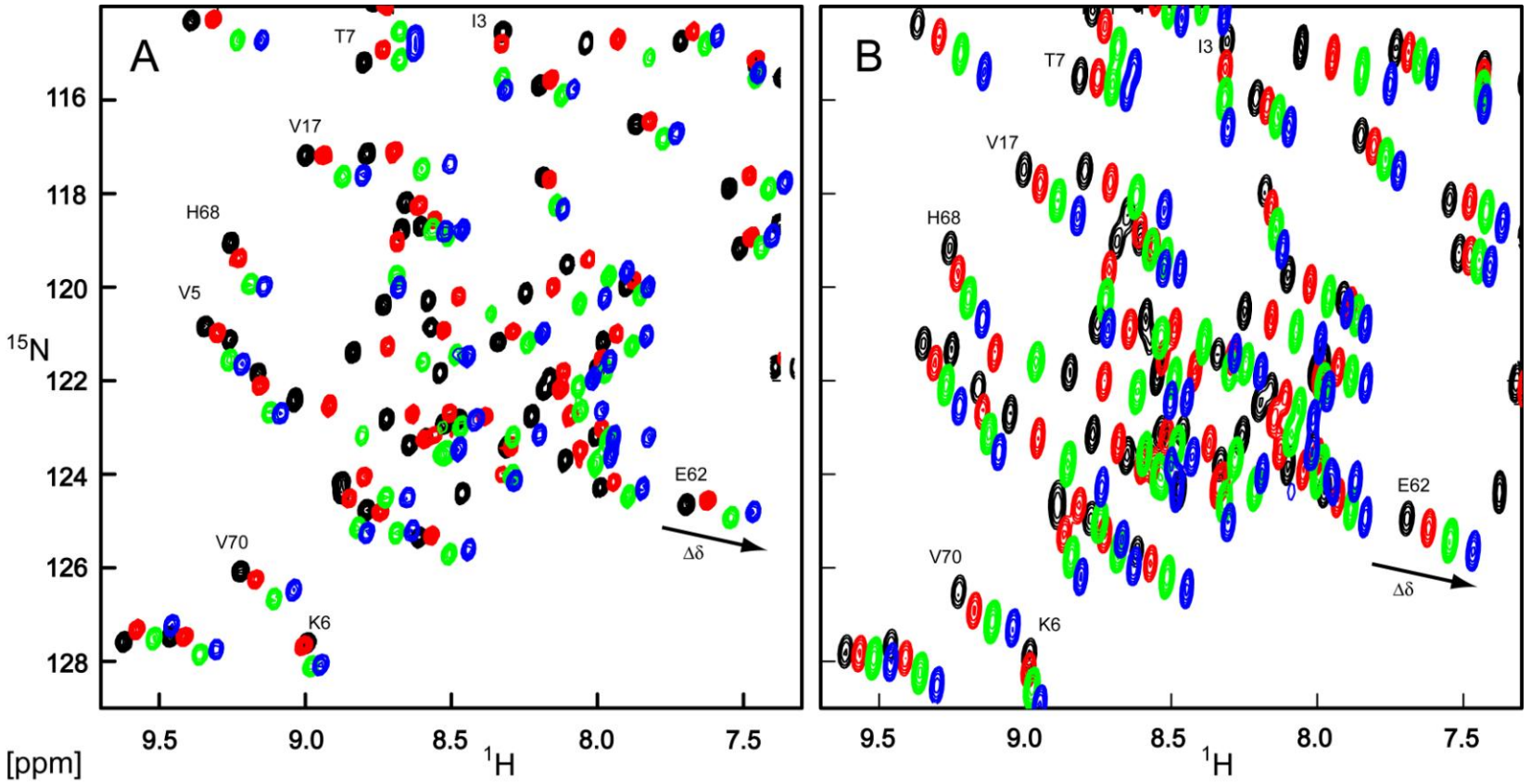

Figure 3.2: An overlay of a region of 2D ^{1}H–^{15}N HSQC spectra of ubiquitin recorded at 15 (black), 30 (red), 45 (green) and 60 ºC (blue) in the absence of the cosolute (A) and in the presence of 1.5 M TMAO (B). There is a clear resolution difference in the ^{15}N dimension between the two spectra. This was due to the lower number of complex points recorded to generate the spectrum in (B).

3.3 The effect of temperature and TMAO on individual H-bonds

In this section the effects of both temperature and TMAO on individual H-bonds in the secondary structure elements of ubiquitin will be examined between 15 to 60 °C. This will be achieved by measuring $^{h3}J_{NC'}$ couplings and will be complemented by measuring $^{1}H_{N}$ chemical shift, $^{1}J_{NH}$ and ^{15}N laboratory-frame relaxation measurements that indirectly probe the stability of the backbone H-bonds in the protein. Measuring changes at higher temperatures was not possible because of hardware limitations, e.g. operation of cryoprobes above 65 °C is not recommended by the manufacturer. Prior to characterising the influence of temperature to each backbone H-bond, the overall influence of temperature and TMAO on the H-bonds in the secondary structure elements will be examined.

Figure 3.3A and B shows the $^{h3}J_{NC'}$ couplings of ubiquitin measured at 15, 30, 45 and 60 ºC in the absence and the presence of 1.5 M TMAO. A general decrease in the size of the $^{h3}J_{NC'}$ couplings were observed as the temperature was increased. This decrease indicates the weakening of H-bonds as a result of thermal expansion of the protein. In the presence and absence of 1.5 M TMAO the thermal expansion of H-bonds (i.e. the weakening of $^{h3}J_{NC'}$ couplings) generally follow the same trend. However in the absence of TMAO (Figure 3.4A) the $^{h3}J_{NC'}$ couplings showed a larger decrease in magnitude as the temperature was increased. In the presence of 1.5 M TMAO, the smaller decreases in $^{h3}J_{NC'}$ couplings are an indication that the backbone H-bonds were protected from thermal expansion. The changes in $^{h3}J_{NC'}$ couplings depicted in Figure 3.3A and B can be translated into changes in the geometry of the H-bonds.

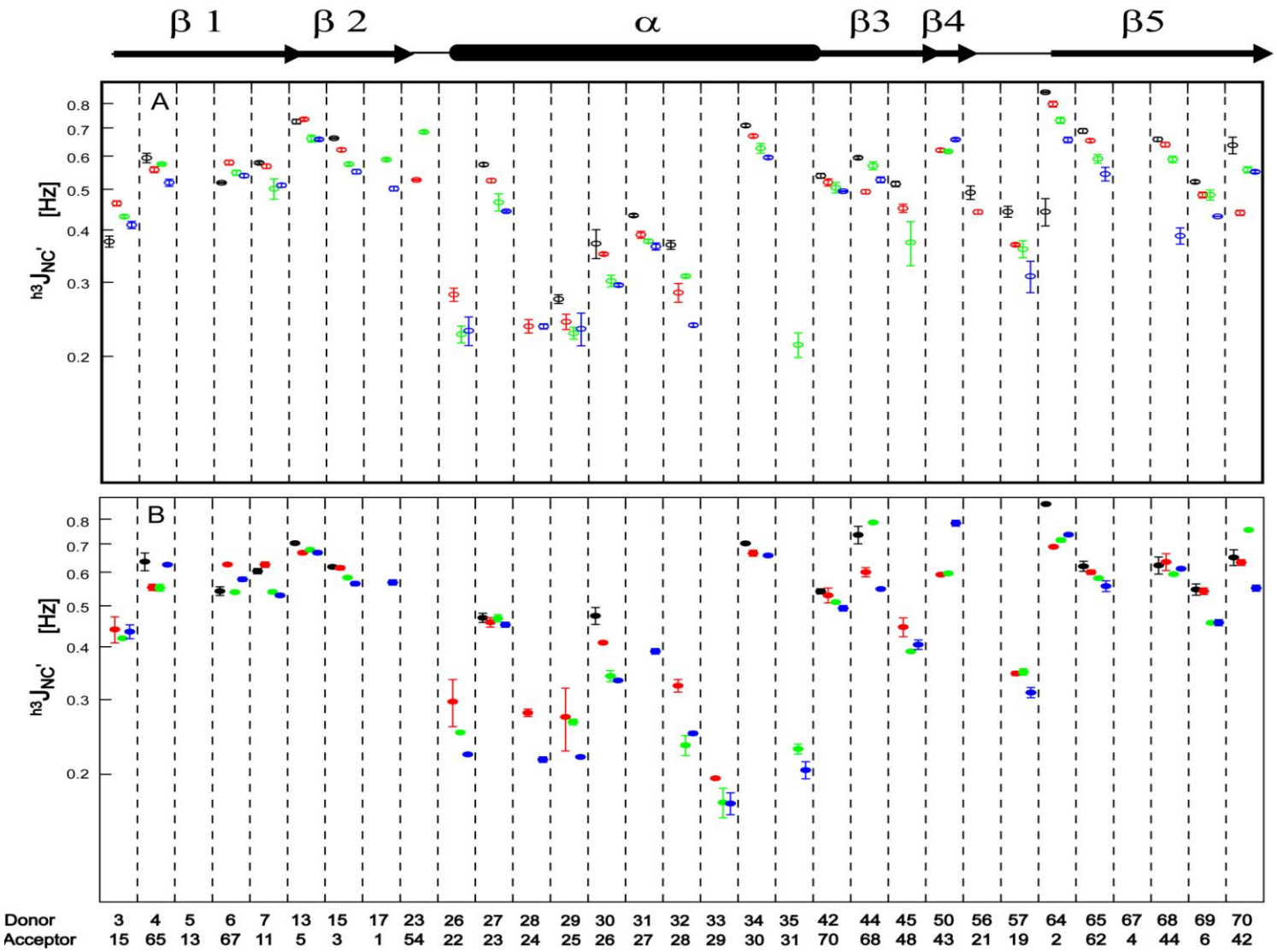

Figure 3.3: The $^{h3}J_{NC'}$ coupling constants for H-bonds in human ubiquitin measured at 15 (black), 30 (red), 45 (green) and 60 ºC (blue) in the absence of solute (A) and in the presence of 1.5 M TMAO (B). Data has been plotted on a logarithmic scale. Error bars correspond to the RMSD deviation of separate experiments.

Although theoretical and experimental studies have indicated that the H-bond length is the dominant factor influencing the size of the $^{h3}J_{NC'}$ coupling (Cornilescu et al., 1999). The multivariate dependencies on distances and angles complicate a direct translation of the changes in the measured $^{h3}J_{NC'}$ coupling values into changes in H-bond geometry. Figure 3.4 shows the theoretical influence of both the r_{HO} and the ∠H•••O=C angle on $^{h3}J_{NC'}$ couplings. Here a change in ∠H•••O=C by 30° at a typical H-bond length of 2.0 Å leads to a change in the $^{h3}J_{NC'}$ coupling of ~0.2 Hz, whereas a change in r_{HO} from 2.2 to 1.8 Å was found to change the coupling by ~1.0 Hz at an ∠H•••O=C angle of 180°. These calculations showed that the $^{h3}J_{NC'}$ couplings are influenced by the ∠H•••O=C to a lesser extent than by the r_{HO} distance. The influence of the ∠N–H•••O angle on the size of the $^{h3}J_{NC'}$ coupling has been theoretically calculated to be even weaker. Interestingly, shorter H-bonds have been found to adopt straighter ∠H•••O=C and ∠N–H•••O values than longer H-bonds (Baker and Hubbard, 1984, Lipsitz et al., 2002). Nonetheless, the HBCs are influenced by both angular and distance dependencies; however, the H-bond distance usually dominates and to a first approximation the effects of the angles on the coupling sizes can be possibly excluded in the analysis (Grzesiek et al., 2004). A comparison of theoretical calculations and experimental HBC values has shown reasonable agreement (Barfield, 2002, Bagno et al., 2000). The difference between the two sets has been ascribed to the internal dynamics in the protein which are absent in the theoretical calculations.(Markwick et al., 2003)

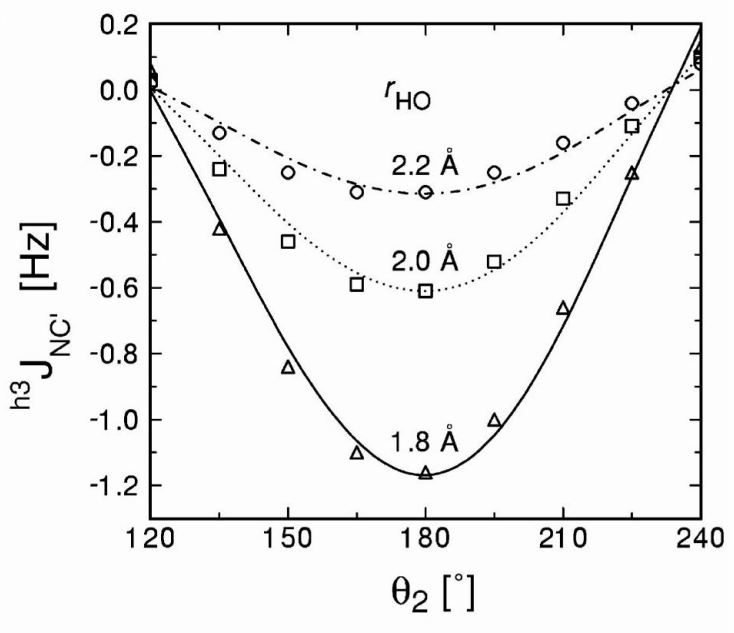

Figure 3.4: DFT results for $^{h3}J_{NC}$ in formamide dimers plotted verses ∠H•••O=C angle in the range 120─240º with r_{HO} = 1.8 Å (triangles), 2.0 Å (squares), and 2.2 Å (circles). The figure is taken from (Barfield, 2002).

Excluding minor variations in H-bond angles and angular dependencies on the couplings (Barfield, 2002), the observed changes in the magnitude of the $^{h3}J_{NC'}$ couplings have been translated into a change in the H-bond length (Cornilescu et al., 1999). Here, an experimental distant relationship between $^{h3}J_{NC'}$ and H-bond length, r_{NO}, has been derived (Figure 3.5):

$$^{h3}J_{NC'} = -5.9\times10^{4}\,Hz\exp(-4r_{NO}/\text{Å}) \pm 0.09\,\text{Hz} \qquad \text{Equation [3.2]}$$

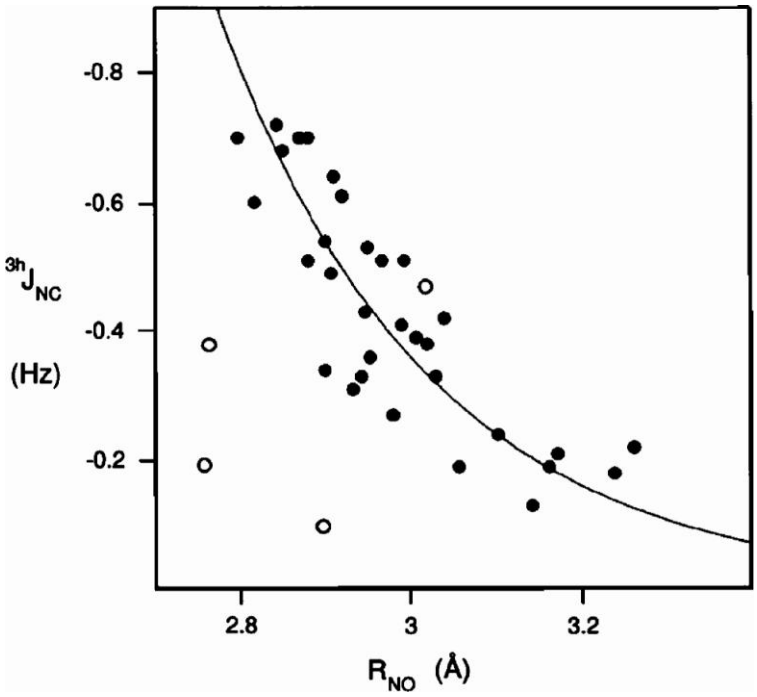

Figure 3.5: Correlation between the $^{h3}J_{NC'}$ values and H-bond lengths in protein G, averaged over three crystal structures (1IGD, 2IGD, and 1PGB), to which protons were added with X-PLOR, assuming r_{NH} = 1.02 Å. Figure has been taken from (Cornilescu et al., 1999).

This relation arises from the electronic orbital overlap which shows an exponential dependence to the atomic nucleus (Cornilescu et al., 1999). Equation [3.2] can be rearranged to calculate the r_{NO} distant as a function of the $^{h3}J_{NC'}$ couplings:

$$d_{NO} = -0.25\text{Å} \ln\left[\frac{^{h3}J_{NC'}}{5.9 \times 10^4 Hz} \right] \qquad \text{Equation [3.3]}$$

The neglect of angular dependencies in Equations 3.2 and 3.3 leads to an overestimation of the distance changes. The measured $^{h3}J_{NC'}$ couplings are presented in Figure 3.3 on a logarithmic scale. Although errors in the $^{h3}J_{NC'}$ measurements for some H-bond couplings were non-negligible, the variations between individual H-bonds lie outside the reproducibility error of the measurement and are therefore meaningful changes. The average $^{h3}J_{NC'}$ couplings recorded at 15, 30, 45 and 60 ºC in the presence and absence of TMAO are depicted in Figure 3.6.

The average $^{h3}J_{NC'}$ couplings calculated were for couplings observed at all four temperatures and in both the presence and absence of TMAO (i.e. eight datasets). Therefore the number of $^{h3}J_{NC'}$ couplings used in this figure for all H-bonds was *n* = 16, for H-bonds in the β-sheet *n* = 12 and for the α-helix H-bonds *n* = 3. The

absence of other H-bond couplings (in particular in the α-helix) in the analysis was due to the absence of data at 15 °C for the protein sample in the presence of TMAO. At this temperature and in the presence of this solute, the viscosity was such that signal intensities for many expected H-bond correlations in the long-range HNCO experiment were broadened and not detected. Longer experiments could have been recorded; however, as experiments were already on the order of 2-3 days, the required increase in signal-to-noise would have resulted in 10 day experiments, which is time-consuming and impractical.

As a first step in interpreting the thermal changes to individual H-bonds, a simple calculation of the change in r_{NO} can be made using Equation [3.3]. The average $^{h3}J_{NC'}$ couplings (n = 16) showed an average increase of 0.049 Å in H-bond length between 15 and 60 ºC in the absence of TMAO. However in the presence of 1.5 M TMAO the H-bonds showed an average increase of 0.030 Å. The smaller average change in the H-bond lengths in the presence of 1.5 TMAO is a clear indication of the stabilising effect TMAO has on the overall structure of the protein. For the secondary structure elements, the average $^{h3}J_{NC'}$ couplings for β-sheets (n = 12) showed an increase of 0.040 Å in the absence of TMAO and an increase of 0.027 Å in the presence of TMAO, whereas for the H-bonds in the α-helix the difference in H-bond length was 0.032 Å in the presence of TMAO and in the absence of TMAO the increase in H-bond length was 0.053 Å. Studies have shown that TMAO increases the water-water H-bond network surrounding the protein. This effect provides stability to the protein in denaturing conditions. The influence of temperature to the length of individual H-bonds was also examined. In particular, and as an example, the H-bond H68/I44 showed the largest thermal expansion in the absence of TMAO of 0.132 Å. The addition of TMAO reduced this change in H-bond length to only 0.006 Å.

As mentioned briefly above, although Equation [3.3] can be used to deduce a lengthening in the average H-bond lengths of ubiquitin, there are inaccuracies in the crystallographic model of the structure that were derived for this equation. In addition, the angular dependence of the $^{h3}J_{NC'}$ couplings and the internal dynamics of the protein influence the sizes of the couplings. The influence of physicochemical conditions of the crystal structure versus the solution measurements should also be considered.

Figure 3.6 depicts the average $^{h3}J_{NC'}$ couplings measured in the absence and presence of 1.5 M TMAO. As previously shown,(Cordier and Grzesiek, 2002) the derivative of the $\ln|^{h3}J_{NC'}|$ with respect to temperature is a measure of the linear thermal expansion coefficient ($\alpha L = r_{NO}\, \delta r_{NO}/\delta T$) of the H-bond. Using the simple assumption that the average r_{NO} is 3.0 Å, αL can be estimated from:

$$\alpha L \approx -\frac{1}{12}\frac{\delta \ln |^{h3} J_{NC'}|}{\delta T} \qquad \text{Equation [3.4]}$$

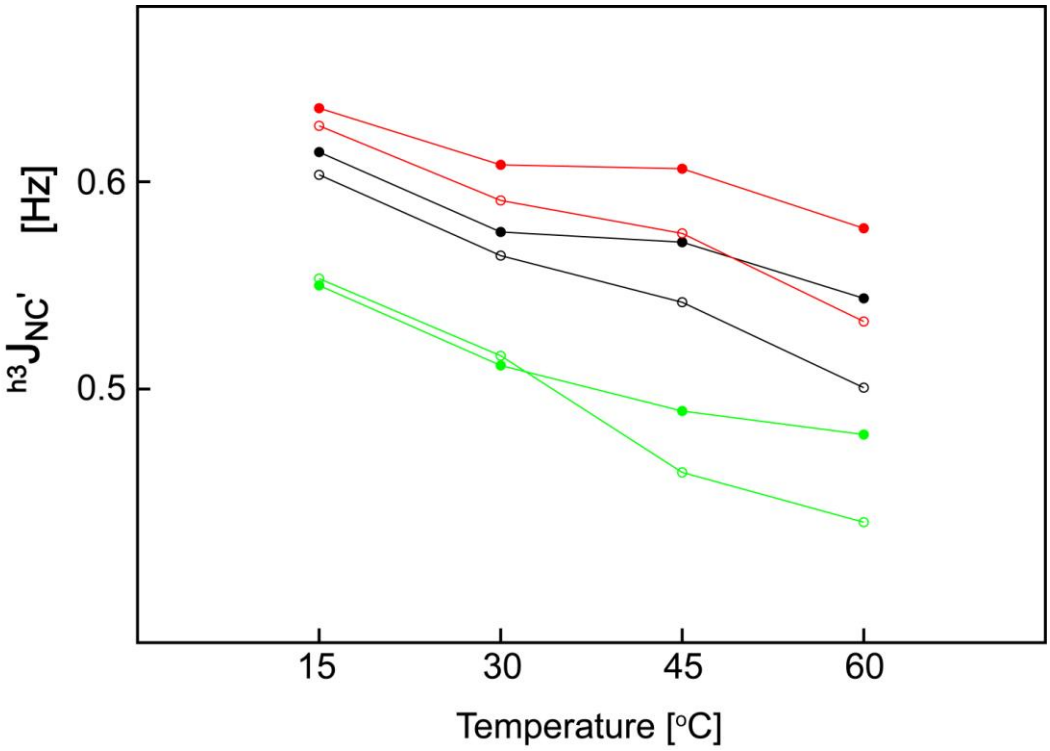

Figure 3.6: The average values of $^{h3}J_{NC'}$ couplings for different regions of the protein: all backbone H-bonds (black); H-bonds involved in the β-sheet (red); and H-bonds involved in the α-helix (green). Open circles represent data in the absence of cosolute and closed circles represent data in the presence of 1.5 M TMAO. The missing data points for weak H-bonds introduce a bias towards stronger average couplings.

From Equation 3.4 and the slopes in Figure 3.6 the thermal expansion coefficients were calculated in the absence and presence of 1.5 M TMAO over the range of 15 to 60 ºC (Table 3.1; Figure 3.7). For all the backbone H-bonds (n = 16) the expansion coefficient αL was 3.3 (± 0.22) × 10^{-4}/K in the absence of TMAO, whereas αL in 1.5 M TMAO was 2.16 (± 0.2) × 10^{-4}/K. The results show that the presence of TMAO reduces the rate of thermal expansion. The secondary structure elements showed an expansion coefficient αL of 3.0 (± 0.37) × 10^{-4}/K for the β-

sheets (n = 12) in the absence of TMAO and a 1.75 (± 0.2) × 10^{-4}/K in the presence of 1.5 M TMAO. The expansion coefficient αL for the α-helical H-bonds (n = 3) were much larger 4.16 (± 0.8) × 10^{-4}/K in the absence of TMAO and 2.4 (± 0.15) × 10^{-4}/K in the presence of 1.5 M TMAO. A previous measure of the thermal expansion coefficient calculated from $^{h3}J_{NC'}$ coupling values for H-bonds in ubiquitin in the absence of solutes were smaller.(Cordier and Grzesiek, 2002) This difference is most likely due to the small number of H-bond couplings (i.e. sixteen from a possible 33) used in this study for data recorded at all four temperatures. Therefore, observing only the strong coupling leads to a bias in the calculations because the weaker coupling generally show a smaller thermal expansion in comparison to the stronger H-bond couplings.

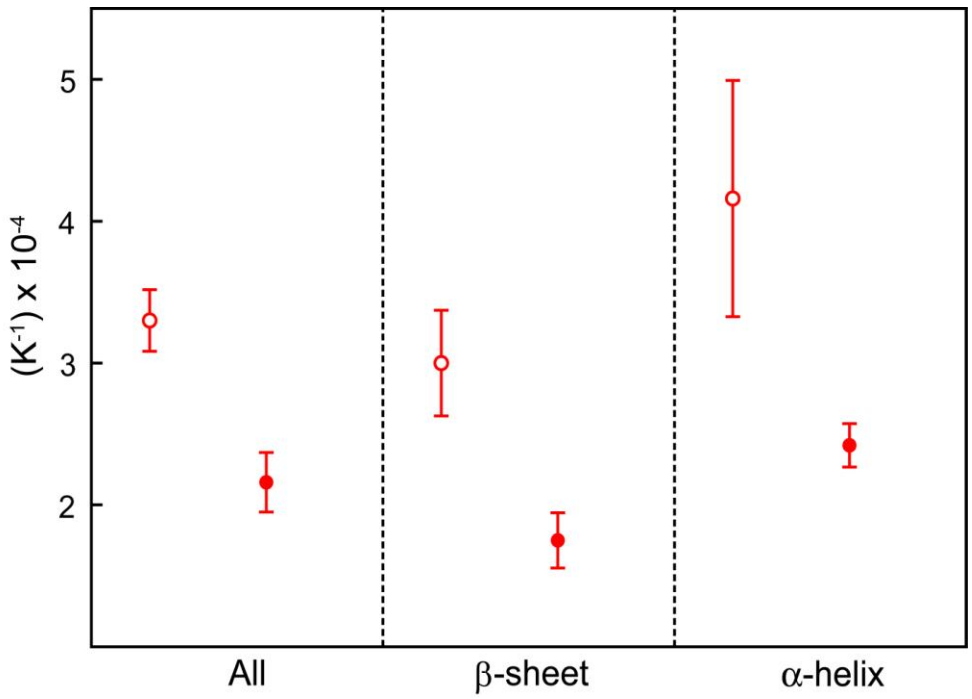

Figure 3.7: The linear thermal expansion coefficient αL of ubiquitin in the absence of cosolute (open circles) and in the presence of 1.5 M TMAO (filled circles) calculated assuming an average r_{NO} value of 3.0 Å and using the expression $\Delta\ln|^{h3}J_{NC'}|/\Delta T$ calculated from linear regression of the average $^{h3}J_{NC'}$ coupling values at each temperature studied**.**

Table 3.1 Thermal expansion coefficient measurements in $K^{-1} \times 10^{-4}$

	No cosolute	1.5 M TMAO
All	3.30 ± 0.22	2.20 ± 0.20
β-sheet	3.30 ± 0.37	1.75 ± 0.20
α-helix	4.16 ± 0.80	2.40 ± 0.15

3.4 The effect of temperature and TMAO on protein dynamics

^{15}N spin relaxation measurements where conducted to probe the effects of temperature and TMAO on the dynamics of ubiquitin in general and on the N–H moieties involved in H-bonds in the secondary structure elements. ^{15}N spin relaxation measurements provide information on the internal bond motion of the protein molecule in various chemical environments and also the overall rotational times of the molecule (Palmer et al., 2001). From the spin relaxation measurements the squared order parameter (S^2) can be extracted which provides important information regarding the conformational states and fluctuations of the amide backbone groups and the effect of TMAO on the thermodynamic stability of ubiquitin.

Spin relaxation measurement provide information on fast motions on the timescale of pico- and nanoseconds, or slow motions on the timescale of micro to milliseconds. For an excited two-spin system (^1H-^{15}N) present in a B_0 field, several relaxation mechanisms exist that bring the system back to equilibrium with its surrounding environment. Usually, these mechanisms are the longitudinal relaxation R_1, the transverse relaxation R_2 and the steady state [1H]–^{15}N heteronuclear Overhauser effect (NOE) (Kay et al., 1989). Dynamic processes of proteins in various environments can be characterised by measuring these three NMR mechanisms (Dyson and Wright, 2004).

The ^{15}N R_1 and R_2 rates and the steady-state [1H]–^{15}N NOE were measured for ubiquitin at 15 and 60 ºC in the presence and absence of 1.5 M TMAO at a field strength of 14.1 Tesla (see Chapter 2.6.4). The determined ^{15}N R_1 and R_2 rates and

the steady-state [1H]–^{15}N NOE values for ^{15}N nuclei in H-bonds in secondary structure elements are shown in Figure 3.8. The average R_1 and R_2 rates for ubiquitin at 15 °C in the absence of TMAO were 1.8 (± 0.003) and 8.0 (± 0.25) s^{-1}, whereas the average values in the presence of 1.5 TMAO were 1.38 (± 0.02) and 11.2 (± 0.5) s^{-1}. At 60 ºC the average R_1 and R_2 in the absence of TMAO were 2.3 (± 0.004) and 3.7 (± 0.15) s^{-1}, and in the presence of 1.5 M TMAO the values were 2.3 (± 0.01) and 4.7 (± 0.026) s^{-1}. The NOE values in the absence and presence of TMAO at 15 ºC were 0.73 (± 0.005) and 0.74 (± 0.16), respectively, and the values for 60 ºC in the absence and presence of TMAO were 0.56 (± 0.006) and 0.66 (± 0.009).

The average R_1 values for H-bond NH donors in the presence (filled black circle) and absence of TMAO (black open circle) at 15 °C were 1.35 (±0.02) and 1.68 (± 0.004) s^{-1} respectively. The R_1 values measured at 60 °C in the presence and absence of 1.5 M TMAO were 2.35 (± 0.007) and 2.22 (± 0.003) s^{-1}, respectively. The lower average value measured for R_1 at 15 °C in the presence of 1.5 M TMAO is due primarily to the much higher viscosity of the solution (see Table 2.3) at this temperature. This leads to a slower overall rotation correlation time and therefore the observed decrease in the R_1 values at this temperature when compared to the R_1 values in the absence of TMAO. At 60 °C the R_1 values showed only a minor difference between the two datasets. This is perhaps not surprising given that the data in Table 2.3 shows that the difference in viscosities in the presence and absence of 1.5 M TMAO at 15 ºC is much larger than the difference at 60 ºC. Hence this larger difference in viscosities at 15 ºC affects the rotational correlation time significantly more at this temperature and leads to the overall larger differences in the relaxation data. In summary, the R_2 and R_1 values are influenced strongly by the differences in the solution viscosities; however, other factors such as internal fast and slow motions, which are not clearly apparent from the relaxation data, were revealed on performing a Modelfree analysis (see below).

For the R_2 values measured for the H-bond NH donors at 15 °C in the absence of 1.5 TMAO the value was 7.56 (±0.25) s^{-1}, whereas in the presence of 1.5 M TMAO the R_2 was 11 (±0.5) s^{-1} demonstrating the influence of viscosity to the measured average rates. In contrast, at 60 °C the difference between the R_2 values

measured in the absence of 1.5 M TMAO (3.53 ± 0.07 s^{-1}) and presence of 1.5 M TMAO (4.6 ± 0.01 s^{-1}) was smaller. Therefore R_2 values were influenced in a similar manner to the R_1 value by the differences in the viscosities of the samples studied.

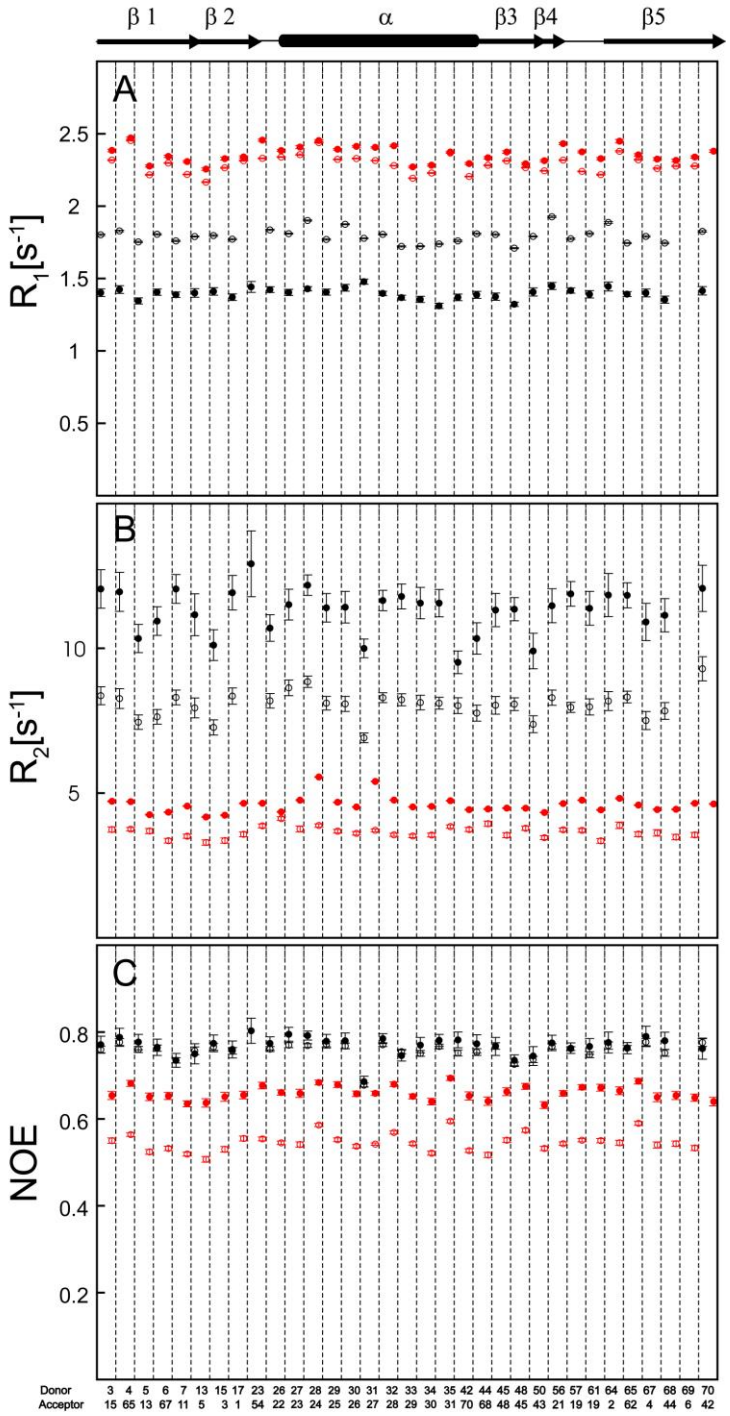

Figure 3.8: Residue specific NMR relaxation rates for H-bond NH donors. Longitudinal (R_1) (A), and transverse (R_2) (B) relaxation rates and the steady state heteronuclear NOE (C) are shown at 15 ºC in the absence of TMAO (open black) in the presence of TMAO (filled black) and at 60 °C in the absence of TMAO (open red) and presence of TMAO (closed red).

The relaxation data were used to extract Modelfree parameters (see Section 2.5.4) for each residue examined. The programme Modelfree uses the extended Lipari-Szabo model formalism (Lipari and Szabo, 1982a,b, Clore et al., 1990) to extract the order-parameters (i.e. S^2) and other motional parameters from the acquired residue specific relaxation data. S^2 is a convenient measure of the amplitude of bond motions, in which a value of one indicates restricted or no motion whereas a value close to zero indicates very low order and essentially unrestricted motion. Below is an overview of the calculated S^2 values.

From the modelfree analysis the average rotational correlation times, τ_c for ubiquitin at 15 and 60 °C in the absence and presence of TMAO determined. The τ_c at 15 °C in the presence and absence of TMAO was 6.0 and 8.5 ns respectively, whereas at 60 °C the correlations timed were 1.8 ns in the absence of cosolute and 2.8 ns in 1.5 M TMAO. The increase in τ_c is consistent with the increase in solution viscosity. The τ_c values obtained from model corroborate with the τ_c values calculates using Stokes-Einstein- Deybe equation (Chapter 2).

The overall average order parameter S^2 values at 15 and 60 ºC in the absence of 1.5 M TMAO were 0.86 ± 0.0013 (n = 55) and 0.81 ± 0.003 (n = 55), respectively. In the presence of TMAO the S^2 values were 0.88 (n = 55) ± 0.013 and 0.83 ± 0.0017 (n = 55) at 15 and 60 °C, respectively. The average S^2 values for the H-bonds in secondary structure elements depicted in Figure 3.10A were 0.81 ± 0.014 (n = 31) and 0.86 ± 0.003 (n = 32) at 15 ºC in the absence and presence of 1.5 M TMAO, respectively, whereas at 60 ºC the S^2 values were 0.79 ± 0.001 (n = 32) and 0.83 ± 0.002 (n = 33). The tabulated residue S^2 values and τ_e and R_{ex} values are provided in the Appendices (9, 10 and 11). The S^2 results showed that backbone N–H groups in ubiquitin in the presence of TMAO at both temperatures show lower amplitudes of internal motions compared with the data in the absence of the cosolute. Consequently, as TMAO reduced the amplitudes of motions of backbone N–H groups in ubiquitin the overall thermal stability of the protein was found to increase. For the H-bond N−H donor atoms the increase in S^2 values at 15 ºC in the presence of TMAO is more pronounced on the terminal ends of the secondary structure elements (Figure 3.11). The β1/β2/β5 secondary structure

residues I3, F4 and V17 showed the highest S^2 values. The more pronounced restriction in the amplitude motion of these three residues can indicate that they are important for the stability of the β1/β2/β5 secondary structure. The two residues L50 and V70 located on the C and N terminus of the β3/β4/β5 structures, respectively, showed the highest S^2 values. As for the α-helix, the S^2 values are on average higher than any other region of ubiquitin. This can be due to the α-helix residues being more solvent exposed; therefore TMAO has a greater effect on stabilising the residues and restricting there motion. Furthermore, the highest S^2 value is for residue A28 which is positioned on the solvent exposed side of the α-helix. At 60 ºC in the absence of TMAO the S^2 values decrease indicating an increase in thermal induced motion of the N−H amide bonds. In the presence of TMAO the S^2 values at 60 °C have increased, indicating that the amide bond motions are restricted and the protein is more stable. In the next section the S^2 values will be compared in more detail with the $^{h3}J_{NC'}$ couplings measured.

A feature of Modelfree models 2, 4 and 5 is the inclusion of the internal correlation time τ_e which accounts for additional picosecond time-scale motions (Clore et al., 1990). Figures 3.9 and 3.10 depict the τ_e (psec) and R_{ex} (μs-ms) motions for H-bond NH donors in ubiquitin. In general there are more τ_e (psec) values observed in the absence of TMAO than in the presence at both 15 and 60 ºC. At 15 °C in the absence of TMAO 25 τ_e values were determined for the NH H-bond donor, whereas in the presence of TMAO 19 values were calculated. The average values for τ_e were 27.5 ± 8 psec and 26.6 ± 4 psec at the two respective temperatures. This indicates that the difference in the fast internal correlations is negligible in the absence and presence of TMAO. Similar to 15 ºC the difference in τ_e values at 60 ºC in the presence of TMAO (25.8 ± 4 psec) and in the absence of TMAO (25.8 ± 2 psec) is insignificant. Since τ_e provides information on very fast internal bond motions on the psec time scale, the values provide a probe on the conformational flexibility of the NH amide donors in the presence and absence of TMAO. However, the differences in τ_e between 15 and 60 ºC were negligible as were the differences in the presence and absence of TMAO.

Slower internal motions (micro to milliseconds μs-ms; R_{ex}) were observed and accounted for by models 3 and 4 of the Modelfree programme. In the absence of

TMAO at 15 °C no R_{ex} was observed, whereas in 1.5 M TMAO three residues showed R_{ex} exchange. At 60 °C in the absence of TMAO only one residue showed R_{ex} exchange in comparison to the 10 residues in 1.5 M TMAO. In the presence of TMAO the three residues that showed R_{ex} exchange at both 15 and 60 °C were K7, K33 and E34. The average R_{ex} exchange for these three residues was higher at 15 ºC (1 ± 0.5 ms) in comparison to 0.18 ± 0.17 at 60 ºC.

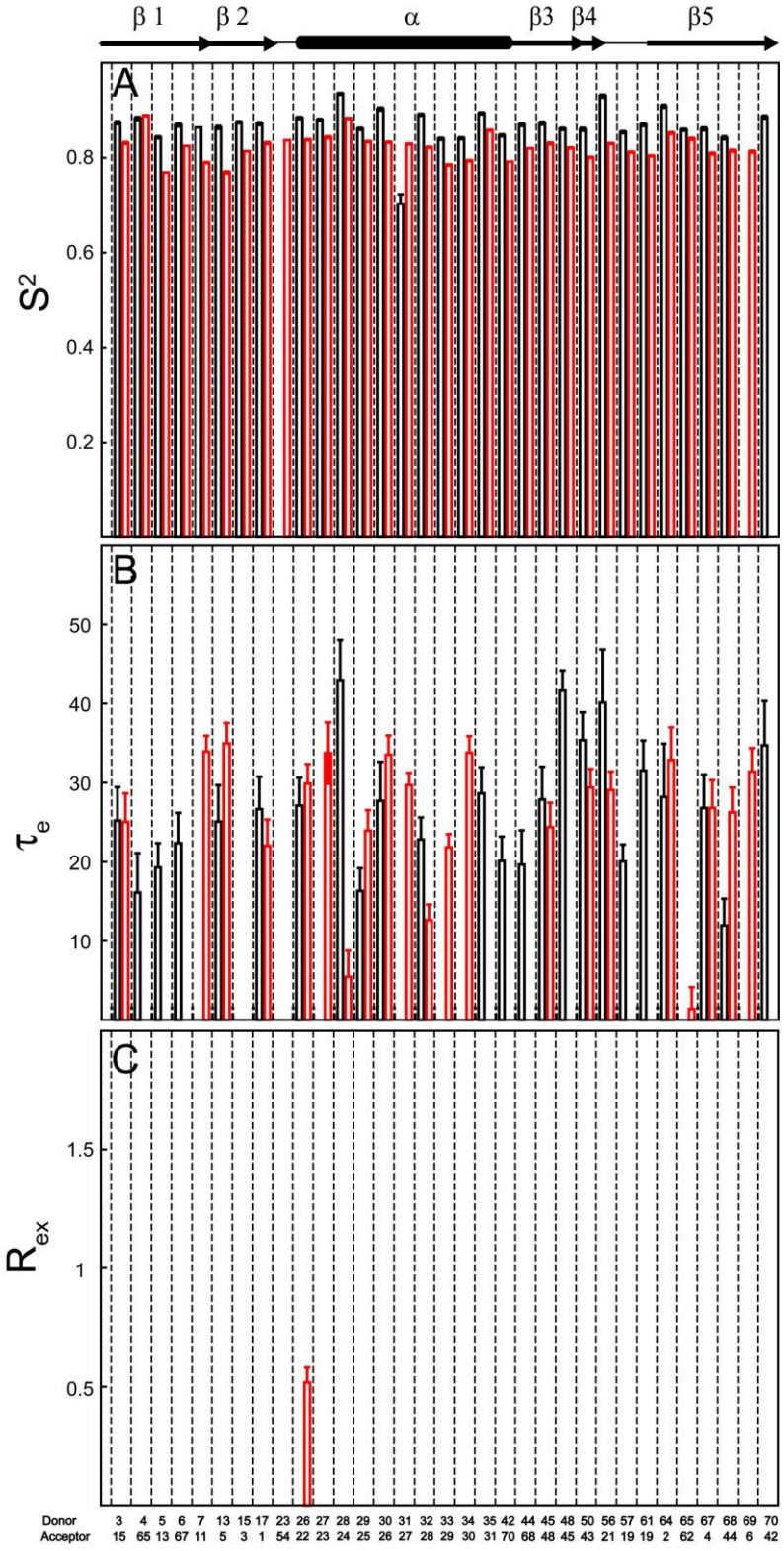

Figure 3.9: Residue specific order parameters S^2 (A), internal correlation time τ_e (B) and conformation exchange rate R_{ex} (C) for H-bond NH donor groups of ubiquitin are presented: 15 ºC (open black histogram), and at 60 ºC (open red histogram) in the absence of TMAO.

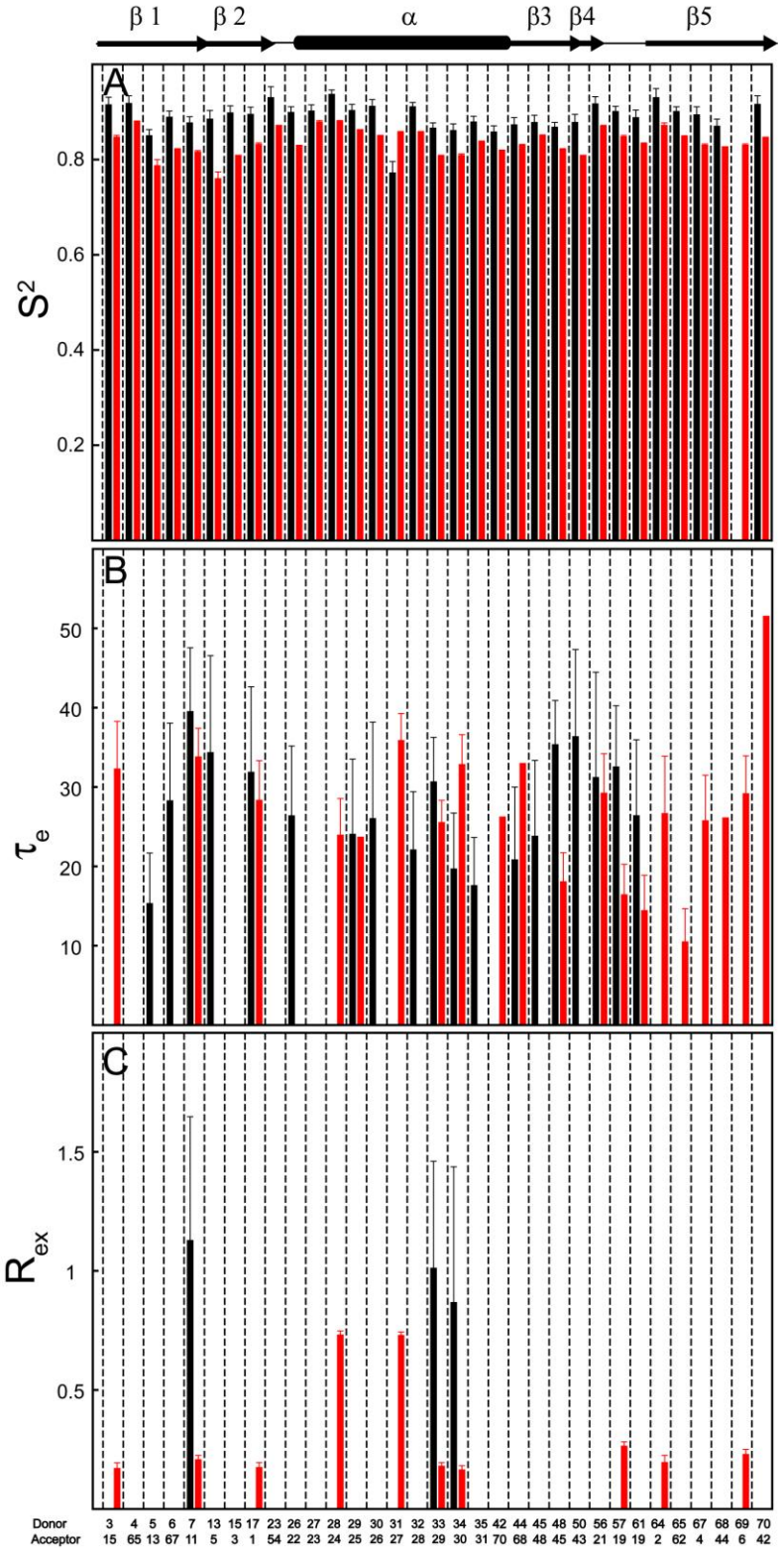

Figure 3.10: Residue specific order parameters S^2 (A), internal correlation time τ_e (B) and conformation exchange rate R_{ex} (C) for H-bond NH donor groups of ubiquitin in the presence of 1.5 M TMAO are presented: 15 ºC (black histogram) and at 60 ºC (red histogram).

3.5 The effect of temperature and TMAO on H-bond properties in secondary structure elements

Figure 3.3 clearly showed that the $^{h3}J_{NC'}$ couplings for various H-bonds in ubiquitin are affected by the increase in temperature. These temperature-dependent changes in $^{h3}J_{NC'}$ couplings are a result of changes in the lengths and angles of the individual H-bonds. The temperature induced changes to the $^{h3}J_{NC'}$ couplings for the H-bonds positioned in the α-helix and between β-strands β5/β3, β3/β4, β2/β1 and β1/β5 will be compared with changes in the $^{1}H_{N}$ chemical shifts and the $^{1}J_{NH}$ couplings. In addition, the NMR data will be examined in relation to the H-bond geometries derived from the 1.8 Å X-ray crystal (1ubq)(Vijay-Kumar et al., 1987) and the 10 lowest-energy NMR derived structures (1d3z) (Cornilescu 1998) The S^2 order parameter derived from ^{15}N laboratory-frame relaxation experiments will also be used in the analysis. The following are simple definitions that will be used in the analysis. These definitions are used to link the changes in the NMR parameter values to approximate geometric changes in the H-bonds:

(i) **$^{1}H_{N}$ chemical shifts**: The changes in the $^{1}H_{N}$ chemical shift are manifested from the change in the geometry of the N–H donor and C=O acceptor groups of the H-bond, where a downfield shift is a result of deshielding of the amide proton nucleus and is likely to indicate a strengthening of the H-bond or, in simplest terms, a decrease in the distance between the amide proton and the oxygen acceptor atom (i.e. electron withdrawal due to the acceptor group). Note angular dependencies are also influencing this change; however, most likely to a lesser degree.(Barfield et al., 2001)

(ii) **$^{1}J_{NH}$ couplings**: Scalar interactions are dependent on the four Ramsay terms, with the Fermi contact term being the dominant of the four terms (Ramsey 1952). In the case of the $^{1}J_{NH}$ coupling, the largest contribution arises from the s-orbital spin-density centred at one nucleus, i.e. ^{1}H, overlapping with the coupled nucleus, i.e. ^{15}N; therefore the size of the coupling is very strongly (but not solely) dependent on the bond length. The N–H bond length thus depends on its immediate electronic environment with H-bonding playing a significant role. Consequently observed changes in the $^{1}J_{NH}$ couplings are a result of changes in the covalent bond length between the ^{15}N and ^{1}H atoms of the donor amide

group. For example, if the H-bond is shortening in length the corresponding $^{1}J_{NH}$ coupling should decrease in absolute magnitude as the N–H bond length increases, i.e. the H atom is drawn to the acceptor group and therefore the bond length increases. Conversely, as the H-bond length increases (weakens), the size of this coupling should increase.

(iii) **$^{h3}J_{NC'}$ coupling**: The $^{h3}J_{NC'}$ coupling will be influenced by both angles and distances associated with the H-bonds.

(iv) **S^2 values**: Relaxation analysis will provide some insights into how amplitude motions of the donor groups influence the character of the H-bonds.

By combining these general rules, some simple interpretations of the changes in the NMR parameters can be used to extract an understanding of the changes in the H-bond geometries.

3.6.1 The α-helix

Ubiquitin has a single α-helix that constitutes residues I23 to G35. The C-terminus end of the helix (i.e. K33 to G35) is bent due to the decrease in the ψ from −44 to 5º and the increase in the ϕ of G35 to 81º (Cordier and Grzesiek, 2002) (Appendix 16). The α-helix whose amide groups are bonded from H^N (i) → O (i−4) are analysed in more detail from V26 to G35. The measured $^{h3}J_{NC'}$ couplings for H-bonds in the α-helix range from −0.2 to −0.7 Hz in magnitude. Figure 3.11A shows the $^{h3}J_{NC'}$ couplings, $^{1}J_{NH}$ couplings, $^{1}H_N$ chemical shifts and the S^2 order parameters. In addition, the H-bond geometries within the α-helix are presented in Figure 3.11B.

At the initial temperature of 15 °C in the absence of cosolute (Figure 3.10A, black symbols) the four H-bonds that gave rise to the strongest $^{h3}J_{NC'}$ couplings are K27/I23, I30/V26, Q31/K27, and E34/I30. These H-bonds are located on one face of the α-helix that is directed towards the hydrophobic side of the β-sheet. As previously indicated (Vijay-Kumar et al., 1987, Cordier and Grzesiek, 2002), this is a result of a slight curvature in the α-helix giving rise to shorter H-bonds (< 2.0 Å) on the hydrophobic side of the α-helix. Note that in the crystal structure of ubiquitin, no such helix curvature is reported and this discrepancy has been

suggested to be due to the limited resolution of the crystal structure of 1.8 Å (Vijay-Kumar et al., 1987). For the K27/I23, I30/V26, Q31/K27, and E34/I30 H-bonds the shorter r_{NO} lengths lead to slightly stronger $^{h3}J_{NC'}$ values, whereas the longer H-bonds (> 2.0 Å; V26/T22, A28/E24, K29/N25, K33/K29 and G35/Q31) are located on the solvent exposed side of the α-helix and give rise to weaker $^{h3}J_{NC'}$ couplings. The only exception is H-bond D32/A28 which has the shortest r_{OH} (X-ray data; ~1.9 Å) yet an $^{h3}J_{NC'}$ coupling which is only slightly stronger than the other solvent exposed H-bonds. However, in the NMR derived structures (Cornilescu et al., 1998), this H-bond length (~2.1 Å) is comparable to the r_{OH} values for H-bonds located on the solvent exposed side of the helix, thus indicating true differences between the crystal and NMR structures for this H-bond. In the presence of 1.5 M TMAO (Figure 3.11A, red) only three $^{h3}J_{NC'}$ couplings were observed, K27/I23, I30/V26 and E34/I30, at 15 ºC and are located on the hydrophobic side of the α-helix. The absence of many of the couplings is due to the presence of 1.5 M TMAO increasing the viscosity of the sample. The increase in viscosity slows the overall tumbling rate of the protein to such an extent that the relaxation rates are too fast to effectively measure the couplings in a reasonable experimental time period (as explained in Section 2.3).

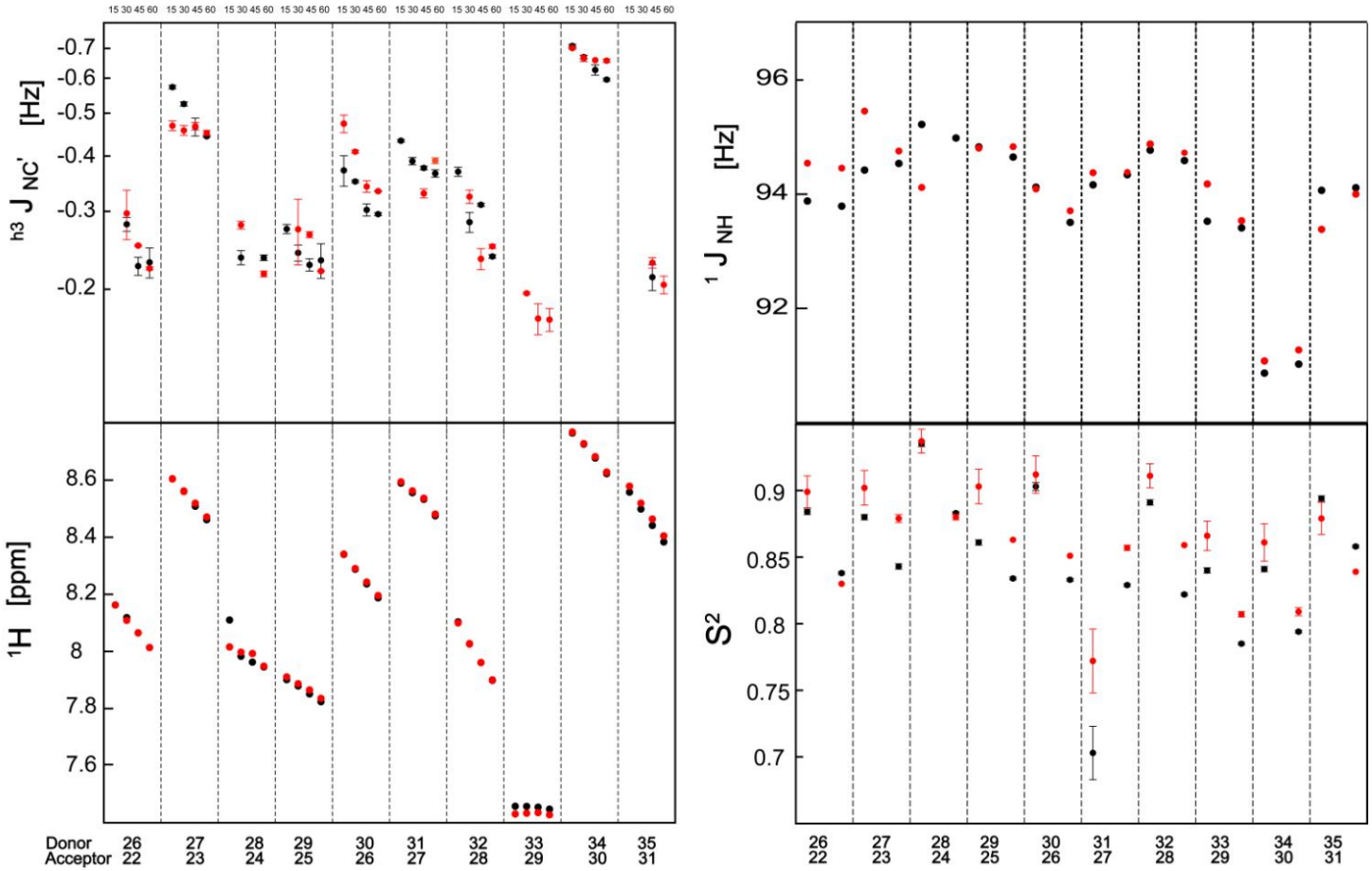

Figure 3.11A: NMR parameters related to the α-helix. Left $^{h3}J_{NC'}$ couplings. $^{1}H_{N}$ chemical shift, $^{1}J_{NH}$ couplings and Lipari-Szabo order parameter S^2. For each H-bond, the data is presented from left to right for the four temperatures 15, 30, 45 and 60 ºC in the absence of solvent (black) and in the presence of 1.5 M TMAO (red).

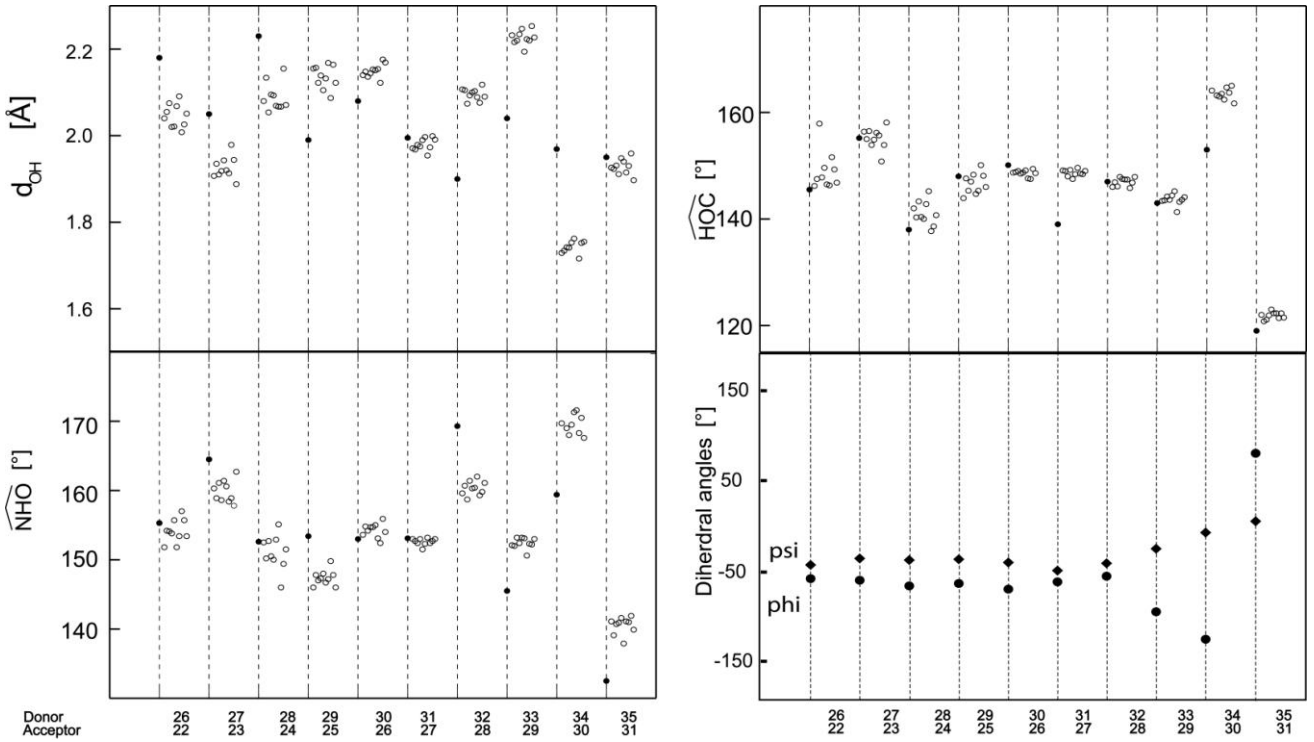

Figure 3.11B: The α-helix H-bond geometric parameters derived from X-ray (1ubq; filled symbols) and NMR (1DZ3; open symbols) structures.

In general, the $^{h3}J_{NC'}$ couplings associated with α-helix H-bonds showed a uniform decrease in magnitude (Figure 3.11A) as the temperature was increased from 15 to 60 ºC in the absence (black) and presence (red) of 1.5 M TMAO. The decrease in the sizes of the $^{h3}J_{NC'}$ couplings are a result of the thermal expansion of the α-helix and therefore a weakening of the H-bonds. Although the decrease in $^{h3}J_{NC'}$ couplings generally follows the same trend, the size of the observed changes in the $^{h3}J_{NC'}$ coupling varies for each H-bond and is dependent on the position of the H-bond in the α-helix. Furthermore in the presence of 1.5 M TMAO the decrease in $^{h3}J_{NC'}$ couplings are affected by the counter-acting mechanism of TMAO against thermal expansion. This is also observed with the $^{1}J_{NH}$ couplings which also showed variable differences in coupling sizes in the absence and presence of TMAO. In contrast, the $^{1}H_N$ chemical shifts for all amide donor groups showed a uniform upfield shift in the presence and absence of TMAO. This indicates that the $^{1}H_N$ chemical shifts are not definitive parameters to examine H-bond geometric changes. Besides I31, the S^2 order parameter showed an increase in the amplitude motions of the N–H group as the temperature was increased. Moreover, in the presence of 1.5 M TMAO the bond motion amplitudes were generally reduced when compared to the same data in the absence of the cosolute.

The H-bonds that will be analysed in detail are those H-bonds in which $^{h3}J_{NC'}$ coupling values were observed at all four temperatures in the presence and absence of 1.5 M TMAO: K27/I23, I30/V26 and E34/I30. The H-bond K27/I23 is located at the N-terminus of the α-helix and has a strong $^{h3}J_{NC'}$ coupling (–0.57 ± 0.005 Hz) at 15 ºC in the absence of TMAO due to a short r_{OH} length of 1.9 Å (NMR structures; Figure 3.11B). This correlates with the strong downfield $^{1}H_N$ chemical shift (8.6 ppm). H-bond E34/I30 is located at the C-terminus and is the shortest H-bond in the α-helix (r_{OH} of 1.7 Å; NMR structure) and coincides with the largest $^{h3}J_{NC'}$ coupling (–0.7 ± 0.006 Hz), and the largest downfield $^{1}H_N$ chemical shift (8.76 ppm). A weaker $^{h3}J_{NC'}$ coupling (–0.4 ± 0.003 Hz) for H-bond I30/V26 is observed as a result of a longer H-bond ($r_{OH} \approx 2.1$ Å; NMR structures).

In the absence of TMAO H-bonds K27/I23, I30/V26 and E34/I30 showed the strongest decrease in $^{h3}J_{NC'}$ couplings as the temperature was increased from 15 to 60 ºC, i.e. the calculated $\Delta^{h3}J_{NC'}$ couplings for H-bonds K27/I23, I30/V26 and

E34/I30 were −0.1294 ± 0.005, −0.0756 ± 0.0295 and −0.1139 ± 0.0073 Hz, respectively. Due to the relatively strong correlation between the $^{h3}J_{NC'}$ coupling size and H-bond length (Figure 3.3), a strong decrease in $^{h3}J_{NC'}$ couplings corresponds to a more pronounced lengthening of these H-bonds. The increase in temperature may result in the geometry of the α-helix becoming more uniform (i.e. loss of curvature), due to the changes in the geometries of the H-bonds K27/I23, I30/V26 and E34/I30. Moreover, examination of the $^{1}J_{NH}$ couplings for K27 and E34 shows that the absolute size of these couplings increases slightly as the temperature was raised, indicating that the N–H bonds shortened which is a direct result of the H-bonds lengthening. At 60 ºC the $^{h3}J_{NC'}$ couplings for H-bonds K27/I23 and E34/I30 are larger than the other couplings for H-bonds in the α-helix. This indicates the important roles H-bonds K27/I23 and E34/I30 contribute in protecting the helix from fraying and thus overall destabilisation of the helix.

In the presence of 1.5 M TMAO H-bonds K27/I23, I30/V26 and E34/I30 showed differences in the changes of the $^{h3}J_{NC'}$ couplings between 15 and 60 ºC. At 15 and 30 ºC the $^{h3}J_{NC'}$ couplings for H-bond K27/I23 in 1.5 M TMAO are weaker than the $^{h3}J_{NC'}$ coupling measured in the absence of TMAO. This weaker H-bond coupling correlates with a larger $^{1}J_{NH}$ coupling at 15 °C. Apparently, the presence of TMAO has lengthened the H-bond leading to a shortening of the N–H bond at this lower temperature. Upon further increase in the temperature, the $^{h3}J_{NC'}$ coupling remained unchanged. This is an indication that the TMAO has stabilised the H-bond against thermal denaturation. The $^{1}J_{NH}$ coupling for K27 decreases between 15 and 60 °C, indicating that the H-bond length has shortened. However, no significant change in the $^{h3}J_{NC'}$ coupling was observed over the whole temperature range. Presumably the absence of change in the coupling value, yet decrease in H-bond length as the temperature was raised, is due to an ∠H•••O=C angular compensatory effect in which this angle deviates further away from the optimal linear arrangement (see Figure 3.4 – theoretical results figure). Although a weaker relationship (as shown by theoretical studies (Barfield et al., 2001)), it is also possible that the ∠N–H•••O shifts to a value further away from 180°. The S^2 value in the presence of TMAO for the K27 shifts to higher values at both temperatures indicative of lower bond amplitude motions. This may also reflect the negligible temperature-dependent changes in the K27/I23 H-bond coupling.

At the other end of the α-helix the $^{h3}J_{NC'}$ coupling measured for H-bond E34/I30 in the presence of TMAO showed small changes in magnitude as the temperature was increased. At the low temperatures, the $^{h3}J_{NC'}$ coupling has similar magnitudes in the absence and presence of TMAO, whereas increasing the temperature to 45 ºC leads to negligible changes in the $^{h3}J_{NC'}$ coupling in the presence of TMAO yet a further decrease in the same coupling in the absence of TMAO. The increase in the $^{1}J_{NH}$ coupling between 15 and 60 °C supports the notion that the H-bond length is increasing.

The rate of change in the size of the $^{h3}J_{NC'}$ coupling for the I30/V26 H-bond in the presence of 1.5 M TMAO (0.14 ± 0.02 Hz) is larger when compared to the data in the absence of TMAO (0.075 ± 0.02 Hz). This may be the result of a compensation effect were the TMAO stabilises the H-bonds K27/I30 and E34/I30 located at the ends of the α-helix to protect the α-helix from unfolding; however, exacerbating the loss of stability of the H-bond I30/V26 located in the centre of the α-helix. The $^{1}H_{N}$ chemical shift for I30 showed an upfield shift which correlates with the decrease in the $^{h3}J_{NC'}$ couplings. However, the $^{1}J_{NH}$ couplings showed a decrease in magnitude indicating a shorter H-bond. Presumably the observed changes in the $^{1}J_{NH}$ is due to a lengthening of the associated N–H bond, whereas the decrease in the $^{h3}J_{NC'}$ coupling is ascribed to a change in the associated H-bond angles. In this case, the angles are decreasing in value as the temperature was increased.

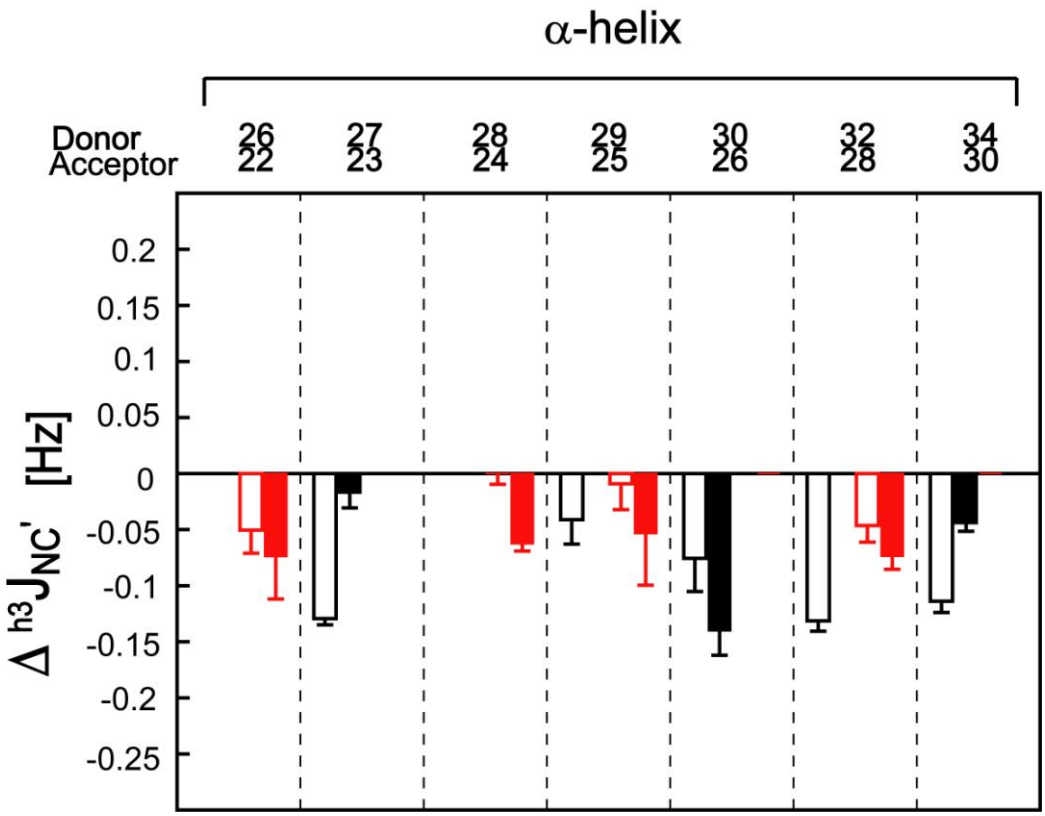

Figure 3.12: $\Delta^{h3}J_{NC'}$ values for α-helix, where $\Delta^{h3}J_{NC'} = |^{h3}J_{NC'}|$ (no cosolute or TMAO) 60 ºC – $|^{h3}J_{NC'}|$ (no cosolute or TMAO) 15 ºC (open black, no cosolute; filled black, TMAO). For H-bonds where no $^{h3}J_{NC'}$ couplings were observed at 15 ºC the $\Delta^{h3}J_{NC'}$ was calculated between 30 and 60 ºC for no cosolute (open red) and in 1.5 M TMAO (filled red).

A positive $\Delta^{h3}J_{NC'}$ value in Figure 3.12 indicates an increase in the magnitude of $^{h3}J_{NC}$ coupling, whereas a negative $\Delta^{h3}J_{NC'}$ value indicates a decrease in $^{h3}J_{NC}$ coupling as the temperature was increased. The missing $\Delta^{h3}J_{NC'}$ values are due to the inability to calculate the $^{h3}J_{NC}$ coupling as a result of very weak (undetectable) signal or peak overlap. All the $\Delta^{h3}J_{NC}$ couplings calculated in the α-helix between 60–15 ºC and 60–30 ºC in the presence and absence of TMAO were negative indicating a decrease in $^{h3}J_{NC}$ coupling magnitudes as the temperature was raised. H-bonds with $^{h3}J_{NC'}$ couplings missing at 15, 30 or 60 ºC in the absence and presence of TMAO are not depicted in the figure above, i.e. H-bonds Q31/K27, K33/K29 and G35/Q31.

The $\Delta^{h3}J_{NC'}$ values for the sample in the absence of TMAO show a greater decrease for H-bonds located on the hydrophobic face of the helix (K27/I23, I30/V26, and E34/I30) with an average decrease of 0.1 ± 0.01 Hz. In contrast, the H-bonds located on the solvent accessible side of the helix show a smaller

decrease in coupling size with the exception of H-bond D32/A28 which has the shortest r_{OH}. The greater negative $\Delta^{h3}J_{NC'}$ couplings observed for H-bonds located on the hydrophobic face of the α-helix is a result of the shorter H-bond distances lengthening more than the H-bond distances located on the solvent exposed side of the α-helix.

The $\Delta^{h3}J_{NC'}$ between 15–60 ºC were calculated for H-bonds K27/I23, I30/V26 and E34/I30 for the sample in the presence of 1.5 M TMAO (black solid bars in Figure 3.12), whereas additional $\Delta^{h3}J_{NC'}$ were calculated between 30─60 ºC (red solid bars). The $\Delta^{h3}J_{NC'}$ for H-bond K27/I23 showed negligible change between 15─60 ºC in the presence of TMAO, whereas the $\Delta^{h3}J_{NC'}$ between E34/I30 showed a small decrease. This contrasts the rather significant $\Delta^{h3}J_{NC'}$ coupling observed for H-bonds K27/I30 and E34/I30 in the absence of TMAO. Clearly TMAO stabilises the helix structure at the termini.

Figure 3.13 represents the changes in the sizes of $^{h3}J_{NC'}$ couplings measured in the presence and absence of TMAO between 15 and 60 ºC. The balls and stick model shows the H-bond network of the α-helix and the H-bonds are coloured according to thermal stability in the presence of 1.5 M TMAO. The H-bonds K27/I23 and E34/I30 are coloured in magenta depicting a more stable H-bond in the presence of TMAO, whereas the yellow coloured H-bonds depict the weakening of the H-bond in the presence of TMAO. This clearly shows that TMAO thermally stabilised the H-bonds at both ends of the α-helix which is compensated by a weakening of the central H-bonds. However the net result is a stabilisation of the α-helix in the presence of TMAO because this cosolute has reduced the thermal denaturation of the terminal H-bonds. Presumably the TMAO protects local non-covalent interactions at the termini of the helix and therefore stabilises the H-bond geometries.

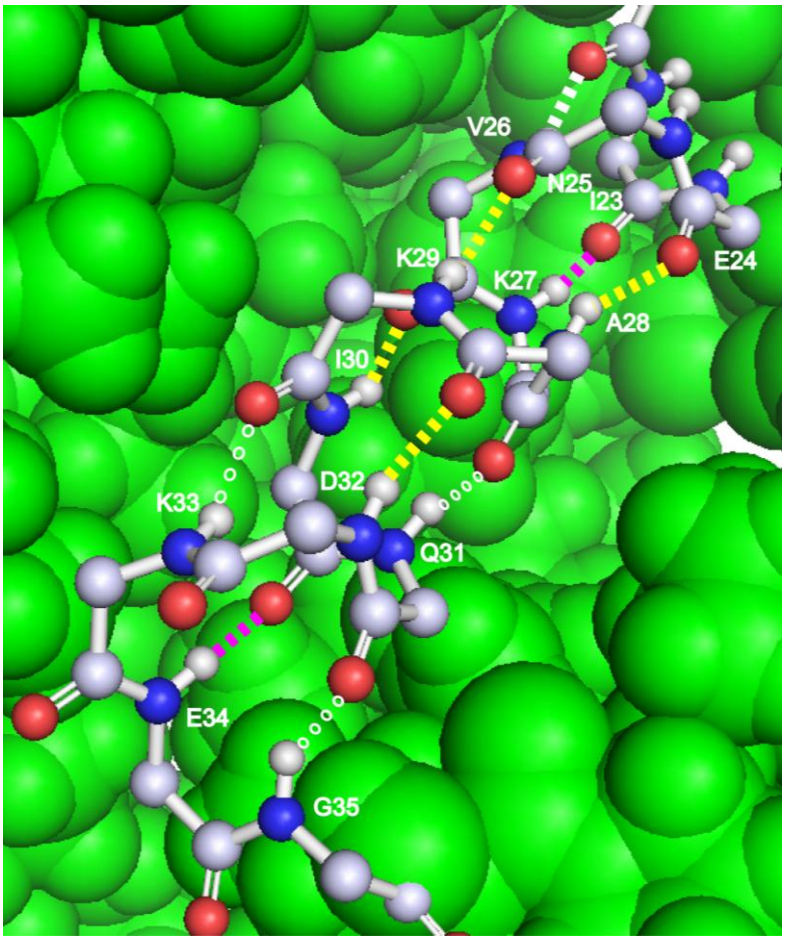

Figure 3.13: Backbone and H-bonds shown as ball and stick models of the α-helix region of ubiquitin. The remaining part (green) of the structure is a space-filled representation. The H-bonds are represented by the dashed lines. Changes in $^{h3}J_{NC'}$ couplings in the presence of 1.5 TMAO are compared to the changes in $^{h3}J_{NC'}$ couplings measured in the absence of this compound. H-bonds coloured magenta have been thermally stabilised by the presence of TMAO, whereas H-bonds coloured yellow showed enhanced thermal weakening in the presence of TMAO. White dashed lines represent no influence of TMAO on the thermal lability of the H-bond. Open dashed lines represent H-bonds for which data is missing.

Generally, the S^2 data shows that in the presence of TMAO, the bond amplitude motions are more restricted at both 15 and 60 °C when compared to the S^2 values in the absence of the cosolute. This observation indicates that the increase in thermal energy leads to increases in both overall protein motion and the amplitude of the motion of the amide groups. The C-terminal H-bond G35/Q31 S^2 values are higher in the absence of TMAO versus the values in the presence of TMAO indicating that TMAO has exacerbated the bond motion at all temperatures. The average S^2 value at 15 °C in the absence of TMAO is 0.86 ± 0.004, whereas the S^2 in the presence of TMAO is 0.89 ± 0.012. The average S^2 reduces to 0.83 ± 0.001

and 0.85 ± 0.001 at 60 °C in the absence and presence of TMAO, respectively. At 15 ºC in the presence of TMAO the bond motion amplitudes are restricted due partly because of the higher viscosity of the sample. In addition the presence of TMAO increases the viscosity by two fold, resulting in a more rigid structure; in turn decreasing the bond vibrations, hence decreasing disorder. As the temperature was increased to 60 ºC, this resulted in an increase in thermal energy, which increased the bond motion amplitudes, i.e. increasing the fluctuations of the N─H bonds. However, in the presence of TMAO at 60 ºC greater restriction was observed when compared to the values measured in the absence of this cosolute.

For K27, I30, D32, K33, E34 and G35, in the presence of TMAO the change in S^2 values between 15 and 60 °C is reduced (i.e. the average $\Delta S^2 = 0.052 \pm 0.0025$ (no TMAO) and $\Delta S^2 = 0.047 \pm 0.01$ (TMAO)). This observation indicates that TMAO reduces the effect of thermal energy on increasing bond vibrations/amplitude motions (i.e. provides stability) for these amide groups. The C-terminal residues K33 and E34 show significant disorder; however, TMAO does provide stability to these residues with S^2 values increasing to be similar in value to S^2 values of other residues. Moreover, TMAO reduces disorder for the four C-terminal residues (i.e. smaller ΔS^2 values), which is not the case for the N-terminal residues (see below). As previously reported,(Cordier and Grzesiek, 2002) the C-terminus of the helix appears to be the most thermally labile region with an increase in disorder as the temperature is raised. Apparently the presence of TMAO plays a key role in stabilizing local non-covalent interactions in this region and therefore reduces the amount of observed disorder (i.e. higher S^2 values).

S^2 values for residues V26, A28 and K29 located at the N-terminus showed an increase in change in the presence of TMAO between 15 and 60 °C (i.e. the average $\Delta S^2 = 0.0416 \pm 0.002$ (no TMAO) and $\Delta S^2 = 0.055\ 0.011\pm$ (TMAO)). This observation indicates that TMAO slightly amplified the influence of thermal energy on bond amplitude motions for these residues (i.e. enhanced disorder in this region of the helix).

In contrast, the S^2 values for the central helix residue Q31 showed a dramatic increase in the presence and absence of TMAO. This observation may be a result of the helix structure undergoing subtle changes in order that forces Q31 to show

less disorder. This reduction in molecular amplitude motion may be due to steric restrictions as Q31 faces the hydrophobic interior of ubiquitin.

3.6.2 The β2/β1 and β1/β5 sheets

This region of the protein consists of both parallel and antiparallel β-sheet secondary structures. This sheet is highly twisted and the residues involved all fall in the range of ϕ (-100° ± 50°) and ψ (150° ± 50°), with the exception of E64/Q2 (Figure 3.14B) (Appendix 16). The irregularity observed with H-bond E64/Q2 is due to the amide proton of S65 located on strand β5 not being paired with its regular C=O acceptor, Q2. Rather the amide proton of S65 is H-bonded with the carbonyl carbon of Q62. This is made possible by a positive ϕ angle of 67º resulting in a very weak H-bond from S65 as the donor and Q62 as the carbonyl acceptor. The S65/Q62 coupling is not observed presumably because of the extremely weak H-bond ≤ –0.1 Hz.

Figure 3.14A depicts the $^{h3}J_{NC'}$ couplings, $^{1}H_N$ chemical shifts, $^{1}J_{NH}$ couplings and Lipari-Szabo order parameter S^2 in the absence (black) and presence of 1.5 M TMAO (red), measured across four temperatures (15, 30, 45, 60 ºC). The overall pattern of the $^{h3}J_{NC'}$ couplings measured in the absence and presence of 1.5 M TMAO showed a decrease in magnitude as the temperature was increased from 15 to 60 ºC. This is correlated with the upfield $^{1}H_N$ chemical shift, and generally an increase in the $^{1}J_{NH}$ couplings. The S^2 values decreased as the temperature was increased, indicative of increases in the bond amplitude motions. In general, in the presence of TMAO the bond amplitude motions were more restricted.

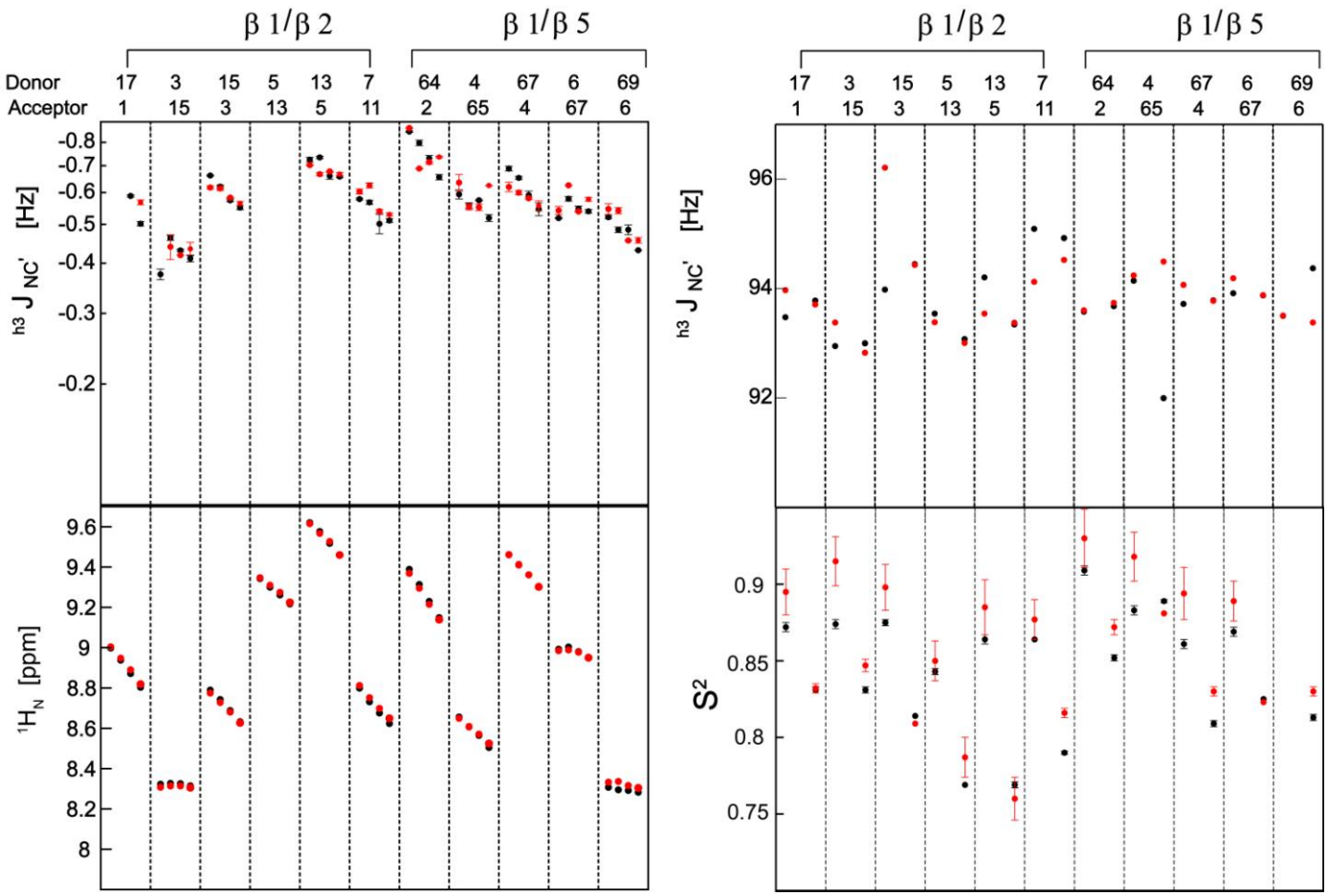

Figure 3.14A: NMR parameters of the β-sheets β1/β2 and β1/β5 (see legend to Figure 3.12A for a description). The filled circles depict the absence of solvent (black) and in the presence of 1.5 M TMAO (red).

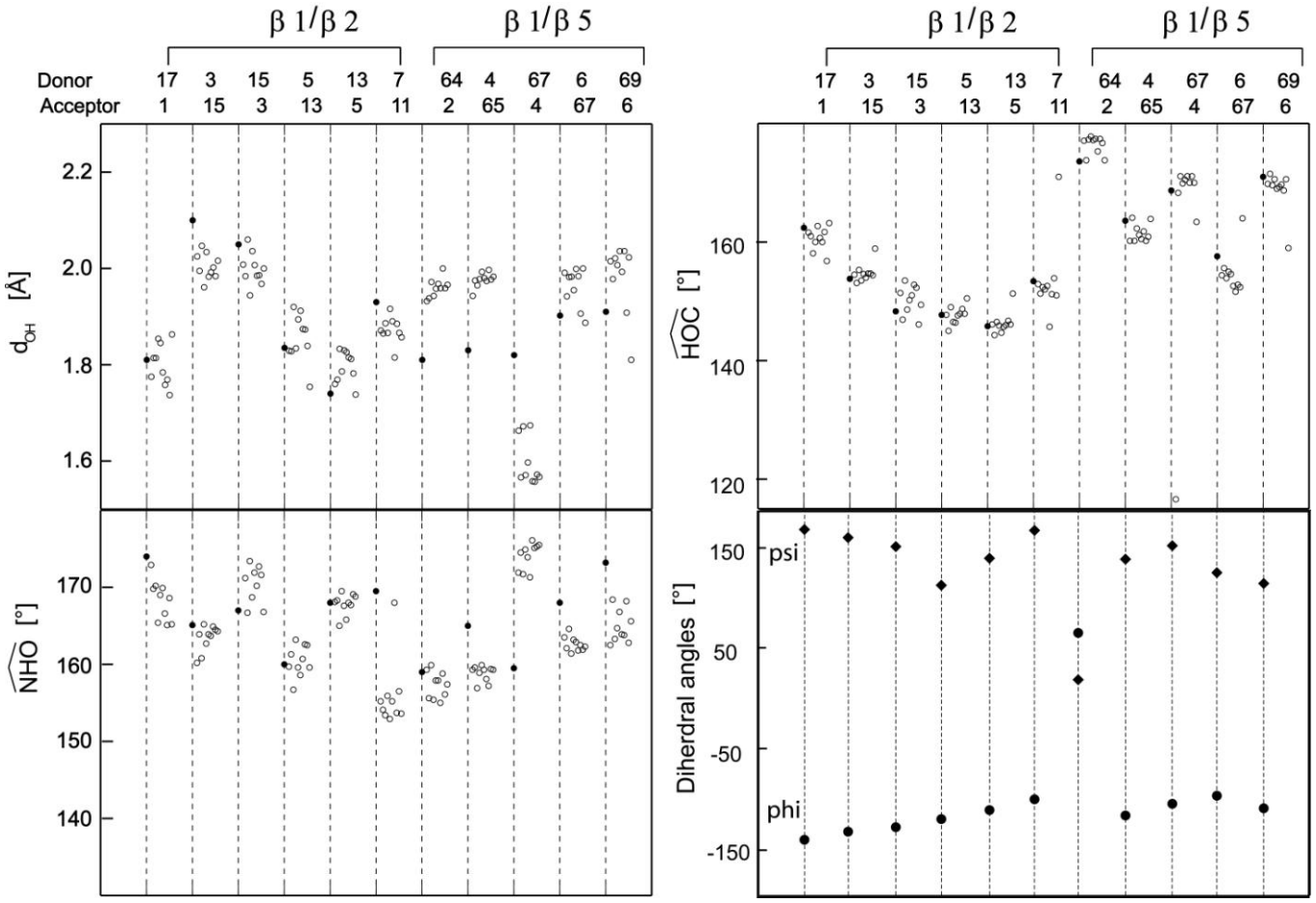

Figure 3.14B: H-bond geometric values of the β-sheets β1/β2 and β1/β5 (see legend to Figure 3.12B for a description).

In the absence of the cosolute the $^{h3}J_{NC'}$ couplings showed a uniform decrease in magnitude as the temperature was increased. The only exceptions are H-bonds I3/L15 and K6/L67, where an increase in $^{h3}J_{NC'}$ coupling sizes was observed between 15 and 30 °C and at higher temperatures the $^{h3}J_{NC'}$ couplings gradually decreased but still remained larger than the couplings measured at 15 °C. The H-bond I3/L15 shares donor and acceptor groups with H-bond L15/I3; however, unlike I3/L15 H-bond L15/I3 showed a uniform decrease in $^{h3}J_{NC'}$ coupling size as the temperature was increased. A similar increase in $^{h3}J_{NC'}$ coupling for H-bond I3/L15 was observed in a temperature dependent study.(Cordier and Grzesiek, 2002) The general decrease in the H-bond couplings indicates that the H-bond lengths have increased as a result of thermal expansion. This weakening of the H-bonds results in the distance between the β1 and β2 strands to increase. In the case of the H-bond I3/L15, the increase in the coupling between 15 and 30 °C may be due to the two strands moving closer together in this region of the secondary structure. This deviation from the trend (i.e. strands moving apart from each other) is most likely a compensatory effect, in which the strands do not uniformly move apart, but there is a rotation of one of the strands with respect to the other close to the N-terminal end of the β1/β2 region. A similar conclusion can be drawn for H-bond K6/L67 where the change in the geometry of the H-bonds connecting β-stands β1 and β5 results in shortening of the H-bond and a consequent increase in the $^{h3}J_{NC'}$ coupling for this H-bond.

Similar to what was observed in the absence of cosolute, the $^{h3}J_{NC'}$ couplings measures in 1.5 M TMAO showed a general uniform decrease in size as the temperature was increased. However the decrease in $^{h3}J_{NC'}$ coupling was less pronounced, indicating that TMAO is counteracting the thermal expansion of the H-bonds. For H-bond I3/L15, negligible changes in the $^{h3}J_{NC'}$ couplings were observed between 30 to 60 ºC in the presence of TMAO. This is corroborated by the insignificant changes in the $^{1}H_N$ chemical shifts. In the presence of TMAO, no observable geometric change has occurred for H-bond I3/L15. In the absence of TMAO, the small change in the $^{h3}J_{NC'}$ couplings as a function of increasing temperature is presumably due to a angular effect since the $^{1}H_N$ chemical shift does not change over the temperature range.

H-bond L15/I3 shares the same donor/acceptor atoms and has the same geometric properties as I3/L15 (Figure 3.14B). The $^{h3}J_{NC'}$ coupling for H-bond I3/L15 in the presence of TMAO at 15 °C is weaker than the same coupling measured in the absence of TMAO. This is corroborated by the observed stronger $^{1}J_{NH}$ coupling. As the temperature was increased from 15 to 60 ºC the $^{h3}J_{NC'}$ coupling values were similar in the presence and absence of TMAO, this is in conjunction with the decrease in $^{1}J_{NH}$ coupling from 15 to 60 ºC and the upfield $^{1}H_{N}$ chemical shift.

H-bond E64/Q2 gives rise to the largest H-bond coupling. In the absence of cosolute there is a uniform decrease in $^{h3}J_{NC'}$ coupling size as the temperature was increased. This is in correlation with the uniform upfield $^{1}H_{N}$ chemical shift and the observed increase in the $^{1}J_{NH}$ coupling. In the presence of 1.5 M TMAO there is a large decrease in the E64/Q2 $^{h3}J_{NC'}$ coupling between 15 to 30 °C; however, from 30 to 60 °C the size of the $^{h3}J_{NC'}$ coupling gradually increased. In contrast, the $^{1}H_{N}$ and $^{1}J_{NH}$ show similar changes as observed for data recorded in the absence of TMAO. Since the upfield shift and increase in $^{1}J_{NH}$ can be attributed to the lengthening of the H-bond, the observed increase in $^{h3}J_{NC'}$ coupling must be a result of a change in the ∠N–H•••O and ∠H•••O=C associated with this H-bond. H-bond E64/Q2 is positioned at the C-terminus of β-sheet β1/β5 and presumably plays an important role in stabilizing this secondary structure. As such, as the rest of the H-bonds are thermally weakened, the E64/Q2 may compensate for these weakened H-bonds and therefore protect the β-sheet from thermal denaturation.

In the presence of TMAO, the $^{h3}J_{NC'}$ coupling for F4/S65 H-bond showed an initial decrease from 15 to 30 °C, negligible change between 30 to 45 °C and a subsequent increase between 45 to 60 °C. Examination of the $^{1}J_{NH}$ for the donor group indicates that the N–H distance shortens (in TMAO) whereas it appears to lengthen in the absence of TMAO. As such, in the presence of TMAO we would expect that the $^{h3}J_{NC'}$ coupling would decrease between 15 and 60 °C; however, the opposite is observed therefore suggesting that there is a strong angular compensation to the apparent lengthening of the H-bond. It appears that the F4/S65 H-bond in the absence of TMAO shortens, as judged from the decrease in the absolute value of the $^{1}J_{NH}$; however the decrease in the F4/S65 $^{h3}J_{NC'}$ coupling suggests that an angular change (or changes) overcompensates the change in the H-bond distance.

In the absence of TMAO the $^{h3}J_{NC'}$ coupling H-bond K6/L67 increased between 15 and 30 ºC, then from 30 to 60 ºC the $^{h3}J_{NC'}$ coupling decreased, but remained slightly stronger (0.54 ± 0.0055 Hz) than the initial $^{h3}J_{NC'}$ coupling value at 15 ºC (0.52 ± 0.0015 Hz). In addition, the $^{1}H_{N}$ chemical shift showed only a slight downfield shift, whilst the $^{1}J_{NH}$ couplings showed negligible change between 15 and 60 ºC. The slight change in the $^{1}H_{N}$ chemical shift and negligible change in the $^{1}J_{NH}$ coupling is indicative that the H-bond length was not significantly changing. Therefore, the changes in the $^{h3}J_{NC'}$ couplings as the temperature was increased must be a result of a change in the ∠N–H•••O and ∠H•••O=C associated with this H-bond. In the presence of TMAO, the $^{h3}J_{NC'}$ couplings fluctuated as the temperature was increased. Similar to what was observed in the absence of TMAO the $^{h3}J_{NC'}$ coupling measured at 60 ºC (0.58 ± 0.007 Hz) was stronger than the coupling measured at 15 ºC (0.54 ± 0.012). Furthermore, the $^{1}J_{NH}$ coupling showed a decrease in magnitude which indicates a lengthening of the N−H, this correlates with the increase in the $^{h3}J_{NC'}$ coupling size, indicating that the H-bond was shorter at the higher temperature.

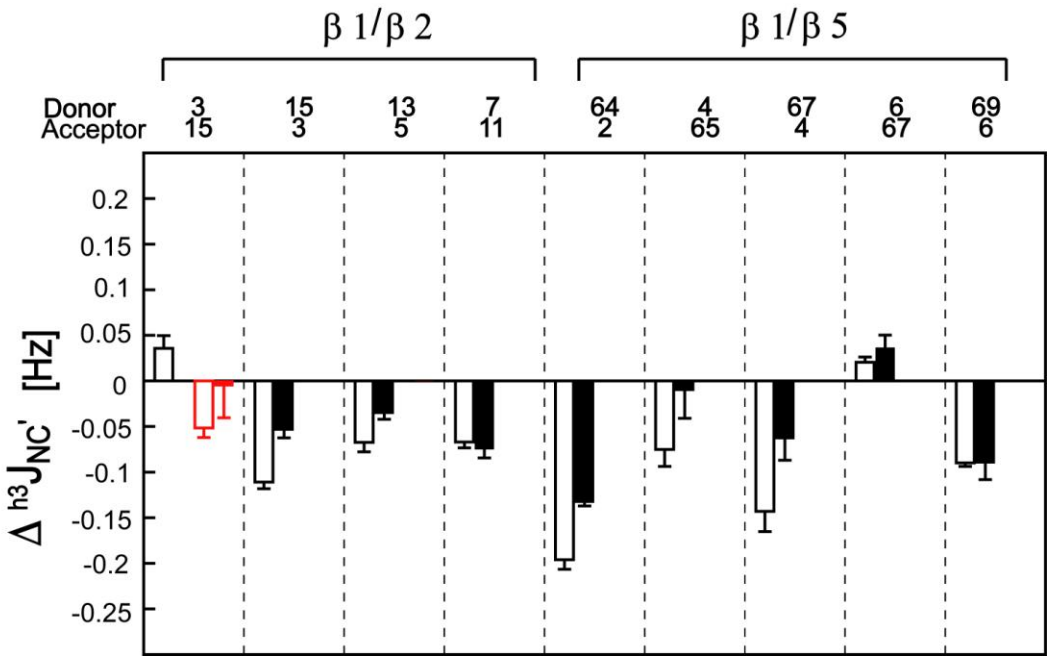

Figure 3.15: $\Delta^{h3}J_{NC'}$ values for β1/β2/β5 (see legend to Figure 3.13)

A negative $\Delta^{h3}J_{NC'}$ coupling is observed in both the presence (filled black) and absence (open black) of 1.5 M TMAO for the majority of the H-bonds (Figure 3.15). This shows that the thermal expansion of this region of the protein has affected the geometries of the H-bonds resulting in an overall decrease in $^{h3}J_{NC'}$

coupling sizes. 1.5 M TMAO provides thermal stability to the H-bonds. Consequently the decrease in $^{h3}J_{NC'}$ coupling magnitude is smaller compared to the decrease of $^{h3}J_{NC'}$ couplings measured in the absence of 1.5 M TMAO. Interestingly, TMAO provides insignificant stability to H-bonds located at the C-terminal ends of the β1/β2 and β1/β5. H-bond K6/L67 appears to be the sole H-bond which is stabilised by an increase in temperature, with little influence of TMAO to this thermal stability.

Figure 3.16 shows a ball and stick model of the β1/β2 and β1/β5 H-bond network. In general, the addition of TMAO slows thermal expansion of the H-bonds connecting β-stands β1, β2 and β5. H-bonds located at the β1/β2 hairpin are unchanged indicating that this region may act as a hinge for the movement of other parts of this secondary structure element. Since strand β1 is sandwiched between β2 and β5 there is little room for this strand to move. Assuming β1 does not significantly change position as a function of temperature, the increase in the stability of the H-bonds is due to the β2 strand rotating anticlockwise around a pivot point located at T7/K11 and the β5 strand rotating clockwise around a pivot point located at L69/K6. The H-bonds I3/L15, F4/65 and L67/F4 located at the center of the β1/β2/β5 H-bond network showed the slowest thermal expansion. This centre region is exposed to the surrounding solvent environment and therefore is stabilised by TMAO due to a highly unfavourable interaction between the osmolyte and the peptide backbone;(Venkatesu et al., 2009, Lin et al., 2009) this mechanism is known as the “osmophobic effect”.

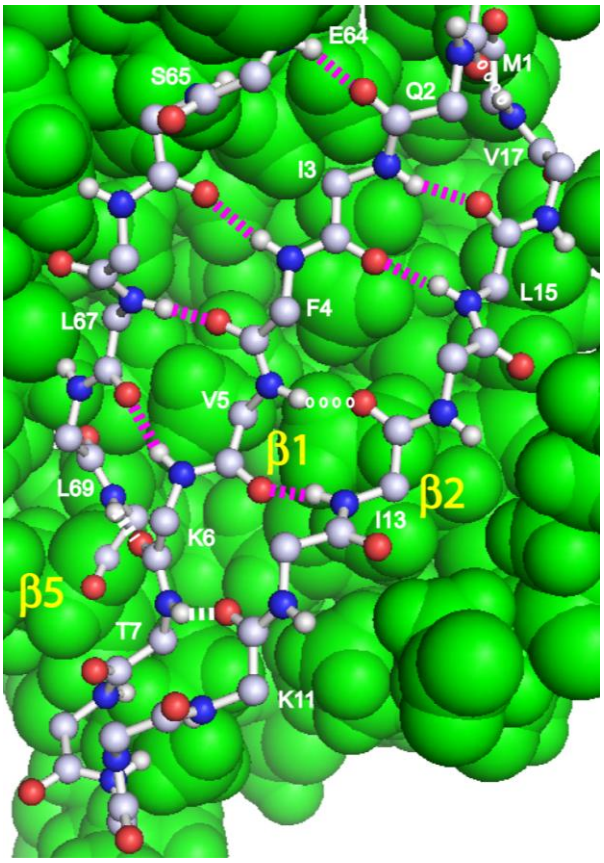

Figure 3.16: Backbone and H-bonds shown as ball and stick models of the β1/β2 and β1/β5 H-bond network region of ubiquitin. (See legend to Figure 3.14 for a description).

In most cases, the S^2 data for β1/β2 and β1/β5 sheets showed an average decrease as the temperature was increased from 15 (0.87 ± 0.002) to 60 ºC (0.82 ± 0.001) in the absence of TMAO. This observation indicates that the increase in thermal energy leads to increases in both motion and the amplitude of the motion of the amide groups. In addition, the average S^2 values are lower than, the average values observed in the α-helix. This supports the suggestion that the most thermally labile regions of ubiquitin are the β1/β2 and β1/β5 sheets.(Cordier and Grzesiek, 2002) When compared with the average S^2 values in the presence of TMAO, in general the bond amplitude motions are more restricted at both 15 (0.9 ± 0.014) and 60 °C (0.83 ± 0.004).

For β1/β2 amide donors V17, I3, L15, V5, I13 and T7 in the absence of TMAO the average S^2 value was 0.87 ± 0.002 at 15 ºC and 0.80 ± 0.001 at 60 ºC, whereas in TMAO the average value was 0.89 ± 0.015 for 15 ºC and 0.81 ± 0.006 at 60 °C. This observation indicates that TMAO reduces the effect of thermal energy on increasing bond vibrations/amplitude motions (i.e. provides stability) for these amide groups. For the β1/β5 residues (E64, F4, L67, K6 and L69) the average S^2

value was 0.89 ± 0.003 at 15 ºC and 0.85 ± 0.001 at 60 ºC, whereas in presence of TMAO the average S^2 was 0.91 ± 0.016 at 15 ºC and 0.85 ± 0.002 at 60 °C. The higher S^2 values observed for the β1/β5 sheet indicates that the bond amplitude motions are smaller compared to the amide groups in the β1/β2 sheet. The most thermally labile region of the β1/β2/5 sheet is the C-terminal region. In the β-sheet β1/β2 (in the absence of TMAO), residues V5, I13 and T7 gave an average S^2 value decrease to 0.78 ± 0.001 demonstrating that this region has the highest amplitude of bond motions, i.e. highest disorder. The observation indicates that the C-terminus of β-sheet β1/β2 is a weak point in the β1/β2 and β1/β5 structure. As such, this region most likely represents a initial point of unfolding of this β-sheet. In the presence of TMAO, the S^2 values slightly increased, signifying a reduction in bond amplitude motion.

In the case of residues F4 and I13, the S^2 at 60 ºC in the absence of TMAO is higher than in the presence of TMAO, which indicates that TMAO slightly amplified the influence of thermal energy on bond amplitude motion for residues I13 and F4.

3.6.3 The β5/β3 and β3/β4 sheets

The β-sheets β5/β3 and β3/β4 have uniform ϕ (-100 º ± -50 º) and ψ (130 º ± 10 º) (Appendix 16) angles for the residues involved in H-bonds. These angles are standard geometric values for residues located in antiparallel β-sheets (Cordier and Grzesiek, 2002, Lehninger et al., 2005). The antiparallel β-sheet β5/β3 has four consecutive H-bonds H68/I44, I44/H68, V70/R42 and R42/V70. The first three H-bonds have uniform H-bond geometries (Figure 3.17B) with H-bond ∠N–H•••O and ∠H•••O=C values ranging between 160–172°. The H-bond R42/V70 has a different geometry with a longer H-bond length and a ∠N–H•••O value which is noticeably smaller in comparison to the same angle for the other three H-bonds in this secondary structure element. Only two $^{h3}J_{NC'}$ couplings were observable in β-sheet β3/β4, because H-bond K48/F45 has a very weak coupling of –0.1 Hz (Cordier and Grzesiek 1999) and is therefore unobservable under most conditions examined. Although H-bond K48/F45 has a r_{HO} distance similar to the other H-bond distances, the much smaller ∠H•••O=C value of 120° presumably leads to the immeasurably small $^{h3}J_{NC'}$ coupling.

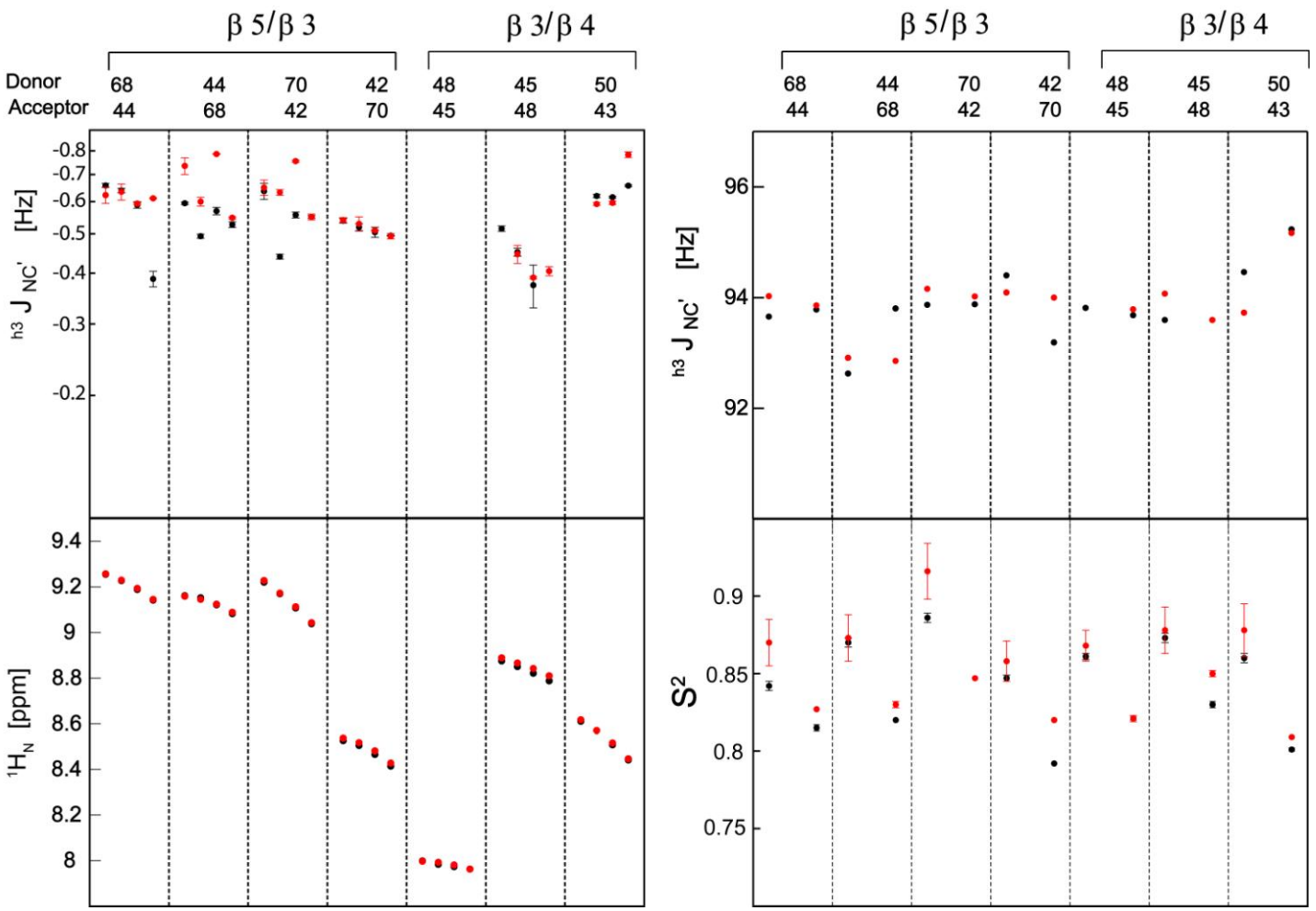

Figure 3.17A: H-bond parameters of the β-sheets β5/β3 and β3/β4 (see legend to Figure 3.12A for a description of the symbols).

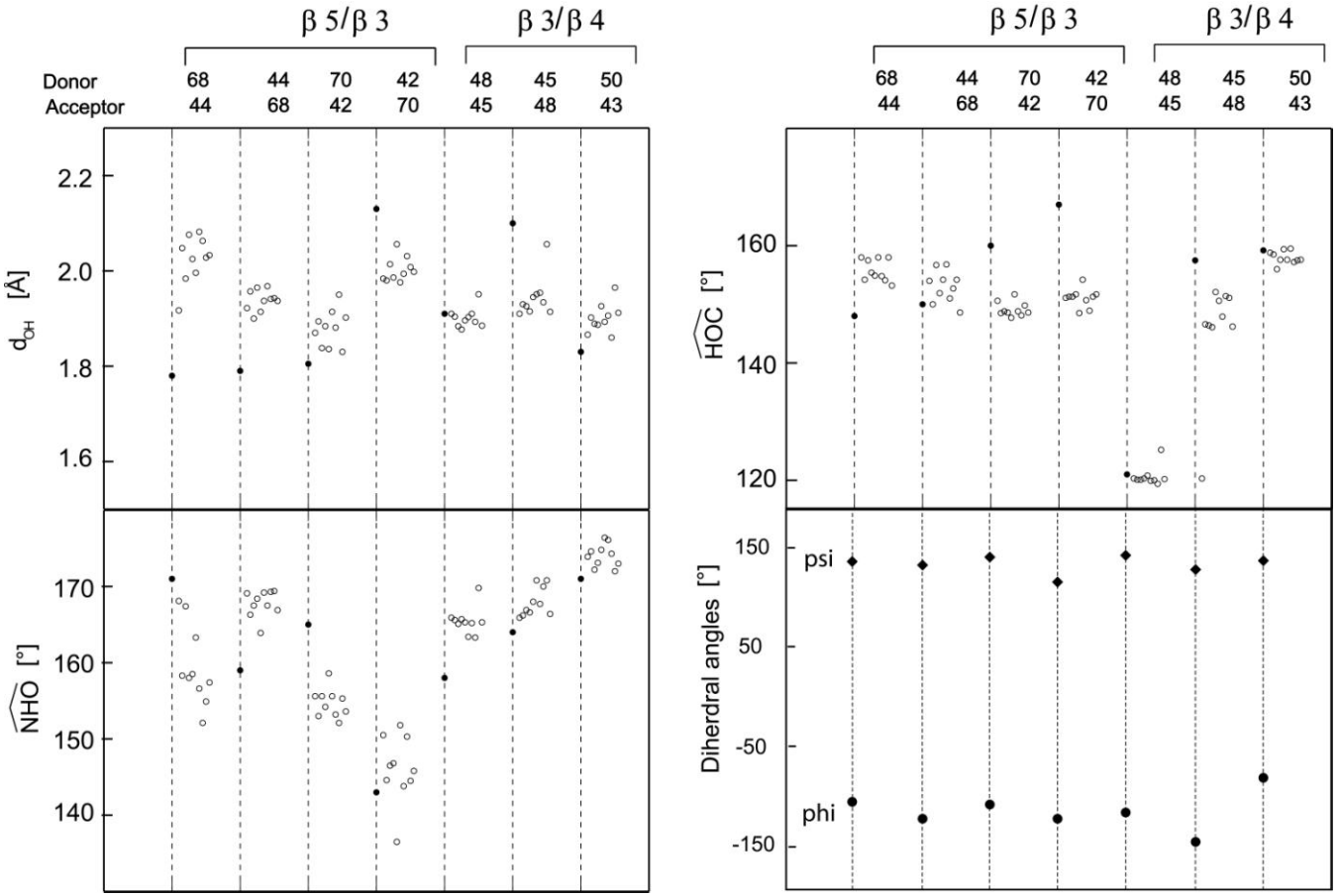

Figure 3.17B H-bond geometric values of the β-sheets β1/β2 and β1/β5 (see legend to Figure 3.12B for a description).

A general decrease in $^{h3}J_{NC'}$ couplings were observed as the temperature was increased from 15 to 60 ºC in the presence and absence of 1.5 M TMAO (Figure 13.17A). This was complemented by an overall upfield change in the $^{1}H_{N}$ chemical shifts. This indicates the β-sheets β5/β3 and β3/β4 are thermally expanding as the temperature was increased. The general decrease in the S^2 order parameters as the temperature was increased indicates increases in the amplitude motion of the N–H groups. However in the presence of 1.5 M TMAO the increase in amplitude motions were attenuated indicating that TMAO has increased the rigidity of the structure.

In β-sheet β5/β3 H-bonds I44/H68, H68/I44 and V70/R42 all showed noticeable variation in the values of the $^{h3}J_{NC'}$ couplings as the temperature was changed. In the absence of 1.5 M TMAO, the $^{h3}J_{NC'}$ coupling for H-bond H68/I44 showed a gradual decrease as the temperature was increased from 15 to 45 ºC; however at 60 ºC there was a significant reduction in the size of this $^{h3}J_{NC'}$ coupling. This observation shows that the H-bond geometry has changed such that the overall strength of the H-bond is significantly weaker. Conversely, in the presence of 1.5 M TMAO the $^{h3}J_{NC'}$ couplings remained essentially uniform at all temperatures indicating that the presence of TMAO has stabilised the H68/I44 H-bond. This observation did not correlate with the change in the $^{1}H_{N}$ chemical shift; however, the $^{1}J_{NH}$ showed a small decrease which also indicates that the H-bond has been stabilised (i.e. shorter H-bond, yet longer N–H bond). The $^{h3}J_{NC'}$ couplings for the adjacent H-bonds I44/H68 and V70/R42 showed fluctuations across the temperature range examined. In the absence of TMAO between 15 and 30 ºC, a large decrease in the I44/H68 and V70/R42 $^{h3}J_{NC'}$ couplings was observed. The couplings increase in value between 30 and 45 ºC. In the presence of 1.5 M TMAO, only the I44/H68 $^{h3}J_{NC'}$ coupling showed a decrease between 15 and 30 ºC. Between 30 and 45 ºC both the I44/H68 and V70/R42 $^{h3}J_{NC'}$ couplings increase beyond coupling values measured at 15 °C. These observations suggest that the H-bonds do not follow a uniform expansion trend, and therefore a more complicated response to thermal energy is assumed. The $^{h3}J_{NC'}$ couplings for H-bond R42/V70 show similar linear thermal expansions in both the presence and absence of TMAO.

For β-sheet β3/β4 the $^{h3}J_{NC'}$ couplings of H-bonds F45/K48 and L50/L43 were measured. The H-bond F45/K48 $^{h3}J_{NC'}$ couplings do not show any differences in the presence and absence of TMAO. This may be due to the H-bond being buried and not

solvent exposed and therefore the direct influence of TMAO or any cosolute is negligible (Appendix 17). The $^{h3}J_{NC'}$ coupling for the H-bond L50/L43 showed an increase as the temperature was increased between 30 and 60 ºC; however in the presence of 1.5 M TMAO the increase in the size of the $^{h3}J_{NC'}$ coupling at 60 ºC is more pronounced. This increase can be the result of the thermal expansion of the H-bonds on β-sheet β5/β3, therefore resulting in geometric changes and a decrease in the length of the L50/L43 H-bond. This observation of a stronger H-bond coupling at higher temperature is contrasted by the increase in the $^{1}J_{NH}$ coupling between 15 and 60 ºC. As such, the observed increase in the H-bond coupling is presumably a result of changes in the two angles associated with this H-bond to values closer to linearity. The S^2 values do decrease noticeably at 60 °C for the H-bond donor group L50. Although the amplitude motion has increased at 60 °C, the overall H-bond geometry appears to have changed to stabilise this H-bond.

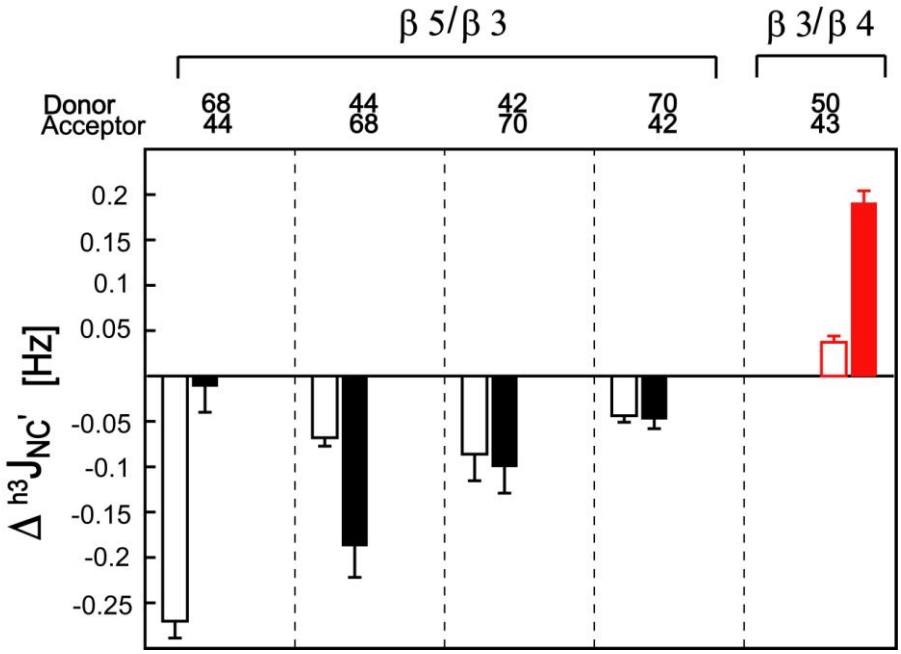

Figure 3.18: $\Delta^{h3}J_{NC'}$ values for β3/β4/β5 (see legend to Figure 3.13)

A negative $\Delta^{h3}J_{NC'}$ is observed in both the presence (filled black) and absence (open black) of 1.5 M TMAO, except for H-bond L50/L43 (Figure 3.18). Figure 3.19 shows a ball and stick model of the β5/β3 and β3/β4 H-bond network. H-bonds coloured in white showed no change in the values of the $^{h3}J_{NC'}$ coupling in the presence of TMAO compared to the same value in the absence of this co-solute. In the absence of 1.5M TMAO the largest decrease in $^{h3}J_{NC'}$ coupling for all the H-bonds in ubiquitin was

observed for H-bond H68/I44. Conversely, for H-bond I44/H68 (involving the same residues), a smaller decrease in $\Delta^{h3}J_{NC'}$ of 0.07 ± 0.002 was determined. The addition of TMAO to the protein sample led to a reversal of the $\Delta^{h3}J_{NC'}$ for these two H-bonds. Here, H-bond H68/I44 showed a negligible $\Delta^{h3}J_{NC'}$, whereas a larger $\Delta^{h3}J_{NC'}$ value was observed for H-bond I44/H68 when compared to the value measured in the absence of TMAO. In Figure 3.18, it appears that as the temperature was increased the β3 strand has rotated in a clockwise direction for the region involving residues L43 and I44; the remaining part of the β3 strand does not change significantly in geometry due to the structural restrictions imposed by the beta-hairpin between strands β3 and β4. Due to this rotation, the length of the L50/L43 H-bond decreases as the carbonyl L43 group moves closer to the donor L50 group. Moreover, the I44 donor group moves away from the H68 acceptor, whereas the I44 carbonyl acceptor group moves closer to the donor H68 moiety. Additional information on other geometric changes is hampered because of the absence of coupling data for a number of the H-bonds in this region (open H-bond symbols in Figure 3.18). The absence of differences around H-bonds V70/R42 is presumably due to the stability of this region.

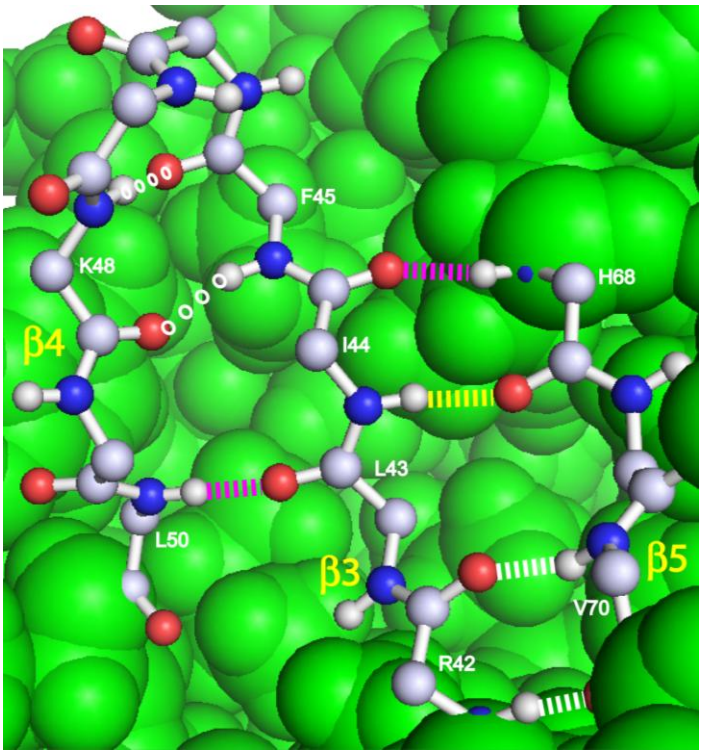

Figure 3.19 Backbone and H-bonds are shown as ball and stick models for the β5/β3 and β3/β4 regions of ubiquitin. (See legend to Figure 3.14 for further information).

Similar to what was observed for the α-helix and the β1/β2/β5 sheet, the S^2 data for the β3/β4β5 sheet showed an average increase in the presence of TMAO. This observation indicates that the motion and the amplitude of the motions of the amide groups were restricted in the presence of cosolute. In the absence of TMAO the average S^2 value at 15 ºC (0.86 ± 0.002) decreased as the temperature increased to 60 ºC (0.81 ± 0.002). The decrease in S^2 values indicates an increase in both motion and the amplitude of the motions of the amide groups. In the presence of TMAO the S^2 values increased (i.e. 0.88 ± 0.014 at 15 ºC and 0.83 ± 0.002 at 60 ºC). This result shows that TMAO provides stability to the amide groups, by reducing the effect of thermal energy on bond amplitude motions.

The highest bond amplitude motions were observed for the C-terminal residues R42 for β3/β4 and L50 for β3/β5. These thermally labile residues may represent the weakest point and the initial point of unfolding of the β3/β4/β5 β-sheet. However, in the presence of TMAO the S^2 values increased, indicating that TMAO has provided stability by decreasing the bond amplitude motions.

Chapter 4

Measuring the stability of H-bonds in ubiquitin by NMR spectroscopy II: the effects of denaturants

4.1 Introduction

In contrast to TMAO, urea and guanidinium.HCl (Gdn.HCl) are denaturants (Figure 4.2) that have been used extensively to characterise protein folding and stability (Arakawa and Timasheff, 1984, Alonso and Dill, 1991, Mayr and Schmid, 1993, Bhuyan, 2002). These compounds are also commonly used in protein purification and separation techniques. Urea and Gdn.HCl function by disrupting weak non-covalent interactions including hydrogen bonds (H-bonds), van der Waals interactions, and hydrophobic forces. The chaotropic behaviour of these two denaturants is dependent on their concentration and the inherent stability of the protein. Besides these two factors, the physicochemical (i.e. temperature and pH) conditions will influence the denaturing strength of urea and Gdn.HCl. For example, studies examining these two denaturants under different pressures and temperatures (St John et al., 1999, St John et al., 2001) have shown that they can act as either chaotropic agents or stabilise protein structures at low concentrations (i.e. kosmotropic) (Baldwin, 1996). Although there is wealth of data on the effect of both denaturants on protein folding and stability, the precise mechanisms of their actions is still not fully understood. An important characteristic of proteins that influences the mechanisms of urea and Gdn.HCl is the water hydration shell of proteins.

The interactions of a protein with solvent or with other molecules are determined primarily by the surface of the protein. The surfaces of most water-soluble globular proteins are covered by charged and polar groups. As such, the most favourable interactions are observed between these hydrophilic side-chains (i.e. charged and polar groups) and water. In general most proteins become soluble in aqueous solution by the addition of detergents or denaturants such as urea and Gdn.HCl, although in the case of denaturants, most proteins will unfold.

Proteins in aqueous solution are surrounded by a tightly bound hydration layer that has different physical properties from those of bulk water. The bound hydration layer is more ordered and less mobile than bulk water and displays a 10% greater density and a 15% greater heat capacity (Murthy and Knox, 2004). On average, this hydration layer contains 0.3 g of water per gram of protein, which is equivalent to nearly two H_2O molecules per amino acid residue (Carrasco et al., 2001).

The solubility of globular proteins is affected by the addition of cosolvents such as salts. A protein molecule in a low ionic strength aqueous solution is surrounded by an ionic atmosphere with an excess of charges opposite to the net charge of the protein molecule (Curtis et al., 2002). The explanation of this "salting in" effect is that at low salt concentrations (Zangi et al., 2007), the addition of counter-ions effectively shield the protein's multiple ionic charges and thereby increase the solubility of the protein. As the ionic strength increases due to an increase in the concentration of salt, the solubility of the protein decreases (Dominy et al., 2002, Zangi et al., 2007). This effect is known as "salting out" and is primarily the result of the competition between the added salt and the protein molecules for hydration (i.e. water) (Zangi et al., 2007). At high salt concentrations, a large body of the salt ions are hydrated and therefore the amount of bulk solvent becomes insufficient to dissolve the protein and the protein precipitates. The magnitude of the "salting in" and "salting-out" effect depends on the nature of the salt and generally follows the Hofmeister series (Figure 4.1) (Zangi and Berne, 2006).

In a folded protein 83% of the most non-polar side chains and 82% of the peptide groups are buried (Myers and Pace, 1996), therefore, the protein interior contains little space and is almost solid in nature. Hence the proportion of the protein surface that is composed of charged side-chains is the most important determinant of the solubility of a protein. When a protein unfolds, many peptide groups and side chains that are buried

in the native state become solvent exposed and more soluble in the aqueous denaturing solution.

Over a century ago, Hofmeister arranged cations and anions into a series based on their effectiveness in precipitating serum globulins. The effect of cations and anions are usually independent and additive, with the anion contributing to the impact on protein precipitation. The first ions of the series (Figure 4.1) disrupt the structure of water; markedly decrease the solubility of non-polar molecules (i.e. "salting out"; or kosmotropic). The last ions of the series generally increase the structure of water, have less effect on its surface tension and increase the solubility of non-polar molecules (i.e. "salting in"; chaotropic). The dividing points between the two effects are taken as Na^+ and Cl^- ions. Figure 4.1 shows the list of anions and cations in ascending order of solubilising strength (left to right).(Hatefi and Hanstein, 1969) The ions that are to the left of the list are regarded as structure makers (kosmotropes), whereas the ions to the right of the list are structure breakers (chaotropes) (Kita et al., 1994, Bolen and Baskakov, 2001).

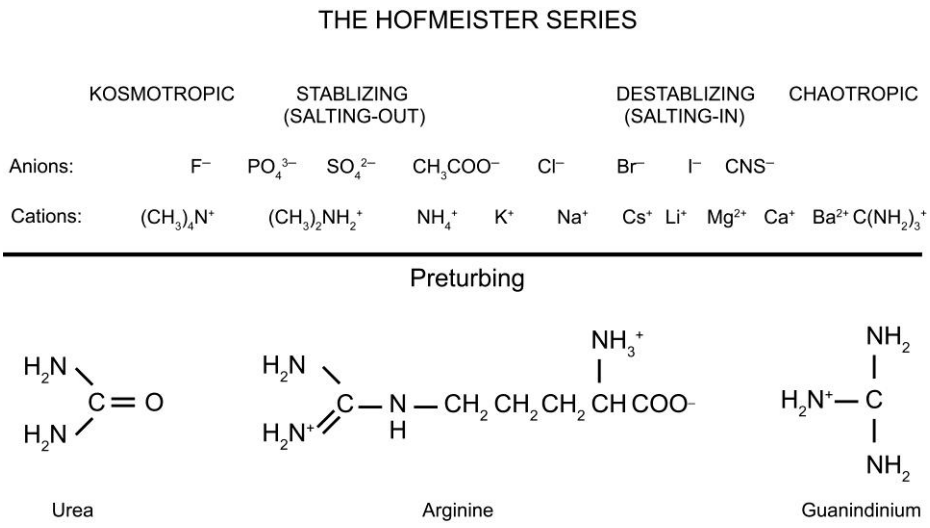

Figure 4.1: The Hofmeister series and perturbing solutes effecting protein structure and function.

The mechanism(s) describing the Hofmeister series is currently believed to not involve changes in general water structure (i.e. bulk water) (Zhang and Cremer, 2006). The Hofmeister concept suggests that more specific interactions between ions and proteins and ions and the water molecules directly contacting the proteins (i.e. hydration shell) are playing a more dominant role in solubilising the protein. Ions that have the greatest such effect (exhibiting weaker interactions with water than water with itself) are known as chaotropes, whereas ions having the opposite effect are known as kosmotropes (exhibiting strong interactions with water molecules) (Moelbert et al.,

2004). Strongly hydrated ions increase the H-bond donating and accepting capacity of the water molecules and do not disrupt the bulk water H-bonding network. This effect leads to the stabilisation of the protein structure. In contrast, weakly hydrated ions (chaotropes, K^+, Rb^+, Cs^+, Br^-, I^-, Gdm^+) may be 'pushed' onto weakly hydrated surfaces by strong water-water interactions. Studies have concluded the Hofmeister trend indicates that stronger denaturation occurs with weakly hydration ions (Arakawa and Timasheff, 1985).

Non-ionic molecules can also affect the physical properties of water. Urea (Figure 4.2A) is a non-ionic molecule which H-bonds to water and at high concentrations disrupts the water H-bond network (Tanford, 1968, Das and Mukhopadhyay, 2009).

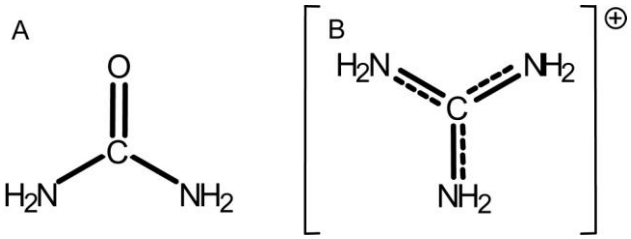

Figure 4.2: The chemical structures of urea (A) and guanidinium (B)

In solution, Gdn.HCl acts as an ionic species (Figure 4.2B) dissociating into Gdm^+ and Cl^- ions. Early studies compared the ionic character of Gdn.HCl to sodium chloride (NaCl). Salts such as NaCl, are well-known to influence the stability and solubility of proteins and are used at various concentrations in buffers for protein studies. The presence of salts is believed to prevent unfavourable charge-charge interaction between amino acid side chains, and this characteristic is often referred to as the "salt effect"(Hagihara et al., 1993, Dempsey et al., 2005). Similar salt effects to protein stability have been observed when proteins are dissolved in low concentrations (i.e. < 3 M) of Gdn.HCl. A study using ITC showed that ubiquitin is more stable (i.e. 18.6 kJ/mol) in low Gdn.HCl concentrations than in the absence of this compound (Makhatadze and Privalov, 1992). This observation is apparently due to the ionic character of Gdn.HCl at low concentrations, whereby the positively charged Gdm^+ interacts with negatively charged side chains of the protein and the Cl^- ions interact with the positively charged side-chains.

At high concentration, Gdm^+ acts as a strong denaturant destabilising the global fold of the protein. Data from ITC and X-ray crystallography of proteins in the presence of Gdn.HCl show that this denaturant interacts with both the folded and the unfolded

states of proteins (Bhuyan, 2002, Lopez and Makhatadze, 2002). This study revealed that as the protein unfolded the amount of bound Gdn.HCl increased (Zou et al., 1998, Dempsey et al., 2005, Alonso and Dill, 1991) which indicates that Gdn.HCl directly interacts with the protein. Further, this study concluded that the protein expanded as the concentration of Gdn.HCl was increased making the hydrophobic part of the protein accessible to the denaturant (Alonso and Dill, 1991, Myers et al., 1995).

There are two fundamental mechanisms by which Gdn.HCl denatures a protein. The first mechanism involves the direct H-bonding interactions with accessible amide and carbonyl H-bond groups of the protein. The amide group of Gdm^+ competes with the hydration shell water for the acceptor carbonyl groups in the protein backbone. This disrupts secondary structure elements, thus destabilising the protein which leads to protein expansion, and therefore exposing the hydrophobic core to solute and solvent (Dempsey et al., 2005).

The second mechanism, which is coupled with the first mechanism, involves the displacement of water molecules that form the protein hydration shell (Makhatadze and Privalov, 1992). The positively charged Gdm^+ ions exhibit weak interactions with bulk water. Consequently, this ion has been shown to not significantly perturb the H-bonding network of water (Mason et al., 2004). Studies indicate that Gdm^+ ions displace water molecules located at the protein-water interface (i.e. protein hydration shell). Moreover, neutron diffraction studies on Gdm^+ and SCN^- (thiocyanate) show that they are both poorly hydrated ions. The partial dehydrated state of the Gdm^+ ions promotes the interaction with poorly hydrated regions on the protein surface, in particular regions that are buried within the protein that become exposed as denaturation proceeds. These results showed that the Gdm^+ ion is flat and rigid with no freely rotating C─N bonds. These properties of Gdm^+ have a twofold effect. First the N–H●●●O H-bond between Gdm^+ and water is about half the strength of the water-water O–H●●●O H-bond (Mason et al., 2003). Secondly the Gdm^+ ions are "sticky" and are "pushed" on to poorly hydrated regions of protein surfaces by the relatively more favourable water-water H-bond interactions.

In contrast to Gdn.HCl, urea is a non-ionic chaotrope, and in some cases regarded as a weak kosmotrope at low concentrations. Although urea is also found to be weakly hydrated, this denaturant more readily forms H-bonds with water compared to Gdn.HCl, due to the C═O acceptor and NH donor atoms.(Dill, 1990) However, as with

Gdm^+, the interaction between water and urea is weaker than water-water interaction. Nonetheless, urea does disrupt the dynamic network of H-bonds in pure water. Due to this disruption of the water-water H-bond network by urea, the relative interaction of water molecules with other molecules is likely to be stronger (Rezus and Bakker, 2006). If a protein molecule is present, the water is therefore more likely to compete for H-bonds of the protein, and thus aid protein unfolding. In the initial unfolding process, urea interacts directly with the protein molecule which facilitates the unfolding of the protein. During the initial unfolding process, water molecules are able to penetrate into the non-polar buried part of the protein. The water molecules begin to compete with the buried amide backbone H-bonds network which results in the weakening of the protein H-bonds (Lim et al., 2009), resulting in further unfolding of the protein. H-bonding by urea to the protein donor and acceptor groups also occurs (see below).

Studies have shown that in conditions where urea is less than optimally hydrated (6–8 mol/L, such as the internal region of proteins), urea will H-bond to itself and to the protein. This absence of sufficient hydration increases the hydrophobic nature of urea and hence this denaturant further interacts with available sites on the protein, leading to localised dehydration-led denaturation (Timasheff and Xie, 2003), NMR studies have concluded that urea interacts directly with the aliphatic side chains of a denatured protein. This interaction with aromatic side chains has also been determined by computational studies (Dotsch et al., 1995), This denaturant clearly interacts directly with the protein, but whether this interaction is the initiation event that causes protein unfolding remains to be resolved.

Some of the initial studies by Tanford and De (1961) (Tanford and De, 1961) examining the effect of urea on protein stability, suggested that this denaturant disrupts the H-bond network in protein secondary structures by H-bonding with donor and acceptor moieties of proteins. This initial suggestion is supported by more recent research examining the denaturing properties of urea (Prakash et al., 1981, Makhatadze and Privalov, 1992, Bhuyan, 2002) and that as the denaturant concentration increases, urea molecules displace water molecules located in close proximity to the protein intramolecular H-bonds. Urea (Figure 4.2A) acts as a strong H-bond donor (amino group) and acceptor (carbonyl group), and therefore will compete with the donor and acceptor groups of the protein to form H-bonds. The proposed mechanism of urea denaturation of proteins involves two stages. In the initial stage of denaturation, urea

interacts with readily accessible backbone H-bond acceptor and donor groups, thus weakening the secondary structure elements. This initial interaction leads to the protein expanding and allowing urea to readily diffuse into the central buried hydrophobic regions of the protein where it further destabilises the protein structure via both H-bonding with donor and acceptor H-bond moieties and destabilising crucial hydrophobic interactions (i.e. hydrophobic effect, see (Section 1.1.3.1)).(Zou et al., 1998)

In this study the effect of urea and Gdn.HCl on ubiquitin (secondary) structure using NMR spectroscopy has been studied. Previous CD, IR and NMR studies on ubiquitin denaturation have shown that there are no folding intermediate states and ubiquitin unfolds via a two-state process. Due to this rapid transition from a folded state to an unfolded state, only the early stages of protein unfolding were examined by NMR spectroscopy. The midpoint of unfolding for ubiquitin in Gdn.HCl and urea was determined to be 4.5 and 5.5 M concentration respectively (Briggs and Roder, 1992, Wintrode et al., 1994, Makhatadze et al., 2003). NMR data collected for ubiquitin close to the mid-point concentrations could not be analysed quantitatively because of the two-state unfolding process which is in the slow-exchange regime (i.e. $< 100\ s^{-1}$).

From a kinetic standpoint, the NMR data showed that at low concentrations of denaturant (i.e. < 4 M) ubiquitin undergoes fast conformational exchange processes. This was observed by small gradual chemical shift changes as the denaturant concentration was increased (Figure 4.3) and is in accord with previously published data (Ibarra-Molero et al., 1999a). These changes in chemical shift represent subtle conformational changes to ubiquitin rather than representing unfolding of the protein. These observed resonance shift changes were seen in both the $^{1}H–^{15}N$ HSQC and the long-range HNCO experiments. At higher denaturant concentrations close to the midpoint (and beyond) of unfolding, additional resonances were clearly observed in the spectra. These resonances clustered at chemical shift values indicative of random coil structures and represent ubiquitin in the denatured state. The intensities of these resonances increased as the denaturant concentration increased concomitantly with a decrease in the intensity of the peaks representing the primarily folded state. The presence of resonances representing both the native and denatured state indicated that the folding-unfolding exchange rate was slow on the NMR chemical shift timescale of the experiments used in this study.

NMR parameters (i.e. $^{h3}J_{NC'}$ couplings, ^{1}H chemical shifts and $^{1}J_{NH}$ couplings) can probe individual H-bond moieties. NMR data enables a direct characterisation of individual H-bonds. These H-bond couplings were analysed on the basis of their location in ubiquitin secondary structures. The $^{h3}J_{NC'}$ couplings observed for the H-bonds of ubiquitin in Gdn.HCl over a concentration range between 0 (no denaturant) ─ 3 M Gdn.HCl showed an overall increase in size at concentrations ≤1.5 M Gdn.HCl, followed by a decrease in the majority of $^{h3}J_{NC'}$ couplings for the H-bonds observed in ubiquitin at 3.0 M Gdn.HCl. This decrease, while not representing an unfolded state of ubiquitin, most likely represented the initial weakening of secondary structure elements. The average $^{h3}J_{NC'}$ couplings in 3.0 M urea showed no change to the average $^{h3}J_{NC'}$ couplings in no denaturant; however, a detailed analysis of individual H-bonds showed that urea affected the hydrophobic part of ubiquitin.

4.2 The chemical shifts and peak intensities of NMR spectra recorded on ubiquitin in varying denaturant concentrations

The $^{1}H_N$ chemical shift is an NMR parameter that has been used to probe protein structure and stability. Changes in $^{1}H_N$ chemical shift values have been an effective method to measure the influence of denaturants on protein secondary structure. Figures 4.3 A and B show a selected region of 2D $^{1}H–^{15}N$ HSQC spectra of ubiquitin recorded in Gdn.HCl and urea. In Figure 4.3A, an overlay of four 2D $^{1}H–^{15}N$ HSQC spectra of ubiquitin recorded in the absence and presence of Gdn.HCl (i.e. 2, 4 and 6 M) is shown. In Figure 4.3B, an overlay of five 2D $^{1}H–^{15}N$ HSQC spectra of ubiquitin recorded in the absence and presence of urea (i.e. 2, 4, 6 and 8 M) is shown. In both figures, the $^{1}H_N$ chemical shift values of the peaks shifted downfield as the concentration of the denaturants was increased. At concentrations above 4 M, a second set of cross peaks were clearly visible in the spectrum. These peaks are clustered around the $^{1}H_N$ random coil chemical shift values which range between ~8.0 ± 0.5 ppm. These peaks represent the population of unfolded protein. The appearance of the second set of peaks is accompanied by a reduction in the intensity of the peaks representing folded ubiquitin. Since the peak intensity is representative of the amount of protein present, the decreases in peak intensities clearly demonstrates that the amount of folded ubiquitin decreases as the denaturant concentration increases.

In general, the changes in the ^{15}N chemical shift values for the peaks representing the folded ubiquitin are modest. Such an observation has been previously made, in which

these studies suggest that the amide ^{15}N nucleus is influenced strongly by other factors such as a side-chain conformation and structure (Wishart et al., 1991).

Unlike the observation in Chapter 3 where an increase in temperature resulted in an upfield shift which correlates with a weakening of the H-bonds (Equation 3.3 Figure 3.5), the increase in denaturant concentration resulted in a downfield shift. Consequently, factors in addition to the effects H-bonding have influenced the $^{1}H_N$ chemical shift. In particular, the chemical environment of the amide groups significantly changes as the denaturant concentration increases. Moreover, the mere presence of the denaturant will impact strongly on the chemical environment of the amide groups (i.e. moving from an H_2O to denaturant "rich" environment. The observation of deshielding often occurs when the observed nucleus is located near a positive charge or electropositive atom/ion (Wishart et al., 1991, Wishart and Case, 2001). Conversely, shielding occurs when the observed nucleus is in the vicinity of a negative charge or an electronegative atom. The charged Gdm^+ and Cl^- ions may therefore also contribute to the observed changes in the $^{1}H_N$ and ^{15}N chemical shifts. For example E62 shows a significantly larger $^{1}H_N$ downfield shift compared to other peaks representing other amide groups. This strong chemical shift change is possibly due to the negatively charged glutamate side chain interacting with a Gdm^+ ion. Similarly, urea also shows a downfield shift similar to that observed for the Gdn.HCl data although the changes in the $^{1}H_N$ chemical shifts are generally smaller in size. This is presumably due to the weaker denaturant properties of urea and possibly the additional influence of the ionic character of Gdn.HCl on the chemical shifts.

By maintaining a constant protein concentration the reduction in peak intensities can be used to calculate the equilibrium of ubiquitin unfolding. As this set of experiments maintained a constant protein concentration (see Section 2.4), it was possible to extract thermodynamic information on the stability of ubiquitin using the 2D $^{1}H–^{15}N$ HSQC spectra.

Figures 4.4 and 4.5 depict the decreasing peak intensities for 10 selected residues of ubiquitin as the denaturant. The peak intensities obtained from Gdn.HCl denaturation (Figures 4.4) do not asymptote. As Gdn.HCl is a salt, increasing the concentration also influences the peak intensities because the charged ions of Gdn.HCl increase the conductivity of the sample which directly effects the sensitivity of the NMR experiment (Kelly et al., 2002). The main factors contributing to the basic signal to

noise (S/N) ratios of NMR measurement are contained in the following equation (Cavanagh, 2007):

$$S/N\alpha \frac{N\gamma_e\gamma_d{}^{3/2}B_0{}^{3/2}K}{\sqrt{\Delta f\left(T_cR_c+T_a\left[R_c+R_s\right]+T_sR_s\right)}} \qquad \text{Equation [4.1]}$$

In which N is the number of observed nuclei γ_e and γ_d are the magnetogyric ratios of the excited and detected nuclei, respectively, B_0 is the static magnetic field strength, K is a factor dependent on the coil design, Δf is the receiver bandwidth (in Hz), R_c and T_c are the resistance and the temperature, respectively, of the coil. T_a is the noise temperature of the preamplifier, T_s is the sample temperature, and R_s is the resistance induced by the sample coil, which is influenced by the Gdm^+ and Cl^- ions.

In contrast, urea is not a charged molecule therefore the decrease in the peak intensity (Figure 4.5) is due to the protein unfolding and therefore this data can be used to extract approximate thermodynamic data.

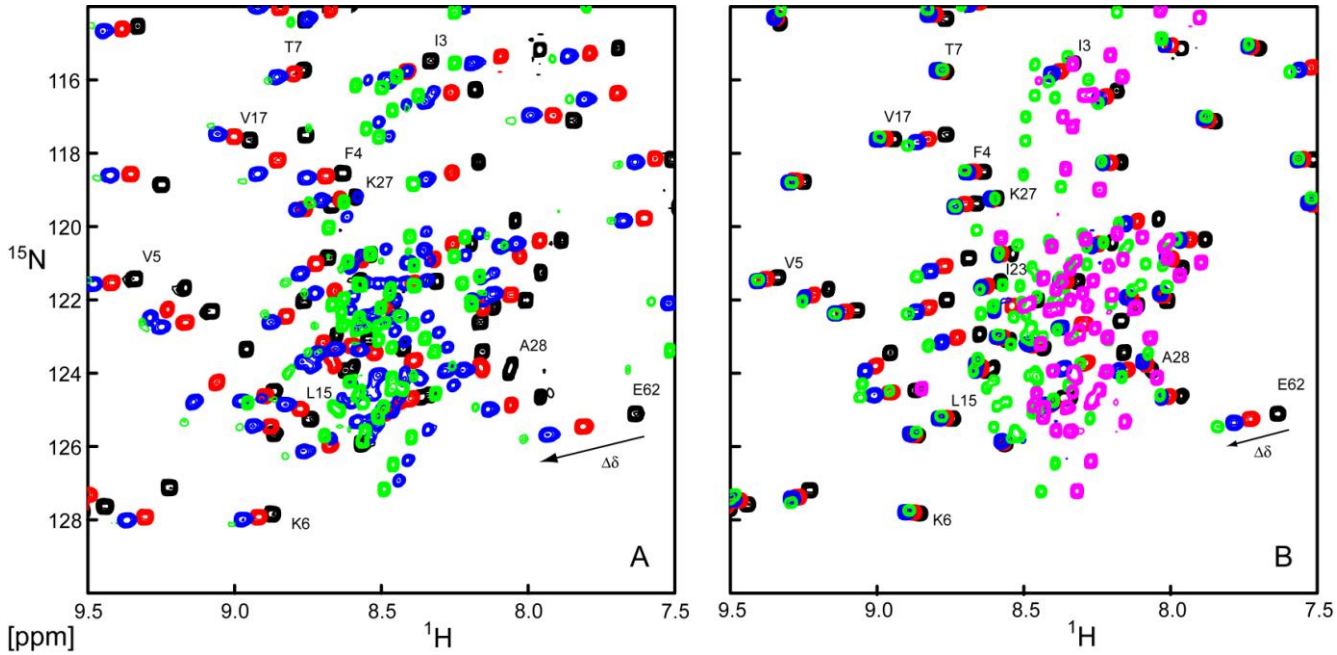

Figure 4.3: (A) Overlay of a region of the 2D ^{1}H-^{15}N HSQC spectra of ubiquitin in the absence (black contours) of denaturant and in the presence of, 2 M (red contours), 4 M (blue contours) and 6 M (green contours) Gdn.HCl. (B) Overlay of a region of the 2D ^{1}H–^{15}N HSQC spectra of ubiquitin in the absence of urea (black contours) and in the presence of 2 M (red contours), 4 M (blue contours), 6 M (green contours) and 8 M (magenta contours) urea.

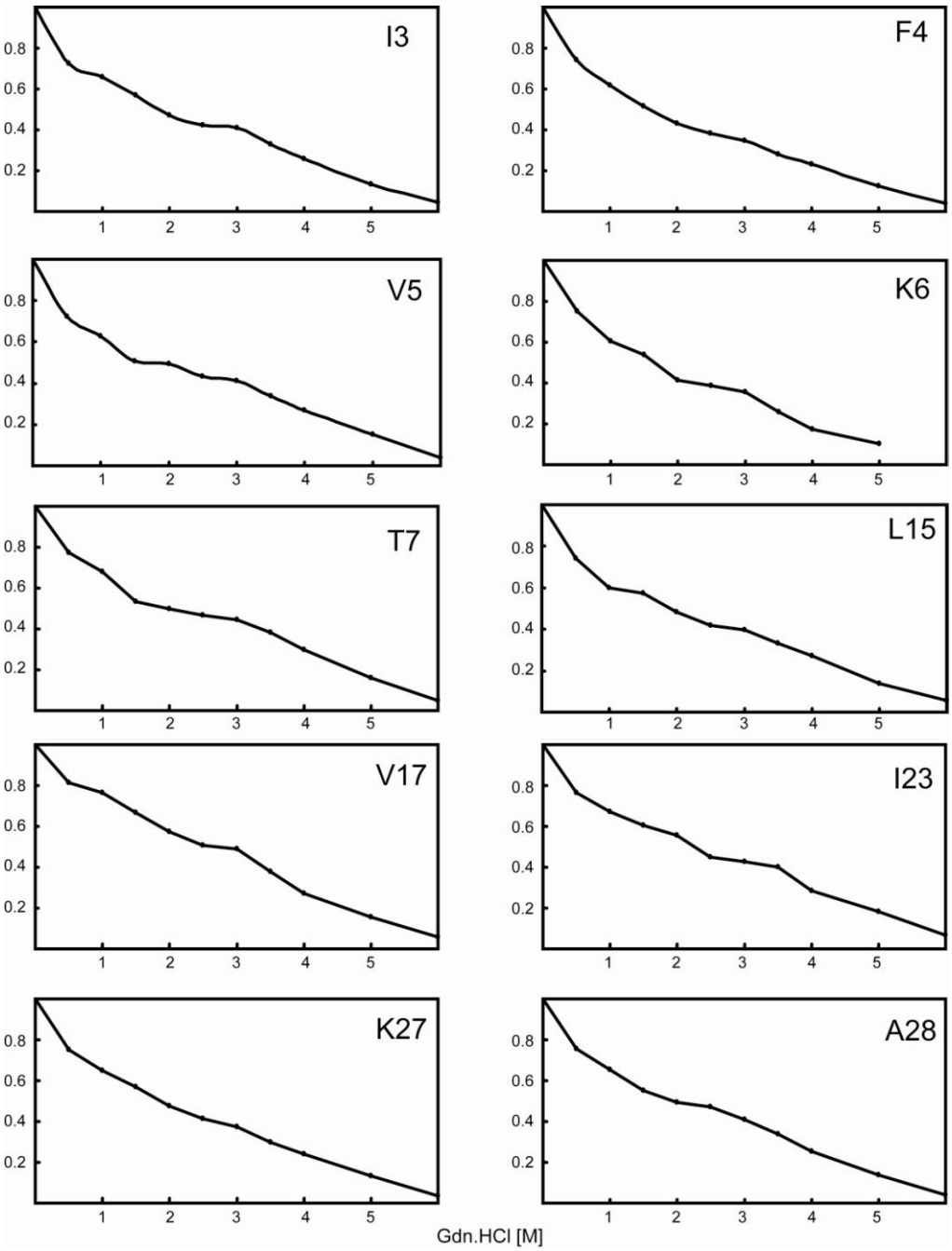

Figure 4.4: Selected residues in which normalised peak intensities have been extracted from the 2D ^{1}H-^{15}N HSQC spectra recorded for ubiquitin in Gdn.HCl concentrations ranging between 0 and 6 M Gdn.HCl.

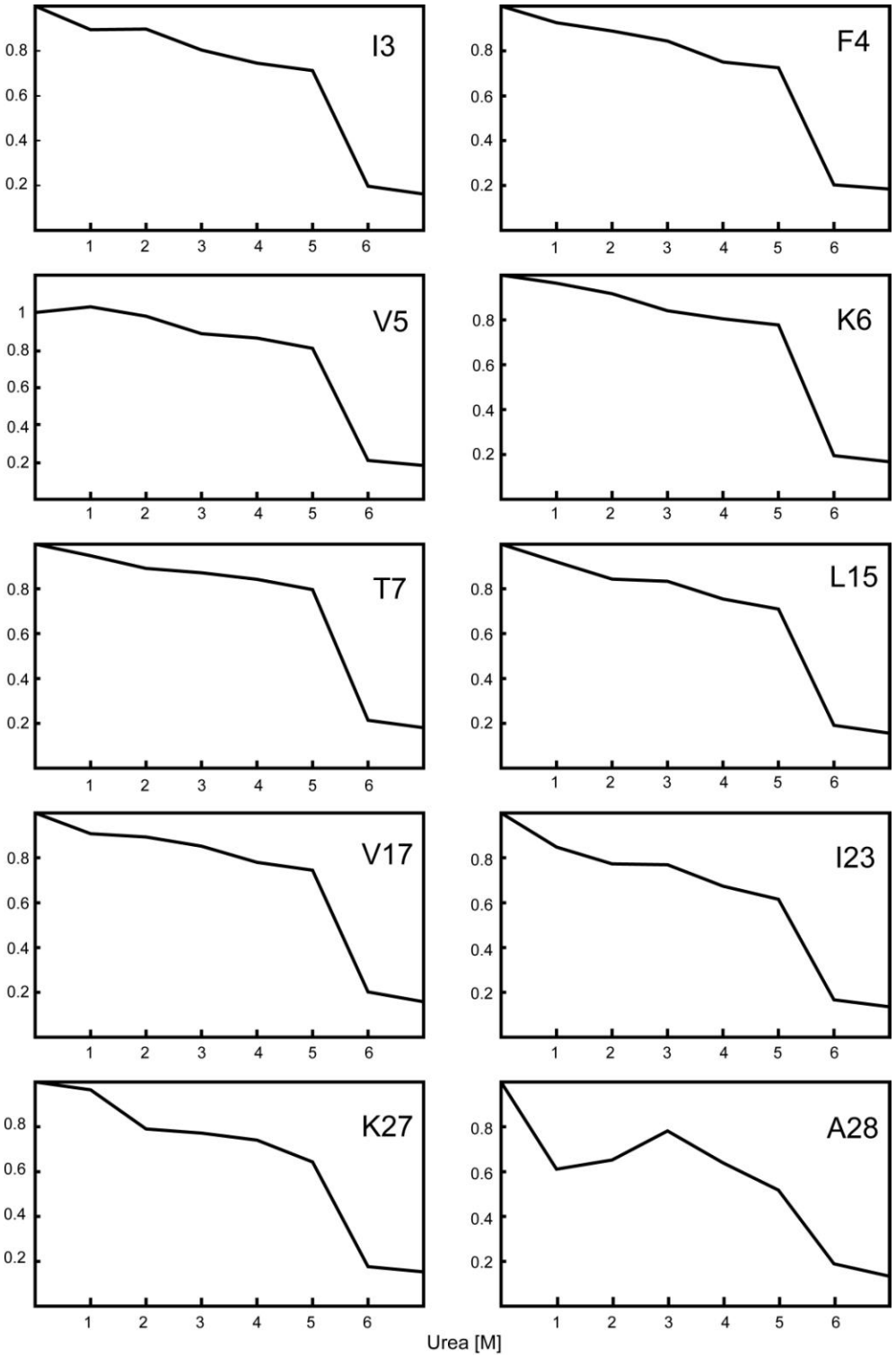

Figure 4.5: Selected residues in which normalised peak intensities have been extracted from 2D ^{1}H-^{15}N HSQC spectra recorded for ubiquitin in urea concentrations ranging between 0 and 7 M urea.

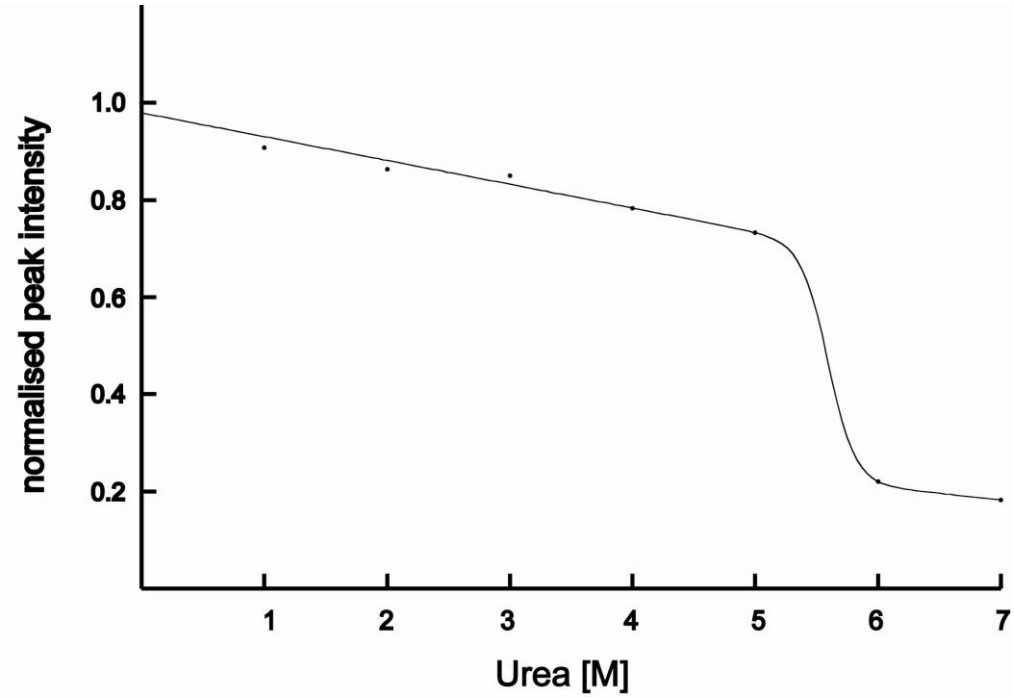

Figure 4.6: The fitted normalised average peak intensities from 2D ^{15}N-^{1}H HSQC titration experiments to equation 4.2 between 0 and 7 M urea, with each dot depicting a 1.0 M increment.

Figure 4.6 shows the average peak intensities of 40 ubiquitin residues between concentrations of 0 to 7 M urea. The intensities where fitted to non-linear least squares fit (equation 4.2). This approach used six parameters to fit the data: a slope and intercept for the pre- and post-transition region, $\Delta G°(H_2O)$ and *m* for the transition region. This gives the following formula (Pace and Shaw, 2000):

$$y = \{(y_F + m_F[ureal]) + (y_U + m_U[urea]) * \exp - ((\Delta G^\circ(H_2O) - m * [urea])/RT)\}/ (1 + \exp - (\Delta G^\circ(H_2O) - m * [urea])/RT) \quad \text{Equation [4.2]}$$

where y_F and y_U are the intercepts and the m_F and m_U are the slopes of the pre- and post-transition baseline, and $\Delta G^o(H_2O)$ and *m* is defined by linear extrapolation method:

$$\Delta G = \Delta G°(H_2O) - m[urea] \quad \text{Equation [4.2]}$$

Table 4.1 The table shows the $\Delta G^{o}(H_2O)$ value and slope in kJ/mol for the non-linear least square fit of ubiquitin in 0 to 7 M urea.

	kJ/mol	**Error**
ΔG^{o} H_2O	127	340
Slope	22.8	60

At pH 4.7 ubiquitin has a Gibbs free energy of unfolding in the absence of urea (i.e. $\Delta G^{o}H_2O$) of 127 kJ/mol (Table 4.1). This is a high value with a very high error. This is the result of only seven data sets collected; none of the data points in the region of the rapid intensity change. As such the value of $\Delta G^{o}H_2O$ is difficult to accurately calculate from the data points collected. The mid-point transition ($C_{1/2}$) is 5.5 M urea (from equation 4.3) and is in agreement with previous studies of ubiquitin in urea at pH 5.0 (Loladze and Makhatadze, 2002).

4.3 Overview of the influence of Gdn.HCl and urea on ubiquitin secondary structure by NMR spectroscopy

Figure 4.7 shows the average change in the $^{h3}J_{NC'}$ couplings recorded on ubiquitin in the presence of either Gdn.HCl or urea. In this figure, the changes in the $^{h3}J_{NC'}$ ($\Delta^{h3}J_{NC'}$) are presented. Here $\Delta^{h3}J_{NC'}$ = $|^{h3}J_{NC}'|$ (denaturant) – $|^{h3}J_{NC}'|$ (no denaturant) and the $^{h3}J_{NC}'$ (denaturant) values are for data recorded in the presence of 1.5 or 3 M denaturant concentrations. In addition, $\Delta^{h3}J_{NC'}$ values for $|^{h3}J_{NC'}|$ (3M Gdn.HCl) – $|^{h3}J_{NC}'|$ (1.5M Gdn.HCl) are reported in Figure 4.7. A positive $\Delta^{h3}J_{NC'}$ indicates a stronger $^{h3}J_{NC'}$ coupling, whereas a negative $\Delta^{h3}J_{NC'}$ indicates a weakening of the coupling.

In Figure 4.7 A, the calculated average $\Delta^{h3}J_{NC'}$ for all $^{h3}J_{NC'}$ couplings measured for ubiquitin in Gdn.HCl and urea is shown. Errors in the figure are weighted uncertainties from the individual datasets (Taylor, 1997). The changes in $\Delta^{h3}J_{NC'}$ couplings between the absence of denaturant and 1.5 M denaturant showed an average increase of 0.04 Hz. Using Equation 3.3 in Chapter 3, in the presence of 1.5 M Gdn.HCl an average increase of ~0.02 Å in H-bond d_{NO} length was calculated. Although a shortening in the average H-bond lengths of ubiquitin was

observed, there are inaccuracies in the crystallographic model of the structure that were derived for this equation. In addition, factors such as the H-bond angular dependence of the $^{h3}J_{NC'}$ couplings and the different physicochemical conditions of the crystal versus the solution structures will influence the coupling magnitudes. As such, the overall calculation of an average decrease of 0.02 of the H-bond lengths is likely to represent an upper limit value.

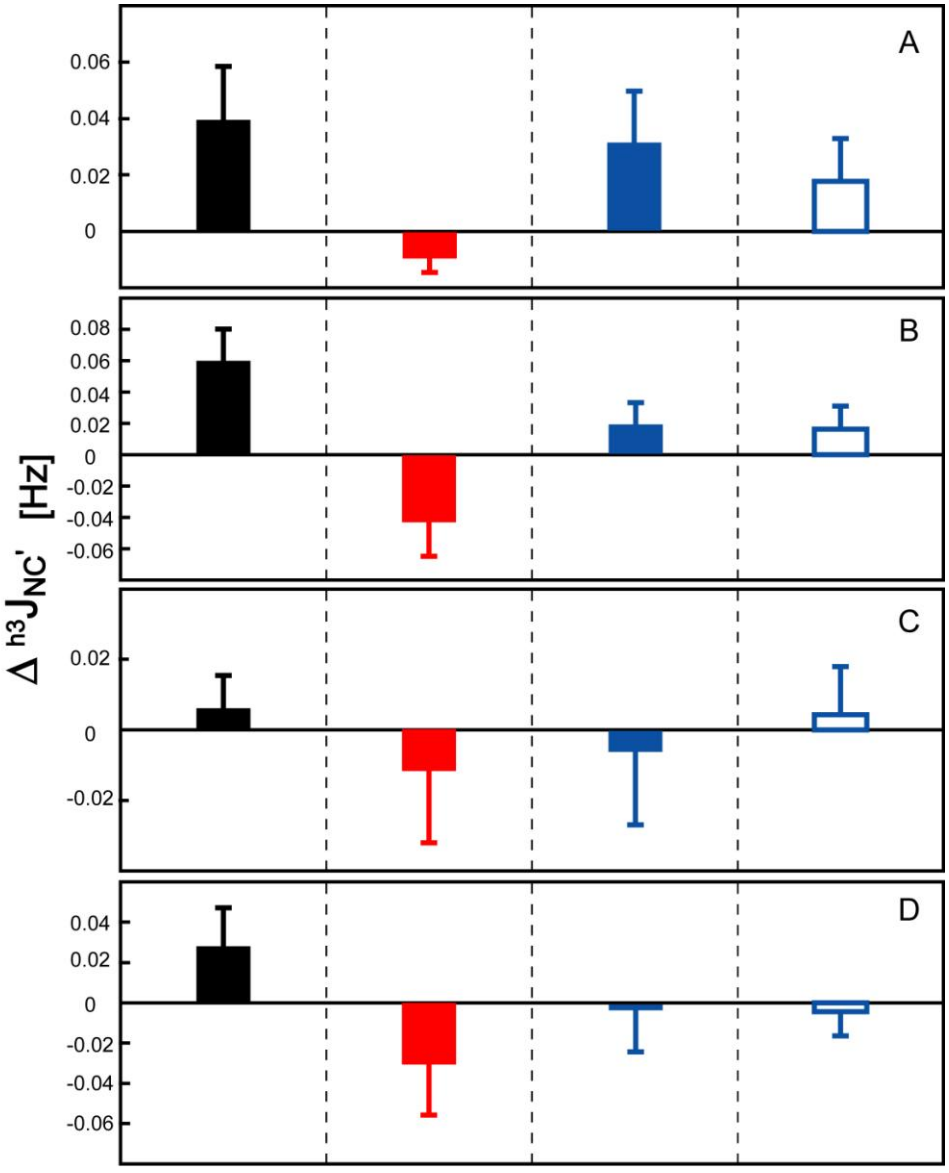

Figure 4.7: Bar graph shows the average changes in $^{h3}J_{NC'}$ values (where $\Delta^{h3}J_{NC'} = |^{h3}J_{NC'}|$ (denaturant) – $|^{h3}J_{NC'}|$ (no denaturant) and ΔME values between no denaturant and 1.5 M Gdn.HCl (black). No denaturant and 3.0 M Gdn.HCl (blue), no denaturant and 3.0 M urea (open blue), and between 3.0 and 1.5 M Gdn.HCl (red). (A) is for all the H-bonds, (B) is for the H-bonds in the α-helix, (C) is for the H-bonds between the β1, β2 and β5 strands. D is for the H-bonds between the β3, β4 and β5 strands.

The $\Delta^{h3}J_{NC'}$ values measured in the presence of 3.0 M denaturant are similar to the values observed in the absence of denaturant. The negative $\Delta^{h3}J_{NC'}$ value observed between 1.5 and 3.0 M denaturant concentrations indicates that the H-bonds are weakening and the protein is expanding in volume. The $\Delta^{h3}J_{NC'}$ between the absence of denaturant and the presence of 3.0 M urea showed an increase in average coupling size. In general what is observed is that at low concentrations of Gdn.HCl and urea the protein is stabilised, which has been shown in previous studies using CD and ITC (Makhatadze and Privalov, 1992). Although a comparison of the $^{h3}J_{NC'}$ coupling data with other biophysical techniques shows similar global trends, the measure of these $^{h3}J_{NC'}$ couplings provides a direct measure of the individual H-bonds. As such, this parameter allows a molecular level investigation of individual H-bonds in secondary structures.

Since the $^{h3}J_{NC'}$ couplings provide direct information on individual H-bonds this NMR parameter also provides insight into the effects of denaturants on different regions of secondary structure elements of ubiquitin. This enabled a comparison of the changes in the H-bond network between secondary structure elements of ubiquitin. The changes between β-sheet regions β1/β2/β5 were compared with the changes in the β-sheet region β3/β4/β5. This provided a more detailed account of how the β-sheets where affected in a different manner with the addition of urea or Gdn.HCl.

The β1/β2 and β1/β5 Figure 4.7C region is the most stable part of the protein with the shortest H-bond lengths and strongest couplings (Appendix 11). This is clearly evident from the average $\Delta^{h3}J_{NC'}$ where there is insignificant change between the absence of Gdn.HCl and 1.5 or 3.0 M Gdn.HCl. The changes in $^{h3}J_{NC'}$ couplings observed between 3.0 M urea and absence of urea where insignificant, which indicate that this region of ubiquitin is stable. The β3/β4 and β4/β5 H-bonded region (Figure 4.7D) showed an increase at 1.5 M Gdn.HCl and then the average drops at 3.0 M Gdn.HCl resulting in a weaker H-bond network for this region of ubiquitin. The average $^{h3}J_{NC'}$ couplings measured in 3.0 M urea showed very similar (i.e. within error) $^{h3}J_{NC'}$ values measured in the absence of urea.

4.4 Detailed observation into the effects of urea and Gdn.HCl on the secondary structure H-bonds of ubiquitin

In the previous section the average $\Delta^{h3}J_{NC'}$ couplings for different secondary structure regions of ubiquitin were compared to understand the influence of Gdn.HCl and urea on ubiquitin structure. Figure 4.8 shows the $\Delta^{h3}J_{NC'}$ values for individual H-bonds, where $\Delta^{h3}J_{NC'} = |^{h3}J_{NC}'|$ (denaturant) $- |^{h3}J_{NC}'|$ (no denaturant). Data is shown for 0.5, 1.0, 1.5, and 3.0 M (Gdn.HCl) and 3.0 M (urea). The changes in individual H-bonds across the different concentrations offers direct insight into which regions of the protein are most influenced as a function of denaturant concentration.

The effect of urea and Gdn.HCl on the $^{h3}J_{NC'}$ couplings vary. In general the $^{h3}J_{NC'}$ coupling increase at low concentrations of denaturant to decreasing as the concentration of denaturant is increased. For some H-bonds, no changes in the magnitude of the $^{h3}J_{NC'}$ couplings were observed. These observations contrast with the temperature study on ubiquitin where a general uniform decrease in $^{h3}J_{NC'}$ couplings as the temperature was increased. This is a result of the thermal expansion of the protein molecule. Presumably, the data presented here indicated that chemical denaturation process, while involving protein expansion and ultimately unfolding, and involves a more complex process on individual chemical moieties of ubiquitin compared to the thermal denaturation processes.

At the lowest concentrations of Gdn.HCl measured (0.5 M, black histogram) the $\Delta^{h3}J_{NC'}$ calculated showed an increase or no change in coupling magnitude across the majority of the H-bonds in ubiquitin. There were three exceptions to this observation: H-bonds T7/K11, I30/V26 and Q31/K27. The H-bonds I30/V26 and Q31/K27 are located in the centre of the α-helix, whereas the H-bond T7/K11 is located in the end of β-sheet β1/β2. The largest increase in $\Delta^{h3}J_{NC'}$ values at 0.5 M Gdn.HCl was observed for H-bonds in the β3, β4 and β5 region of ubiquitin. This was sharply contrasted by the observation that the $^{h3}J_{NC'}$ couplings showed no change for the H-bonds between strands β1 and β2 and for H-bonds constituting the α-helix.

At 1.0 M Gdn.HCl (red histogram) further increases in the $^{h3}J_{NC'}$ couplings were observed, with the largest changes observed for H-bonds in the α-helix. This increase in the sizes of the $^{h3}J_{NC'}$ couplings indicate that the increase in the concentration of Gdm^+ and Cl^- ions increased the stability of the protein.

The α-helix side-chains are more solvent exposed (Appendix 17) hence the Gdm^+ and Cl^- may affect charge-charge repulsions greatest in this secondary structure and this has resulted in the largest increase in $^{h3}J_{NC'}$ coupling values. Excluding the T7/K11 H-bond, the $^{h3}J_{NC'}$ couplings showed no change (within error) for the H-bonds between strands β1 and β2, indicating that the influence of this denaturant to this region of ubiquitin is negligible.

Examination of the three $^{h3}J_{NC'}$ values for H-bonds T7/K11, I30/V26 and Q31/K27 showed that the $^{h3}J_{NC'}$ couplings for H-bonds T7/K11 and Q31/K27 did not change in size (change compared to data recorded at 0.5 M), whereas the H-bond coupling for the I30/V26 H-bond showed an increase in size from 0.5 to 1.0 M Gdn.HCl.

At 1.5 M Gdn.HCl concentration (green histogram) the highest number of $^{h3}J_{NC'}$ couplings showed an increase is size. This observation correlates with the observed data presented in Section 4.3. The greatest increase was observed in the α-helix, β3/β4/β5 and β1/β5 regions of ubiquitin. In contrast, the H-bonds between the β1 and β2 strands showed essentially no change in the size of the $^{h3}J_{NC'}$ couplings or a decrease was observed for couplings related to the H-bonds F4/S65 and L15/I3. Therefore as Gdn.HCl concentration was increased most regions of ubiquitin were more stable while the H-bonds involved in the β1/β2 sheet were not influenced or appear to weaken. In the α-helix two more $^{h3}J_{NC'}$ couplings were measured for H-bonds K27/I23 and K33/K29, which were not detected at lower Gdn.HCl concentrations due to signal overlap.

At a Gdn.HCl concentration of 3.0 M (blue histogram) smaller $^{h3}J_{NC'}$ couplings were observed. The decrease in the magnitude of the $^{h3}J_{NC'}$ couplings were observed across the protein. This indicates that the H-bonds of the protein are weakening and thus the protein is shifting from a tighter more stable packing to an unfolded state. This has been proven by X-ray and ITC studies of proteins soaked in low concentrations of Gdn.HCl which suggest the denaturants reduce the mobility of the protein in its native state (Makhatadze and Privalov, 1992). At concentration beyond 3.0 M the protein starts to unfold. In general, the $^{h3}J_{NC'}$ values for the H-bonds of ubiquitin decreased when the protein was in the presence of 3.0 M Gdn.HCl. Only $^{h3}J_{NC'}$ couplings for the H-bonds I3/L15,

D32/A28, L67/F4, L69/K6 and S57/P19 showed an increase in value. The largest decreases in $^{h3}J_{NC'}$ couplings were observed for H-bonds located in β1/β2. This highlights that the H-bonds of this region of the protein are the first to collectively weaken and may represent the initial point of ubiquitin denaturation.

There are cases were an increase in $^{h3}J_{NC'}$ couplings was observed at all the denaturant concentrations used (i.e. I3/L15, D32/A28, S57/P19, L69/K6). In contrast, there were a few H-bonds (i.e. Q31/K27 and R42/V70) that showed a decrease in $\Delta^{h3}J_{NC'}$ at all the Gdn.HCl concentrations measured. The β2/β1 donor acceptor region of ubiquitin showed a general decrease in $^{h3}J_{NC'}$ coupling size as the Gdn.HCl concentration was increased.

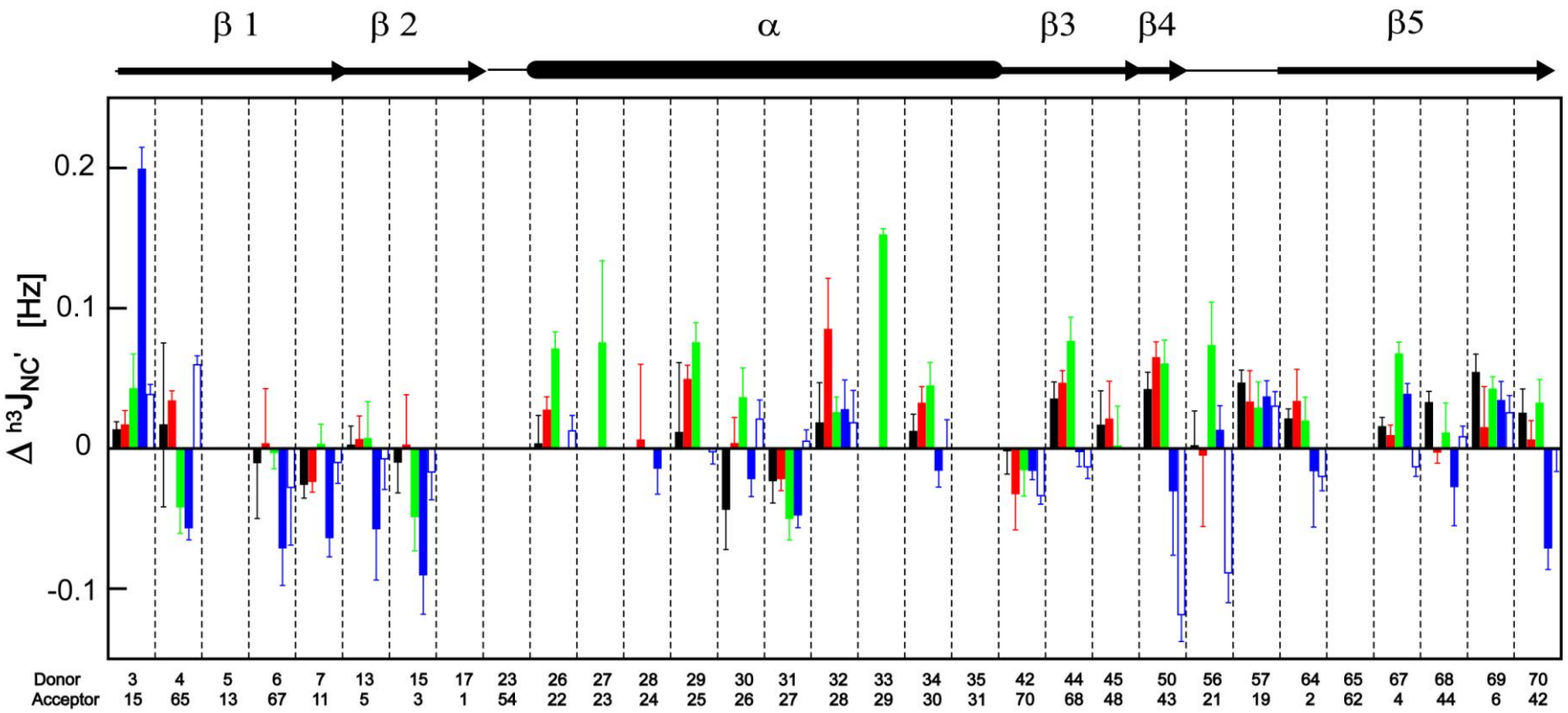

Figure 4.8: Histogram of $\Delta\,{}^{h3}J_{NC'}$ couplings between 0 M and 0.5 M Gdn.HCl (black), 1.0 M Gdn.HCl (red), 1.5 M Gdn.HCl (green), 3.0 M Gdn.HCl (blue) and 3.0 M Urea (blue open). Upper limits values for ${}^{h3}J_{NC'}$ couplings were determined for H-bonds where either peak overlap or the absence of a peak in the ${}^{h3}J_{NC'}$ couplings active experiment obfuscated the ability to determine the coupling size (explained in Section 2.5.2)

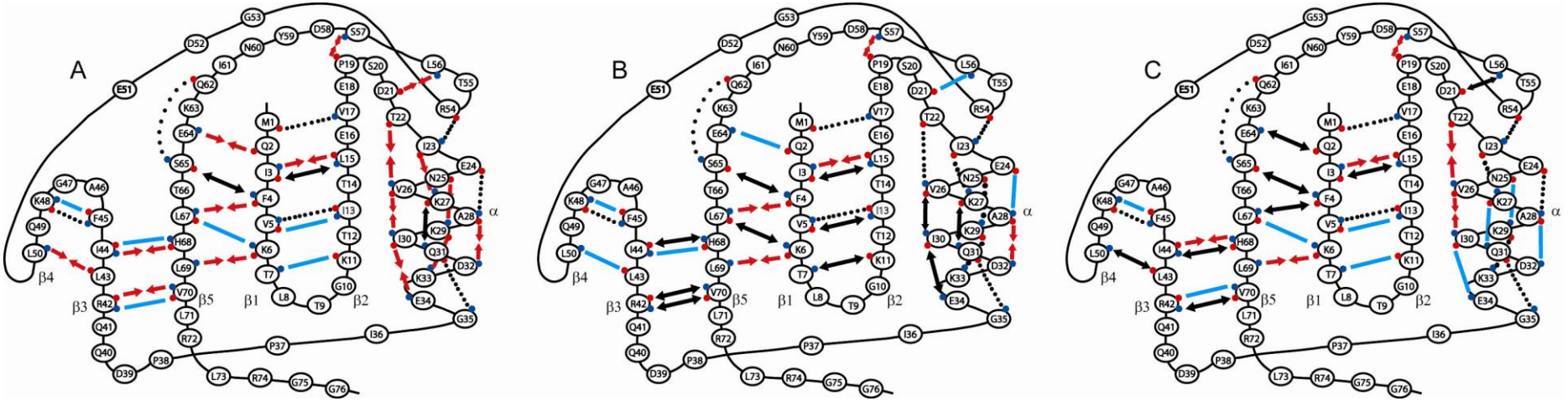

Figure 4.9: Ubiquitin secondary structure topology and the backbone H-bonds as observed by the $\Delta^{h3}J^{NC'}$ couplings between (A) 0 and 1.5 M Gdn.HCl, (B) 0 and 3.0 M Gdn.HCl and (C) 0 and 3.0 M urea. The H-bonds are depicted by a dotted line between the amide proton donor (blue circle) and the oxygen acceptor (red circle). The red arrows depict and increase in $^{h3}J_{NC'}$ coupling, black arrows depict a decrease and blue line depicts no change.

The influence of urea on the $^{h3}J_{NC'}$ couplings (open blue histogram) showed a weaker effect on ubiquitin compared to Gdn.HCl. This is presumably due to urea being a weaker denaturant. This is clearly evident in Figure 4.8 were the changes in couplings are smaller in comparison to the 3.0 M Gdn.HCl. Although weaker most of the changes in $^{h3}J_{NC'}$ couplings in 3.0 M urea followed the same trend observed for the 3.0 M Gdn.HCl data. However, six H-bonds showed an increase in $^{h3}J_{NC'}$ coupling sizes in 3 M urea whilst the couplings for these H-bonds decreased in 3 M Gdn.HCl (i.e. F4/S65, V26/T22, I30/V26, L56/D21, L67/F4 and L69/K6) This is presumably due to the different denaturing mechanism of urea to Gdn.HCl (Dempsey et al., 2005, Loladze and Makhatadze, 2002). The most affected region of ubiquitin in 3 M urea was the β3/β4 region, which is regarded as the most hydrophobic region of ubiquitin (Vijay-Kumar et al., 1987). Consequently, this suggests that urea has a preference to interact with the more hydrophobic surface of ubiquitin. This is supported by previous studies examining protein denaturation, including ubiquitin. These studies suggest that urea preferentially targets the most hydrophobic part of the protein structure (Das and Mukhopadhyay, 2009, Timasheff and Xie, 2003, Zou et al., 1998).

4.5 Analysis of the effects of Gdn.HCl and urea on ubiquitin H-bonds in secondary structures

In this section the various NMR parameters used to analyse the stability of ubiquitin at low denaturant concentrations will be compared at three concentrations: 1.5 M (Gdn.HCl), 3.0 M (Gdn.HCl) and 3.0 M (urea). The observed $\Delta^{h3}J_{NC'}$ couplings for H-bonds in the α-helix (Figure 4.10) and H-bonds between the β-strands β1/β2, β1/β5, β5/β3 and β3/β4 (Figures 4.12 and 4.14) will be compared with the corresponding changes in $^{1}J_{NH}$ couplings and $^{1}H_{N}$ chemical shifts. Both these latter NMR parameters have been used to probe H-bond functionality. The $^{h3}J_{NC'}$ couplings are divided into three sections due to each H-bond network reacting differently to the influence of Gdn.HCl and urea. The changes in the $^{h3}J_{NC'}$ couplings between 0–1.5 and 0–3.0 M are plotted on the ubiquitin secondary structure topology diagram. Here, the backbone H-bonds are presented as arrows. Red arrows represent an increase in $^{h3}J_{NC'}$ coupling values, black arrows represent an observed decrease in $^{h3}J_{NC'}$ couplings and blue lines represent no change in $^{h3}J_{NC'}$ coupling (Figure 4.9).

4.5.1 The α-helix

Figure 4.10 shows a histogram of $\Delta^{h3}J_{NC'}$ couplings, $\Delta^{1}J_{NH}$ couplings and $\Delta^{1}H_{N}$ chemical shifts measured between no denaturant and the presence of 1.5 M Gdn.HCl (black), no denaturant and 3M Gdn.HCl (blue), and 1.5 and 3 M (red). The same NMR parameters are presented for ubiquitin in the presence of 3 M urea (open blue). The four H-bonds that give rise to the strongest $^{h3}J_{NC'}$ couplings in the α-helix in the absence of denaturant are residue pairings K27/I23, I30/V26, Q31/K27, and E34/I30. These H-bonds are located on one face of the α-helix that is directed towards the hydrophobic core, or more specifically to the hydrophobic side of the β2 strand. The slight curvature in the α-helix gives rise to shorter H-bonds (average of four H-bonds = 1.93 Å), on the interior side and slightly longer H-bonds on the opposite face of the helix (average of six H-bonds = 2.09 Å). Consequently, in the absence of denaturant the shorter H-bonds led to slightly stronger $^{h3}J_{NC'}$ (average of −0.45 Hz) values, whereas the longer H-bonds (i.e. V26/T22, A28/E24, K29/N25, K33/K29 and G35/Q31) give rise to weaker $^{h3}J_{NC'}$ couplings (average −0.20 Hz). The addition of 1.5 M Gdn.HCl led to an increase for most $\Delta^{h3}J_{NC'}$ values for H-bonds positioned on both the interior and solvent exposed side of the α-helix. The $^{h3}J_{NC'}$ coupling for the H-bond Q31/K27 which is located in the centre of the α-helix was the sole exception (Figures 4.10 and 4.11).

Despite being one of the weakest couplings in the helix (i.e. 0.19 ± 0.004 Hz), the largest change in $^{h3}J_{NC'}$ occurred for the K33/K29 H-bond upon the addition of 1.5 M Gdn.HCl, which may be a result of the Cl^- ion preventing the charge-charge repulsion of both solvent exposed lysine side-chains. Charge repulsion is a long-range effect (1/r, where r is the inter-atomic distance between charged groups) (Aqvist, 1999). As such side chains with like charges that are distal from each other (i.e. 10 Å radius) can still have a weak charge-charge repulsion effect on one another. This effect will influence the overall stability of the α-helix (Loladze and Makhatadze, 2002). The addition of Gdn.HCl leads to the positive Gdm^+ interacting with negatively charged side-chains and the Cl^- ions interacting with the positive side-chains (Makhatadze et al., 1998). Such an interaction will screen long-range electrostatic charge-charge repulsions that are present. The shielding of charge repulsions presumably led to an increase in the stability of the α-helix of ubiquitin. The size of the $^{h3}J_{NC'}$ couplings

increased as a result of this greater stability. This increase in $^{h3}J_{NC'}$ coupling of the K33/K29 H-bond coincides with the strongest downfield $^{1}H_N$ chemical shift. This correlates with either the strengthening of the H-bond or the positively charged Gdm^+ ion deshielding the amide proton atom. The $^{h3}J_{NC'}$ coupling size for H-bond G35/Q31 must be weaker than $^{h3}J_{NC'}$ coupling measured for the H-bond K33/K29 (−0.19 ± 0.004 Hz). The size of this coupling is at the detection limit of the quantitative long-range $J_{NC'}$ experiment (explained in Section 2.3).

The measured $^{h3}J_{NC'}$ couplings for the ubiquitin α-helix in the presence of 3.0 M Gdn.HCl decreased with the exception of the coupling for the D32/A28 H-bond. The change in $^{h3}J_{NC'}$ values between no denaturant and 3 M is very small, which indicated that the α-helix remains structured. This is shown in the topological diagram (Figures 4.11A ($\Delta^{h3}J_{NC'}$, 0−1.5 M) and 4.11B ($\Delta^{h3}J_{NC'}$, 0−3.0 M)). However the $^{h3}J_{NC'}$ couplings for H-bonds on the buried side of the α-helix were influenced by the presence of Gdm^+ and Cl^- to a greater degree than the H-bonds on the exposed surface. This observation correlates with the temperature study where the H-bonds on the inner side of the α-helix were more affected by the change in temperature than the H-bonds on the solvent exposed side. In contrast, studies of $^{h3}J_{NC'}$ couplings in ubiquitin in the presence of 60 % methanol showed a uniform change in the α-helix $^{h3}J_{NC'}$ couplings from native to A-state (Cordier and Grzesiek, 2004). The $^{h3}J_{NC'}$ data highlights that the centre of the α-helix could represent the weak point. Here the H-bond Q31/K27 decreased in $\Delta^{h3}J_{NC'}$ couplings size as the Gdn.HCl concentration was increased. The largest increase in $^{h3}J_{NC'}$ couplings in the presence of low concentrations (i.e. 1.5 M) was observed for H-bonds at the N and C termini of the α-helix. These H-bonds are crucial in preventing the α-helix structure from fraying. Similar observations were made for the temperature denaturation study of ubiquitin. Here, the $^{h3}J_{NC'}$ for the two terminal H-bonds, K27/I23 and E34/30, showed the slowest change in size as a function of increasing temperature ((Cordier and Grzesiek, 2002) and Chapter 3). H-bond cooperativity studies have shown that as the α-helix increases in length the H-bonds present in the centre become stronger (Wieczorek and Dannenberg, 2003b, Wieczorek and Dannenberg, 2003a, Salvador et al., 2007). What is observed from the temperature study is that the central H-bonds weaken due to the thermal expansion of the α-helix. The relaxing of the H-bonds in the centre over-compensate for the H-

bonds at each end of the α-helix. This ensures that these terminal H-bonds remain stable preventing the structure from unfolding. The $^{h3}J_{NC'}$coupling for H-bond E34/I30 showed little change from the absence of denaturant to 3.0 M Gdn.HCl.

Only four $^{h3}J_{NC'}$ couplings were measured at both 1.5 and 3.0 M Gdn.HCl for H-bonds I30/V26, Q31/K27, D32/A28 and E34/I30 H-bonds. The influence of denaturant on the H-bonds I30/V26 and Q31/K27 which are facing into the hydrophobic core of the protein showed a different trend with respect to changes in the $^{h3}J_{NC'}$ couplings. An increase in the size of the $^{h3}J_{NC'}$ coupling for I30/V26 was observed when ubiquitin was dissolved in 1.5 M Gdn.HCl, yet showed a marked decrease in value when increasing the denaturant concentration from 1.5 to 3.0 M (0.05 Hz). In contrast, the $^{h3}J_{NC'}$ coupling for Q31/K27 decreased in value when the protein was in the presence of 1.5 M Gdn.HCl and showed no significant change in coupling size at 3.0 M Gdn.HCl. The $^{h3}J_{NC'}$ coupling results do not correlate with the $^{1}H_{N}$ chemical shift which show a constant downfield chemical shift, while the $^{1}J_{NH}$ coupling showed a very subtle increase in size.

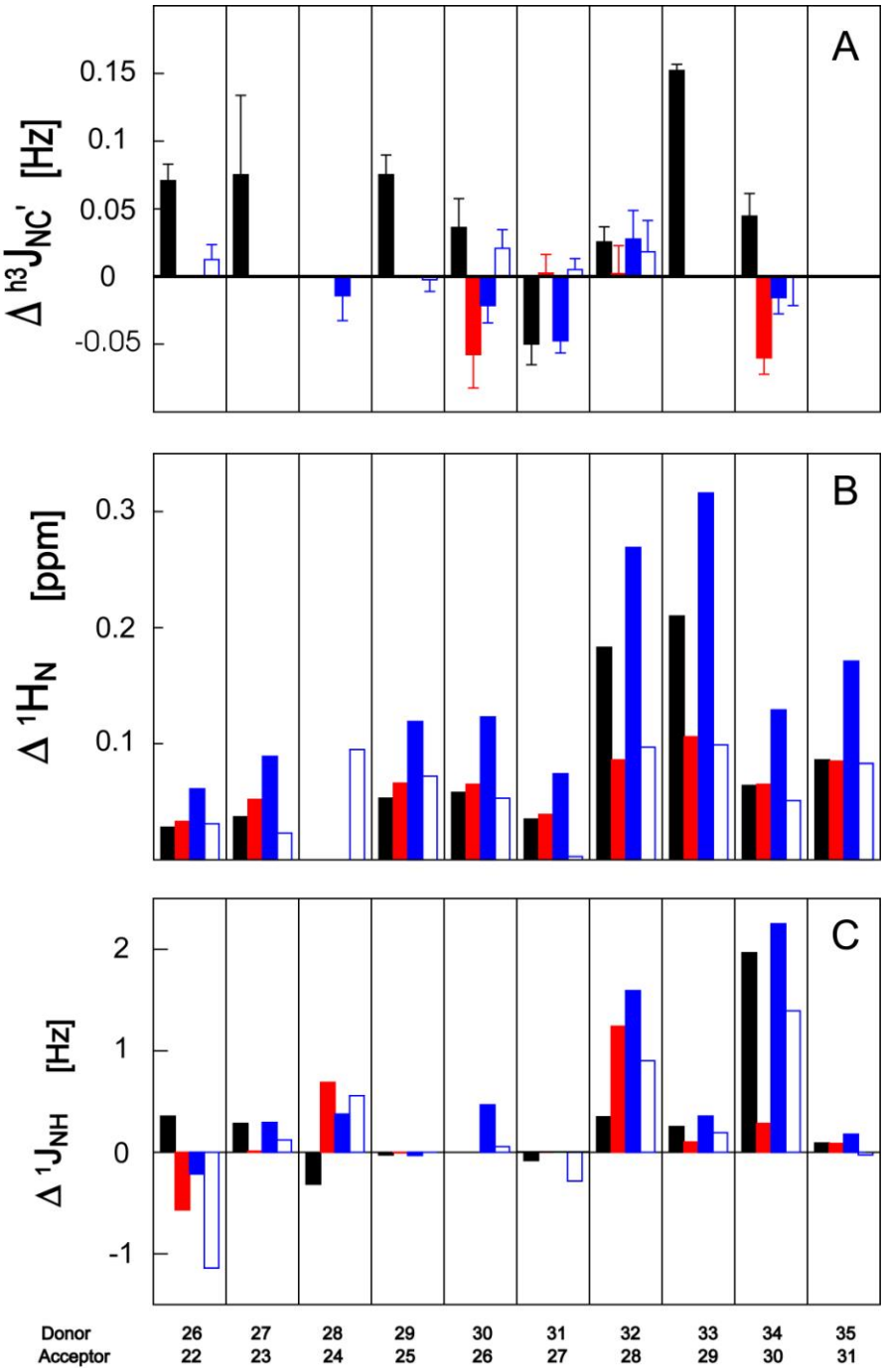

Figure 4.10: Changes in $^{h3}J_{NC'}$ scalar coupling values of the α-helix H-bonds, amide proton $^{1}H_N$ chemical shifts and $^{1}J_{NH}$ couplings. (A) shows the changes in $^{h3}J_{NC'}$ values where $\Delta^{h3}J_{NC'} = |^{h3}J_{NC'}|$ (denaturant) – $|^{h3}J_{NC'}|$ (no denaturant) between no denaturant and 1.5 M Gdn.HCl (black), no denaturant and 3.0 M Gdn.HCl (blue), no denaturant and 3.0 M urea (open blue). The red histogram represents the difference in $^{h3}J_{NC'}$ values between 3.0 and 1.5 M Gdn.HCl. (B) shows the changes in $^{1}H_N$ chemical shifts where the $^{1}H_N$ (denaturant) – $^{1}H_N$ (no denaturant). (C) Shows the changes in the $^{1}J_{NH}$ values where $\Delta^{1}J_{NH} = |^{1}J_{NH}|$ (denaturant) – $|^{1}J_{NH}|$ (no denaturant).

The $^{h3}J_{NC'}$ couplings for H-bond D32/A28 showed an increase in value upon the addition of 1.5 M Gdn.HCl. The coupling showed no further change between 1.5 and 3.0 M Gdn.HCl, yet the donor D32 group is one of the most solvent exposed H-bond donor atoms in the α-helix (30 $Å^2$). Both H-bonds Q31/K27 and D32/A28 are located in the centre of the α-helix but are positioned on opposite faces. Here, Q31/K27 is located on the hydrophobic side and D32/A28 on the solvent exposed side. As the Gdn.HCl concentration is increased Q31/K27 and D32/A28 showed opposite trends in changes in the $^{h3}J_{NC'}$ values. The $^{h3}J_{NC'}$ couplings for the Q31/K27 H-bond decreased at 1.5 M denaturant and remained constant upon an increase of Gdn.HCl to 3.0 M, whereas the $^{h3}J_{NC'}$ couplings for the D32/A28 H-bond increased at 1.5 M Gdn.HCl and showed an insignificant change as the denaturant was increased to 3.0. This could be a result of a compensating effect between the two H-bonds.

The C-terminal H-bond E34/I30 has been shown to be important in providing α-helix stability and is the shortest H-bond in the helix (Vijay-Kumar et al., 1987). Therefore, it is not surprising to observe that for all H-bonds the largest $^{h3}J_{NC'}$ value is for the E34/I30 H-bond (–0.66 ± 0.01Hz). An increase in this $^{h3}J_{NC'}$ coupling to –0.7 Hz was calculated as the Gdn.HCl concentration was increased to 1.5 M. Conversely, the largest decrease in coupling value was observed (0.06 Hz) for the E34/I30 $^{h3}J_{NC'}$ coupling at a denaturant concentration of 3 M. This decrease is similar in magnitude for I30/V26 H-bond coupling between 1.5 and 3.0 M Gdn.HCl (i.e. 0.057 Hz). Both of these H-bonds are located on the hydrophobic side of the α-helix. As mentioned earlier, the H-bonds on this side of the helix were affected the most as the Gdn.HCl concentration increased. Structural studies have shown that the α-helix is slightly bent. This curvature results in shorter H-bond lengths for the H-bonds located on the hydrophobic face. Consequently, the larger decreases in the $^{h3}J_{NC'}$ couplings associated with the H-bonds on this hydrophobic face indicates that the addition of the denaturant loosens and straightens the α-helix.

The five $\Delta^{h3}J_{NC'}$ couplings observed in 3.0 M urea (V26/T22, I30/V26, Q31/K27, D32/A28 and E34/I30) all showed an increase or no change in magnitude which clearly indicates that a higher urea concentration is required to cause a weakening in the α-helix H-bonds. The most significant increase in $^{h3}J_{NC'}$ coupling was observed for H-bond I30/V26 and contrasts to the $^{h3}J_{NC'}$ couplings measured for I30/V26 in 3.0

M Gdn.HCl which showed a significant decrease. This may indicate that urea affects the α-helix in a different manner than to Gdn.HCl. The changes in the $^{h3}J_{NC'}$ couplings observed (i.e. V26/T22, Q31/K27, D32/A28 and E34/I30) showed changes within the error which indicates α-helix stability at 3 M urea. The $^{1}H_{N}$ chemical shifts in urea show a downfield change similar to what was observed for the $^{1}H_{N}$ chemical shift in Gdn.HCl, although the $^{1}H_{N}$ chemical shifts are weaker in comparison to the Gdn.HCl $^{1}H_{N}$ shifts (explained in Section 4.2). Overall, the $^{1}J_{NH}$ couplings show an increase, yet there is no clear correlation with the $^{h3}J_{NC'}$ couplings which has previously been shown (i.e. increase in $^{h3}J_{NC'}$ leads to a decrease in the $^{1}J_{NH}$).

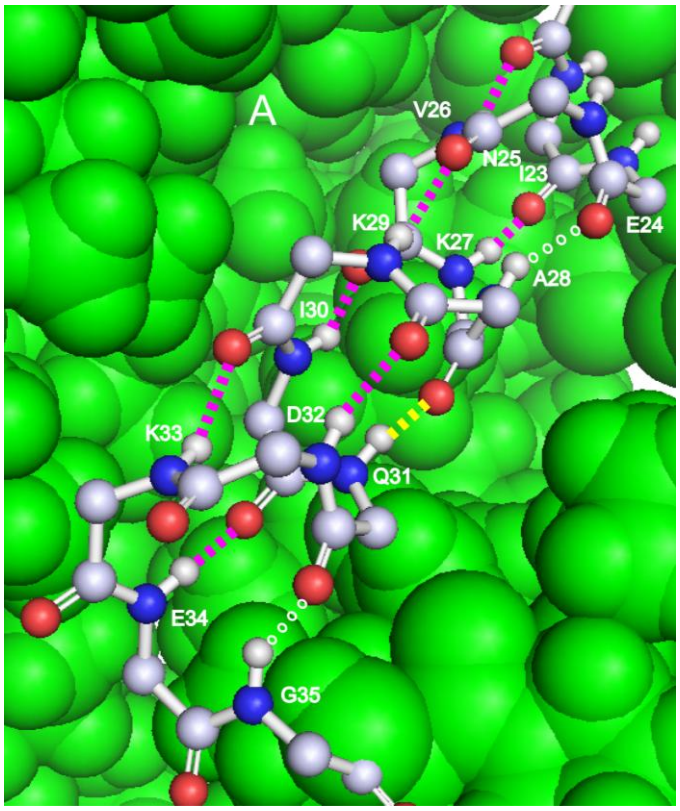

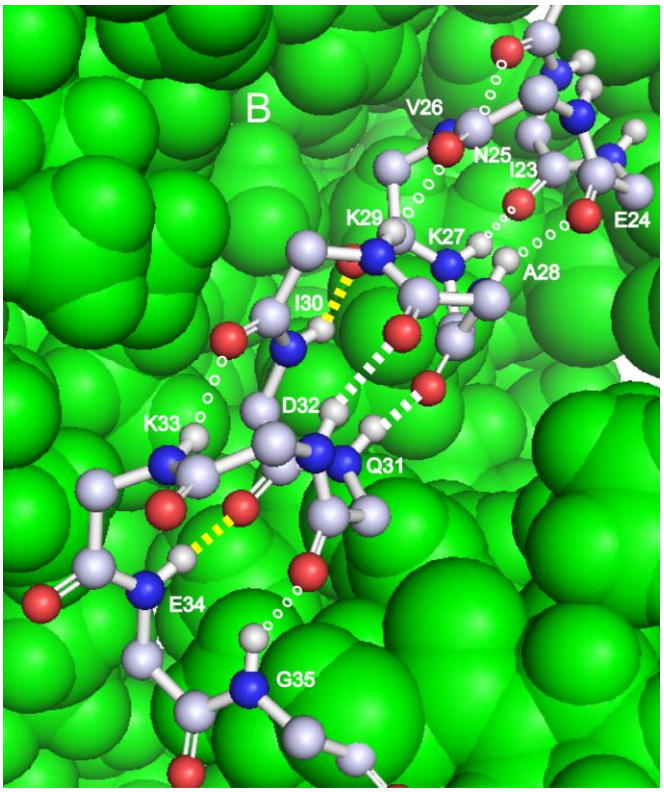

Figure 4.11: Backbone and H-bond structure of the α-helix (ball and stick) of ubiquitin. The remaining part of the structure is shown as a space-filled representation. The H-bonds are represented by dashed lines. Iincrease in $^{h3}J_{NC'}$ values (magenta), decrease in $^{h3}J_{NC'}$ values (yelllow), No change in $^{h3}J_{NC'}$ values (white) and the $^{h3}J_{NC'}$ values not calculated (white open circles). (A) shows the changes in $^{h3}J_{NC'}$ values between no denaturant and 1.5 M Gdn.HCl. (B) shows the difference in $^{h3}J_{NC'}$values between 3.0 and 1.5 M Gdn.HCl.

4.5.2 H-bond connectivities between β2/β1 and β1/β5 strands

In the absence of denaturant, the H-bonds connecting β strands β1/β5 (E64/Q2, F4/S65, L67/F4, K6/L67 and L69/K6) had the strongest $^{h3}J_{NC'}$ couplings with an average value of 0.61 Hz, which correlates with a shorter average H-bond length of ~1.90 Å (Figure 4.12). The strongest $^{h3}J_{NC'}$ coupling observed in ubiquitin was for the E64/Q2 H-bond 0.8 Hz. This coupling correlates with the short H-bond length (r_{OH}) of 1.86 Å. The H-bonds between stands β1/β2 (V17/M1, I3/L15, L15/I3, V5/I3, I13/V5 and T7/K11) showed a weaker $^{h3}J_{NC'}$ coupling average of 0.56 Hz and is presumably due to the longer r_{NO} distances (average of ~1.99 Å) as compared to the H-bonds between the β1/β5 strands. The $^{h3}J_{NC'}$ couplings where not measured for H-bonds M17/I3 and V5/I13 due to peak overlap (Cordier and Grzesiek, 2002).

A general increase in $^{h3}J_{NC'}$ couplings was observed for H-bonds connecting β-strands β1, β2 and β5 in the presence of 1.5 M Gdn.HCl (Figure 4.12A). The increase in the size of $^{h3}J_{NC'}$ coupling size is presumably due to the stabilising effect of Gdn.HCl at low concentrations. This increase in $^{h3}J_{NC'}$ couplings is similar to that observed for the α-helix. The results observed for the $^{h3}J_{NC'}$ couplings did not correlate with the $^{1}H_{N}$ chemical shift (black histogram Figure 4.12B) as explained in Section 4.2. The $^{1}J_{NH}$ couplings (black histogram Figure 4.12C) also did not show a correlation with the $^{h3}J_{NC'}$ coupling data.

The H-bonds in β-sheets β1/β2 showed a smaller average increase in $^{h3}J_{NC'}$ couplings of 0.17 Hz in comparison to couplings measured for β-sheet β1/β5 0.043 Hz. This can be due to the H-bonds located on β1/β2 have only one charged residue presented by H-bond T7/K11, therefore the charge-charge repulsion only effected the β1/β2 sheets slightly, and that is evident from the couplings observed in Figure 4.12A. Whereas β-sheet β1/β5 has three solvent exposed charged side chains E64 (81 $Å^3$), Q2 (68 $Å^3$) and K6 (98 $Å^3$) therefore the Gdm^+ and the Cl^- ions may have a greater effect on H-bonds that connect β-sheet β1/β5. Only two H-bonds L15/ I3 (β1/β2) and F4/S65 (β1/β5) showed a decrease in $^{h3}J_{NC'}$ coupling. The increase in $^{h3}J_{NC'}$ couplings for the rest of the H-bonds lead predominantly in a decrease in H-bond length. Therefore the decrease in $^{h3}J_{NC'}$ couplings for H-bonds L15/I3 and F4/S65 may be a due a over compensation effect for the increase in $^{h3}J_{NC'}$ couplings for the H-bonds connecting β-strands β1/β2 and β1/β5. This observation is similar to the cooperativity effect between H-bonds in the α-helix (Section 4.5.1) where an increase in $^{h3}J_{NC'}$ coupling at the ends of the α-helix resulted in weakening of the $^{h3}J_{NC'}$ couplings in the centre. The H-bond L15/I3 shares an amide donor and a carbonyl acceptor with I3/L15. The changes in $^{h3}J_{NC'}$ couplings for both H-bonds were very similar in magnitude (i.e. 0.042 and 0.048 Hz); however, the changes are in opposite directions. Presumably, the near equal changes in the $^{h3}J_{NC'}$ couplings in I3/L15 and L15/I3 may be a result of changes in the H-bond length where H-bond I3/L15 decreased in length and L15/I3 increased in length.

The increase in the concentration of Gdn.HCl from 1.5 to 3.0 M depicted by the red histograms in Figure 4.12 resulted in an overall decrease in $^{h3}J_{NC'}$ couplings for H-bonds in β-sheets β1/β2 and β1/β5. In the presence of 3.0 M urea, The H-bond

network was less affected showing both increase and decrease in $^{h3}J_{NC'}$ coupling size. These results do not correlate with the $^{1}H_{N}$ chemical shift and the $^{1}J_{NH}$ couplings figures red histograms (Figures 4.12B and C). Though the only H-bond that showed a further increase in $^{h3}J_{NC'}$ coupling size between 1.5 and 3.0 M Gdn.HCl was I3/L5 (0.15 Hz). The dramatic increase in $^{h3}J_{NC'}$ coupling size for H-bond I3/L15 may be a result of the increase in the length of the weakening H-bonds in the β1/β2 structure As the weakening of the $^{h3}J_{NC'}$ coupling can be attributed to the lengthening of the H-bond what is observed is as the H-bonds increase in the length, the open up in a manner that results in a shorter H-bond for I3/L15.

The increase in Gdn.HCl concentration from 1.5 to 3.0 M resulted in a decrease in $^{h3}J_{NC'}$ couplings for H-bonds connecting β-strands β1/β2 (T7/K11 0.064 Hz), (I13/V5 0.066 Hz) and (I3/L15 0.041 Hz) with an average decrease of 0.057 Hz between 1.5 and 3.0 M Gdn.HCl. Whereas the H-bonds connecting β-strands β1/β5 showed a decrease of (F4/S65 0.015 Hz), (E64/Q2 0.035 Hz), (L67/F4 0.028), (F4/S65 0.067) and (L69/K6 0.008 Hz) with an average of 0.031 Hz. The higher average change in the $^{h3}J_{NC'}$ couplings observed for H-bonds connecting β1/β2 may suggest that this is the weak point of the β1/β2/β5 H-bond network where the structure unfolds. The most effected H-bonds in the β1/β2 sheets are ones with residues that have their backbone slightly exposed T7, K11 and L15 (Appendix 17). On the other hand the residues with the most solvent exposed backbone are for H-bonds E64/Q2 and L69/K6 but they were less affected by the increase in Gdn.HCl concentration. Another point is the H-bonds in the beginning and the ends of the three connecting strands β1/β2/β3, I3/L15 and L69/K6 increased in $^{h3}J_{NC'}$ coupling while the other H-bonds decreased. This might indicate that these two H-bonds are the pivot for keeping the β1/β2/β5 sheets structured.

The $^{h3}J_{NC'}$ couplings observed in 3.0 M (open blue histogram) urea show a similar pattern to what was observed for 3.0 M Gdn.HCl. Although the effect of urea on the couplings is weaker which indicates that urea is a weaker denaturant. The only exception is H-bond F4/S65 which increased by 0.06 Hz. The side chain of F4 is solvent exposed (55 $Å^3$) although it is hydrophobic in nature, and it is well documented that urea targets the hydrophobic regions of the protein, therefore the presence of urea in the moiety created a change in the surrounding water molecules

which resulted in a change in length of the H-bond thus increasing the $^{h3}J_{NC'}$ coupling size. The H-bonds I3/L15 and L69/K6 are both in the positive side of the $^{h3}J_{NC'}$ coupling magnitude between no denaturant and 3.0 M urea. This further indicates that these two H-bonds located at each end of the β1/β2/β5 H-bond network are protecting the secondary structure from collapsing. The $^{1}H_{N}$ chemical shifts show a downfield shift although weaker than what is observed in 3.0 M Gdn.HCl.

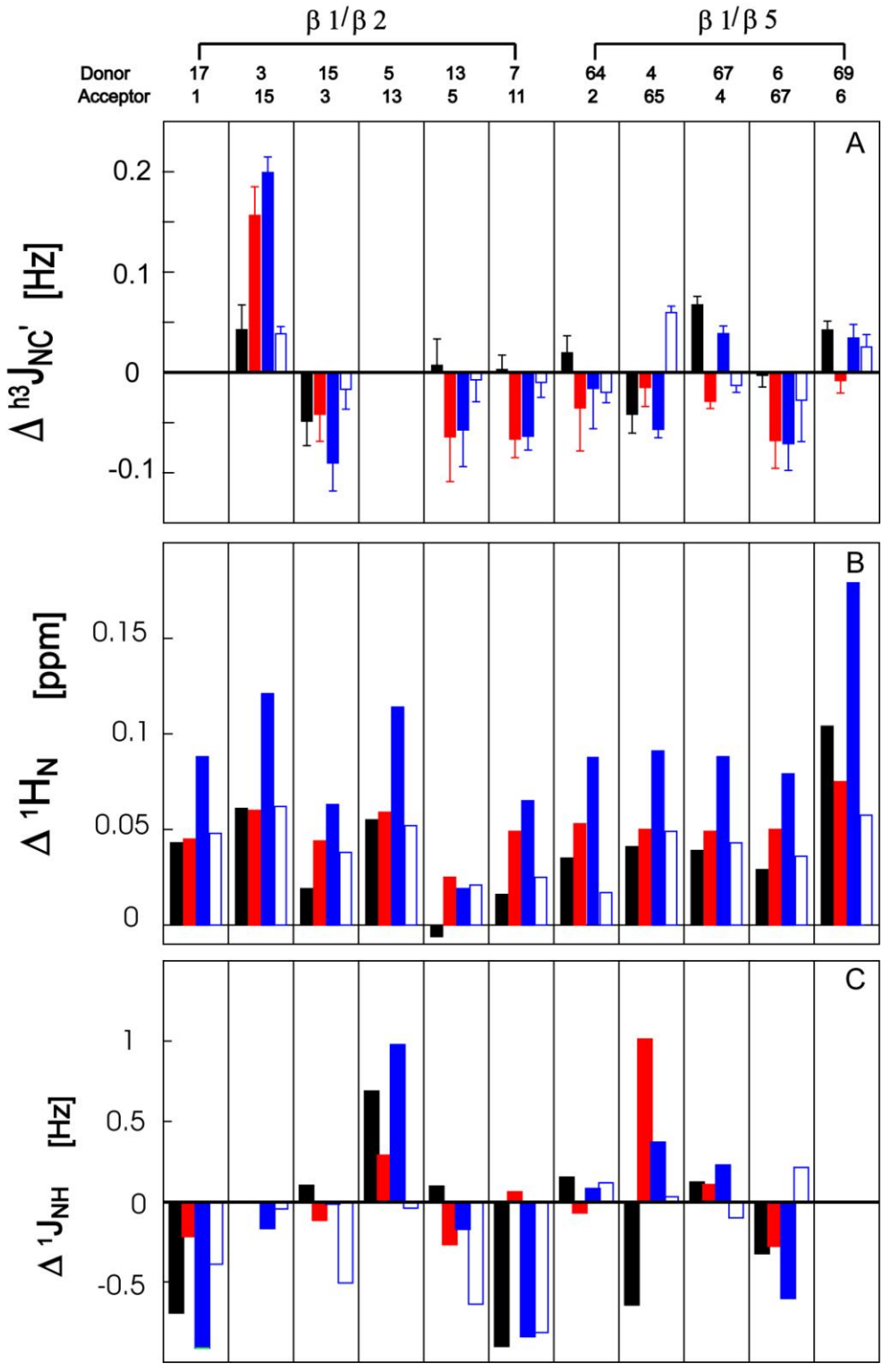

Figure 4.12: H-bond parameters of β-sheets β1/β2 and β1/β5 in ubiquitin (see legend for Figure 4.10 for a description)

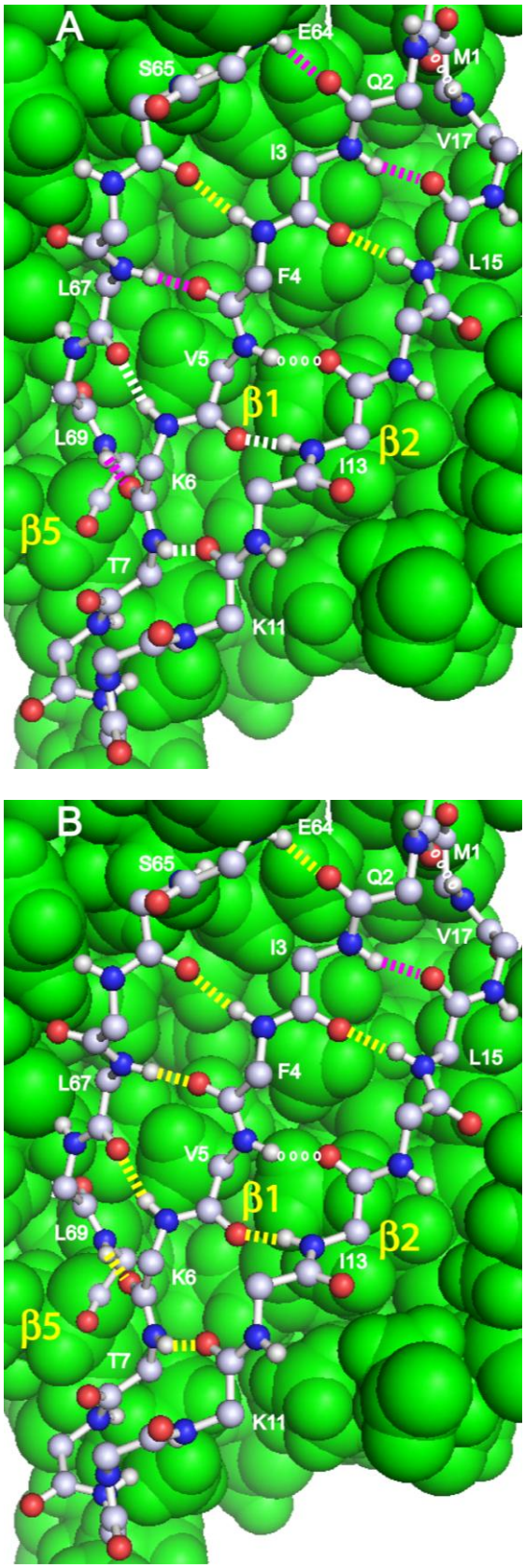

Figure 4.13: Backbone and H-bond structure of β1/β2/β5 (ball and stick) strands of ubiquitin. The remaining part of the protein structure is shown as a space-filled representation. (see legend for Figure 4.11 for a description)

4.5.3 The H-bond connectivities between β5/β3 and β3/β4 strands

In general the $^{h3}J_{NC'}$ couplings calculated between no denaturant and 1.5 M Gdn.HCl (black histogram Figure 4.14A) showed no change or an increase in size for H-bonds connecting β-strands β3, β4 and β5. The H-bonds that showed an increase in $^{h3}J_{NC'}$ couplings were H-bonds I44/H68 (0.076 Hz), L50/L43 (0.060 Hz) and V70/R42 (0.032 Hz).

The H-bonds that showed the greatest increase in $^{h3}J_{NC'}$ coupling between no denaturant and 1.5 M Gdn.HCl are located in the centre of β3/β5 sheet (I44/H68 and V70/R42). Whilst the H-bonds located at each end H68/I44 and R42/V70 where only slightly effected (i.e. within error). This may indicate that the connecting H-bonds in the centre of β-strands β3 and β5 are most affected by the 1.5 M Gdn.HCl. The observed increase in $^{h3}J_{NC'}$ couplings are presumably due to changes in the geometry of the H-bonds in the β-sheets β3/β4 and β4/β5. This could be due to the salt effect of Gdn.HCl stabilising the secondary structure via weak non-covalent interactions with side-chain and potentially backbone groups. In particular, both the R42 and H68 side-chains are solvent exposed. In support of this postulate, the $^{h3}J_{NC'}$ couplings associated with these two residues do show an increase at low concentrations of denaturant. The $^{1}H_N$ chemical shifts (Figure 4.14B) did not correlate with the increase in Gdn.HCl concentration as explained in section 4.4.

As the Gdn.HCl concentration was increased from 1.5 to 3.0 M a decrease in $^{h3}J_{NC'}$ coupling size was observed for all the H-bonds connecting β-stands β3/β4 and β3/β5 (Figure 4.14C). A decrease in the $^{h3}J_{NC'}$ couplings were also observed in 3.0 M urea (histogram), although the decrease was much weaker than in Gdn.HCl. The H-bonds located in the centre of β3/β5 sheet (I44/H68 and V70/R42) showed the greatest weakening in $^{h3}J_{NC'}$ coupling between 1.5 and 3.0 M Gdn.HCl 0.07 and 0.1 Hz respectively. Whilst the H-bonds on each end showed a smaller decrease of 0.04 Hz for H68/I44 and H-bond R42/V70 showed no change (i.e. with in error). This can point to the H-bonds in the centre of the β3/β5 being the weak point at which the structure breaks, while the H-bonds at each end remain more stable to protect the structure from breaking. Whereas the greatest decrease in $^{h3}J_{NC'}$ coupling size between no denaturant and 3.0 M urea was observed for H-bond R42/V70. This may indicate that urea affected the C-terminal end of the β3/β5 as the weak point of unfolding.

The H-bond L50/L43 located on the C-terminus of β-strands β3 and β4 showed a dramatic decrease in $^{h3}J_{NC'}$ as the Gdn.HCl concentration was increased (0.09 Hz) from 1.5 to 3.0 M. This decrease was in $^{h3}J_{NC'}$ coupling was also observed in 3.0 M urea 0.12 Hz. Both the H-bond donor and acceptor atoms are hydrophobic yet the back bone of L50 is slightly expose (5.56 $Å^3$) which may result in the Gdn.HCl and urea competing for the H-bond donor atom and resulting in a weaker H-bond. The $^{h3}J_{NC'}$ coupling does not correlate with the ^1H_N (Figure 4.14B) chemical shift as a continuous downfield shift is observed. The $^1J_{NH}$ coupling (Figure 4.14C) shows a correlation with the $^{h3}J_{NC'}$ coupling where an increase in coupling size is observed which correlates with the decrease in $^{h3}J_{NC'}$ coupling.

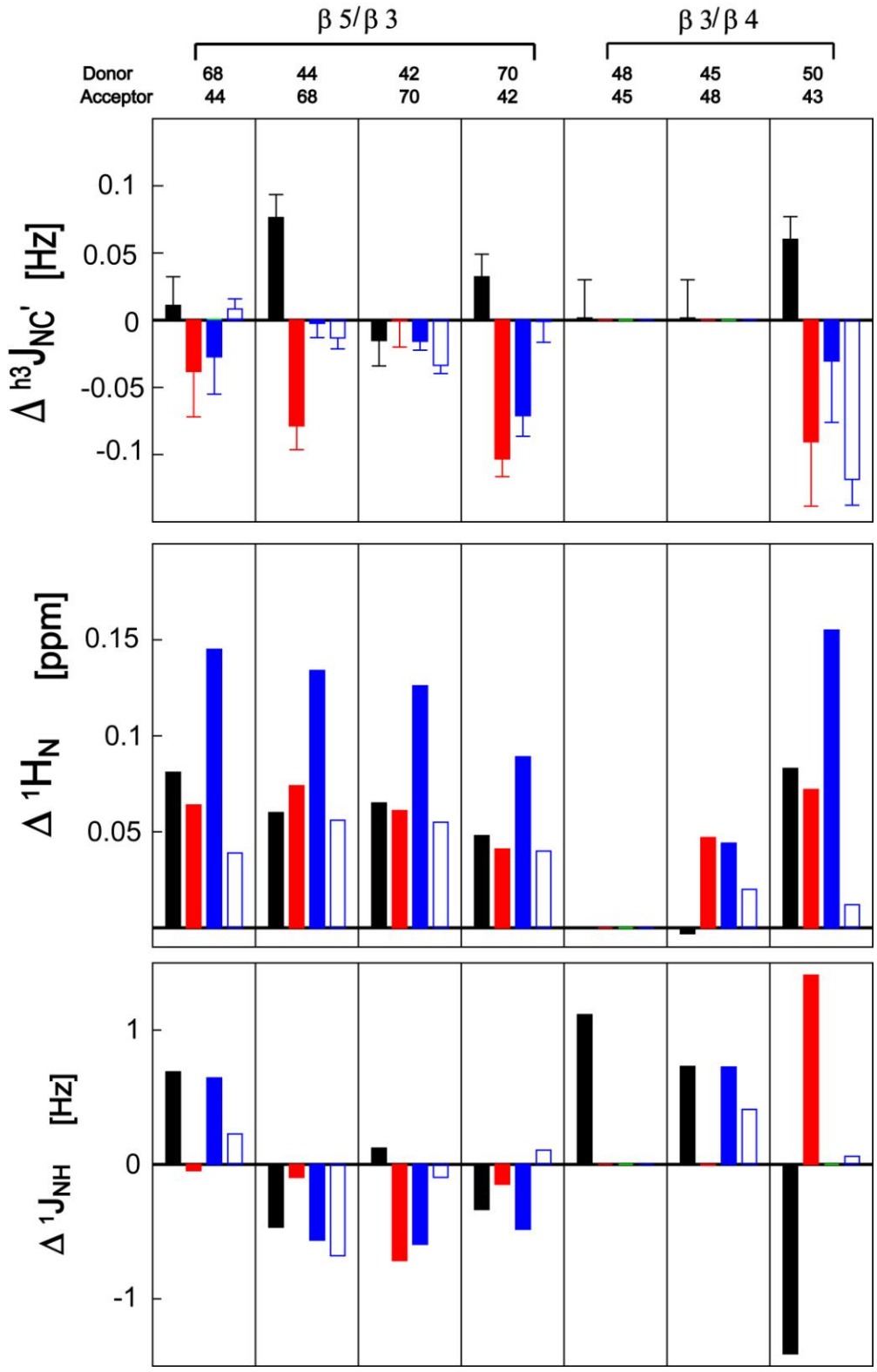

Figure 4.14: H-bond parameters of β-sheets β3/β5 and β3/β4 in ubiquitin (see figure legend to Figure 4.10. for a description of colour coding of the histograms).

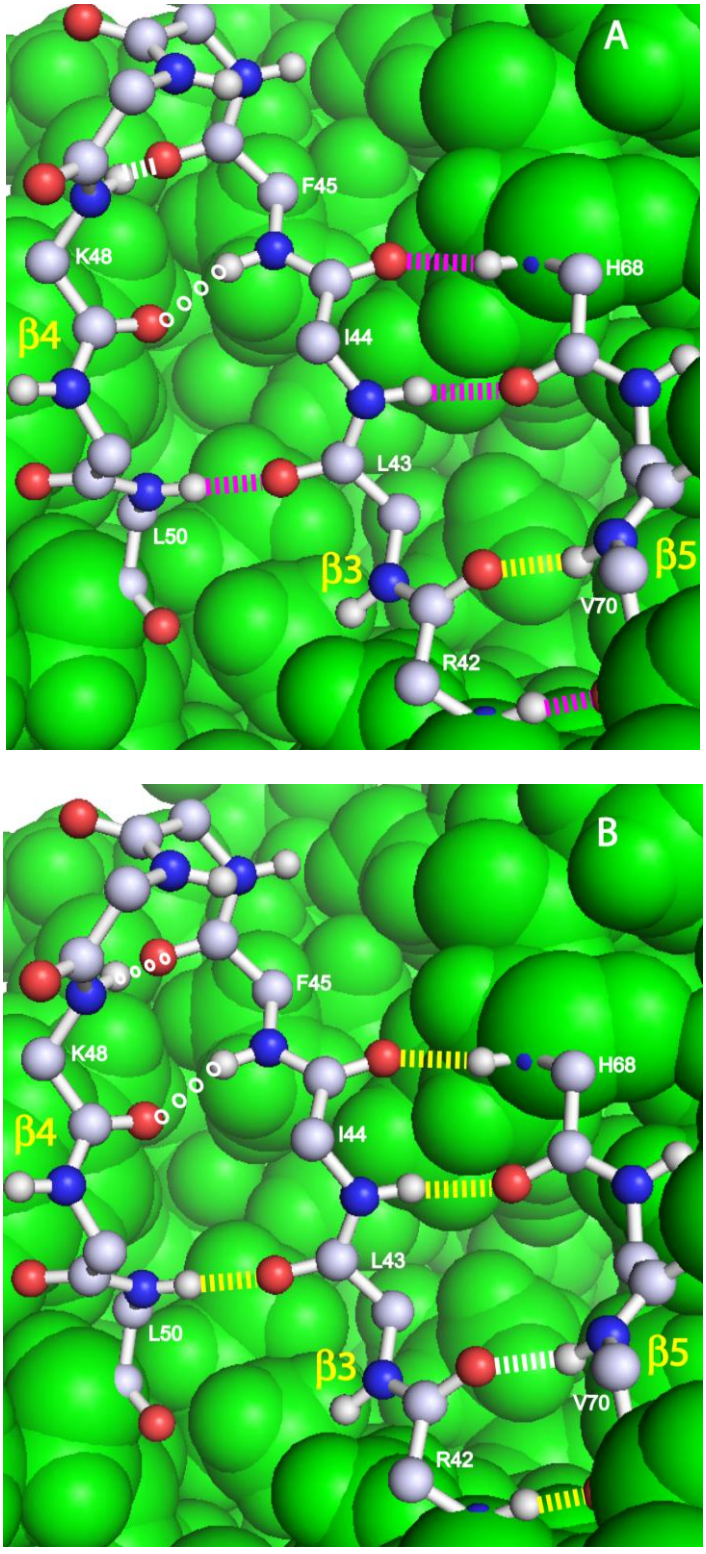

Figure 4.15: Backbone and H-bond structure of β3/β4/β5 (ball and stick) strands of ubiquitin. The remaining part of the protein structure is shown as a space-filled representation. (see legend for Figure 4.11 for the explanation to the colour coding of H-bonds)

4.6 Analysis of the effects of Gdn.HCl and urea on ubiquitin H-bonds in secondary structures

The effects of co-solutes guanidinium chloride (Gdn.HCl) and urea on the hydrogen bond (H-bond) properties of protein ubiquitin where examined using and various NMR parameters. The NMR parameters comprise of hydrogen bond (H-bond) scalar couplings ($^{h3}J_{NC'}$), amide proton $^{1}H_{N}$ chemical shifts, $^{1}J_{NH}$ couplings. Studies on ubiquitin denaturation have shown that ubiquitin unfolds via a two-state process. Due to this rapid transition from a folded state to an unfolded state, only the early stages of protein unfolding were examined by NMR spectroscopy. Urea and guanidinium chloride (Gdn.HCl) are denaturants that have been used extensively in protein folding and stability studies. Urea denaturation of ubiquitin was monitored by $^{1}H_{N}$ chemical shift over a concentration range of 0 (no denaturant) to 8.5 M, whereas Gdn.HCl denaturation was measured over a concentration range of 0 (no denaturant) to 7.5 M. The $^{h3}J_{NC'}$ couplings observed for the H-bonds of ubiquitin in Gdn.HCl over a concentration range between 0 (no denaturant) ─ 3 M Gdn.HCl showed an over all increase in size at concentrations ≤1.5 M Gdn.HCl. The highest number of H-bonds increasing in $^{h3}J_{NC'}$ couplings were observed at 1.5 M Gdn.HCl. This was followed by a decrease in the majority of $^{h3}J_{NC'}$ couplings for the H-bonds observed in ubiquitin at 3.0 M Gdn.HCl. The changes in the $^{h3}J_{NC'}$ couplings can be correlated to the changes in the N●●●O distance of the H-bond, which get shorter as the $^{h3}J_{NC'}$ couplings increased in size. The average $^{h3}J_{NC'}$ couplings in 3.0 M urea showed no change to the average $^{h3}J_{NC'}$ couplings in no denaturant, but a detailed analysis of individual H-bond showed urea affected the hydrophobic part of ubiquitin.

Chapter 5

Summary and Conclusions

The influence of cosolutes on individual H-bonds was successfully compared using H-bonds scalar couplings ($^{h3}J_{NC'}$) and other NMR parameters. The H-bond properties as a function of temperature and the counteracting mechanism of the osmolyte TMAO were studied in Chapter 3, whereas in Chapter 4 the influence of denaturing cosolutes urea and Gdn.HCl were examined.

In Chapter 3, the initial stages of thermal induced denaturation of ubiquitin were presented. Here, the thermal expansion of ubiquitin was monitored using $^{h3}J_{NC'}$ couplings, in which reduction in the sizes of $^{h3}J_{NC'}$ couplings can be attributed to the thermal expansion of the protein. In the presence of TMAO the $^{h3}J_{NC'}$ couplings also showed a decrease in magnitude as a result of thermal expansion. However, in the presence of TMAO the thermal expansion coefficient (αL) of ubiquitin was lower compared to the αL value calculated in the absence of this osmolyte. Between 15 and 60 ºC the average H-bond length increase was reduced by 0.019 Å in the presence of 1.5 M TMAO. While the absolute difference in αL is small, the results are meaningful and show that ubiquitin is thermally stabilized in the presence of 1.5 M TMAO. This was further corroborated by calculating the average ΔS^2 values for H-bond N-H donors at 15 and 60 ºC in the presence and absence of TMAO. At 15 ºC the presence of 1.5 M TMAO increased the S^2 by 0.05 ± 0.01, whereas at 60 ºC the increase was 0.04 ± 0.002, which is a result of reductions in amplitudes of internal bond motions in the presence of TMAO. Similar thermal stability effects of TMAO were observed in recent studies examining bovine pancreatic ribonuclease (RNase A) (Mukaiyama et al., 2008)

and hyperthermophile protein ribonuclease HII. In these studies, the presence of 1.0 M TMAO shifted the temperature (T_d) denaturation of ribonuclease (RNase A) from 63.9 to 67.2 ºC, whereas for hyperthermophile protein ribonuclease HII protein the presence of 0.5 M TMAO increased the T_m a further 3.6 ºC. This further indicates that TMAO shifts the denaturation temperature of proteins regardless of there natural stability at high temperatures.

The analysis of individual H-bonds in the α-helix revealed that H-bonds K27/I23 and E34/I30 positioned at the ends of the α-helix and on the hydrophobic side showed a significantly slower rate of heat-induced thermal expansion in the presence of TMAO, whereas TMAO exacerbated the thermal expansion of H-bonds in the center of the α-helix. Consequently, the mechanism of TMAO stabilising the helix from thermal denaturation is by enhancing the stability of the terminal H-bonds at the expense of weakening the central H-bonds.

Consequently, the β-strands most likely move apart due to thermal expansion. The H-bond E64/Q2 located at the N-terminus of β-strand β5 was found to be the least thermostable part of the β1/β2 and β1/β5 secondary structural elements with a decrease in $^{h3}J_{NC'}$ coupling size of 0.2 ± 0.01 Hz from 15 to 60 ºC. This pronounced decrease in $^{h3}J_{NC'}$ coupling size of H-bond E64/Q2 has been observed in previously for temperatures ranging between 5 and 65 ºC (Cordier and Grzesiek, 2002). This is further corroborated with sharp upfield chemical shift and a large decrease in the S^2 order parameter between 15 to 60 ºC. This is perhaps not surprising since the donor Q2 group lies at the N-terminus and may be labile to fraying upon the introduction of thermal energy. As such, the addition of TMAO slowed the thermal expansion of the H-bonds connecting β-stands β1, β2 and β5. The three H-bonds located at the center of the β1/β2/β5 H-bond network showed the slowest thermal expansion between 15 and 60 ºC were I3/L15, F4/65 and L67/F4. H-bonds I3/L15 and F4/S65 were 0.005 ± 0.035 and 0.01 ± 0.03 respectively, whereas H-bond K6/L67 showed a further increase in $^{h3}J_{NC'}$ coupling of 0.035 ± 0.02 Hz. The $\Delta\ ^{h3}J_{NC'}$ couplings for H-bonds I3/L15, F4/65 and L67/F4 all show high error values indicating that no significant decrease in coupling magnitude was observed, hence the H-bonds remained stable/The stabilising mechanism of TMAO is due to a highly unfavouable interaction between the osmolyte and the peptide backbone, this mechanism is known as the "osmophobic effect".

Studies have also shown that TMAO restricts the conformational space sampled by the N–H vectors in the presence of (heat or chemical denaturant) (Bolen and Baskakov, 2001). Thus TMAO leads to a more restricted conformation similar to a native-like fluctuation, thereby limiting access to a higher energy, more loosely packed, conformation.

The H-bonds for β-sheet region β3/β4/β5 showed a decrease in H-bond strength as a result of thermal expansion. H-bond H68/I44 showed a decrease in $^{h3}J_{NC'}$ coupling magnitude of 0.27 ± 0.018 Hz between 15 and 60 ºC, which is the greatest thermal expansion for all the H-bonds in ubiquitin. Consequently, this expansion might explain the observed increase in the size of the H-bond L50/L43 coupling (0.03 ± 0.0002 Hz) due to the geometric repositioning of β-stand β3 leading to this strand moving towards β-stand β4. This leads to a change in the geometry of the L50/L43 H-bond. In the presence of TMAO (Figure 5.3B) the dramatic thermal expansion of H-bond H68/I44 located in the β3/β5 region was not observed, whereas an increase in thermal expansion is observed for the "reverse" H-bond I44/H68.

In Chapter 4 the effects of the chemical denaturants, Gdn.HCl and urea, on H-bond properties were examined. The $^{h3}J_{NC'}$ couplings and other NMR parameters were measured in the absence and presence of the denaturants.

At 1.5 M Gdn.HCl ubiquitin is more stable than in the absence of the cosolute. This observation is the result of the salt effect (Hagihara et al., 1993). Here, studies have shown that at low concentrations the Gdn.HCl, this cosolute acts as a salt and prevents charge-charge repulsions. A recent study has shown that proteins have charge ion binding capabilities through the side-chain groups, therefore when Gdn.HCl dissociates into Gdm^+ (cation) and Cl^- (anion) the Gdm^+ and Cl^- ions readily interact with these groups to bring about stabilisation (Mason et al., 2007). Moreover, H-bonds located on the solvent exposed side were observed to be influence to a greater degree than the H-bonds buried within the interior of the protein. Such influences were observed by increases in the H-bond coupling magnitudes. The only exception is H-bond Q31/K27 where a decrease in H-bond strength was observed. H-bond Q31/K27 is located in the centre of the α-helix and could represent the weakest point within the helix, or the H-bond which is the most labile to chemical denaturation. Alternatively this H-bond may weaken to compensate for the geometric changes observed for the

other H-bonds, which appear to increase in strength due to an increase in the H-bond coupling values. The increase in Gdn.HCl concentration to 3.0 M led to an observed decrease in the $^{h3}J_{NC'}$ couplings, therefore Gdn.HCl at this higher concentration begins to act as a denaturant.

In general, at 1.5 M Gdn.HCl the majority of the H-bonds couplings present in the β-sheet increase (Figure 5.2A). Therefore, the β-sheets were observed to be more stabile in the presence of 1.5 M Gdn.HCl. However, H-bonds L15/I3 and F4/S65 showed a decrease in $^{h3}J_{NC'}$ coupling magnitude, which maybe a result of a compensation type effect, i.e. accommodate the shortening of the other H-bonds leading to subtle geometric changes at the local H-bond level. A study (O'Brien et al., 2007) has shown that Gdn.HCl interacts directly with the protein backbone and amino acid side chains resulting in a change in protein geometry. The study used ^{1}H and ^{15}N chemical shift to map any shifts in peaks induced by the addition of Gdn.HCl to Fyn SH3 domain protein. The results showed that Gdn.HCl binds to arginine pockets in the SH3 domain resulting in thermodynamic stability.

The increase in Gdn.HCl concentration to 3.0 M resulted in a general weakening of the $^{h3}J_{NC'}$ couplings and hence the H-bonds became less stable. Nonetheless, three H-bonds become more stable with the increase in Gdn.HCl concentration; I3/L15, K6/L67. This observation can broadly be interpreted as local changes in the geometry around these H-bonds leading to an increase in the couplings rather than "global" strand movements or geometric changes. Perhaps the "salt effect" is not uniform in effect and these H-bonds are thereby stabilised by the 3.0 M denaturant concentration. At higher concentrations, not presented herein, the H-bonds weaken as the denaturing characteristics of Gdn.HCl come into play.

In most cases, the majority of the $^{h3}J_{NC'}$ couplings for the 34 H-bonds in ubiquitin were observed in the various cosolute conditions. This was significant enough to achieve the aims of this project by probing the effects of cosolutes on protein stability in general and the secondary structure elements in particular. However, the H-bonds not observed were mainly due to either rather non-linear H-bond associated angles or a long H-bond length (as determined structurally) resulting in the inability to detect H-bond correlations in the NMR spectra acquired. In addition various cosolute conditions also contributed to the loss of signal and limited the number of $^{h3}J_{NC'}$ couplings detected in

the long-range 2D H(N)CO spectra. This in turn limited the ability to probe all individual H-bonds and in some cases regions of secondary structure. In the case of Gdn.HCl the maximum concentration that we could work with was 3.0 M because as the concentration increased the actual ionic strength lengthened the pulse lengths to unreasonably high values and reducing the signal-to-noise value. In 1.5 M TMAO at 15 ºC the majority of the smaller $^{h3}J_{NC'}$ couplings were not detected due to the high viscosity of the sample leading to poor signal-to-noise. Consequently, while an interest in characterising these couplings at higher TMAO concentrations was planned, at concentrations such as 3.0 M the solution viscosity would most likely obfuscate the ability to measure the majority of these couplings over a reasonable acquisition period. Furthermore, in a two-state equilibrium which is in the slow-exchange regime on the chemical shift time-scale for the experiment, the long-range 2D H(N)CO only measures the ensemble average coupling value for the folded state species. The unfolded state was not examined. Therefore this thesis was focused on measuring changes in the early stages of chemical and thermal denaturation where the folded state is predominant, yet subtle expansion or changes are observable to this state. There is a point where the transition from the folded to unfolded state is a rapid process, at which point, the ability to measure this observable shift by the H-bond scalar coupling method is not feasible.

Future research includes increasing the concentration of TMAO to higher than 1.5 M and characterising the effects this increase in TMAO concentration has on individual H-bonds. This set of experiments would be performed at higher temperatures, e.g. 45 °C, to overcome issues with sensitivity due to increases in solution viscosity. Comparing, the $^{h3}J_{NC'}$ coupling data with S^2 order parameter should provide insight into the effects increases in viscosity have on H-bond donors. The effects of other osmolytes can also be compared with the effects of TMAO, to understand if they have different mechanisms of action on the protein structure, and particularly, H-bonds. In the case of the denaturants study, the effects of other kosmotropic solutes can be compared with the effect of Gdn.HCl and urea on protein stability. The effects of the denaturing cosolutes may also be compared with the effects on the overall protein dynamics, a parameter that was not extended to in this thesis.

An additional set of experiments that may be useful from a comparative perspective include further understanding of the importance of specific H-bonds in ubiqiutin

stability by changing amino acids involved in H-bonds. Such mutations can be characterised using H-bond scalar couplings and the results examined with respect to the native protein data. In particular, characterising the α-helix H-bonds via mutagenesis would provide valuable complementary data to a large field of research that has examined H-bond cooperativity and the role of helix capping residues to the overall helix stability (Wieczorek and Dannenberg, 2005, Salvador et al., 2004, Oliva et al., 2008, Chin et al., 2002) in isolated helices. The work would also complement research on helix stability within the protein context.

Appendix

Appendix 1: $^{h3}J_{NC'}$ scalar couplings in Hz at four temperatures in the absence of cosloute

Don.	Acc.	15 ºC	err	30 ºC	err	45 ºC	err	60 ºC	err
1	17	–	–	–	–	–	–	–	–
2	–	–	–	–	–	–	–	–	–
3	15	0.375	0.011	0.463	0.007	0.431	0.003	0.411	0.008
4	65	0.594	0.016	0.557	0.009	0.574	0.002	0.518	0.010
5	13								
6	67	0.518	0.001	0.579	0.008	0.547	0.008	0.539	0.006
7	11	0.578	0.003	0.567	0.007	0.501	0.028	0.511	0.006
8	–	–	–	–	–	–	–	–	–
9	–	–	–	–	–	–	–	–	–
10	–	–	–	–	–	–	–	–	–
11	–	–	–	–	–	–	–	–	–
12	–	–	–	–	–	–	–	–	–
13	5	0.725	0.009	0.734	0.005	0.660	0.013	0.657	0.004
14									
15	3	0.661	0.002	0.621	0.006	0.574	0.004	0.550	0.007
16	–	–	–	–	–	–	–	–	–
17	1	–	–	–	–	0.588	0.003	0.502	0.007
18	–	–	–	–	–	–	–	–	–
19	–	–	–	–	–	–	–	–	–
20	–	–	–	–	–	–	–	–	–
21	–	–	–	–	–	–	–	–	–
22	–	–	–	–	–	–	–	–	–
23	54	–	–	0.526	0.002	0.684	0.004	–	–
24	–	–	–	–	–	–	–	–	–
25	–	–	–	–	–	–	–	–	–
26	22	–		0.281	0.010	0.226	0.011	0.230	0.018
27	23	0.573	0.005	0.524	0.006	0.466	0.022	0.443	0.002
28	24	–	–	0.236	0.009	–	–	0.236	0.003
29	25	0.274	0.007	0.242	0.010	0.227	0.007	0.233	0.021
30	26	0.371	0.029	0.350	0.002	0.302	0.009	0.296	0.002
31	27	0.433	0.003	0.390	0.007	0.376	0.004	0.365	0.007
32	28	0.369	0.009	0.284	0.015	0.310	0.002	0.237	0.002
33	29	–	–	–	–	–	–	–	–
34	30	0.709	0.006	0.670	0.006	0.626	0.017	0.595	0.004
35	31	–	–	–	–	0.213	0.014	–	–
36	–	–	–	–	–	–	–	–	–
37	–	–	–	–	–	–	–	–	–
38	–	–	–	–	–	–	–	–	–
39	–	–	–	–	–	–	–	–	–
40	–	–	–	–	–	–	–	–	–

41	–	–	–	–	–	–	–	–	–
42	70	0.538	0.007	0.519	0.010	0.504	0.015	0.495	0.001
43	–	–	–	–	–	–	–	–	–
44	68	0.595	0.004	0.493	0.006	0.569	0.012	0.527	0.008
45	–	–	–	–	–	–	–	–	–
46	–	–	–	–	–	–	–	–	–
47	–	–	–	–	–	–	–	–	–
48	45	0.515	0.008	0.450	0.010	0.374	0.045	–	–
49	–	–	–	–	–	–	–	–	–
50	43	–	–	0.619	0.006	0.615	0.003	0.657	0.004
51	–	–	–	–	–	–	–	–	–
52	–	–	–	–	–	–	–	–	–
53	–	–	–	–	–	–	–	–	–
54	–	–	–	–	–	–	–	–	–
55	–	–	–	–	–	–	–	–	–
56	21	0.491	0.018	0.441	0.005	–	–	–	–
57	19	0.442	0.013	0.369	0.002	0.360	0.017	0.310	0.027
58	–	–	–	–	–	–	–	–	–
59	–	–	–	–	–	–	–	–	–
60	–	–	–	–	–	–	–	–	–
61	56	–	–	–	–	–	–	–	–
62	–	–	–	–	–	–	–	–	–
63	–	–	–	–	–	–	–	–	–
64	2	0.851	0.003	0.798	0.012	0.730	0.012	0.655	0.010
65	–	0.442	0.033	–	–	–	–	–	–
66	–	–	–	–	–	–	–	–	–
67	4	0.688	0.009	0.653	0.006	0.591	0.014	0.544	0.020
68	44	0.657	0.007	0.639	0.008	0.589	0.011	0.387	0.017
69	6	0.521	0.004	0.485	0.008	0.485	0.014	0.431	0.000
70	42	0.637	0.029	0.439	0.006	0.556	0.009	0.550	0.004
71	–	–	–	–	–	–	–	–	–
72	–	–	–	–	–	–	–	–	–
73	–	–	–	–	–	–	–	–	–
74	–	–	–	–	–	–	–	–	–
75	–	–	–	–	–	–	–	–	–
76	–	–	–	–	–	–	–	–	–

Appendix 2: $^{h3}J_{NC'}$ scalar couplings in Hz at four temperatures in 1.5 M TMAO

Don.	Acc.	15 ºC	err	30 ºC	err	45 ºC	err	60 ºC	err
1	17	–	–	–	–	–	–	–	–
2	–	–	–	–	–	–	–	–	–
3	15	–	–	0.440	0.031	0.419	0.000	0.434	0.016
4	65	0.635	0.031	0.552	0.010	0.551	0.011	0.625	0.001
5	13	–	–	–	–	–	–	–	–
6	67	0.541	0.013	0.625	0.001	0.538	0.002	0.577	0.007
7	11	0.603	0.009	0.625	0.009	0.539	0.005	0.529	0.005
8	–	–	–	–	–	–	–	–	–
9	–	–	–	–	–	–	–	–	–
10	–	–	–	–	–	–	–	–	–
11	–	–	–	–	–	–	–	–	–
12	–	–	–	–	–	–	–	–	–
13	5	0.702	0.001	0.667	0.006	0.677	0.000	0.667	0.006
14	–	–	–	–	–	–	–	–	–
15	3	0.618	0.005	0.614	0.007	0.582	0.002	0.564	0.007
16	–	–	–	–	–	–	–	–	–
17	1	–	–	–	–	–	–	0.567	0.008
18	–	–	–	–	–	–	–	–	–
19	–	–	–	–	–	–	–	–	–
20	–	–	–	–	–	–	–	–	–
21	–	–	–	–	–	–	–	–	–
22	–	–	–	–	–	–	–	–	–
23	54	–	–	–	–	–	–	–	–
24	–	–	–	–	–	–	–	–	–
25	–	–	–	–	–	–	–	–	–
26	22	–	–	0.297	0.038	0.251	0.001	0.223	0.002
27	23	0.468	0.012	0.457	0.012	0.467	0.009	0.451	0.006
28	24	–	–	0.279	0.006	–	–	0.217	0.003
29	25	–	–	0.273	0.046	0.266	0.004	0.220	0.000
30	26	0.473	0.022	0.409	0.003	0.341	0.010	0.333	0.001
31	27	–	–	–	–	0.329	0.008	0.390	0.006
32	28	–	–	0.324	0.011	0.234	0.013	0.250	0.003
33	29	–	–	0.196	0.001	0.172	0.014	0.171	0.010
34	30	0.701	0.004	0.665	0.011	–	–	0.657	0.006
35	31	–	–	–	–	0.230	0.006	0.205	0.009
36	–	–	–	–	–	–	–	–	–
37	–	–	–	–	–	–	–	–	–
38	–	–	–	–	–	–	–	–	–
39	–	–	–	–	–	–	–	–	–
40	–	–	–	–	–	–	–	–	–
41	–	–	–	–	–	–	–	–	–
42	70	0.540	0.008	0.529	0.021	0.510	0.001	0.493	0.007
43	–	–	–	–	–	–	–	–	–
44	68	0.734	0.035	0.600	0.015	0.786	0.001	0.548	0.003
45	–	–	–	–	–	–	–	–	–

46	–	–	–	–	–	–	–	–	–
47	–	–	–	–	–	–	–	–	–
48	45	–		0.445	0.023	0.390	0.003	0.405	0.010
49	–	–	–	–	–	–	–	–	–
50	43	–	–	0.592	0.004	0.596	0.005	0.783	0.013
51	–	–	–	–	–	–	–	–	–
52	–	–	–	–	–	–	–	–	–
53	–	–	–	–	–	–	–	–	–
54	–	–	–	–	–	–	–	–	–
55	–	–	–	–	–	–	–	–	–
56	21	–	–	–	–	–	–	–	–
57	19	0.529	0.242	0.346	0.004	0.349	0.006	0.312	0.009
58	–	–	–	–	–	–	–	–	–
59	–	–	–	–	–	–	–	–	–
60	–	–	–	–	–	–	–	–	–
61	56	–	–	0.171	0.001	–	–	–	–
62	–	–	–	–	–	–	–	–	–
63	–	–	–	–	–	–	–	–	–
64	2	0.869	0.003	0.689	0.003	0.714	0.008	0.735	0.003
65	–	–	–	–	–	–	–	–	–
66	–	–	–	–	–	–	–	–	–
67	4	0.620	0.017	0.600	0.007	0.581	0.004	0.556	0.016
68	44	0.623	0.029	0.634	0.029	0.593	0.003	0.611	0.002
69	6	0.546	0.017	0.541	0.010	0.456	0.000	0.456	0.007
70	42	0.650	0.028	0.632	0.010	0.755	0.004	0.550	0.009
71	–	–	–	–	–	–	–	–	–
72	–	–	–	–	–	–	–	–	–
73	–	–	–	–	–	–	–	–	–
74	–	–	–	–	–	–	–	–	–
75	–	–	–	–	–	–	–	–	–
76	–	–	–	–	–	–	–	–	–

Appendix 3: $^{1}H_{N}$ chemical shifts (ppm) at four temperatures in absence of cosolute

Res	15 ºC	30 ºC	45 ºC	60 ºC
1	–	–	–	–
2	9.0352	8.9198	8.8077	8.6921
3	8.3229	8.3268	8.3254	8.3147
4	8.6561	8.6097	8.5649	8.5045
5	9.3428	9.3004	9.2615	9.217
6	8.9926	9.0035	8.9805	8.949
7	8.7995	8.7316	8.676	8.6239
8	9.2591	–	–	–
9	7.6848	–	–	–
10	7.8766	7.8364	7.8116	–
11	7.3151	7.2812	7.2505	–
12	8.7315	8.6158	–	8.6796
13	9.6205	9.5764	9.5177	9.4584
14	8.8363	8.7169	8.5968	–
15	8.79	8.7426	8.6882	8.633
16	8.1787	8.1255	8.0625	7.9597
17	8.998	8.9382	8.8716	8.8034
18	8.6696	8.6834	8.6886	8.5213
19	–	–	–	–
20	7.0724	7.0383	7.008	6.9783
21	8.0051	8.0595	8.0069	7.951
22	7.9502	7.8679	7.7974	7.7358
23	8.571	8.5299	8.4873	8.4436
24	–	–	10.0562	10.0176
25	7.9811	7.931	7.8808	7.8337
26	8.1631	8.1135	–	8.0139
27	8.6041	8.5601	8.5086	8.4614
28	8.1103	7.9833	7.9627	7.9459
29	7.9013	7.8793	7.8514	7.8243
30	8.3399	8.2879	8.2366	8.1879
31	8.5895	8.556	8.5328	8.4753
32	8.1039	8.0278	7.961	7.9007
33	7.4581	7.4576	7.4549	7.4478
34	8.7648	8.726	8.6775	8.6231
35	8.5581	8.4989	8.4414	8.3837
36	6.1795	6.1717	6.1672	6.1641
37	–	–	–	–
38	–	–	–	–
39	8.5942	8.5316	8.4759	8.4307
40	7.8662	7.8191	7.7727	7.7299
41	7.5491	7.4769	7.415	7.3585
42	8.526	8.5048	8.4655	8.4142
43	8.8765	8.7966	8.7244	8.6497

44	9.1619	9.1527	9.1216	9.0828
45	8.8756	8.8505	8.8215	8.7882
46	9.067	—	—	—
47	8.1875	8.075	7.9619	7.853
48	7.9992	7.9838	7.9736	—
49	8.7226	8.6306	—	—
50	8.6108	8.5659	8.5076	8.4413
51	8.4742	8.3851	8.2904	7.9851
52	8.2469	8.1553	8.0591	7.9779
53	—	—	9.6574	9.5891
54	7.5124	7.474	7.4388	7.4017
55	8.8726	8.8446	8.8102	8.7709
56	8.1865	8.1612	8.1393	8.1198
57	8.5544	8.4703	8.3937	8.3194
58	7.991	7.9453	7.8957	7.8464
59	7.2919	7.2667	7.2444	7.2215
60	8.1988	8.159	8.1213	8.0819
61	7.3024	7.2509	7.195	7.1438
62	7.6948	7.621	7.5437	7.4662
63	8.5793	8.4771	8.3627	—
64	9.389	9.3137	9.2298	9.1493
65	7.7153	7.67	7.6275	7.5886
66	8.7885	8.6961	8.6002	—
67	9.4622	9.413	9.3611	9.3049
68	9.2552	9.2275	9.1887	9.1421
69	8.3073	8.2952	8.2918	8.2825
70	9.2206	9.1701	9.1079	9.0388
71	8.2253	8.0922	8.0589	7.8231
72	8.644	8.5954	8.5214	8.4141
73	8.4622	8.3261	—	8.1991
74	8.5388	—	—	—
75	8.5803	—	—	—
76	8.0397	7.9294	7.8201	7.7258

Appendix 4: $^{1}H_{N}$ chemical shifts (ppm) at four temperatures in 1.5 M TMAO

Res	15 ºC	30 ºC	45 ºC	60 ºC
1	–	–	–	–
2	9.1	8.9562	8.8534	8.7377
3	8.3078	8.3144	8.3169	8.3057
4	8.6496	8.6064	8.5703	8.5248
5	9.3472	9.3099	9.2699	9.2245
6	8.9851	8.9885	8.9776	8.9504
7	8.8125	8.7522	8.7005	8.6497
8	9.2513	9.1028	8.9628	8.8211
9	–	7.6419	7.6013	–
10	7.9304	7.8953	7.8602	7.8187
11	7.3189	7.2888	7.2619	7.2302
12	8.752	8.642	8.5361	8.4297
13	9.6157	9.5669	9.5192	9.4598
14	8.8465	8.729	8.6147	8.5036
15	8.7749	8.7279	8.6807	8.6271
16	8.1953	8.1465	8.088	8.0167
17	9.0043	8.9482	8.8886	8.8192
18	8.6865	8.7125	8.7254	8.7155
19	–	–	–	–
20	7.0773	7.0464	7.0217	6.9953
21	8.0995	8.0465	7.9929	7.9487
22	7.8884	7.8518	7.7981	7.7247
23	8.5743	8.5292	8.4888	8.4456
24	–	–	–	10.128
25	7.9971	7.9289	7.8838	7.834
26	8.1627	8.1091	8.0653	8.0138
27	8.6054	8.5624	8.5193	8.4712
28	8.0159	7.9977	7.9929	7.9487
29	7.9111	7.8872	7.8652	7.836
30	8.3411	8.2907	8.2435	8.1959
31	8.5942	8.5626	8.5367	8.4811
32	8.1	8.0259	7.9612	7.8987
33	7.431	7.4336	7.4356	7.4281
34	8.7686	8.7283	8.6822	8.6283
35	8.5788	8.5194	8.4639	8.4048
36	6.1673	6.1614	6.1631	6.1561
37	–	–	–	–
38	–	–	–	–
39	8.6098	8.5523	8.5072	8.4637

40	7.8506	7.8067	7.7659	7.7217
41	7.5474	7.477	7.4228	7.3658
42	8.5371	8.5175	8.4813	8.4278
43	8.8892	8.8157	8.7449	8.6677
44	9.1593	9.1457	9.1246	9.089
45	8.8892	8.8666	8.8429	8.8106
46	9.084	9.0072	8.9261	—
47	8.2436	8.1312	8.0207	7.908
48	7.9971	7.9929	7.9809	7.9629
49	8.7687	8.6817	8.5923	8.5008
50	8.6179	8.571	8.5159	8.4464
51	8.4616	8.3705	8.2802	8.1888
52	8.2488	8.1582	8.0726	7.9907
53	—	—	—	9.7009
54	7.515	7.4779	7.445	7.4082
55	8.8704	8.8469	8.8202	8.7834
56	8.1795	8.1573	8.1417	8.1195
57	8.5488	8.4691	8.3935	8.3191
58	7.9764	7.9289	7.8843	7.8372
59	7.2873	7.2638	7.2438	7.2175
60	8.2096	8.1707	8.1352	8.0965
61	7.2886	7.2349	7.1839	7.1274
62	7.6918	7.6185	7.5465	7.4668
63	8.5874	8.4886	8.3867	8.2822
64	9.3689	9.2947	9.2211	9.1393
65	7.73	7.6878	7.6496	7.6056
66	8.7955	8.7082	8.6181	8.5233
67	9.4606	9.4102	9.3608	9.3017
68	9.2576	9.23	9.1937	9.1451
69	8.3326	8.3363	8.3163	8.3044
70	9.2283	9.1732	9.1132	9.0434
71	8.2575	8.1259	7.9929	7.8705
72	8.6512	8.6007	8.5367	8.4811
73	8.4746	8.3363	8.2122	8.0892
74	8.5476	8.4198	8.2983	—
75	8.621	8.4992	8.3882	—
76	8.0556	7.9481	7.8466	7.7504

Appendix 4: $^{1}J_{NH}$ scalar couplings (absolute value Hz) at four temperatures

Res	15 ºC	60 ºC	15 ºC TMAO	60 ºC TMAO
1	–	–	–	–
2	93.5	93.9	94.0	94.0
3	92.9	93.0	93.4	93.4
4	94.1	92.0	94.2	94.2
5	93.5	93.1	93.4	93.4
6	93.9	93.9	94.2	94.2
7	95.1	94.9	94.1	94.1
8	93.2	–	93.3	93.3
9	92.8	–	–	–
10	93.4	–	–	–
11	93.9	–	–	–
12	93.0	92.9	92.4	92.4
13	94.2	93.3	93.5	93.5
14	93.1	–	93.5	93.5
15	94.0	94.4	96.2	96.2
16	92.3	93.7	92.8	92.8
17	93.5	93.8	94.0	94.0
18	92.9	93.8	93.4	93.4
19	–	–	–	–
20	92.6	92.3	92.8	92.8
21	94.7	94.8	95.2	95.2
22	93.9	93.6	–	–
23	94.9	100.4	95.6	95.6
24	–	93.1	–	–
25	95.0	94.9	94.9	94.9
26	93.9	93.8	94.5	94.5
27	94.4	94.5	95.5	95.5
28	95.2	95.0	94.1	94.1
29	94.8	94.6	94.8	94.8
30	94.1	93.5	94.1	94.1
31	94.2	94.3	94.4	94.4
32	94.8	94.6	94.9	94.9
33	93.5	93.4	94.2	94.2
34	90.9	91.0	91.1	91.1
35	94.1	94.1	93.4	93.4
36	91.7	91.5	91.7	91.7
37	–	–	–	–
38	–	–	–	–
39	93.9	93.9	94.3	94.3

40	93.3	93.9	93.2	93.2
41	94.2	94.1	94.3	94.3
42	94.4	93.2	94.1	94.1
43	93.8	93.7	122.5	122.5
44	92.6	93.8	92.9	92.9
45	93.8	93.7	65.1	65.1
46	94.6	—	94.8	94.8
47	93.3	93.2	93.4	93.4
48	93.6	—	94.1	94.1
49	93.4	—	93.9	93.9
50	94.5	95.2	93.7	93.7
51	94.0	93.7	93.7	93.7
52	93.6	93.4	93.8	93.8
53	—	92.9	—	—
54	93.7	94.5	94.0	94.0
55	92.9	92.6	92.8	92.8
56	97.8	95.1	94.3	94.3
57	94.4	94.1	94.5	94.5
58	95.2	537.2	95.7	95.7
59	92.8	-347.5	93.6	93.6
60	94.7	94.4	94.7	94.7
61	93.6	93.5	93.6	93.6
62	93.7	92.5	93.9	93.9
63	93.9	—	93.8	93.8
64	93.6	93.7	93.6	93.6
65	94.6	94.3	95.2	95.2
66	92.4	—	92.1	92.1
67	93.7	93.8	94.1	94.1
68	93.7	93.8	94.0	94.0
69	93.5	94.4	93.5	93.5
70	93.9	93.9	94.2	94.2
71	93.8	—	93.9	93.9
72	93.7	—	93.5	93.5
73	93.8	92.7	93.8	93.8
74	93.2	—	93.5	93.5
75	94.3	—	94.1	94.1
76	93.5	90.6	93.5	93.5

Appendix 5: R_1 (s^{-1}) at 15 and 60 ºC in the presence and absence of 1.5 M TMAO

Res	R1 15 ºC	err	R1 60 ºC	err	R1 15 ºC TMAO	err	R1 60 ºC TMAO	err
1	–	–	–	–	–	–	–	–
2	1.70	0.004	2.17	0.011	1.29	0.02	2.19	0.03
3	1.80	0.005	2.32	0.004	1.40	0.03	2.39	0.01
4	1.83	0.005	2.45	0.003	1.42	0.03	2.47	0.01
5	1.75	0.004	2.22	0.003	1.35	0.02	2.28	0.01
6	1.81	0.004	2.30	0.003	1.41	0.02	2.34	0.01
7	1.76	0.004	2.22	0.003	1.39	0.02	2.31	0.01
8	1.80	0.004	–	–	1.52	0.02	–	–
9	1.66	0.004	–	–	1.38	0.02	–	–
10	1.74	0.003	–	–	1.44	0.01	–	–
11	1.61	0.003	–	–	1.36	0.01	–	–
12	1.71	0.003	2.23	0.011	1.37	0.02	2.20	0.03
13	1.79	0.005	2.17	0.004	1.40	0.03	2.26	0.01
14	1.72	0.004	–	–	1.33	0.02	–	–
15	1.80	0.005	2.27	0.004	1.41	0.03	2.33	0.01
16	1.62	0.003	2.13	0.004	1.25	0.01	2.17	0.01
17	1.77	0.004	2.31	0.003	1.37	0.02	2.34	0.01
18	1.67	0.004	2.26	0.003	1.26	0.02	2.26	0.01
19	–	–	–	–	–	–	–	–
20	1.69	0.003	2.27	0.005	1.33	0.02	2.33	0.01
21	1.85	0.003	2.14	0.005	1.43	0.02	2.22	0.01
22	1.82	0.004	2.25	0.004	1.41	0.02	2.31	0.01
23	1.88	0.006	2.33	0.003	1.44	0.04	2.46	0.01
24	–	–	2.40	0.007	–	–	2.46	0.02
25	1.81	0.004	2.41	0.002	1.40	0.02	2.42	0.01
26	1.84	0.004	2.34	0.002	1.42	0.02	2.38	0.01
27	1.81	0.004	2.36	0.004	1.40	0.02	2.41	0.01
28	1.90	0.003	2.44	0.002	1.43	0.01	2.45	0.01
29	1.77	0.004	2.32	0.003	1.41	0.02	2.39	0.01
30	1.88	0.004	2.33	0.003	1.44	0.02	2.41	0.01
31	1.78	0.003	2.32	0.002	1.48	0.02	2.41	0.01
32	1.81	0.003	2.28	0.002	1.40	0.01	2.42	0.01
33	1.72	0.003	2.19	0.002	1.37	0.02	2.27	0.01
34	1.72	0.004	2.23	0.003	1.36	0.02	2.28	0.01
35	1.74	0.003	2.37	0.002	1.31	0.02	2.37	0.01
36	1.49	0.003	1.96	0.002	1.17	0.01	2.05	0.00
37	–	–	2.24	0.007	–	–	–	–
38	–	–	–	–	–	–	–	–
39	1.74	0.002	–	–	1.42	0.01	2.19	0.02
40	1.76	0.004	2.26	0.003	1.38	0.02	2.35	0.01
41	1.80	0.004	2.21	0.003	1.41	0.02	2.30	0.01
42	1.76	0.004	2.21	0.003	1.37	0.02	2.29	0.01
43	1.76	0.006	2.22	0.004	1.35	0.03	2.30	0.01
44	1.81	0.005	2.28	0.003	1.39	0.02	2.33	0.01
45	1.80	0.005	2.31	0.004	1.38	0.02	2.37	0.01
46	–	–	–	–	1.42	0.03	–	–

47	1.75	0.003	2.12	0.015	1.37	0.02	2.09	0.04
48	1.71	0.003	2.27	0.003	1.32	0.02	2.29	0.01
49	1.63	0.003	–	–	1.33	0.01	–	–
50	1.79	0.005	2.24	0.003	1.41	0.03	2.31	0.01
51	1.67	0.005	2.16	0.003	1.27	0.03	2.22	0.01
52	1.60	0.002	2.20	0.003	1.20	0.01	2.18	0.01
53	–	–	2.20	0.026	–	–	2.30	0.06
54	1.68	0.003	2.22	0.003	1.29	0.02	2.24	0.01
55	1.75	0.005	2.25	0.004	1.36	0.03	2.29	0.01
56	1.93	0.005	2.32	0.003	1.45	0.02	2.43	0.01
57	1.78	0.003	2.24	0.003	1.42	0.02	2.38	0.01
58	1.84	0.004	2.38	0.003	1.45	0.02	2.44	0.01
59	1.74	0.004	2.25	0.004	1.36	0.02	2.29	0.01
60	1.83	0.004	2.32	0.006	1.41	0.02	2.37	0.01
61	1.81	0.005	2.22	0.003	1.39	0.03	2.33	0.01
62	1.58	0.004	1.94	0.004	1.28	0.02	2.03	0.01
63	1.72	0.003	2.10	0.011	1.29	0.01	–	–
64	1.89	0.006	2.38	0.005	1.45	0.03	2.45	0.01
65	1.75	0.003	2.32	0.004	1.39	0.02	2.35	0.01
66	1.72	0.004	2.24	0.007	–	–	2.32	0.01
67	1.79	0.005	2.26	0.004	1.40	0.03	2.33	0.01
68	1.75	0.005	2.28	0.004	1.35	0.02	2.32	0.01
69	1.83	0.002	2.28	0.004	1.66	0.01	2.34	0.01
70	1.83	0.006	–	–	1.42	0.03	2.38	0.01
71	1.74	0.003	–	–	1.41	0.02	–	–
72	1.85	0.003	–	–	1.44	0.02	–	–
73	–	–	–	–	1.39	0.02	–	–
74	–	–	–	–	–	–	–	–
75	–	–	–	–	–	–	–	–
76	–	–	–	–	–	–	–	–

Appendix 6: R_2 (s^{-1}) at 15 and 60 ºC in the presence and absence of 1.5 M TMAO

Res	R2 15 C	err	R2 60 C	err	R2 15 C TMAO	err	R2 60 C TMAO	err
1	–	–	–	–	–	–	–	–
2	8.10	0.27	3.83	0.31	10.76	0.46	5.10	0.06
3	8.36	0.31	3.74	0.09	12.05	0.67	4.72	0.02
4	8.26	0.34	3.75	0.06	11.95	0.68	4.70	0.01
5	7.45	0.25	3.69	0.09	10.34	0.49	4.25	0.01
6	7.63	0.25	3.35	0.08	10.94	0.49	4.34	0.01
7	8.30	0.26	3.51	0.07	12.05	0.50	4.55	0.01
8	7.08	0.22	–	–	9.99	0.44	–	–
9	7.25	0.24	–	–	10.41	0.41	–	–
10	6.70	0.15	–	–	9.44	0.26	–	–
11	6.77	0.14	–	–	9.29	0.24	–	–
12	7.01	0.19	3.65	0.22	9.88	0.33	4.39	0.06
13	7.94	0.34	3.29	0.09	11.16	0.72	4.17	0.02
14	8.08	0.27	–	–	10.46	0.47	–	–
15	7.27	0.26	3.36	0.09	10.11	0.53	4.23	0.02
16	7.50	0.19	3.83	0.13	10.21	0.35	4.38	0.02
17	8.35	0.28	3.58	0.08	11.92	0.60	4.65	0.01
18	8.29	0.24	3.56	0.08	11.41	0.56	4.53	0.01
19	–	–	–	–	–	–	–	–
20	7.75	0.20	3.56	0.12	10.73	0.39	4.46	0.02
21	8.66	0.22	3.99	0.14	11.53	0.43	5.29	0.03
22	7.76	0.25	3.50	0.08	10.61	0.51	4.31	0.01
23	10.76	0.52	3.87	0.07	12.92	1.14	4.65	0.01
24	–	–	3.78	0.15	–	–	4.58	0.04
25	13.23	0.45	4.07	0.06	16.96	1.00	5.08	0.01
26	8.19	0.25	4.12	0.06	10.70	0.46	4.35	0.01
27	8.64	0.27	3.76	0.10	11.51	0.53	4.76	0.02
28	8.85	0.20	3.88	0.06	12.18	0.35	5.55	0.01
29	8.11	0.24	3.68	0.06	11.40	0.49	4.68	0.01
30	8.08	0.26	3.61	0.06	11.42	0.55	4.52	0.01
31	6.91	0.16	3.71	0.05	10.00	0.32	5.40	0.01
32	8.29	0.17	3.56	0.05	11.65	0.35	4.76	0.01
33	8.22	0.21	3.52	0.06	11.79	0.43	4.52	0.01
34	8.13	0.25	3.55	0.07	11.56	0.54	4.54	0.01
35	8.10	0.20	3.84	0.06	11.56	0.47	4.74	0.01
36	7.46	0.20	3.18	0.05	10.61	0.42	4.06	0.01
37	–	–	3.71	0.17	–	–	–	–
38	–	–	–	–	–	–	–	–
39	8.08	0.14	–	–	11.35	0.28	4.66	0.04
40	8.26	0.25	3.54	0.07	11.88	0.53	4.69	0.01
41	7.93	0.25	3.52	0.07	11.45	0.53	4.54	0.01
42	8.02	0.27	3.74	0.07	9.52	0.39	4.43	0.01
43	7.94	0.36	3.36	0.10	11.64	0.64	4.40	0.02
44	7.76	0.28	3.94	0.09	10.34	0.54	4.45	0.02

45	8.03	0.31	3.55	0.09	11.32	0.57	4.48	0.02
46	—	—	—	—	12.37	0.81	—	—
47	7.07	0.18	3.37	0.37	10.44	0.36	4.35	0.08
48	8.07	0.22	3.78	0.07	11.35	0.40	4.48	0.01
49	7.68	0.17	—	—	10.17	0.32	—	—
50	7.38	0.29	3.46	0.07	9.91	0.61	4.33	0.01
51	8.84	0.42	3.62	0.08	10.58	0.68	4.83	0.01
52	7.84	0.17	3.51	0.07	10.95	0.32	4.60	0.02
53	—	—	8.71	2.93	—	—	9.74	0.48
54	8.14	0.22	3.53	0.07	11.69	0.44	4.51	0.01
55	8.87	0.34	3.51	0.09	11.56	0.70	4.35	0.02
56	8.29	0.26	3.73	0.06	11.47	0.59	4.64	0.01
57	7.96	0.17	3.71	0.06	11.88	0.42	4.75	0.01
58	8.06	0.21	3.71	0.07	11.89	0.44	4.76	0.01
59	8.45	0.27	3.52	0.09	10.79	0.46	4.56	0.02
60	8.17	0.22	3.70	0.13	11.81	0.45	4.97	0.03
61	7.98	0.28	3.35	0.08	11.38	0.58	4.42	0.01
62	6.39	0.21	3.28	0.11	9.43	0.45	4.01	0.02
63	8.22	0.18	3.64	0.31	11.02	0.36	—	—
64	8.18	0.33	3.89	0.11	11.84	0.74	4.82	0.02
65	8.32	0.20	3.58	0.09	11.83	0.43	4.59	0.01
66	7.81	0.24	3.68	0.17	—	—	4.72	0.03
67	7.50	0.31	3.63	0.11	10.91	0.65	4.43	0.02
68	7.84	0.29	3.48	0.09	11.14	0.58	4.44	0.02
69	4.76	0.09	3.56	0.09	7.36	0.13	4.65	0.01
70	9.29	0.42	—	—	12.07	0.80	4.62	0.02
71	7.85	0.18	—	—	10.07	0.32	—	—
72	8.65	0.20	—	—	11.38	0.42	—	—
73	—	—	—	—	11.14	0.49	—	—
74	—	—	—	—	—	—	—	—
75	—	—	—	—	—	—	—	—
76	—	—	—	—	—	—	—	—

Appendix 7: NOE at 15 and 60 ºC in the presence and absence of 1.5 M TMAO

Res	noe 15 ºC	err	noe 60 ºC	err	noe 15 ºC TMAO	err	noe 60 ºC TMAO	err
1	–	–	–	–	–	–	–	–
2	0.74	0.01	0.60	0.01	0.73	0.02	0.69	0.02
3	0.76	0.01	0.55	0.01	0.77	0.02	0.65	0.01
4	0.78	0.01	0.56	0.00	0.79	0.02	0.68	0.01
5	0.76	0.01	0.52	0.01	0.78	0.02	0.65	0.01
6	0.76	0.01	0.53	0.00	0.76	0.02	0.65	0.01
7	0.74	0.01	0.52	0.00	0.73	0.02	0.64	0.01
8	0.66	0.01	–	–	0.67	0.02	–	–
9	0.61	0.01	–	–	0.58	0.01	–	–
10	0.61	0.00	–	–	0.58	0.01	–	–
11	0.57	0.00	–	–	0.53	0.01	–	–
12	0.67	0.01	0.59	0.01	0.66	0.01	0.69	0.02
13	0.76	0.01	0.51	0.01	0.75	0.02	0.64	0.01
14	0.76	0.01	–	–	0.75	0.02	–	–
15	0.77	0.01	0.53	0.01	0.77	0.02	0.65	0.01
16	0.72	0.01	0.57	0.01	0.72	0.01	0.67	0.01
17	0.76	0.01	0.55	0.01	0.76	0.02	0.66	0.01
18	0.75	0.01	0.57	0.01	0.74	0.02	0.67	0.01
19	–	–	–	–	–	–	–	–
20	0.73	0.00	0.58	0.00	0.73	0.01	0.67	0.01
21	0.76	0.00	0.52	0.01	0.79	0.01	0.62	0.01
22	0.76	0.01	0.53	0.00	0.76	0.02	0.66	0.01
23	0.77	0.01	0.55	0.00	0.80	0.03	0.68	0.01
24	–	–	0.59	0.01	–	–	0.70	0.02
25	0.79	0.01	0.58	0.00	0.79	0.02	0.68	0.01
26	0.76	0.01	0.54	0.00	0.77	0.02	0.66	0.01
27	0.77	0.01	0.54	0.01	0.79	0.02	0.66	0.01
28	0.77	0.00	0.59	0.00	0.79	0.01	0.68	0.01
29	0.77	0.01	0.55	0.00	0.78	0.02	0.68	0.01
30	0.77	0.01	0.54	0.00	0.78	0.02	0.66	0.01
31	0.68	0.00	0.54	0.00	0.69	0.01	0.66	0.00
32	0.77	0.00	0.57	0.00	0.79	0.01	0.68	0.01
33	0.76	0.00	0.54	0.00	0.75	0.01	0.65	0.01
34	0.75	0.01	0.52	0.00	0.77	0.02	0.64	0.01
35	0.77	0.01	0.59	0.00	0.78	0.01	0.69	0.01
36	0.75	0.01	0.60	0.00	0.75	0.01	0.68	0.01
37	–	–	0.58	0.01	–	–	–	–
38	–	–	–	–	–	–	–	–
39	0.76	0.00	–	–	0.77	0.01	0.68	0.01
40	0.76	0.01	0.56	0.00	0.78	0.02	0.66	0.01
41	0.75	0.01	0.53	0.00	0.75	0.02	0.64	0.01
42	0.76	0.01	0.53	0.00	0.78	0.02	0.65	0.01
43	0.75	0.01	0.52	0.01	0.76	0.02	0.65	0.01

44	0.77	0.01	0.52	0.01	0.77	0.02	0.64	0.01
45	0.76	0.01	0.55	0.01	0.77	0.02	0.66	0.01
46	—	—	—	—	0.71	0.02	—	—
47	0.72	0.00	0.58	0.01	0.70	0.01	0.66	0.02
48	0.73	0.01	0.57	0.00	0.73	0.01	0.67	0.01
49	0.68	0.00	—	—	0.66	0.01	—	—
50	0.74	0.01	0.53	0.00	0.75	0.02	0.63	0.01
51	0.72	0.01	0.56	0.00	0.74	0.02	0.67	0.01
52	0.36	0.00	0.61	0.00	0.72	0.01	0.69	0.01
53	—	—	0.60	0.02	—	—	0.73	0.04
54	0.76	0.01	0.59	0.00	0.76	0.01	0.69	0.01
55	0.75	0.01	0.55	0.01	0.76	0.02	0.66	0.01
56	0.77	0.01	0.54	0.00	0.78	0.02	0.66	0.01
57	0.76	0.00	0.55	0.00	0.76	0.01	0.67	0.01
58	0.78	0.01	0.59	0.00	0.77	0.01	0.69	0.01
59	0.76	0.01	0.54	0.01	0.76	0.02	0.64	0.01
60	0.75	0.01	0.59	0.01	0.77	0.01	0.69	0.01
61	0.75	0.01	0.55	0.01	0.77	0.02	0.67	0.01
62	0.58	0.01	0.49	0.01	0.55	0.02	0.58	0.01
63	0.74	0.00	0.61	0.01	0.74	0.01	—	—
64	0.77	0.01	0.55	0.01	0.78	0.02	0.67	0.01
65	0.76	0.00	0.59	0.00	0.76	0.01	0.69	0.01
66	0.78	0.01	0.57	0.01	—	—	0.68	0.01
67	0.75	0.01	0.54	0.01	0.79	0.02	0.65	0.01
68	0.78	0.01	0.54	0.01	0.78	0.02	0.65	0.01
69	0.46	0.00	0.53	0.01	0.49	0.01	0.65	0.01
70	0.75	0.01	—	—	0.76	0.02	0.64	0.01
71	0.70	0.00	—	—	0.70	0.01	—	—
72	0.77	0.00	—	—	0.78	0.01	—	—
73	—	—	—	—	0.77	0.02	—	—
74	—	—	—	—	—	—	—	—
75	—	—	—	—	—	—	—	—
76	—	—	—	—	—	—	—	—

Appendix 8: S^2 at 15 and 60 ºC in the presence and absence of 1.5 M TMAO

Res	S^2 15 ºC	err	S^2 60 ºC	err	S^2 15 ºC TMAO	err	S^2 60 ºC TMAO	err
1	–	–	–	–	–	–	–	–
2	0.85	0.002	0.79	0.004	0.85	0.01	–	–
3	0.87	0.003	0.83	0.002	0.92	0.02	0.85	0.004
4	0.88	0.003	0.89	0.001	0.92	0.02	0.88	–
5	0.84	0.002	0.77	–	0.85	0.01	0.84	0.004
6	0.87	0.003	0.83	–	0.89	0.01	0.82	–
7	0.86	–	0.79	0.001	0.88	0.01	0.82	0.003
8	0.88	–	–	–	0.77	0.03	–	–
9	–	–	–	–	0.84	0.01	–	–
10	–	–	–	–	0.89	0.02	–	–
11	–	–	–	–	0.84	0.01	–	–
12	0.83		0.81	0.004	0.84	0.01	0.79	0.010
13	0.86	0.003	0.77	0.002	0.89	0.02	0.83	0.005
14	0.84	0.002	0.81		0.84	0.01	–	–
15	0.88	0.002	–	–	0.90	0.02	0.81	–
16	0.79	0.002	0.77		0.80	0.01	0.80	0.003
17	0.87	0.003	0.83	0.002	0.90	0.02	0.83	0.003
18	0.85	0.002	0.81	0.002	–	–	0.82	0.002
19	0.84	0.002	–	–	–	–	–	–
20	0.91	0.002	0.82	0.002	0.85	0.01	0.83	0.003
21	–	–	0.77	–	0.93	0.01	0.82	–
22	0.88	0.002	0.80	0.002	0.88	0.01	0.87	–
23	–	–	0.84	–	0.93	0.02	–	–
24	–	–	0.87	0.003	–	–	0.86	–
25	–	–	0.87	–	–	–	0.87	0.002
26	0.88	0.002	0.84	0.001	0.90	0.01	0.83	–
27	0.88	0.002	0.84	0.002	0.90	0.01	0.88	0.003
28	0.94	0.002	0.88	0.001	0.94	0.01	0.88	0.002
29	0.86	0.002	0.83	0.001	0.90	0.01	0.95	–
30	0.90	0.003	0.83	0.001	0.91	0.01	0.85	–
31	0.70	0.020	0.83	0.001	0.77	0.02	0.86	0.002
32	0.89	0.002	0.82	0.001	0.91	0.01	0.86	–
33	0.84	0.002	0.79	0.001	0.87	0.01	0.81	0.002
34	0.84	0.002	0.79	0.001	0.86	0.01	0.81	0.003
35	0.89	0.002	0.86	0.001	0.88	0.01	0.84	–
36	0.77	0.002	0.71	0.001	–	–	0.74	–
37	–	–	–	–	–	–	–	–
38	–	–	–	–	–	–	–	–
39	0.85	–	0.81	0.003	0.90	0.01	0.78	0.008
40	0.87	0.002	0.81	0.001	0.90	0.01	0.84	0.003

41	0.87	0.002	0.79	0.001	0.89	0.01	0.81	0.003
42	0.85	0.002	0.79	—	0.86	0.01	0.99	—
43	0.84	0.003	0.80	—	0.87	0.02	0.82	0.003
44	0.87	0.003	0.82	—	0.87	0.02	1.00	0.002
45	0.87	0.003	0.83	0.002	0.88	0.02	0.85	0.002
46	—	—	—	—	0.89	0.02	—	—
47	0.85		0.77	0.006	0.85	0.01	0.78	0.010
48	0.86	0.002	0.82	0.001	0.87	0.01	0.82	0.002
49	0.81	—	—	—	0.83	0.01	—	—
50	0.86	0.003	0.80	0.001	0.88	0.02	0.81	—
51	—	—	0.78	0.001	0.84	0.02	0.79	0.003
52	—	—	0.80	0.001	—	—	0.78	0.003
53	—	—	—	—	—	—	—	—
54	0.84	0.002	0.80	0.001	—	—	0.80	—
55	0.86	0.002	0.81	0.002	0.88	0.02	0.81	—
56	0.93	0.003	0.83	0.001	0.92	0.02	0.87	0.002
57	0.85	0.002	0.81	0.001	0.90	0.01	0.85	0.003
58	0.90	0.002	0.86	0.001	0.93	0.01	0.89	0.002
59	0.85	0.002	0.80	0.002	0.86	0.01	0.81	0.003
60	0.88	0.002	0.84	0.002	0.91	0.01	0.85	0.005
61	0.87	0.003	0.80	0.001	0.89	0.02	0.83	0.002
62	—	—	—	—	—	—	—	—
63	0.87	0.002	0.76	0.004	0.85	0.01	—	—
64	0.91	0.003	0.85	0.002	0.93	0.02	0.87	0.005
65	0.86	0.002	0.84	0.002	0.90	0.01	0.85	0.002
66	0.83	0.002	0.81	0.003	—	—	0.86	0.004
67	0.86	0.003	0.81	0.002	0.89	0.02	0.83	0.003
68	0.84	0.003	0.82	0.002	0.87	0.02	0.99	—
69	—	—	0.81	0.002	—	—	0.83	0.003
70	0.89	0.003	—	—	0.92	0.02	0.98	—
71	0.83	0.002	—	—	0.87	0.01	—	—
72	0.92	0.002	—	—	0.92	0.01	—	—
73	—	—	—	—	0.88	0.01	—	—
74	—	—	—	—	—	—	—	—
75	—	—	—	—	—	—	—	—
76	—	—	—	—	—	—	—	—

Appendix 9: τe (psec) values at 15 and 60 ºC in the presence and absence of 1.5 M TMAO

Res	τe 15 ºC	err	τe 60 ºC	err	τe 15º C TMAO	err	τe 60 ºC TMAO	err
1	–	–	–	–	–	–	–	–
2	33.2	2.9	–	–	32.4	6.4	–	–
3	25.2	4.2	25.0	3.6	–	–	32.3	6.0
4	16.1	5.0	–	–	–	–	–	–
5	19.3	3.1	–	–	15.3	6.4	0.9	0.0
6	22.4	3.8	–	–	28.3	9.8	–	–
7	–	–	33.9	2.0	39.5	8.0	33.8	3.6
8	–	–	–	–	0.8	0.0	–	–
9	–	–	–	–	–	–	–	–
10	–	–	–	–	–	–	–	–
11	–	–	–	–	–	–	–	–
12	–	–	1.5	4.6	56.8	5.9	0.2	0.1
13	25.1	4.6	35.0	2.6	34.3	12.2	0.9	0.0
14	–	–	–	–	23.2	5.9	–	–
15	–	–	–	–	–	–	–	–
16	28.0	1.7	–	–	27.2	3.6	–	–
17	26.6	4.1	22.0	3.3	31.9	10.8	28.3	5.0
18	24.5	2.8	11.2	2.7	–	–	–	–
19	–	–	–	–	–	–	–	–
20	32.1	1.9	6.3	2.7	34.1	4.8	21.3	4.5
21	–	–	–	–	26.4	10.2	–	–
22	24.3	3.6	31.7	2.3	30.9	8.9	–	–
23	–	–	–	–	–	–	–	–
24	–	–	0.7	7.8	–	–	–	–
25	–	–	–	–	–	–	23.1	4.1
26	27.1	3.5	29.9	2.5	26.4	8.8	–	–
27	–	–	33.8	3.9	–	–	–	–
28	43.0	5.1	5.4	3.3	–	–	23.9	4.6
29	16.3	2.9	23.9	2.6	24.0	9.5	0.9	0.0
30	27.7	4.9	33.5	2.4	26.0	12.2	–	–
31	0.8	0.0	29.7	1.6	0.9	0.0	35.9	3.4
32	22.8	2.8	12.6	2.0	22.1	7.3	–	–
33	–	–	21.8	1.7	30.6	5.6	25.5	2.8
34	–	–	33.8	2.1	19.7	7.0	32.8	3.8
35	28.6	3.3	2.7		17.6	6.1	–	–
36	16.0	1.3	1.1	–	–	–	–	–
37	–	–	–	–	–	–	–	–
38	–	–	–	–	–	–	–	–

39	—	—	3.6	2.9	31.1	5.6	9.4	5.1
40	25.5	2.9	18.5	2.4	—	—	27.3	4.1
41	28.4	3.1	27.8	2.0	36.3	9.1	32.2	3.4
42	20.1	3.1	—	—	—	—	0.8	—
43	22.0	3.8	—	—	—	—	25.7	5.2
44	19.6	4.3	—	—	20.8	9.2	0.8	—
45	27.9	4.1	24.4	3.1	23.8	9.6	—	—
46	—	—	—	—	57.2	14.4	—	—
47	—	—	4.5	4.0	45.9	5.4	—	—
48	41.8	2.4	—	—	35.3	5.6	18.1	3.7
49	—	—	—	—	49.9	4.7	—	—
50	35.4	3.5	29.4	2.3	36.4	11.0	—	—
51	—	—	—	—	24.2	7.0	22.5	3.5
52	—	—	—	—	—	—	10.0	2.4
53	—	—	—	—	—	—	—	—
54	18.5	2.3	2.7	2.2	—	—	—	—
55	—	—	22.9	2.8	—	—	—	—
56	40.1	6.7	29.1	2.3	31.2	13.3	29.2	5.0
57	20.0	2.1	—	—	32.5	7.7	16.4	3.8
58	16.9	3.6	1.8	2.8	40.9	12.8	5.0	4.7
59	—	—	25.9	2.7	23.2	6.2	28.5	4.3
60	30.6	3.1	3.8	3.3	—	—	6.1	5.9
61	31.5	3.8	—	—	26.4	9.6	14.4	4.5
62	—	—	—	—	—	—	—	—
63	39.9	2.4	—	—	30.6	4.5	—	—
64	28.2	6.7	32.9	4.1	—	—	26.7	7.2
65	—	—	1.4	2.8	—	—	10.5	4.2
66	10.2	2.5	8.8	3.3	—	—	8.6	7.2
67	26.8	4.2	26.8	3.5	—	—	25.7	5.7
68	11.9	3.4	26.3	3.1	—	—	0.8	—
69	—	—	31.4	3.0	—	—	29.2	4.8
70	34.7	5.6	—	—	—	—	0.9	4.7
71	43.5	2.0	—	—	55.5	6.8	—	—
72	—	—	—	—	25.7	10.1	—	—
73	—	—	—	—	22.3	8.6	—	—
74	—	—	—	—	—	—	—	—
75	—	—	—	—	—	—	—	—
76	—	—	—	—	—	—	—	—

Appendix 10: R_{ex} (msec) values at 15 and 60 ºC in the presence and absence of 1.5 M TMAO

Res	Rex 15 ºC	err	Rex 60 ºC	err	Rex 15 ºC TMAO	err	Rex 60 ºC TMAO	err
1	–	–	–	–	–	–	–	–
2	–	–	–	–	–	–	–	–
3	–	–	–	–	–	–	32.28	0.17
4	–	–	–	–	–	–	–	–
5	–	–	–	–	–	–	980.65	0.00
6	–	–	–	–	–	–	–	–
7	–	–	–	–	1.13	0.52	33.81	0.21
8	–	–	–	–	1295.66	209.30	–	–
9	–	–	–	–	–	–	–	–
10	–	–	–	–	–	–	–	–
11	–	–	–	–	–	–	–	–
12	–	–	–	–	–	–	–	–
13	–	–	–	–	–	–	1228.97	0.00
14	–	–	–	–	–	–	–	–
15	–	–	–	–	–	–	–	–
16	–	–	–	–	–	–	–	–
17	–	–	–	–	–	–	28.32	0.17
18	–	–	–	–	–	–	–	–
19	–	–	–	–	–	–	–	–
20	–	–	–	–	–	–	21.28	0.00
21	–	–	–	–	–	–	–	–
22	–	–	–	–	–	–	–	–
23	–	–	–	–	–	–	–	–
24	–	–	–	–	–	–	–	–
25	–	–	–	–	–	–	23.06	0.34
26	–	–	0.52	0.06	–	–	–	–
27	–	–	–	–	–	–	–	–
28	–	–	–	–	–	–	23.93	0.73
29	–	–	–	–	–	–	23.68	0.00
30	–	–	–	–	–	–	–	–
31	1476.48	161.71			1329.28	179.92	35.87	0.73
32	–	–	–	–	–	–	–	–
33	–	–	–	–	1.01	0.45	25.52	0.18
34	–	–	–	–	0.87	0.57	32.83	0.16
35	–	–	–	–	–	–	–	–
36	–	–	–	–	–	–	–	–
37	–	–	–	–	–	–	–	–
38	–	–	–	–	–	–	–	–
39	–	–	–	–	–	–	9.42	0.51
40	–	–	–	–	–	–	27.34	0.21

41	–	–	–	–	–	–	32.21	0.18
42	–	–	–	–	–	–	26.22	0.00
43	–	–	–	–	–	–	25.74	0.00
44	–	–	–	–	–	–	32.96	0.00
45	–	–	–	–	–	–	–	–
46	–	–	–	–	1.40	0.84	–	–
47	–	–	–	–	–	–	–	–
48	–	–	–	–	–	–	18.06	0.00
49	–	–	–	–	–	–	–	–
50	–	–	–	–	–	–	–	–
51	–	–	–	–	–	–	22.46	0.40
52	–	–	–	–	–	–	10.02	0.25
53	–	–	–	–	–	–	–	–
54	–	–	–	–	–	–	–	–
55	–	–	–	–	–	–	–	–
56	–	–	–	–	–	–	29.21	0.00
57	–	–	–	–	–	–	16.42	0.26
58	–	–	–	–	–	–	5.02	0.00
59	–	–	–	–	–	–	28.55	0.26
60	–	–	–	–	–	–	6.13	0.43
61	–	–	–	–	–	–	14.41	0.00
62	–	–	–	–	–	–	–	–
63	–	–	–	–	–	–	–	–
64	–	–	–	–	–	–	26.66	0.20
65	–	–	–	–	–	–	10.49	0.00
66	–	–	–	–	–	–	8.56	0.00
67	–	–	–	–	–	–	25.75	0.00
68	–	–	–	–	–	–	26.11	0.00
69	–	–	–	–	–	–	29.16	0.23
70	–	–	–	–	–	–	51.52	0.00
71	–	–	–	–	–	–	–	–
72	–	–	–	–	–	–	–	–
73	–	–	–	–	–	–	–	–
74	–	–	–	–	–	–	–	–
75	–	–	–	–	–	–	–	–
76	–	–	–	–	–	–	–	–

Appendix 11: $^{h3}J_{NC'}$ scalar couplings (Hz) in Guanidinium Chloride (Gdn.HCl) (25 ^{o}C)

Don.	Acc.	0 M	err	0.5 M	err	1.0 M	err	1.5 M	err	3.0 M	err
1	17	–	–	–	–	–	–	–	–	–	–
2	–	–	–	–	–	–	–	–	–	–	–
3	15	0.434	0.005	0.447	0.004	0.451	0.009	0.477	0.024	0.633	0.015
4	65	0.577	0.006	0.594	0.058	0.611	0.004	0.536	0.018	0.521	0.006
5	13	–	–	–	–	0.577	0.008				
6	67	0.566	0.007	0.556	0.039	0.569	0.039	0.563	0.010	0.495	0.026
7	11	0.544	0.005	0.519	0.008	0.521	0.006	0.547	0.013	0.480	0.013
8	–	–	–	–	–	–	–	–	–	–	–
9	–	–	–	–	–	–	–	–	–	–	–
10	–	–	–	–	–	–	–	–	–	–	–
11	–	–	–	–	–	–	–	–	–	–	–
12	–	–	–	–	–	–	–	–	–	–	–
13	5	0.677	0.005	0.680	0.013	0.684	0.016	0.684	0.026	0.620	0.036
14	–	–	–	–	–	–	–	–	–	–	–
15	3	0.632	0.018	0.623	0.012	0.635	0.031	0.584	0.016	0.542	0.021
16	–	–	–	–	–	–	–	–	–	–	–
17	1	–	–	–	–	–	–	–	–	0.623	0.023
18	–	–	–	–	–	–	–	–	–	–	–
19	–	–	–	–	–	–	–	–	–	–	–
20	–	–	–	–	–	–	–	–	–	–	–
21	–	–	–	–	–	–	–	–	–	–	–
22	–	–	–	–	–	–	–	–	–	–	–
23	54	–	–	–	–	0.854	0.111	–	–	–	–
24	–	–	–	–	–	–	–	–	–	–	–
25	–	–	–	–	–	–	–	–	–	–	–
26	22	0.272	0.009	0.275	0.018	0.299	0.003	0.342	0.008	–	–
27	23	0.494	0.026	–	–	–	–	0.569	0.052	–	–
28	24	0.297	0.014	–	–	0.303	0.052	–	–	0.283	0.012
29	25	0.254	0.007	0.266	0.049	0.303	0.008	0.330	0.013	–	–
30	26	0.346	0.001	0.303	0.029	0.349	0.019	0.382	0.021	0.325	0.013
31	27	0.283	0.008	0.260	0.014	0.262	0.004	0.233	0.013	0.235	0.004
32	28	0.293	0.009	0.311	0.027	0.378	0.036	0.319	0.007	0.321	0.019
33	29	0.197	0.005	–	–	–	–	0.349	–	–	–
34	30	0.660	0.012	0.673	0.003	0.693	0.001	0.705	0.012	0.645	0.003
35	31	–	–	–	–	–	–	–	–	–	–
36	–	–	–	–	–	–	–	–	–	–	–
37	–	–	–	–	–	–	–	–	–	–	–
38	–	–	–	–	–	–	–	–	–	–	–
39	–	–	–	–	–	–	–	–	–	–	–
40	–	–	–	–	–	–	–	–	–	–	–
41	–	–	–	–	–	–	–	–	–	–	–
42	70	0.552	0.003	0.550	0.016	0.520	0.026	0.537	0.019	0.536	0.006

43	–	–	–	–	–	–	–	–	–	–	–
44	68	0.547	0.007	0.582	0.010	0.594	0.006	0.624	0.016	0.545	0.008
45	48	0.453	0.018	0.469	0.017	0.474	0.021	0.454	0.022	–	–
46	–	–	–	–	–	–	–	–	–	–	–
47	–	–	–	–	–	–	–	–	–	–	–
48	45	–	–	–	–	–	–	–	–	–	–
49	–	–	–	–	–	–	–	–	–	–	–
50	43	0.730	0.007	0.772	0.010	0.795	0.009	0.791	0.016	0.700	0.045
51	–	–	–	–	–	–	–	–	–	–	–
52	–	–	–	–	–	–	–	–	–	–	–
53	–	–	–	–	–	–	–	–	–	–	–
54	–	–	–	–	–	–	–	–	–	–	–
55	–	–	–	–	–	–	–	–	–	–	–
56	21	0.465	0.017	0.467	0.018	0.460	0.048	0.538	0.026	0.478	0.004
57	19	0.344	0.009	0.390	0.001	0.377	0.021	0.372	0.016	0.380	0.007
58	–	–	–	–	–	–	–	–	–	–	–
59	–	–	–	–	–	–	–	–	–	–	–
60	–	–	–	–	–	–	–	–	–	–	–
61	56	–	–	–	–	–	–	–	–	–	–
62	–	–	–	–	–	–	–	–	–	–	–
63	–	–	–	–	–	–	–	–	–	–	–
64	2	0.800	0.006	0.821	0.004	0.833	0.022	0.819	0.016	0.784	0.040
65	–	–	–	–	–	–	–	–	–	–	–
66	–	–	–	–	–	–	–	–	–	–	–
67	4	0.631	0.006	0.646	0.002	0.640	0.004	0.698	0.006	0.669	0.005
68	44	0.606	0.007	0.639	0.004	0.604	0.004	0.617	0.020	0.579	0.027
69	6	0.502	0.007	0.556	0.011	0.516	0.028	0.544	0.005	0.536	0.011
70	42	0.642	0.013	0.667	0.011	0.648	0.004	0.674	0.011	0.571	0.008
71	–	–	–	–	–	–	–	–	–	–	–
71	–	–	–	–	–	–	–	–	–	–	–
73	–	–	–	–	–	–	–	–	–	–	–
74	–	–	–	–	–	–	–	–	–	–	–
75	–	–	–	–	–	–	–	–	–	–	–
76	–	–	–	–	–	–	–	–	–	–	–

Appendix 12: $^{h3}J_{NC'}$ scalar couplings (Hz) in Urea (25 ºC)

Don.	Acc.	0 M	err	3.0 M	err
1	17	–	–	–	–
2	–	–	–	–	–
3	15	0.43	0.00	0.47	0.005
4	65	0.58	0.01	0.64	0.003
5	13	–	–	–	–
6	67	0.57	0.01	0.54	0.041
7	11	0.54	0.01	0.53	0.014
8	–	–	–	–	–
9	–	–	–	–	–
10	–	–	–	–	–
11	–	–	–	–	–
12	–	–	–	–	–
13	5	0.68	0.00	0.67	0.021
14	–	–	–	–	–
15	3	0.63	0.02	0.62	0.008
16	–	–	–	–	–
17	1	–	–	–	–
18	–	–	–	–	–
19	–	–	–	–	–
20	–	–	–	–	–
21	–	–	–	–	–
22	–	–	–	–	–
23	54	–	–	–	–
24	–	–	–	–	–
25	–	–	–	–	–
26	22	0.27	0.01	0.28	0.006
27	23	0.49	0.03	–	–
28	24	0.30	0.01	–	–
29	25	0.25	0.01	0.25	0.006
30	26	0.35	0.00	0.37	0.014
31	27	0.28	0.01	0.29	0.002
32	28	0.29	0.01	0.31	0.021
33	29	0.20	0.00		
34	30	0.66	0.01	0.66	0.017
35	31	–	–	–	–
36	–	–	–	–	–
37	–	–	–	–	–
38	–	–	–	–	–
39	–	–	–	–	–
40	–	–	–	–	–
41	–	–	–	–	–
42	70	0.55	0.00	0.52	0.005
43	–	–	–	–	–

44	68	0.55	0.01	0.53	0.005
45	48	0.45	0.02	–	–
46	–	–	–	–	–
47	–	–	–	–	–
48	45	–	–	–	–
49	–	–	–	–	–
50	43	0.73	0.01	0.61	0.018
51	–	–	–	–	–
52	–	–	–	–	–
53	–	–	–	–	–
54	–	–	–	–	–
55	–	–	–	–	–
56	21	0.46	0.02	0.38	0.013
57	19	0.34	0.01	0.37	0.005
58	–	–	–	–	–
59	–	–	–	–	–
60	–	–	–	–	–
61	56	–	–	–	–
62	–	–	–	–	–
63	–	–	–	–	–
64	2	0.80	0.01	0.78	0.008
65	–	–	–	–	–
66	–	–	–	–	–
67	4	0.63	0.01	0.62	0.003
68	44	0.61	0.01	0.61	0.003
69	6	0.50	0.01	0.53	0.010
70	42	0.64	0.01	0.64	0.008
71	–	–	–	–	–
71	–	–	–	–	–
73	–	–	–	–	–
74	–	–	–	–	–
75	–	–	–	–	–
76	–	–	–	–	–

Appendix 13: $^{1}J_{NH}$ scalar couplings (Hz) in Guanidinium Chloride and Urea (25 ºC)

Ref	0M	1.5 M	3.0 M	3m Urea
1	–	–	–	–
2	93.77	93.75	93.61	93.59
3	93.29	–	93.24	93.12
4	94.07	93.43	94.10	94.44
5	93.20	93.88	93.16	94.17
6	93.78	93.90	93.68	94.01
7	95.47	94.57	94.65	94.63
8	93.20	93.15	93.05	93.07
9	92.68	92.86	92.87	92.71
10	100.50	97.47	93.87	93.85
11	93.88	93.85	93.93	93.90
12	93.11	92.95	92.82	92.82
13	94.21	94.31	93.58	94.04
14	93.20	93.26	93.21	93.01
15	94.45	94.55	93.94	94.43
16	93.16	92.31	92.32	92.26
17	94.69	93.99	94.30	93.77
18	92.39	92.71	92.77	93.01
19	–	–	–	–
20	92.42	92.45	92.27	92.60
21	94.65	94.34	95.21	94.80
22	93.91	93.78	93.77	93.68
23	94.75	94.54	94.25	96.29
24	–	–	–	–
25	95.17	95.06	95.23	95.10
26	93.90	94.25	92.76	93.68
27	94.25	94.54	94.38	94.55
28	94.65	94.34	95.21	95.03
29	94.80	94.78	94.80	94.77
30	94.11	–	94.16	94.57
31	93.98	93.90	93.70	77.36
32	94.74	95.09	95.64	96.33
33	93.56	93.81	93.75	93.92
34	89.39	91.35	90.78	91.64
35	94.25	94.35	94.23	94.43
36	91.74	91.57	91.66	91.89
37	–	–	–	–
38	–	–	–	–
39	94.39	–	94.12	94.28
40	93.57	93.51	92.89	92.84
41	94.24	94.16	94.12	93.89
42	94.50	94.16	94.60	94.02
43	94.45	93.52	93.97	94.04
44	93.08	92.62	92.41	92.52
45	93.29	94.02	93.70	94.02
46	94.69	94.68	94.60	94.73
47	93.37	93.14	93.30	93.13
48	92.91	94.47	93.66	94.09

49	93.51	93.48	93.21	93.55
50	94.95	93.54	95.01	94.95
51	93.06	93.48	93.35	92.01
52	93.37	93.39	93.15	93.27
53	0.00	0.00	0.00	0.00
54	93.67	94.25	93.74	93.81
55	92.86	93.07	92.84	93.05
56	96.09	95.31	94.20	95.49
57	93.87	94.37	94.31	94.38
58	95.36	95.36	95.94	95.30
59	92.91	93.13	93.18	93.35
60	94.73	93.90	94.55	93.97
61	93.53	93.50	93.29	93.31
62	93.58	93.90	93.69	93.68
63	94.15	94.07	93.00	93.98
64	93.60	93.75	93.72	93.68
65	97.31	94.78	94.61	94.79
66	91.39	92.94	92.08	92.02
67	94.20	93.88	94.42	93.60
68	93.72	94.41	93.95	94.36
69	0.00	0.00	0.00	0.00
70	94.69	94.81	94.59	94.09
71	93.82	93.94	93.90	93.79
72	93.64	93.53	93.70	108.14
73	93.70	93.33	93.59	94.16
74	93.45	93.42	93.55	93.25
75	94.13	93.98	94.00	93.80
76	93.44	93.53	93.48	93.62

Appendix 14: $^{1}H_{N}$ chemical shifts (ppm) in Gdn.HCl at 25 ºC

Res	0M	1M	2M	3M	4M	5M	6M
1	–	–	–	–	–	–	–
2	8.957	9.009	–	–	–	–	–
3	8.330	8.371	8.412	8.451	–	–	–
4	8.626	8.652	8.685	8.717	8.754	8.795	8.813
5	9.341	9.373	9.415	9.455	8.972	–	–
6	8.868	8.883	8.916	8.947	8.856	8.989	9.005
7	8.763	8.764	8.797	8.828	9.289	8.862	8.885
8	9.167	9.192	9.227	9.260	7.839	9.295	9.314
9	7.657	7.721	7.769	7.809	–	7.864	7.883
10	7.835	7.900	7.948	7.991	–	–	–
11	7.268	7.280	7.266	–	–	–	–
12	8.675	8.693	8.717	8.750	8.774	8.804	–
13	9.515	9.502	9.523	9.534	–	–	–
14	8.756	8.788	8.821	8.853	8.875	8.876	8.896
15	8.738	8.747	8.773	8.801	8.826	8.848	8.864
16	8.155	–	–	–	–	–	–
17	8.941	8.964	8.997	9.029	9.058	9.057	9.077
18	8.661	8.725	8.756	8.782			
19	–	–	–	–	–	–	–
20	7.059	7.124	7.176	7.227	–	–	–
21	8.063	8.118	–	–	–	–	–
22	7.931	7.961	8.026	8.097	8.163		
23	8.569	8.620	8.658	8.695	8.726	8.745	8.763
24	9.918	9.749	9.686	9.647	–	–	–
25	7.954	7.989	8.027	8.065	–	–	–
26	8.114	8.131	8.153	8.175	–	–	–
27	8.586	8.607	8.640	8.675	–	–	–
28	8.057	8.113	–	–	–	–	–
29	7.884	7.916	7.959	8.003	–	–	–
30	8.309	8.346	8.388	8.432	–	–	–
31	8.623	8.647	8.673	8.697	8.720	8.732	8.749
32	8.042	8.188	8.257	8.311	–	–	–
33	7.447	8.797	–	–	–	–	–
34	8.754	8.607	8.843	8.883	8.921	8.962	8.981
35	8.547	6.208	8.661	8.718	8.770	8.824	8.851
36	6.172		6.239	6.272	6.293	6.306	6.325
37	–	–	–	–	–	–	–
38	–	–	–	–	–	–	–
39	8.571	8.626	8.673	8.716	8.754	8.788	8.809
40	7.841	7.869	7.914	7.955	7.991	7.980	–
41	7.507	7.531	7.567	7.605	7.635	7.672	7.693
42	8.539	8.566	8.597	8.628	8.656	8.688	8.712
43	8.861	8.858	8.894	8.936	–	–	–
44	9.077	9.117	9.166	9.211	9.248	9.274	9.300
45	8.865	8.852	8.877	8.909	8.938	8.959	8.982

46	8.874	8.842	8.873	8.905	8.934	8.951	8.971
47	8.165	–	–	–	–	–	–
48	8.002	8.019	8.056	8.094	–	–	–
49	8.652	8.667	8.699	8.735	–	–	–
50	8.569	8.628	8.677	8.724	8.766	8.753	–
51	8.425	8.486	8.523	8.554	8.574	8.576	8.590
52	8.191	8.266	8.317	8.367	–	–	–
53	–	7.554	–	–	–	–	–
54	7.477	7.582	7.602	7.646	7.674	7.694	7.716
55	8.804	8.821	8.848	8.869	8.886	8.847	8.867
56	8.168	8.212	8.259	8.306	8.348	8.371	8.390
57	8.505	8.552	8.604	8.652	8.693	8.719	8.743
58	7.960	8.013	8.060	8.103	–	–	–
59	7.267	–	–	–	–	–	–
60	8.181	8.217	8.263	8.311	8.352	–	–
61	7.270	7.342	7.376	7.419	7.450	7.461	7.486
62	7.631	7.743	7.813	7.877	7.934	7.939	8.015
63	8.531	8.538	8.561	8.585	–	–	–
64	9.330	9.350	9.384	9.418	–	–	–
65	7.695	7.749	7.791	–	–	–	–
66	8.753	8.811	8.851	–	–	–	–
67	9.436	9.460	9.494	9.524	–	–	–
68	9.244	9.308	9.351	9.389	–	–	–
69	8.361	–	8.492	8.540	–	–	–
70	9.216	8.437	–	–	–	–	–
71	8.155	9.265	–	–	–	–	–
72	8.595	8.623	8.661	8.703	–	–	–
73	8.339	8.406	8.438	8.470	–	–	–
74	8.451	8.444	8.482	8.522	–	–	–
75	8.506	8.517	8.552	8.587	8.618	8.638	8.659
76	7.961	8.036	8.094	8.149	8.192	8.176	–

Appendix 15: $^{1}H_{N}$ chemical shifts (ppm) in Urea at 25 ºC

Res	0M	1M	2M	3M	4M	5M	6M	7M
1								
2	8.955	8.982	9.004	9.026	9.040	9.054	–	9.069
3	8.332	8.356	8.377	8.394	8.405	8.419	8.415	8.433
4	8.634	8.653	8.671	8.683	8.691	8.704	8.700	8.715
5	9.338	9.363	9.377	9.390	9.404	9.414	9.407	9.419
6	8.853	8.867	8.875	8.889	8.900	8.907	8.889	8.906
7	8.765	8.775	8.782	8.790	8.796	8.801	8.777	8.789
8	9.164	9.193	9.216	9.235	9.247	9.260	9.253	9.271
9	7.658	7.667	7.679	7.688	7.692	7.699	–	–
10	7.836	7.845	7.855	7.865	7.869	7.877	7.857	7.872
11	7.265	7.273	7.279	–	–	–	–	–
12	8.684	8.731	8.768	8.797	8.817	8.842	8.861	8.884
13	9.500	9.514	9.510	9.521	9.531	9.531	–	–
14	8.761	8.795	8.821	8.845	8.865	8.884	8.892	8.913
15	8.740	8.755	8.765	8.778	8.785	8.794	8.777	8.793
16	8.168	8.233	8.293	8.340	8.374	8.414	8.386	8.407
17	8.939	8.957	8.972	8.987	8.996	9.004	8.988	9.005
18	8.660	8.685	8.698	8.716	8.732	8.742	8.733	8.752
19	–	–	–	–	–	–	–	–
20	7.064	7.087	7.109	7.126	7.134	7.149	7.147	7.163
21	8.063	8.075	8.083	8.092	8.096	8.101	8.076	8.090
22	7.942	7.966	7.988	8.005	8.010	8.026	8.027	8.044
23	8.578	8.603	8.624	8.639	8.644	8.657	8.649	8.665
24	9.846	9.790	9.721	9.705	9.714	9.687	9.588	9.600
25	7.958	7.977	7.993	8.007	8.014	8.025	8.014	8.030
26	8.111	8.122	8.132	8.142	8.148	8.154	8.131	8.612
27	8.590	8.599	8.606	8.613	8.615	8.621	8.598	–
28	8.076	8.112	8.149	8.171	8.179	8.202	8.216	8.234
29	7.881	7.909	7.933	7.953	7.966	7.980	7.977	7.996
30	8.314	8.335	8.353	8.367	8.374	8.385	8.375	8.398
31	8.626	–	–	–	–	–	–	–
32	8.040	8.079	8.113	8.137	8.152	8.171	8.177	8.197
33	7.448	7.487	7.521	7.547	7.563	7.583	7.593	7.614
34	8.762	8.787	8.802	8.813	8.821	8.835	8.824	8.842
35	8.554	8.588	8.616	8.637	8.646	8.663	8.664	8.680
36	6.171	6.185	6.199	6.211	6.218	6.226	6.209	6.225
37	–	–	–	–	–	–	–	–
38	–	–	–	–	–	–	–	–
39	8.579	8.616	8.649	8.672	8.683	8.704	8.713	8.732
40	7.848	7.859	7.872	7.881	7.883	7.891	7.874	7.890
41	7.513	7.531	7.547	7.561	7.566	7.576	7.563	7.578
42	8.548	8.565	8.575	8.588	8.588	8.596	–	–
43	8.865	8.915	8.954	8.987	9.009	9.034	9.055	9.076
44	9.068	9.095	9.107	9.124	9.137	9.148	9.139	9.157
45	8.863	8.870	8.874	8.883	8.887	8.891	8.865	8.877

46	8.857	8.857	8.856	8.866	8.875	8.877	8.846	8.862
47	8.169	8.194	8.215	8.227	8.232	8.244	8.228	8.244
48	8.004	8.012	8.020	8.027	8.028	8.035	8.011	8.021
49	8.650	8.690	8.727	8.759	8.780	8.804	8.825	8.848
50	8.565	8.571	8.573	8.577	8.578	8.579	—	—
51	8.432	8.452	8.467	8.478	8.481	8.492	—	—
52	8.198	8.220	8.242	8.258	8.265	8.282	8.284	8.302
53	—	—	9.372	7.525	—	—	—	—
54	7.481	7.498	7.507	—	7.529	7.534	7.521	7.530
55	8.782	8.790	8.795	8.810	8.828	8.829	8.798	8.815
56	8.168	8.187	8.205	8.220	8.230	8.242	8.234	8.251
57	8.506	8.519	8.528	8.537	8.540	8.546	8.521	8.533
58	7.963	7.986	8.008	8.024	8.032	8.045	8.036	8.053
59	7.268	7.276	7.279	—	—	—	—	—
60	8.184	8.204	8.222	8.237	8.245	8.257	8.247	8.262
61	7.272	—	—	—	—	—	—	—
62	7.633	7.683	7.727	7.761	7.784	7.811	7.837	7.862
63	8.537	8.556	8.572	8.585	8.589	8.599	8.583	8.598
64	9.331	9.338	9.341	9.348	9.351	9.356	9.328	9.341
65	7.698	7.711	7.723	7.734	7.738	7.747		
66	8.762	8.797	8.826	8.848	8.862	8.883	8.893	8.913
67	9.437	9.462	9.468	9.480	9.489	9.498	9.493	9.508
68	9.249	9.270	9.276	9.288	9.295	9.305	9.286	9.302
69	8.362	—	—	—	—	—	—	—
70	9.226	9.253	9.267	9.281	9.288	9.301	9.289	9.307
71	8.157	8.223	8.289	8.335	8.364	8.404	8.456	8.479
72	8.604	8.632	8.647	8.660	8.665	8.673	8.672	8.688
73	8.341	8.392	8.416	8.437	8.449	8.466	8.466	8.480
74	8.450	8.498	8.540	8.575	8.599	8.624	8.646	8.671
75	8.508	8.525	8.540	8.555	8.562	8.574	—	8.581
76	7.963	7.982	7.999	8.015	8.021	8.034	8.564	—

Appendix 16: Phi and psi angles of ubiquitin x-ray crystal structure (1UBQ)

Res	Phi (ϕ)	Psi (ψ)
1	0	149.6288
2	-91.0203	138.2642
3	-131.099	163.0466
4	-115.991	140.2261
5	-118.03	114.2244
6	-95.2261	127.5416
7	-99.5796	170.7542
8	-73.4253	-6.93582
9	-101.397	14.92934
10	77.44474	16.54442
11	-96.2712	138.079
12	-119.945	131.7569
13	-109.474	141.9886
14	-101.441	139.7376
15	-126.413	154.0003
16	-111.795	121.1288
17	-139.02	170.7172
18	-120.043	144.5116
19	-54.9367	-24.527
20	-79.8385	-8.13681
21	-71.006	148.4355
22	-83.7038	160.4343
23	-61.3276	-37.21
24	-57.5668	-40.4877
25	-65.4883	-44.4443
26	-58.4233	-46.4089
27	-60.8123	-37.9648
28	-66.1219	-38.1201
29	-64.2164	-37.259
30	-69.9996	-39.564
31	-62.1262	-48.6279
32	-53.4121	-41.7666
33	-93.58	-24.3986
34	-123.579	-6.34567
35	81.21639	5.321256
36	-79.7333	124.8668
37	-57.003	136.9671
38	-57.1842	-32.1653
39	-68.2389	-15.5716
40	-95.7981	-10.4692
41	-84.8312	129.6955
42	-121.243	115.9565

43	-103.558	130.2409
44	-122.075	131.807
45	-144.27	129.6366
46	48.17127	45.99398
47	61.7145	21.6164
48	-115.066	142.7131
49	-85.7723	130.2829
50	-79.5553	138.333
51	-101.829	139.9596
52	-48.1901	-42.21
53	-82.9252	-8.88863
54	-85.4496	165.4644
55	-104.51	164.5928
56	-61.218	-36.2052
57	-63.8914	-29.6222
58	-55.5523	-39.3028
59	-91.0217	4.651424
60	57.93961	45.35533
61	-88.6669	116.4408
62	-103.437	169.5413
63	-54.7883	143.0572
64	66.8974	19.14719
65	-71.147	159.5174
66	-119.152	126.6734
67	-103.136	154.6118
68	-105.583	135.6702
69	-106.974	115.7756
70	-108.115	139.9337
71	-96.0197	138.8
72	-117.62	98.81109
73	-83.7244	150.394
74	-97.6604	93.87963
75	120.4149	125.558
76	174.1602	0

Appendix 17: Solvent accessible surface area (SASA) individual ubiquitin amino acids were calculated by GETAREA (Fraczkiewicz and Braun, 1998).

Residue	Total	Apolar	Backbone	Sidechain	Ratio (%)	In/Out
1	55.95	41.57	36.44	19.51	12.3	i
2	70.03	14.5	1.65	68.38	47.6	
3	0	0	0	0	0	i
4	55.78	55.78	0	55.78	31	
5	0	0	0	0	0	i
6	98.97	58.06	0.69	98.28	59.7	o
7	18.07	15.08	2.98	15.09	14.2	i
8	138.06	110.34	31.34	106.71	73	o
9	126.9	93.82	36.12	90.78	85.5	o
10	68.48	36.9	68.48	0	78.5	o
11	106.59	84.79	8.23	98.37	59.8	o
12	60.94	30.14	19.05	41.9	39.4	
13	5.76	5.76	4.23	1.53	1	i
14	62.31	37.16	4.12	58.19	54.8	o
15	7.26	7.24	4.13	3.13	2.1	i
16	137.57	48.66	6.39	131.18	92.9	o
17	6.15	5.34	6.15	0	0	i
18	100.51	40.76	0	100.51	71.2	o
19	52.29	52.29	0	52.29	49.7	
20	81.79	55.44	14.49	67.3	86.9	o
21	31.25	4.03	4.03	27.22	24.1	
22	49.17	44.72	0.1	49.07	46.2	
23	0	0	0	0	0	i
24	113.59	33.16	1.28	112.31	79.5	o
25	49.9	20.91	4.55	45.34	39.7	
26	0	0	0	0	0	i
27	16.08	1.84	0	16.08	9.8	i
28	48.59	46.49	2.16	46.42	71.5	o
29	66.1	39.41	4.74	61.37	37.3	
30	0	0	0	0	0	i
31	69.04	15.99	2.71	66.32	46.2	
32	127.58	23.54	30.55	97.03	85.9	o
33	111.14	54.62	29.82	81.32	49.4	
34	60.46	11.5	31.12	29.34	20.8	
35	51.2	33.48	51.2	0	58.7	o
36	28.98	28.98	1.71	27.27	18.5	i
37	56.91	56.91	0	56.91	54.1	o
38	51.02	48.59	2.43	48.59	46.2	
39	82.3	53.35	13.83	68.47	60.6	o
40	36.52	1.78	0	36.52	25.4	
41	0.05	0	0.05	0	0	i
42	83.11	29.84	1.79	81.32	41.6	
43	0.17	0	0.17	0	0	i
44	29.04	29.04	0	29.04	19.7	i

45	39.14	39.14	0.89	38.25	21.2	
46	74.66	58.47	41.74	32.92	50.7	o
47	73.86	39.48	73.86	0	84.7	o
48	100.28	72.66	8.07	92.2	56.1	o
49	98.05	27.55	17.38	80.66	56.1	o
50	5.56	0	5.56	0	0	i
51	115.59	35.08	8.3	107.29	76	o
52	59.95	24.46	0.81	59.14	52.3	o
53	48.09	35.49	48.09	0	55.2	o
54	118.03	43.2	0.09	117.94	60.3	o
55	34.3	33.37	0	34.3	32.3	
56	0	0	0	0	0	i
57	62.17	36.45	16.05	46.12	59.6	o
58	83.55	19.26	37.28	46.27	41	
59	34.22	23.77	9.36	24.86	12.9	i
60	112.45	35.39	10.4	102.05	89.3	o
61	3.31	0	3.31	0	0	i
62	119.29	42.41	3.32	115.97	80.7	o
63	135.12	82.98	12.97	122.15	74.3	o
64	96.7	30.83	15.36	81.34	57.6	o
65	21.29	14.44	14.2	7.09	9.2	i
66	50.84	27.67	8.29	42.55	40.1	
67	0	0	0	0	0	i
68	75.8	54.04	0	75.8	49	
69	1.82	0.43	1.39	0.43	0.3	i
70	39.31	39.31	0.24	39.07	31.9	
71	75.25	56.33	18.92	56.33	38.5	
72	116.67	69	10.57	106.1	54.3	o
73	122.2	98.13	24.23	97.97	67	o
74	203.36	90.37	34.36	169	86.4	o
75	75.4	48.51	75.4	0	86.5	o
76	145.95	55.06	103.5	42.46	100	o

References

ALONSO, D. O. & DILL, K. A. (1991) Solvent denaturation and stabilization of globular proteins. *Biochemistry,* 30, 5974-85.

ANJUM, F., RISHI, V. & AHMAD, F. (2000) Compatibility of osmolytes with Gibbs energy of stabilization of proteins. *Biochim Biophys Acta,* 1476, 75-84.

AQVIST, J. (1999) Long-range electrostatic effects on peptide folding. *FEBS Lett,* 457, 414-8.

ARAKAWA, T. & TIMASHEFF, S. N. (1984) Protein stabilization and destabilization by guanidinium salts. *Biochemistry,* 23, 5924-9.

ARAKAWA, T. & TIMASHEFF, S. N. (1985) Mechanism of poly(ethylene glycol) interaction with proteins. *Biochemistry,* 24, 6756-62.

ASSADI-PORTER, F. M., ABILDGAARD, F., BLAD, H. & MARKLEY, J. L. (2003) Correlation of the sweetness of variants of the protein brazzein with patterns of hydrogen bonds detected by NMR spectroscopy. *J Biol Chem,* 278, 31331-9.

ATHAWALE, M. V., DORDICK, J. S. & GARDE, S. (2005) Osmolyte trimethylamine-N-oxide does not affect the strength of hydrophobic interactions: origin of osmolyte compatibility. *Biophys J,* 89, 858-66.

ATKINS, P. W. (1994) *Physical Chemistry,* Oxford, ELBS with Oxford University Press.

AUNE, K. C. & TANFORD, C. (1969a) Thermodynamics of the denaturation of lysozyme by guanidine hydrochloride. I. Dependence on pH at 25 degrees. *Biochemistry,* 8, 4579-85.

AUNE, K. C. & TANFORD, C. (1969b) Thermodynamics of the denaturation of lysozyme by guanidine hydrochloride. II. Dependence on denaturant concentration at 25 degrees. *Biochemistry,* 8, 4586-90.

BAGNO, A., GERARD, S., KEVELAM, J., MENNA, E. & SCORRANO, G. (2000) Detecting hydrogen bonding by NMR relaxation of the acceptor nuclei. *Chemistry,* 6, 2915-24.

BAI, Y., MILNE, J. S., MAYNE, L. & ENGLANDER, S. W. (1993) Primary structure effects on peptide group hydrogen exchange. *Proteins,* 17, 75-86.

BAKER, E. N. & HUBBARD, R. E. (1984) Hydrogen bonding in globular proteins. *Prog Biophys Mol Biol,* 44, 97-179.

BALDWIN, R. L. (1996) How Hofmeister ion interactions affect protein stability. *Biophys J,* 71, 2056-63.

BARFIELD, M. (2002) Structural dependencies of interresidue scalar coupling (h3)J(NC') and donor (1)H chemical shifts in the hydrogen bonding regions of proteins. *J Am Chem Soc,* 124, 4158-68.

BARFIELD, M., DINGLEY, A. J., FEIGON, J. & GRZESIEK, S. (2001) A DFT study of the interresidue dependencies of scalar J-coupling and magnetic shielding in the hydrogen-bonding regions of a DNA triplex. *J Am Chem Soc,* 123, 4014-22.

BASKAKOV, I. & BOLEN, D. W. (1998a) Forcing thermodynamically unfolded proteins to fold. *J Biol Chem,* 273, 4831-4.

BASKAKOV, I. & BOLEN, D. W. (1998b) Time-dependent effects of trimethylamine-N-oxide/urea on lactate dehydrogenase activity: an unexplored dimension of the adaptation paradigm. *Biophys J,* 74, 2658-65.

BAX, A. & TJANDRA, N. (1997) High-resolution heteronuclear NMR of human ubiquitin in an aqueous liquid crystalline medium. *J Biomol NMR,* 10, 289-92.

BENNION, B. J. & DAGGETT, V. (2003) The molecular basis for the chemical denaturation of proteins by urea. *Proc Natl Acad Sci U S A,* 100, 5142-7.

BENNION, B. J., DEMARCO, M. L. & DAGGETT, V. (2004) Preventing misfolding of the prion protein by trimethylamine N-oxide. *Biochemistry,* 43, 12955-63.

BHUYAN, A. K. (2002) Protein stabilization by urea and guanidine hydrochloride. *Biochemistry,* 41, 13386-94.

BLUNDELL, T., BARLOW, D., BORKAKOTI, N. & THORNTON, J. (1983) Solvent-induced distortions and the curvature of alpha-helices. *Nature,* 306, 281-3.

BOLEN, D. W. (2004) Effects of naturally occurring osmolytes on protein stability and solubility: issues important in protein crystallization. *Methods,* 34, 312-22.

BOLEN, D. W. & BASKAKOV, I. V. (2001) The osmophobic effect: natural selection of a thermodynamic force in protein folding. *J Mol Biol,* 310, 955-63.

BOLEN, D. W. & SANTORO, M. M. (1988) Unfolding free energy changes determined by the linear extrapolation method. 2. Incorporation of delta G degrees N-U values in a thermodynamic cycle. *Biochemistry,* 27, 8069-74.

BONDI, A. (1964) van der Waals volumes and radii. *J Phys Chem*, 68, 441_451.

BONVIN, A. M., HOUBEN, K., GUENNEUGUES, M., KAPTEIN, R. & BOELENS, R. (2001) Rapid protein fold determination using secondary chemical shifts and cross-hydrogen bond 15N-13C' scalar couplings (3hbJNC'). *J Biomol NMR,* 21, 221-33.

BRANDEN, C. & TOOZE, J. (1999) *Introduction to Protein Structure,* New York, Garland Pub.

BRIGGS, M. S. & RODER, H. (1992) Early hydrogen-bonding events in the folding reaction of ubiquitin. *Proc Natl Acad Sci U S A,* 89, 2017-21.

CARRASCO, B., GARCIA DE LA TORRE, J., DAVIS, K. G., JONES, S., ATHWAL, D., WALTERS, C., BURTON, D. R. & HARDING, S. E. (2001) Crystallohydrodynamics for solving the hydration problem for multi-domain proteins: open physiological conformations for human IgG. *Biophys Chem,* 93, 181-96.

CARY, P. D., KING, D. S., CRANE-ROBINSON, C., BRADBURY, E. M., RABBANI, A., GOODWIN, G. H. & JOHNS, E. W. (1980) Structural studies on two high-mobility-group proteins from calf thymus, HMG-14 and HMG-20 (ubiquitin), and their interaction with DNA. *Eur J Biochem,* 112, 577-80.

CASSIDY, C. S., LIN, J. & FREY, P. A. (2000) The deuterium isotope effect on the NMR signal of the low-barrier hydrogen bond in a transition-state analog complex of chymotrypsin. *Biochem Biophys Res Commun,* 273, 789-92.

CAVALLI, A., FERRARA, P. & CAFLISCH, A. (2002) Weak temperature dependence of the free energy surface and folding pathways of structured peptides. *Proteins,* 47, 305-14.

CAVANAGH, J. (1996) *Protein NMR spectroscopy : principles and practice,* San Diego ; London, Academic Press.

CAVANAGH, J. (2007) *Protein NMR spectroscopy : principles and practice,* Amsterdam ; Boston, Academic Press.

CELINSKI, S. A. & SCHOLTZ, J. M. (2002) Osmolyte effects on helix formation in peptides and the stability of coiled-coils. *Protein Sci,* 11, 2048-51.

CHAN, S. I., LIN, L., CLUTTER, D. & DEA, P. (1970) The anomalous deuterium isotope effect on the chemical shift of the bridge hydrogen in the enol tautomer of 2,4-Pentanedione. *Proc Natl Acad Sci U S A,* 65, 816-822.

CHEN, J., TOPTYGIN, D., BRAND, L. & KING, J. (2008) Mechanism of the efficient tryptophan fluorescence quenching in human gammaD-crystallin studied by time-resolved fluorescence. *Biochemistry,* 47, 10705-21.

CHIN, D. H., WOODY, R. W., ROHL, C. A. & BALDWIN, R. L. (2002) Circular dichroism spectra of short, fixed-nucleus alanine helices. *Proc Natl Acad Sci U S A,* 99, 15416-21.

CIECHANOVER, A. (2005) Proteolysis: from the lysosome to ubiquitin and the proteasome. *Nat Rev Mol Cell Biol,* 6, 79-87.

CLORE G, M., SZABO A., BAX, A., KAY, L, E., DRISCOLL, P, C., GRONENBORN, A, M. (1990). Deviations from the simple two-parameter model-free approach to the interpretation of ^{15}N nuclear magnetic-relaxation of proteins. *J. Am. Chem. Soc*., 112, 4989-4991.

CORDIER, F., DINGLEY, A. J. & GRZESIEK, S. (1999a) A doublet-separated sensitivity-enhanced HSQC for the determination of scalar and dipolar one-bond J-couplings. *J Biomol NMR,* 13, 175-80.

CORDIER, F. & GRZESIEK, S. (2002) Temperature-dependence of protein hydrogen bond properties as studied by high-resolution NMR. *J Mol Biol,* 317, 739-52.

CORDIER, F. & GRZESIEK, S. (2004) Quantitative comparison of the hydrogen bond network of A-state and native ubiquitin by hydrogen bond scalar couplings. *Biochemistry,* 43, 11295-301.

CORDIER, F., ROGOWSKI, M., GRZESIEK, S. & BAX, A. (1999b) Observation of through-hydrogen-bond 2hJHC' in a perdeuterated protein. *J Magn Reson,* 140, 510-2.

CORDIER, F., WANG, C., GRZESIEK, S. & NICHOLSON, L. K. (2000) Ligand-induced strain in hydrogen bonds of the c-Src SH3 domain detected by NMR. *J Mol Biol,* 304, 497-505.

CORDIER, F. & GRZESIEK, S. (1999). Direct observation of hydrogen bonds in proteins by interresidue $^{3h}J_{NCO}$ scalar couplings. *J Am Chem Soc,* 121, 1601-1602.

CORNILESCU, G., HU J. S., BAX A. (199) Identification of the hydrogen bonding network in a protein by scalar couplings. *J Am Chem Soc,* 121, 2949-2950.

CORNILESCU, G., RAMIREZ, B. E., FRANK M. K., CLORE GM, GRONENBORN A. M., BAX, A. (1999) Correlation between $^{3h}J_{NC}$ and hydrogen bond length in proteins. *J Am Chem Soc*, 121, 6275-6279.

CORNILESCU, G., MARQUARDT, J, L., OTTIGER, M., BAX, A. (1998) Validation of protein structure from anisotropic carbonyl chemical shifts in a dilute liquid crystalline phase. *J.Am.Chem.Soc.* 120, 6836-6837

CREIGHTON, T. E. (1992) *Protein folding,* New York, W.H. Freeman.

CURNOW, P. & BOOTH, P. J. (2009) The transition state for integral membrane protein folding. *Proc Natl Acad Sci U S A,* 106, 773-8.

CURTIS, R. A., ULRICH, J., MONTASER, A., PRAUSNITZ, J. M. & BLANCH, H. W. (2002) Protein-protein interactions in concentrated electrolyte solutions. *Biotechnol Bioeng,* 79, 367-80.

DALEY, M. E., GRAETHER, S. P. & SYKES, B. D. (2004) Hydrogen bonding on the ice-binding face of a beta-helical antifreeze protein indicated by amide proton NMR chemical shifts. *Biochemistry,* 43, 13012-7.

DAS, A. & MUKHOPADHYAY, C. (2009) Urea-mediated protein denaturation: a consensus view. *J Phys Chem B,* 113, 12816-24.

DELAGLIO, F., TORCHIA, D. A. & BAX, A. (1991) Measurement of 15 N-13 CJ couplings in staphylococcal nuclease. *Journal of biomolecular NMR,* 1**,** 439-446.

DELANO, W. L. (2002) The PyMOL molecular graphics system.

DEMPSEY, C. E., PIGGOT, T. J. & MASON, P. E. (2005) Dissecting contributions to the denaturant sensitivities of proteins. *Biochemistry,* 44, 775-81.

DENISOV, V. P. & HALLE, B. (1995a) Hydrogen exchange and protein hydration: the deuteron spin relaxation dispersions of bovine pancreatic trypsin inhibitor and ubiquitin. *J Mol Biol,* 245, 698-709.

DENISOV, V. P. & HALLE, B. (1995b) Protein hydration dynamics in aqueous solution: a comparison of bovine pancreatic trypsin inhibitor and ubiquitin by oxygen-17 spin relaxation dispersion. *J Mol Biol,* 245, 682-97.

DEREWENDA, Z. S., DEREWENDA, U. & KOBOS, P. M. (1994) (His)C epsilon-H...O=C < hydrogen bond in the active sites of serine hydrolases. *J Mol Biol,* 241, 83-93.

DEREWENDA, Z. S., LEE, L. & DEREWENDA, U. (1995) The occurrence of C-H...O hydrogen bonds in proteins. *J Mol Biol,* 252, 248-62.

DI STEFANO, D. L. & WAND, A. J. (1987) Two-dimensional 1H NMR study of human ubiquitin: a main chain directed assignment and structure analysis. *Biochemistry,* 26, 7272-81.

DILL, K. A. (1990) Dominant forces in protein folding. *Biochemistry,* 29, 7133-55.

DINGLEY, A. & GRZESIEK, S. (1998). Direct observation of hydrogen bonds in nucleic acid base pairs by internucleotide $^{2}J_{NN}$ couplings. *J Am Chem Soc,* 120, 8293-8297.

DINGLEY, A. J., MASSE, J. E., FEIGON, J. & GRZESIEK, S. (2000) Characterization of the hydrogen bond network in guanosine quartets by internucleotide $^{3h}J_{(NC)'}$ and $^{2h}J_{(NN)}$ scalar couplings. *J Biomol NMR,* 16, 279-89.

DINGLEY, A., CORDIER, F & GRZESIEK, S. (2001) An introduction to hydrogen bond scalar couplings, *Concepts Magn. Reson,* 13, 103-117

DOBSON, C. M. (1992) Resting places on folding pathways. *Curr Biol,* 2, 343-5.

DOBSON, C. M. (2003) Protein folding and misfolding. *Nature,* 426, 884-90.

DOMINY, B. N., PERL, D., SCHMID, F. X. & BROOKS, C. L., 3RD (2002) The effects of ionic strength on protein stability: the cold shock protein family. *J Mol Biol,* 319, 541-54.

DOTSCH, V., WIDER, G., SIEGAL, G. & WUTHRICH, K. (1995) Salt-stabilized globular protein structure in 7 M aqueous urea solution. *FEBS Lett,* 372, 288-90.

DYSON, H. J. & WRIGHT, P. E. (2004) Unfolded proteins and protein folding studied by NMR. *Chem Rev,* 104, 3607-22.

FABER-BARATA, J. & SOLA-PENNA, M. (2005) Opposing effects of two osmolytes--trehalose and glycerol--on thermal inactivation of rabbit muscle 6-phosphofructo-1-kinase. *Mol Cell Biochem,* 269, 203-7.

FABIOLA, G. F., KRISHNASWAMY, S., NAGARAJAN, V. & PATTABHI, V. (1997) C-H...O hydrogen bonds in beta-sheets. *Acta Crystallogr D Biol Crystallogr,* 53, 316-20.

FARIA, T. Q., LIMA, J. C., BASTOS, M., MACANITA, A. L. & SANTOS, H. (2004) Protein stabilization by osmolytes from hyperthermophiles: effect of mannosylglycerate on the thermal unfolding of recombinant nuclease a from Staphylococcus aureus studied by picosecond time-resolved fluorescence and calorimetry. *J Biol Chem,* 279, 48680-91.

FERSHT, A. (1999) *Structure and mechanism in protein science : a guide to enzyme catalysis and protein folding,* New York, W.H. Freeman.

FORSTER, R. P. & GOLDSTEIN, L. (1976) Intracellular osmoregulatory role of amino acids and urea in marine elasmobranchs. *Am J Physiol,* 230, 925-31.

FRACZKIEWICZ, R. and BRAUN, W. (1998) "Exact and efficient analytical calculation of the accessible surface areas and their gradients for macromolecules" *J. Comp. Chem.*, 19, 319-333

FREY, P. A., WHITT, S. A. & TOBIN, J. B. (1994) A low-barrier hydrogen bond in the catalytic triad of serine proteases. *Science,* 264, 1927-30.

GARCIA-MIRA, M. M. & SANCHEZ-RUIZ, J. M. (2001) pH corrections and protein ionization in water/guanidinium chloride. *Biophys J,* 81, 3489-502.

GARRETT, D, S., POWERS, R., GRONENBORN, A, M. & CLORE, G, M. (1991) A common sense approach to peak picking two-, three- and four-dimensional spectra using automatic computer analysis of contour diagrams. *J. Magn. Reson. 95*, 214-220

GOLDSTEIN, G. (1974) Isolation of bovine thymin: a polypeptide hormone of the thymus. *Nature,* 247, 11-4.

GRANT, D. M. & HARRIS, R. K. (1996) *Encyclopedia of nuclear magnetic resonance,* Chichester ; New York, John Wiley.

GREENE, R. F., JR. & PACE, C. N. (1974) Urea and guanidine hydrochloride denaturation of ribonuclease, lysozyme, alpha-chymotrypsin, and beta-lactoglobulin. *J Biol Chem,* 249, 5388-93.

GRIBENKO, A. V., GUZMAN-CASADO, M., LOPEZ, M. M. & MAKHATADZE, G. I. (2002) Conformational and thermodynamic properties of peptide binding to the human S100P protein. *Protein Sci,* 11, 1367-75.

GRIKO, Y. V., MAKHATADZE, G. I., PRIVALOV, P. L. & HARTLEY, R. W. (1994) Thermodynamics of barnase unfolding. *Protein Sci,* 3, 669-76.

GRZESIEK, S. & BAX, A. (1997) A three-dimensional NMR experiment with improved sensitivity for carbonyl-carbonyl J correlation in proteins. *J Biomol NMR,* 9, 207-11.

GRZESIEK, S., CORDIER, F. & DINGLEY, A. J. (2001) Scalar couplings across hydrogen bonds. *Methods Enzymol,* 338, 111-33.

GRZESIEK, S., CORDIER, F., JARVINE, V. & BARFIELD, M, (2004) Insights into biomolecular hydrogen bonds from hydrogen bond scalar couplings. *Progress in Nuclear Magnetic Resonance Spectroscopy,* 45, 275-300.

GUPTA, R., YADAV, S. & AHMAD, F. (1996) Protein stability: urea-induced versus guanidine-induced unfolding of metmyoglobin. *Biochemistry,* 35, 11925-30.

HAGARMAN, A., DUITCH, L. & SCHWEITZER-STENNER, R. (2008) The conformational manifold of ferricytochrome c explored by visible and far-UV electronic circular dichroism spectroscopy. *Biochemistry,* 47, 9667-77.

HAGIHARA, Y., AIMOTO, S., FINK, A. L. & GOTO, Y. (1993) Guanidine hydrochloride-induced folding of proteins. *J Mol Biol,* 231, 180-4.

HARDING, M. M., WILLIAMS, D. H. & WOOLFSON, D. N. (1991) Characterization of a partially denatured state of a protein by two-dimensional NMR: reduction of the hydrophobic interactions in ubiquitin. *Biochemistry,* 30, 3120-8.

HATEFI, Y. & HANSTEIN, W. G. (1969) Solubilization of particulate proteins and nonelectrolytes by chaotropic agents. *Proc Natl Acad Sci U S A,* 62, 1129-36.

HERBERHOLD, H. & WINTER, R. (2002) Temperature- and pressure-induced unfolding and refolding of ubiquitin: a static and kinetic Fourier transform infrared spectroscopy study. *Biochemistry,* 41, 2396-401.

HERNANDEZ, G. & LEMASTER, D. M. (2009) NMR analysis of native-state protein conformational flexibility by hydrogen exchange. *Methods Mol Biol,* 490, 285-310.

HERRMANN, J., LERMAN, L. O. & LERMAN, A. (2007) Ubiquitin and ubiquitin-like proteins in protein regulation. *Circ Res,* 100, 1276-91.

HERSHKO, A. & CIECHANOVER, A. (1992) The ubiquitin system for protein degradation. *Annu Rev Biochem,* 61, 761-807.

HERSHKO, A. & CIECHANOVER, A. (1998) The ubiquitin system. *Annu Rev Biochem,* 67, 425-79.

HWANG, T. L. & SHAKA, A. J. (1998) Multiple-pulse mixing sequences that selectively enhance chemical exchange or cross-relaxation peaks in high-resolution NMR spectra. *J Magn Reson,* 135, 280-7.

HWANG, T. L., VAN ZIJL, P. C. & MORI, S. (1998) Accurate quantitation of water-amide proton exchange rates using the phase-modulated CLEAN chemical EXchange (CLEANEX-PM) approach with a Fast-HSQC (FHSQC) detection scheme. *J Biomol NMR,* 11, 221-6.

IBARRA-MOLERO, B., LOLADZE, V. V., MAKHATADZE, G. I. & SANCHEZ-RUIZ, J. M. (1999a) Thermal versus guanidine-induced unfolding of ubiquitin. An analysis in terms of the contributions from charge-charge interactions to protein stability. *Biochemistry,* 38, 8138-49.

IBARRA-MOLERO, B., MAKHATADZE, G. I. & SANCHEZ-RUIZ, J. M. (1999b) Cold denaturation of ubiquitin. *Biochim Biophys Acta,* 1429, 384-90.

JAMESON, D. M., CRONEY, J. C. & MOENS, P. D. (2003) Fluorescence: basic concepts, practical aspects, and some anecdotes. *Methods Enzymol,* 360, 1-43.

JARAVINE, V. A., ALEXANDRESCU, A. T. & GRZESIEK, S. (2001) Observation of the closing of individual hydrogen bonds during TFE-induced helix formation in a peptide. *Protein Sci,* 10, 943-50.

JENSON, J., GOLDSTEIN, G. & BRESLOW, E. (1980) Physical-chemical properties of ubiquitin. *Biochim Biophys Acta,* 624, 378-85.

JURANIC, N., ATANASOVA, E., STREIFF, J. H., MACURA, S. & PRENDERGAST, F. G. (2007) Solvent-induced differentiation of protein backbone hydrogen bonds in calmodulin. *Protein Sci,* 16, 1329-37.

JURANIC, N., MONCRIEFFE, M. C., LIKIC, V. A., PRENDERGAST, F. G. & MACURA, S. (2002) Structural dependencies of h3JNC' scalar coupling in protein H-bond chains. *J Am Chem Soc,* 124, 14221-6.

KAY L, E., KEIFER P., SAARINEN T. (1992). Pure absorption gradient enhanced heteronuclear single quantum correlation spectroscopy with improved sensitivity. *J Am Chem Soc*, 114, 10663-1066

KAY, L. E., TORCHIA D. A. & BAX, A. (1989). Backbone dynamics of proteins as studied by ^{15}N inverse detected heteronuclear NMR spectroscopy: application to staphylococcal nuclease. *Biochemistry*, 28, 8972-8979.

KAVITHA, M. & SWAMY, M. J. (2009) Spectroscopic and differential scanning calorimetric studies on the unfolding of Trichosanthes dioica seed lectin. Similar modes of thermal and chemical denaturation. *Glycoconj J,* 26, 1075-84.

KAWAHARA, K., KIRSHNER, A. G. & TANFORD, C. (1965) DISSOCIATION OF HUMAN CO-hemoglobin by urea, guanidine hydrochloride, and other reagents. *Biochemistry,* 4, 1203-13.

KEELER, J. (2005) *Understanding NMR spectroscopy,* Chichester, England ; Hoboken, NJ, Wiley.

KELLY, A. E., OU, H. D., WITHERS, R. & DOTSCH, V. (2002) Low-conductivity buffers for high-sensitivity NMR measurements. *J Am Chem Soc,* 124, 12013-9.

KITA, Y., ARAKAWA, T., LIN, T. Y. & TIMASHEFF, S. N. (1994) Contribution of the surface free energy perturbation to protein-solvent interactions. *Biochemistry,* 33, 15178-89.

KORADI, R., BILLETER, M. & WUTHRICH, K. (1996) MOLMOL: a program for display and analysis of macromolecular structures. *J Mol Graph,* 14, 51-5, 29-32.

KRISHNA, M. M., HOANG, L., LIN, Y. & ENGLANDER, S. W. (2004) Hydrogen exchange methods to study protein folding. *Methods,* 34, 51-64.

KUNTZ, I. D. (1972) Tertiary structure in carboxypeptidase. *J Am Chem Soc,* 94, 8568-72.

KUPCE, E., FREEMAN, R. (1995) Adiabatic pulses for wideband inversion and broadband decoupling, *J. Magn. Reson A*, 115 273-276.

LAMOSA, P., GONCALVES, L. G., RODRIGUES, M. V., MARTINS, L. O., RAVEN, N. D. & SANTOS, H. (2006) Occurrence of 1-glyceryl-1-myo-inosityl phosphate in hyperthermophiles. *Appl Environ Microbiol,* 72, 6169-73.

LAMOSA, P., MARTINS, L. O., DA COSTA, M. S. & SANTOS, H. (1998) Effects of temperature, salinity, and medium composition on compatible solute accumulation by thermococcus spp. *Appl Environ Microbiol,* 64, 3591-8.

LARSON, J.W. & McMAHON, T, B., (1982) Gas-phase bifluoride ion. An ion cyclotron resonance determination of the hydrogen bond energy in FHF_ from gasphase fluoride transfer equilibrium measurements. *J Am Chem Soc*, 104, 5848-5849.

LATHAM, M. P., ZIMMERMANN, G. R. & PARDI, A. (2009) NMR chemical exchange as a probe for ligand-binding kinetics in a theophylline-binding RNA aptamer. *J Am Chem Soc,* 131, 5052-3.

LEE, L. K., RANCE, M., CHAZIN, W. J. & PALMER, A. G., 3RD (1997) Rotational diffusion anisotropy of proteins from simultaneous analysis of 15N and 13C alpha nuclear spin relaxation. *J Biomol NMR,* 9, 287-98.

LEHNINGER, A. L., NELSON, D. L. & COX, M. M. (2005) *Lehninger principles of biochemistry*, New York, W. H. Freeman.

LEVITT, M. H. (2001) *Spin dynamics : basics of nuclear magnetic resonance*, Chichester ; New York, John Wiley & Sons.

LI, H., YAMADA, H., AKASAKA, K. & GRONENBORN, A. M. (2000) Pressure alters electronic orbital overlap in hydrogen bonds. *J Biomol NMR*, 18, 207-16.

Li WANG, A. C. & BAX A. (1996) Equilibrium protium_deuterium fractionation of backbone amides in U-^{13}C-^{15}N labeled human ubiquitin by triple resonance NMR. *J Am Chem* Soc, 118, 12864-12865

LIM, W. K., ROSGEN, J. & ENGLANDER, S. W. (2009) Urea, but not guanidinium, destabilizes proteins by forming hydrogen bonds to the peptide group. *Proc Natl Acad Sci U S A*, 106, 2595-600.

LIN, S. L., ZARRINE-AFSAR, A. & DAVIDSON, A. R. (2009) The osmolyte trimethylamine-N-oxide stabilizes the Fyn SH3 domain without altering the structure of its folding transition state. *Protein Sci*, 18, 526-36.

LIN, T. Y. & TIMASHEFF, S. N. (1994) Why do some organisms use a urea-methylamine mixture as osmolyte? Thermodynamic compensation of urea and trimethylamine N-oxide interactions with protein. *Biochemistry*, 33, 12695-701.

LINS, L. & BRASSEUR, R. (1995) The hydrophobic effect in protein folding. *Faseb J*, 9, 535-40.

LIPARI G. & SZABO A. (1982a). Model-free approach to the interpretation of nuclear magnetic-resonance relaxation in macromolecules. 1. Theory and range of validity. *J. Am. Chem. Soc*., 17, 4546-4559.

LIPARI, G. & SZABO, A. (1982b). Model-free approach to the interpretation of nuclear magnetic-resonance relaxation in macromolecules. 2. Analysis of experimental results *J Am Chem Soc*, 104, 4559-4570.

LIPSITZ, R. S., SHARMA, Y., BROOKS, B. R. & TJANDRA, N. (2002) Hydrogen bonding in high-resolution protein structures: a new method to assess NMR protein geometry. *J Am Chem Soc*, 124, 10621-6.

LIU, A., HU, W., MAJUMDAR, A., ROSEN, M. K. & PATEL, D. J. (2000) NMR detection of side chain-side chain hydrogen bonding interactions in 13C/15N-labeled proteins. *J Biomol NMR*, 17, 305-10.

LIWANG, A. C. & BAX, A. (1997) Solution NMR characterization of hydrogen bonds in a protein by indirect measurement of deuterium quadrupole couplings. *J Magn Reson*, 127, 54-64.

LOH, S. N. & MARKLEY, J. L. (1994) Hydrogen bonding in proteins as studied by amide hydrogen D/H fractionation factors: application to staphylococcal nuclease. *Biochemistry*, 33, 1029-36.

LOLADZE, V. V. & MAKHATADZE, G. I. (2002) Removal of surface charge-charge interactions from ubiquitin leaves the protein folded and very stable. *Protein Sci*, 11, 174-7.

LOPEZ, M. M. & MAKHATADZE, G. I. (2002) Isothermal titration calorimetry. *Methods Mol Biol*, 173, 121-6.

MAKHATADZE, G. I., CLORE, G. M. & GRONENBORN, A. M. (1995) Solvent isotope effect and protein stability. *Nat Struct Biol*, 2, 852-5.

MAKHATADZE, G. I., LOLADZE, V. V., ERMOLENKO, D. N., CHEN, X. & THOMAS, S. T. (2003) Contribution of surface salt bridges to protein stability: guidelines for protein engineering. *J Mol Biol,* 327, 1135-48.

MAKHATADZE, G. I., LOLADZE, V. V., GRIBENKO, A. V. & LOPEZ, M. M. (2004) Mechanism of thermostabilization in a designed cold shock protein with optimized surface electrostatic interactions. *J Mol Biol,* 336, 929-42.

MAKHATADZE, G. I., LOPEZ, M. M., RICHARDSON, J. M., 3RD & THOMAS, S. T. (1998) Anion binding to the ubiquitin molecule. *Protein Sci,* 7, 689-97.

MAKHATADZE, G. I. & PRIVALOV, P. L. (1992) Protein interactions with urea and guanidinium chloride. A calorimetric study. *J Mol Biol,* 226, 491-505.

MANALO, M. N., KONG, X. & LIWANG, A. (2005) 1JNH values show that N1...N3 hydrogen bonds are stronger in dsRNA A:U than dsDNA A:T base pairs. *J Am Chem Soc,* 127, 17974-5.

MANDEL, A. M., AKKE, M. & PALMER, A. G., 3RD (1995) Backbone dynamics of Escherichia coli ribonuclease HI: correlations with structure and function in an active enzyme. *J Mol Biol,* 246, 144-63.

MARION, D., IKURA, M., TSCHUDIN, R. & BAX, A. (1989) Rapid recording of 2D NMR spectra without phase cycling. Application to the study of hydrogen exchange in proteins. *J Magn Reson,* 85, 393-399.

MARKLEY, J. L., WESTLER, W. M., CHAN, T. M., KOJIRO, C. L. & ULRICH, E. L. (1984) Two-dimensional NMR approaches to the study of protein structure and function. *Fed Proc,* 43, 2648-56.

MARKWICK, P. R., SPRANGERS, R. & SATTLER, M. (2003) Dynamic effects on j-couplings across hydrogen bonds in proteins. *J Am Chem Soc,* 125, 644-5.

MARTINS, L. O., HUBER, R., HUBER, H., STETTER, K. O., DA COSTA, M. S. & SANTOS, H. (1997) Organic Solutes in Hyperthermophilic Archaea. *Appl Environ Microbiol,* 63, 896-902.

MASON, P. E., BRADY, J. W., NEILSON, G. W. & DEMPSEY, C. E. (2007) The interaction of guanidinium ions with a model peptide. *Biophys J,* 93, L04-6.

MASON, P. E., NEILSON, G. W., DEMPSEY, C. E., BARNES, A. C. & CRUICKSHANK, J. M. (2003) The hydration structure of guanidinium and thiocyanate ions: implications for protein stability in aqueous solution. *Proc Natl Acad Sci U S A,* 100, 4557-61.

MASON, P. E., NEILSON, G. W., ENDERBY, J. E., SABOUNGI, M. L., DEMPSEY, C. E., MACKERELL, A. D., JR. & BRADY, J. W. (2004) The structure of aqueous guanidinium chloride solutions. *J Am Chem Soc,* 126, 11462-70.

MAYOR, U., GUYDOSH, N. R., JOHNSON, C. M., GROSSMANN, J. G., SATO, S., JAS, G. S., FREUND, S. M., ALONSO, D. O., DAGGETT, V. & FERSHT, A. R. (2003) The complete folding pathway of a protein from nanoseconds to microseconds. *Nature,* 421, 863-7.

MAYR, L. M. & SCHMID, F. X. (1993) Stabilization of a protein by guanidinium chloride. *Biochemistry,* 32, 7994-8.

MCDONALD, I. K. & THORNTON, J. M. (1994) Satisfying hydrogen bonding potential in proteins. *J Mol Biol,* 238, 777-93.

MERRIL, C. R. (1990) Gel-staining techniques. *Methods Enzymol,* 182, 477-88.

MOELBERT, S., NORMAND, B. & DE LOS RIOS, P. (2004) Kosmotropes and chaotropes: modelling preferential exclusion, binding and aggregate stability. *Biophys Chem,* 112, 45-57.

MOGLICH, A., KRIEGER, F. & KIEFHABER, T. (2005) Molecular basis for the effect of urea and guanidinium chloride on the dynamics of unfolded polypeptide chains. *J Mol Biol,* 345, 153-62.

MUKAIYAMA, A., KOGA, Y., TAKANO, K. & KANAYA, S. (2008) Osmolyte effect on the stability and folding of a hyperthermophilic protein. *Proteins,* 71, 110-8.

MURTHY, N. S. & KNOX, J. R. (2004) Hydration of proteins: SAXS study of native and methoxy polyethyleneglycol (mPEG)-modified L-asparaginase and bovine serum albumin in mPEG solutions. *Biopolymers,* 74, 457-66.

MYERS, J. K. & PACE, C. N. (1996) Hydrogen bonding stabilizes globular proteins. *Biophys J,* 71, 2033-9.

MYERS, J. K., PACE, C. N. & SCHOLTZ, J. M. (1995) Denaturant m values and heat capacity changes: relation to changes in accessible surface areas of protein unfolding. *Protein Sci,* 4, 2138-48.

NELSON, J. W. & KALLENBACH, N. R. (1989) Persistence of the alpha-helix stop signal in the S-peptide in trifluoroethanol solutions. *Biochemistry,* 28, 5256-61.

NONIN, S., JIANG, F. & PATEL, D. J. (1997) Imino proton exchange and base-pair kinetics in the AMP-RNA aptamer complex. *J Mol Biol,* 268, 359-74.

NOZAKI, Y. & TANFORD, C. (1970) The solubility of amino acids, diglycine, and triglycine in aqueous guanidine hydrochloride solutions. *J Biol Chem,* 245, 1648-52.

O'BRIEN, E. P., DIMA, R. I., BROOKS, B. & THIRUMALAI, D. (2007) Interactions between hydrophobic and ionic solutes in aqueous guanidinium chloride and urea solutions: lessons for protein denaturation mechanism. *Journal of the American Chemical Society,* 129**,** 7346-7353.

OLDFIELD, E. (2002) Chemical shifts in amino acids, peptides, and proteins: from quantum chemistry to drug design. *Annu Rev Phys Chem,* 53, 349-78.

OLIVA, A., BERTRAN, J. & DANNENBERG, J. J. (2008) Attractive strain: the disadvantages of rigid multiple H-bond donors and acceptors. A theoretical analysis of the hydrogen-bonding interactions in complexes of tetraazaanthracenedione with pyridylureas. *J Phys Chem B,* 112, 1765-9.

OLIVEIRA, L. M., CORDEIRO, C., FREIRE, A. P., ASCENSO, C. & QUINTAS, A. (2007) Unveiling heme proteins conformational stability through a UV absorbance ratio method. *Anal Biochem,* 371, 253-5.

PACE, C. N. (1986) Determination and analysis of urea and guanidine hydrochloride denaturation curves. *Methods Enzymol,* 131, 266-80.

PACE, C. N., ALSTON, R. W. & SHAW, K. L. (2000) Charge-charge interactions influence the denatured state ensemble and contribute to protein stability. *Protein Sci,* 9, 1395-8.

PACE, C. N., LAURENTS, D. V. & THOMSON, J. A. (1990) pH dependence of the urea and guanidine hydrochloride denaturation of ribonuclease A and ribonuclease T1. *Biochemistry,* 29, 2564-72.

PACE, C. N. & SHAW, K. L. (2000) Linear extrapolation method of analyzing solvent denaturation curves. *Proteins,* Suppl 4, 1-7.

PALMER, A. G., 3RD, KROENKE, C. D. & LORIA, J. P. (2001) Nuclear magnetic resonance methods for quantifying microsecond-to-millisecond motions in biological macromolecules. *Methods Enzymol,* 339, 204-38.

PARDI, A., WAGNER, G. & WUTHRICH, K. (1983) Protein conformation and proton nuclear-magnetic-resonance chemical shifts. *Eur J Biochem,* 137, 445-54.

PAUL, S. & PATEY, G. N. (2007a) The influence of urea and trimethylamine-N-oxide on hydrophobic interactions. *J Phys Chem B,* 111, 7932-3.

PAUL, S. & PATEY, G. N. (2007b) Structure and interaction in aqueous urea-trimethylamine-N-oxide solutions. *J Am Chem Soc,* 129, 4476-82.

PAULING, L. (1940) *The nature of the chemical bond, and the structure of molecules and crystals; an introduction to modern structural chemistry,* Ithaca, N.Y. London,, Cornell University Press; H. Milford, Oxford Universty Press.

PAULING, L. (1960) *The nature of the chemical bond and the structure of molecules and crystals; an introduction to modern structural chemistry,* Ithaca, N. Y., Cornell University Press.

PAULING, L. & COREY, R. B. (1951) The pleated sheet, a new layer configuration of polypeptide chains. *Proc Natl Acad Sci U S A,* 37, 251-6.

PAULING, L., COREY, R. B. & BRANSON, H. R. (1951) The structure of proteins; two hydrogen-bonded helical configurations of the polypeptide chain. *Proc Natl Acad Sci U S A,* 37, 205-11.

PERUTZ, M. F. & RAIDT, H. (1975) Stereochemical basis of heat stability in bacterial ferredoxins and in haemoglobin A2. *Nature,* 255, 256-9.

PERVUSHIN, K., ONO, A., FERNANDEZ, C., SZYPERSKI, T., KAINOSHO, M. & WUTHRICH, K. (1998) NMR scalar couplings across Watson-Crick base pair hydrogen bonds in DNA observed by transverse relaxation-optimized spectroscopy. *Proc Natl Acad Sci U S A,* 95, 14147-51.

PERVUSHIN, K., RIEK, R., WIDER, G. & WUTHRICH, K. (1997) Attenuated T2 relaxation by mutual cancellation of dipole-dipole coupling and chemical shift anisotropy indicates an avenue to NMR structures of very large biological macromolecules in solution. *Proc Natl Acad Sci U S A,* 94, 12366-71.

PIMENTEL, G. C. & MCCLELLAN, A. L. (1960) *The hydrogen bond,* San Francisco, W. H. Freeman; trade distributor., New York.

PRAKASH, V., LOUCHEUX, C., SCHEUFELE, S., GORBUNOFF, M. J. & TIMASHEFF, S. N. (1981) Interactions of proteins with solvent components in 8 M urea. *Arch Biochem Biophys,* 210, 455-64.

QU, Y. & BOLEN, D. W. (2003) Hydrogen exchange kinetics of RNase A and the urea:TMAO paradigm. *Biochemistry,* 42, 5837-49.

RAMSEY N, F. (1953) Electron coupled interactions between nuclear spins in molecules. *Phys Rev,* 91, 303-307.

RAUSELL, C., MUNOZ-GARAY, C., MIRANDA-CASSOLUENGO, R., GOMEZ, I., RUDINO-PINERA, E., SOBERON, M. & BRAVO, A. (2004) Tryptophan spectroscopy studies and black lipid bilayer analysis indicate that the oligomeric structure of Cry1Ab toxin from Bacillus thuringiensis is the membrane-insertion intermediate. *Biochemistry,* 43, 166-74.

REZUS, Y. L. & BAKKER, H. J. (2006) Effect of urea on the structural dynamics of water. *Proc Natl Acad Sci U S A,* 103, 18417-20.

RICHARDSON, J. M. & MAKHATADZE, G. I. (2004) Temperature dependence of the thermodynamics of helix-coil transition. *J Mol Biol,* 335, 1029-37.

RICHARDSON, J. S. (1977) beta-Sheet topology and the relatedness of proteins. *Nature,* 268, 495-500.

ROZWADOWSKI, Z. (2007) Chiral recognition of the Schiff bases by NMR spectroscopy in the presence of a chiral dirhodium complex. Deuterium isotope effect on 13C chemical shift of the optically active Schiff bases and their dirhodium adducts. *Magn Reson Chem,* 45, 605-10.

SALVADOR, P., KOBKO, N., WIECZOREK, R. & DANNENBERG, J. J. (2004) Calculation of trans-hydrogen-bond 13C-15N three-bond and other scalar J-couplings in cooperative peptide models. A density functional theory study. *J Am Chem Soc,* 126, 14190-7.

SALVADOR, P., WIECZOREK, R. & DANNENBERG, J. J. (2007) Direct calculation of trans-hydrogen-bond 13C-15N 3-bond J-couplings in entire polyalanine alpha-helices. A density functional theory study. *J Phys Chem B,* 111, 2398-403.

SCHIFFER, M. & EDMUNDSON, A. B. (1967) Use of helical wheels to represent the structures of proteins and to identify segments with helical potential. *Biophys J,* 7, 121-35.

SCHILF, W., BLOXSIDGE, J. P., JONES, J. R. & LU, S. Y. (2004) Investigations of intramolecular hydrogen bonding in three types of Schiff bases by 2H and 3H NMR isotope effects. *Magn Reson Chem,* 42, 556-60.

SHAKA A, J., BARKER P, B., FREEMAN R. (1985) Computer-optimized decoupling scheme for wideband applicationsand low-level operation. *J Magn Reson,* 64, 547-552.

SHAKA, A,J., LEE, C, J., PINES, A. (1988) Iterative schemes for bilinear operators; application to spin decoupling. *J Magn Reson,* 77, 274-293.

SHARIF, S., HUOT, M. C., TOLSTOY, P. M., TONEY, M. D., JONSSON, K. H. & LIMBACH, H. H. (2007) 15N nuclear magnetic resonance studies of acid-base properties of pyridoxal-5'-phosphate aldimines in aqueous solution. *J Phys Chem B,* 111, 3869-76.

SHOUP, R. R., MILES, H. T. & BECKER, E. D. (1966) NMR evidence of specific base-pairing between purines and pyrimidines. *Biochem Biophys Res Commun,* 23, 194-201.

SINGER, M. A. & LINDQUIST, S. (1998) Thermotolerance in Saccharomyces cerevisiae: the Yin and Yang of trehalose. *Trends Biotechnol,* 16, 460-8.

SMITH, J. S. & SCHOLTZ, J. M. (1996) Guanidine hydrochloride unfolding of peptide helices: separation of denaturant and salt effects. *Biochemistry,* 35, 7292-7.

SOMERO, G. N. (1986) Protons, osmolytes, and fitness of internal milieu for protein function. *Am J Physiol,* 251, R197-213.

ST JOHN, R. J., CARPENTER, J. F., BALNY, C. & RANDOLPH, T. W. (2001) High pressure refolding of recombinant human growth hormone from insoluble aggregates. Structural transformations, kinetic barriers, and energetics. *J Biol Chem,* 276, 46856-63.

ST JOHN, R. J., CARPENTER, J. F. & RANDOLPH, T. W. (1999) High pressure fosters protein refolding from aggregates at high concentrations. *Proc Natl Acad Sci U S A,* 96, 13029-33.

STRYER, L. (1995) *Biochemistry,* New York, W.H. Freeman.

SUNDD, M., IVERSON, N., IBARRA-MOLERO, B., SANCHEZ-RUIZ, J. M. & ROBERTSON, A. D. (2002) Electrostatic interactions in ubiquitin: stabilization of carboxylates by lysine amino groups. *Biochemistry,* 41, 7586-96.

TAFAZZOLI, M. & AMINI, S. K. (2008) Theoretical 13C chemical shift, 14N, and 2H quadrupole coupling- constant studies of hydrogen bonding in L-alanylglycine dipeptide. *Magn Reson Chem,* 46, 370-6.

TJANDRA, N., GRZESIEK, S. & BAX, A. (1996) Magnetic field dependence of nitrogen-proton J splittings in ^{15}N-enriched human ubiquitin resulting from relaxation interference and residual dipolar coupling. *J Am Chem Soc* 118, 26, 6264-6272.

TJANDRA, N., FELLER, S. E., PASTOR, R. W. & BAX, A. (1995) Rotational diffusion anisotropy of human ubiquitin from 15N NMR relaxation. *J. Am. Chem. Soc.* 117, 12562-12565

TAKANO, K., SAITO, M., MORIKAWA, M. & KANAYA, S. (2004) Mutational and structural-based analyses of the osmolyte effect on protein stability. *J Biochem,* 135, 701-8.

TANFORD, C. (1968) Protein denaturation. *Adv Protein Chem,* 23, 121-282.

TANFORD, C. & DE, P. K. (1961) The unfolding of beta-lactoglobulin at pH 3 by urea, formamide, and other organic substances. *J Biol Chem,* 236, 1711-5.

TAYLOR, J. R. (1997) *An introduction to error analysis : the study of uncertainties in physical measurements,* Sausalito, Calif., University Science Books.

TIMASHEFF, S. N. (1992) Water as ligand: preferential binding and exclusion of denaturants in protein unfolding. *Biochemistry,* 31, 9857-64.

TIMASHEFF, S. N. & XIE, G. (2003) Preferential interactions of urea with lysozyme and their linkage to protein denaturation. *Biophys Chem,* 105, 421-48.

TOLMAN, J. R. & PRESTEGARD, J. H. (1996) A quantitative J-correlation experiment for the accurate measurement of one-bond amide 15N-1H couplings in proteins. *J Magn Reson B,* 112, 245-52.

TRAVASSO, R. D., TELO DA GAMA, M. M. & FAISCA, P. F. (2007) Pathways to folding, nucleation events, and native geometry. *J Chem Phys,* 127, 145106-145110

TUTTLE, T., KRAKA, E., WU, A. & CREMER, D. (2004) Investigation of the NMR spin-spin coupling constants across the hydrogen bonds in ubiquitin: the nature of the hydrogen bond as reflected by the coupling mechanism. *J Am Chem Soc,* 126, 5093-107.

VAN MOURIK, T. & DINGLEY, A. J. (2005) Characterization of the monovalent ion position and hydrogen-bond network in guanine quartets by DFT calculations of NMR parameters. *Chemistry,* 11, 6064-79.

VENKATESU, P., LEE, M. J. & LIN, H. M. (2009) Osmolyte counteracts urea-induced denaturation of alpha-chymotrypsin. *J Phys Chem B,* 113, 5327-38.

VIJAY-KUMAR, S., BUGG, C. E. & COOK, W. J. (1987) Structure of ubiquitin refined at 1.8 A resolution. *J Mol Biol,* 194, 531-44.

VIJAY-KUMAR, S., BUGG, C. E., WILKINSON, K. D. & COOK, W. J. (1985) Three-dimensional structure of ubiquitin at 2.8 A resolution. *Proc Natl Acad Sci U S A,* 82, 3582-5.

VRANKEN, W. F., BOUCHER, W., STEVENS, T. J., FOGH, R. H., PAJON, A., LLINAS, M., ULRICH, E. L., MARKLEY, J. L., IONIDES, J. & LAUE, E. D. (2005) The CCPN data model for NMR spectroscopy: development of a software pipeline. *Proteins,* 59, 687-96.

WAGNER, G., PARDI, A., WUTHRICH, K. (1983) Hydrogen bond length and proton NMR chemical shifts in proteins J . Am. Chem. Soc, 105 (1983) 5948.

WAGNER, G. & WUTHRICH, K. (1982) Sequential resonance assignments in protein 1H nuclear magnetic resonance spectra. Basic pancreatic trypsin inhibitor. *J Mol Biol,* 155, 347-66.

WANG, A. C. & BAX, A. (1995) Reparametrization of the karplus relation for 3J(H.alpha.-N) and 3J(HN-C') in Peptides from Uniformly 13C/15N-Enriched Human Ubiquitin *J. Am. Chem. Soc.* 117, 6, 1810-1813.

WANG, A. C., BAX, A. (1996) Determination of the Backbone Dihedral Angles in Human Ubiquitin from Reparametrized Empirical Karplus Equations *J. Am. Chem. Soc.* 118, 10, 2483-2494.

WANG, A. & BOLEN, D. W. (1996) Effect of proline on lactate dehydrogenase activity: testing the generality and scope of the compatibility paradigm. *Biophys J,* 71, 2117-22.

WANG, A. & BOLEN, D. W. (1997) A naturally occurring protective system in urea-rich cells: mechanism of osmolyte protection of proteins against urea denaturation. *Biochemistry,* 36, 9101-8.

WANG, L., EGHBALNIA, H. R. & MARKLEY, J. L. (2007) Nearest-neighbor effects on backbone alpha and beta carbon chemical shifts in proteins. *J Biomol NMR,* 39, 247-57.

WANG, Y. X., JACOB, J., CORDIER, F., WINGFIELD, P., STAHL, S. J., LEE-HUANG, S., TORCHIA, D., GRZESIEK, S. & BAX, A. (1999) Measurement of 3hJNC' connectivities across hydrogen bonds in a 30 kDa protein. *J Biomol NMR,* 14, 181-4.

WEBER, P. L., BROWN, S. C. & MUELLER, L. (1987) Sequential 1H NMR assignments and secondary structure identification of human ubiquitin. *Biochemistry,* 26, 7282-90.

WEISS, S. (2000) Measuring conformational dynamics of biomolecules by single molecule fluorescence spectroscopy. *Nat Struct Biol,* 7, 724-9.

WHITFORD, D. (2005) *Proteins : structure and function,* Hoboken, NJ, J. Wiley & Sons.

WIECZOREK, R. & DANNENBERG, J. J. (2003a) H-bonding cooperativity and energetics of alpha-helix formation of five 17-amino acid peptides. *J Am Chem Soc,* 125, 8124-9.

WIECZOREK, R. & DANNENBERG, J. J. (2003b) Hydrogen-bond cooperativity, vibrational coupling, and dependence of helix stability on changes in amino acid sequence in small 3 10-helical peptides. A density functional theory study. *J Am Chem Soc,* 125, 14065-71.

WIECZOREK, R. & DANNENBERG, J. J. (2005a) The energetic and structural effects of single amino acid substitutions upon capped alpha-helical peptides containing 17 amino acid residues. An ONIOM DFT/AM1 study. *J Am Chem Soc,* 127, 17216-23.

WIECZOREK, R. & DANNENBERG, J. J. (2005b) Enthalpies of hydrogen-bonds in alpha-helical peptides. An ONIOM DFT/AM1 study. *J Am Chem Soc,* 127, 14534-5.

WIGGINS, P. M. (2001) High and low density intracellular water. *Cell Mol Bio,* 47, 735-44.

WILKINSON, K. D. (2005) The discovery of ubiquitin-dependent proteolysis. *Proc Natl Acad Sci U S A,* 102, 15280-2.

WINTRODE, P. L., MAKHATADZE, G. I. & PRIVALOV, P. L. (1994) Thermodynamics of ubiquitin unfolding. *Proteins,* 18, 246-53.

WISHART, D. S. & CASE, D. A. (2001) Use of chemical shifts in macromolecular structure determination. *Methods Enzymol,* 338, 3-34.

WISHART, D. S., SYKES, B. D. & RICHARDS, F. M. (1991) Relationship between nuclear magnetic resonance chemical shift and protein secondary structure. *J Mol Biol,* 222, 311-33.

WOHNERT, J., DINGLEY, A. J., STOLDT, M., GORLACH, M., GRZESIEK, S. & BROWN, L. R. (1999) Direct identification of NH...N hydrogen bonds in non-canonical base pairs of RNA by NMR spectroscopy. *Nucleic Acids Res,* 27, 3104-10.

WOESSNER, D.E. (1962) Spin relaxation processes in a two-proton system undergoing anisotropic reorientation. *J Chem Phy*, 36, 1–4

WU, P. & BOLEN, D. W. (2006) Osmolyte-induced protein folding free energy changes. *Proteins*, 63, 290-6.

WUTHRICH, K., BILLETER, M. & BRAUN, W. (1984) Polypeptide secondary structure determination by nuclear magnetic resonance observation of short proton-proton distances. *J Mol Biol*, 180, 715-40.

YANCEY, P. H. (2005) Organic osmolytes as compatible, metabolic and counteracting cytoprotectants in high osmolarity and other stresses. *J Exp Biol*, 208, 2819-30.

YANCEY, P. H., CLARK, M. E., HAND, S. C., BOWLUS, R. D. & SOMERO, G. N. (1982) Living with water stress: evolution of osmolyte systems. *Science*, 217, 1214-22.

YANCEY, P. H. & SOMERO, G. N. (1979) Counteraction of urea destabilization of protein structure by methylamine osmoregulatory compounds of elasmobranch fishes. *Biochem J*, 183, 317-23.

ZANCAN, P. & SOLA-PENNA, M. (2005) Trehalose and glycerol stabilize and renature yeast inorganic pyrophosphatase inactivated by very high temperatures. *Arch Biochem Biophys*, 444, 52-60.

ZANGI, R. & BERNE, B. J. (2006) Aggregation and dispersion of small hydrophobic particles in aqueous electrolyte solutions. *J Phys Chem B*, 110, 22736-41.

ZANGI, R., HAGEN, M. & BERNE, B. J. (2007) Effect of ions on the hydrophobic interaction between two plates. *J Am Chem Soc*, 129, 4678-86.

ZERBST-BOROFFKA, I., KAMALTYNOW, R. M., HARJES, S., KINNE-SAFFRAN, E. & GROSS, J. (2005) TMAO and other organic osmolytes in the muscles of amphipods (Crustacea) from shallow and deep water of Lake Baikal. *Comp Biochem Physiol A Mol Integr Physiol*, 142, 58-64.

ZHANG, Y. & CREMER, P. S. (2006) Interactions between macromolecules and ions: The Hofmeister series. *Curr Opin Chem Biol*, 10, 658-63.

ZHOU, Y. & KARPLUS, M. (1999) Interpreting the folding kinetics of helical proteins. *Nature*, 401, 400-3.

ZOU, Q., HABERMANN-ROTTINGHAUS, S. M. & MURPHY, K. P. (1998) Urea effects on protein stability: hydrogen bonding and the hydrophobic effect. *Proteins*, 31, 107-15.

.